ZESZYTY NAUKOWE
Akademia Morska w Szczecinie

2013

36(108) z. 1

SCIENTIFIC JOURNALS
Maritime University of Szczecin

Szczecin 2013

Edition of this publication was curried out with the participation of financial resources received from the budget of West Pomeranian Province

Wydanie publikacji zrealizowano przy udziale środków finansowych otrzymanych z budżetu Województwa Zachodniopomorskiego

The printed version of *Scientific Journals Maritime University of Szczecin* is the original version of the issued journal

Patronage / Pod patronatem
Baltic Association of Mechanical Engineering, Kaliningrad, Rosja
Polskie Naukowo-Techniczne Towarzystwo Eksploatacyjne

CONTENTS / SPIS TREŚCI

Scientific Journals
Maritime University of Szczecin

Zeszyty Naukowe
Akademia Morska w Szczecinie

2013, 36(108) z. 1 pp. 5–14
ISSN 1733-8670

2013, 36(108) z. 1 s. 5–14

Simplified steady-state analytical model for manoeuvring and control of ASD tug in escort push operations

Jarosław Artyszuk

Maritime University of Szczecin, Faculty of Navigation
72-500 Szczecin, ul. Wały Chrobrego 1–2, e-mail: j.artyszuk@am.szczecin.pl

Key words: analytical model, manoeuvring, tug hydrodynamics, control parameters, escort push operations

Abstract

This paper evaluates an ASD tug's main control parameters in terms of: the propeller thrust, a direction thereof (the thruster angle), and the hull drift angle for given escort speed and required push force. Such a relation is sometimes referred to as the tug performance diagram. A simplified model of tug hydrodynamics is used to arrive at the qualitative and most representative relations of the above variables. This model is rather generic that can also suit any type of tug hydrodynamics, including even that related to a conventional tug.

Introduction

For safe and efficient ship-tug operation from the viewpoint of a tug's master (towmaster) we need to have exact knowledge and understanding of the complex relations between multiple input control variables and the output performance. The output performance is mostly indicated by the force applied on the towed ship, either in pull or push mode.

In steering / manoeuvring a tug (of any type of propulsion) there are direct and inverse control problems. In the direct problem we are interested in the tow force (the effective force applied on the towed ship) excited under given speed and control parameters. On the contrary, the inverse problem consists in establishing necessary control parameters for the assumed tow force and escort speed. The direct and inverse problems are sometimes called passive and active ones accordingly. In both tasks, a convenient mathematical description of the above mentioned input/output dependence is absolutely essential in reaching an efficient solution to the control problem.

A good understanding of control principles ensures i.a. a self-confidence of the towmaster and especially his right response in rapid and emergency situations, involving many different hydrodynamic and mechanical effects. Such skills or competences will certainly supplement those outlined e.g. in [1] or [2].

The required control parameters for a tug essentially change with the speed of the assisted ship. ASD tugs are specially capable of executing the tow assistance with high speed, much better (in wider limits) than conventional tugs.

Some research centres claim they developed software for computing tow forces, as well as necessary control parameter values on a tug in steady state situations. However, appropriate results concerning both an applied mathematical model and a detailed, well documented tug performance output in the form of charts are practically not published. Such data are needed for the training process and many optimisation studies on tug control and design as recently undertaken in Poland in view of the new LNG import terminal in Świnoujście. For an ASD tug of 50 t BP (bollard pull) in pushing mode [3, page 58] presents only a single and not complete chart of control, which rather originates in [4]. Similarly, for a VSP (Voith-Schneider Propeller) tractor tug while pushing stern-first, as compatible to an ASD tug operation (bow-first), one can also refer to [5]. In addition, seemingly a very valuable reference [6] provides control variables in a difficult, implicit format that is hard to be handled.

Under such somehow negative background, the objectives of this paper are:

- to prepare an initial platform / framework for computing the control parameters of a tug in the escort (non-zero speed) steady-state conditions of movement, which as far as possible avoids numerical solving of nonlinear equations, thus attempting to reach a direct / explicit analytical formulation;
- to test and evaluate at present this model with simple, analytically given hydrodynamic data, but only for the push mode of towing, as being relatively easier.

All these efforts shall bring to light the mechanism of equilibrium for a tug and her limits of operation. The explicit formulation ensures a parameterisation of the model, with which we can easily investigate various hydrodynamic designs of the tug, quickly conduct sensitivity analyses, and validate any simulation (numerical) results as based on more sophisticated models.

Though it is further indirectly assumed that azimuth thruster(-s) is installed, the obtained solution is general enough for any propulsor type.

Basic formulation of force equilibrium

The mutual ship-tug arrangement during the so-called indirect pushing operation, together with forces, is presented in figure 1. The indirect towing involves taking advantage of a tug's underwater hull hydrodynamic force while rendering assistance at significant escort speed. The tug-fixed coordinate system *Mxy* is positioned for convenience at the intersection of her centre plane and midship section, with *x* axis pointing forward and *y* axis to starboard side.

It shall be further kept in mind that escorting on starboard side of the ship is related to negative drift angles β and positive thruster angles δ. The thruster angle means the angle of the resulting thrust in tug's body axes. Though we generically assume a single thruster, this thrust force can also be equally distributed to dual propulsors (as usual in modern tugs), if such exist and are steered parallel. If the thrust force is provided by the classical rudder-propeller complex, the positive thrust angle is provided by deflecting the rudder to portside. Though both angles for the latter case – the resulting thrust angle and the rudder angle – are by convention positive in the ship manoeuvring hydrodynamics, there is no easy relation between them as compared to azimuth thrusters. In the case of azimuth thrusters, at least for a stationary tug or ship, both angles are identical.

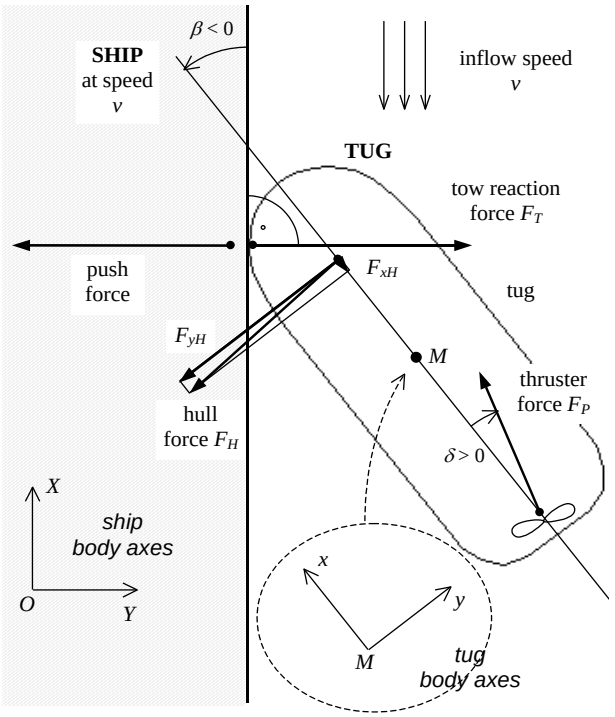

Fig. 1. Steady-state condition of indirect pushing operation

On the contrary, for the rudder-propeller system based on the Schilling rudder the maximum rudder angle of 65–70°, while running the propeller ahead, diverts the effective thrust to 90°. The Becker flapped rudder at its nominal 45° gives here slightly lower value of the thrust force angle, likely around 80–85°. For the conventional stern rudder such data are mostly not analysed and published – the propeller and rudder forces are described and computed (or measured) quite independently and such substituted to motion equations. The direction of the combined (thrust) force against the rudder angle is here not revealed due to a lack of interest. In general, the rudder-propeller system involves very complex propeller-rudder interactions, varying with the hull speed much more than that for azimuth thrusters. In addition, the helm angle for the conventional rudder is traditionally/historically limited to 35°. It also shall be remembered that for the propeller running astern the rudder is not so effective and the resulting force, almost entirely dominated by the propeller negative thrust and to some extent by its lateral component (well known to navigators), is almost constant and does not provide any means of control. Such a significant limitation in performance for the rudder-propeller system, and thus in the towing performance, is often shown in the so-called polar vector diagrams of the effective thrust as published for conventional tugs, see for example [3]. However, the relation between the rudder angle and the resulting thrust is almost omitted there.

The tow elastic reaction force F_T, hereafter briefly called also the tow force, is considered normal to the ship's hull in that no friction exists at the contact point. The tow force is equal in the absolute value to the effective push force applied on the ship. However, the latter force by the earlier definition is the proper tow force. The lack of tangential forces at the interacting surfaces, here arising from friction, is also equivalent in our model to the absence of mooring line(-s) for making fast the tug's bow alongside. This line, either applied as spring line or bow-line from the tug's viewpoint, is sometimes used to support escorting. Adopting a longitudinal component (in the ship body axes) that the tug would exert on the ship will certainly make the following mathematical model little complicated. The real need for such additional assumptions and possible improvements to the present formulation will be examined in next reports.

The equilibrium condition between the hull (*H*), thruster/propeller (*P*), and tow (*T*) forces in the tug's coordinates take the form:

$$\begin{cases} F_{xH} + F_{xP} + F_{xT} = 0 \\ F_{yH} + F_{yP} + F_{yT} = 0 \\ M_H + M_P + M_T = 0 \end{cases} \tag{1}$$

where:

F_x, F_y – longitudinal and lateral components of each force;

M – moment developed by particular force (however, in the case of hull this could incorporate also the effect of the hydrodynamic couple of forces that results in the zero force).

The tug's hull hydrodynamic forces are commonly written as follows:

$$\begin{bmatrix} F_{xH} \\ F_{yH} \\ M_{zH} \end{bmatrix} = 0.5\rho LTv^2 \cdot \begin{bmatrix} c_{fxh}(\beta) \\ c_{fyh}(\beta) \\ L \cdot c_{mzh}(\beta) \end{bmatrix} \tag{2}$$

where:

ρ – water density [kg/m^3];

L, T – tug's length (between perpendiculars) and draft (extreme) in [m];

v – absolute inflow speed [m/s];

c_{fxh}, c_{fyh}, c_{mzh} – nondimensional hydrodynamic coefficients [–].

For further calculations we adopt the following conditions of the tug and the environment: water density 1000 kg/m^3, L = 30.5 m, T = 5 m. However, most of obtained numerical and graphical data are nondimensional and thus independent of these quantities.

The product LT constitutes the reference or representative area for defining the nondimensional hydrodynamic coefficients and thus the resulting hydrodynamic forces. Since the tug is considered in the steady-state oblique movement, i.e. without turning, the hydrodynamic coefficients are functions of the drift angle β solely. Otherwise, we have to incorporate the other input variable of the hull hydrodynamic forces and moment – namely the nondimensional yaw velocity. Data on the yaw effect in hull hydrodynamics, especially over full range of the drift angle, are considerably missing in the literature. This might be contributed to some extent to difficulties in measurements in the model scale. On the other hand, the hydrodynamic coefficients as pure functions of the drift angle are frequently and quite accurately provided. The drift angle in ship hydrodynamics is adopted negative when the inflow comes from starboard side of the ship, as in our case of the tug, giving the hydrodynamic force to portside.

For the objectives of the present paper – development and initial appraisal of the mathematical model, and getting some reference numerical (quantitative) results – simple trigonometric functions will be used to approximate the hull hydrodynamic coefficients at even keel:

$$\begin{aligned} c_{fxh}(\beta) &= -0.03\cos\beta \\ c_{fyh}(\beta) &= +0.5\sin\beta \\ c_{mzh}(\beta) &= +0.1\sin 2\beta \end{aligned} \tag{3}$$

where $\beta \in \langle -180°, +180° \rangle$.

These rough but practically sufficient and very handy relations are illustrated in figure 2. For the assumptions of the present paper, we will look here for an equilibrium solution in the negative range of drift angles: from 0° up to the practical limiting value –90° and combined with positive thruster angles δ (to starboard side). A validation of these first choice expressions (3) was undertaken in [7].

Let's define at this point for subsequent derivations the following useful ratios with the hull nondimensional lateral force in the denominator (as practically avoiding the division by zero):

$$c'_{fxh}(\beta) = \frac{c_{fxh}(\beta)}{c_{fyh}(\beta)}, \qquad c'_{mzh}(\beta) = \frac{c_{mzh}(\beta)}{c_{fyh}(\beta)} \tag{4}$$

The relations (4) for data given by (3) are graphically demonstrated in figure 3. The functions (4) are fundamental in the process of getting the balance of forces as will be shown later.

The first ratio of (4) can be interpreted as a deflection angle, strictly its tangent, of the resultant

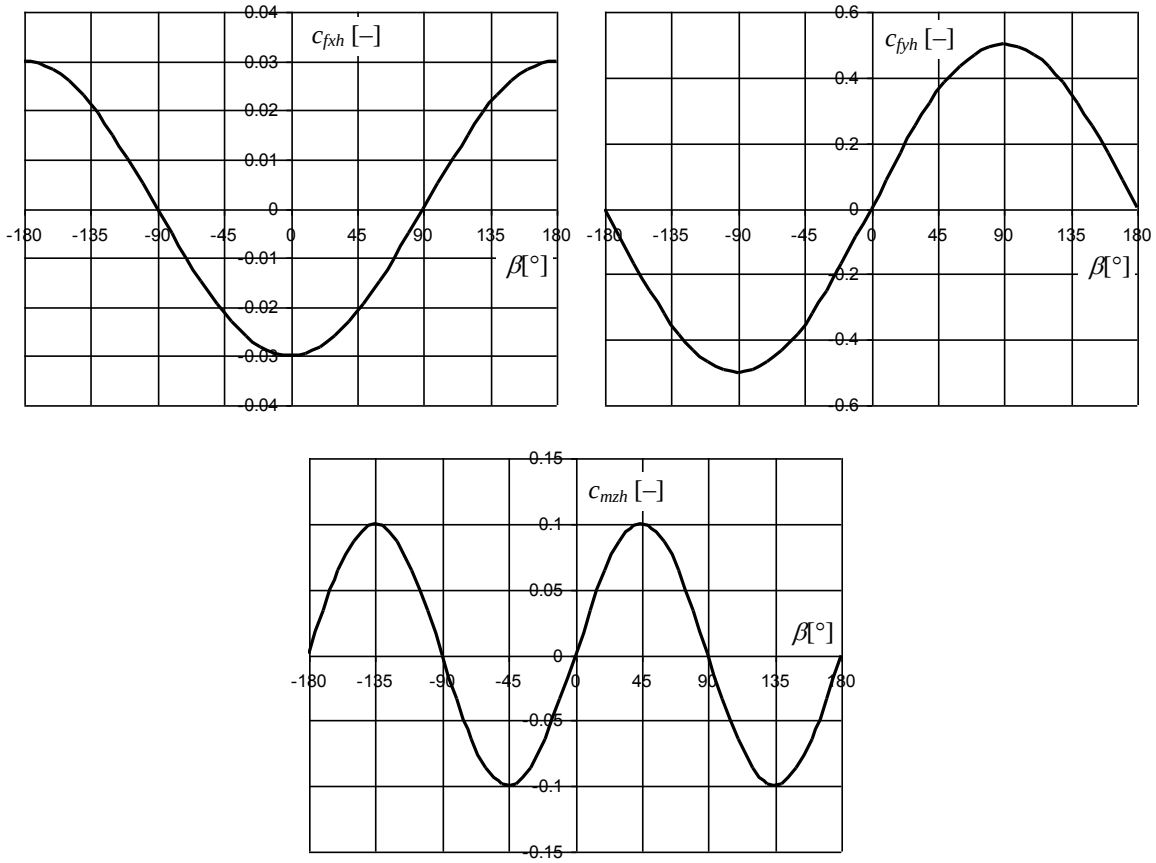

Fig. 2. Exemplary simple analytical approximations to the hull hydrodynamic coefficients

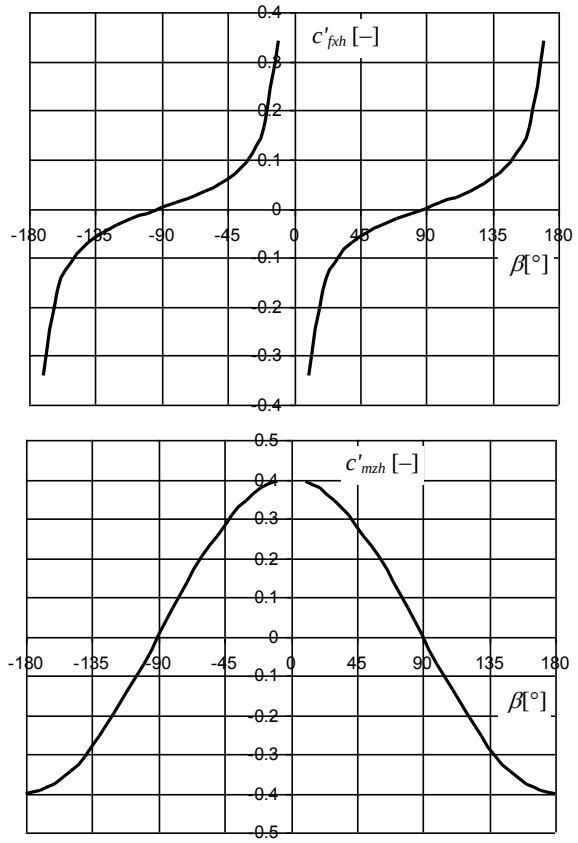

Fig. 3. Relative hull longitudinal force and yaw moment coefficients

hull force from the normal (perpendicular) direction to the hull. This direction is normal only in ideal fluid. However, in real (viscous) fluids and ship flows there are significant tangential stresses at the ship's hull surface. This deflection angle could reach even 20° and more.

The second ratio of (4) can be explained as the nondimensional arm, in ship's length units, counted from the midship section (the *M* origin). This could be quite abstract if it assumes values beyond the ship physical limits in that a certain hydrodynamic couple of forces, as aforementioned in the comments to equation (2), exists in the ship flow.

The thruster forces and moment in (1) read:

$$\begin{bmatrix} F_{xP} \\ F_{yP} \\ M_{zP} \end{bmatrix} = F_P \begin{bmatrix} \cos\delta \\ \sin\delta \\ \sin\delta \cdot x_P \end{bmatrix} \approx F_P \begin{bmatrix} \cos\delta \\ \sin\delta \\ -0.5L \cdot \sin\delta \end{bmatrix} \quad (5)$$

where:

F_P – absolute value of thrust (always positive);
x_P – thruster position (negative in aft direction).

In (5) we have already adopted the thruster location in the centre plane and its fore and aft coordinate at the aft perpendicular ($x_P \approx -0.5L$). The real values for x_P in the case of harbour or escort tugs

might go towards the midship section up to even $-0.3L$.

The thruster (or thrust) angle δ takes value from the range $(-180°, +180°\rangle$.

One should also be aware that assuming in (5) the constant value of the thrust force means its independence of other variables, particularly of the inflow speed v. This is a crucial item that needs our further investigation in the future and a possible improvement made to the mathematical model, however, being paid for with an additional sophistication of the model and difficulties in analysing the simulation results. Over the last years, there has been a tremendous progress in the research on the advance speed effect, particularly for azimuth thrusters, and such data are available: [8, 9] and many others. Also, some inspiration can be taken from [10]. Although the latter directly deals with VSP, but with respect to thrust and torque coefficients (as function of the advance coefficient and pitch ratio), this unconventional propeller reveals very similar hydrodynamic modelling properties to those well known for conventional propellers and thus for azimuth thrusters, as essentially consisting of a conventional yet rotatable propeller.

The tow (push) force in tug's coordinates is described by:

$$\begin{bmatrix} F_{xT} \\ F_{yT} \\ M_{zT} \end{bmatrix} = F_T \begin{bmatrix} \sin\beta \\ \cos\beta \\ \cos\beta \cdot x_T \end{bmatrix} \approx F_T \begin{bmatrix} \sin\beta \\ \cos\beta \\ +0.5L \cdot \cos\delta \end{bmatrix} \quad (6)$$

where:

F_T – absolute value of tow force (always positive);

x_P – tow point position (positive in forward direction).

In (6) we have just assumed that the moment of the tow force F_T comes only from the longitudinal abscissa of the contact point in that the tug's beam is completely disregarded. In addition, the tow position is at the forward perpendicular. Both assumptions are rather valid for higher drift angle in the vicinity of ±90° and will be rectified in the future, though it is believed they have no significant influence.

Fundamental derivations

Rearranging the three equations in (1) and dividing side-by-side in pairs: first and second, and third and second, supported by formulations (2), (4), (5), and (6), one finally gets:

$$c'_{fxh}(\beta) = \frac{-\cos\delta - F'_T \sin\beta}{-\sin\delta - F'_T \cos\beta} \quad (7)$$

$$c'_{mzh}(\beta) = \frac{+0.5\sin\delta - 0.5F'_T \cos\beta}{-\sin\delta - F'_T \cos\beta} \quad (8)$$

where:

$$F'_T = \frac{F_T}{F_P} \quad (9)$$

that can be considered as the nondimensional (relative) tow force. Having a brief look at (1), (2), (5), and (6) one can easily conclude that the absolute tow force F_T, as one of the equilibrium variables, is always proportional to the absolute thruster force F_T that is another variable (or parameter) of the these equations. The ratio of both is always constant in the equilibrium solution, if such exists.

A supplement of (7), (8), and (9) to the full equilibrium is the following equation for the tug's hull hydrodynamic lateral force F_{yH}:

$$F_{yH} = 0.5\rho LTv^2 c_{fyh}(\beta) = -F_P(\sin\delta + \cos\beta \cdot F'_T) \quad (10)$$

which can be split into two but more convenient relations:

$$F'_{yH} = -(\sin\delta + \cos\beta \cdot F'_T) \quad (11)$$

$$F'_{yH} = \frac{F_{yH}}{F_P} = \frac{0.5\rho LTv^2 c_{fyh}(\beta)}{F_P} \quad (12)$$

The absolute hull lateral force F_{yH} is the only term in our equations that comprises the speed dependence. So, the expression (12) turns into:

$$v = \sqrt{\frac{F'_{yH} \cdot F_P}{0.5\rho LTc_{fyh}(\beta)}} \quad (13)$$

This way the escort speed, enabling the desired steady-state condition of towing, is linearly related to the square root of the absolute thruster force F_P, and inversely proportional to the water density ρ or the tug's lateral area of the underwater hull LT.

Finally, we have arrived at the four basic relations: (7), (8), (11), (13). The first three directly originate from the equilibrium equations (1) and the last one is a part the hull hydrodynamic force formulation (2). We are going to further look for mutual relations of five variables:

β, δ, F_T, F_P, and v

or

β, δ, F'_T, F_P, and v.

However, the equations (7), (8), and (11) provide unique triples of (β, δ, F'_T) in that the drift angle β shall serve as parameter (the independent variable), since the thruster angle δ and the relative tow force F'_T can then be formulated as direct func-

tions of β thus avoiding the numerical solution of the essentially nonlinear equations (if other variable from the above set is taken for the domain). The drift angle is also one of the important steering parameters for the tug's master.

There are two strategies possible for steering the tug – active (inverse) and passive (direct) – which are defined according to the input parameters (initial assumptions or requests) and the chosen unknowns as steering variables. One can namely select the required absolute tow force F_T at the speed of advance v, in which the absolute thruster force F_P is searched for, together with the other basic steering parameters: β and δ. Such strategy we can call an active steering. A passive steering is obtained if we want to find the effective tow force F_T (apart from β and δ) if the thruster force F_P is known at the speed v.

The solutions provided later in the paper encompass the passive steering in that two distinct absolute thruster force are simulated as corresponding to 10 t and 50 t.

The expressions (7) and (8) can be transformed into:

$$F'_T = \frac{-\cos\delta + \sin\delta \cdot c'_{cfxh}(\beta)}{+\sin\beta - \cos\beta \cdot c'_{cfxh}(\beta)} \tag{14}$$

$$F'_T = \frac{\sin\delta}{\cos\beta} \cdot \frac{0.5 + c'_{mzh}(\beta)}{0.5 - c'_{mzh}(\beta)} \tag{15}$$

and made equal, thus leading to the direct function $\delta = \delta(\beta)$:

$$\frac{1}{\tan\delta} = \frac{1 + 2c'_{mzh}(\beta)}{1 - 2c'_{mzh}(\beta)} \cdot \left[-\tan\beta + c'_{fxh}(\beta)\right] + c'_{fxh}(\beta) \tag{16}$$

The next step now is to compute the relative tow force F'_T by means of (14) or (15). The both equations supply the same value.

The third and final stage is to evaluate the relative hull lateral force F'_{yH}, according to (11), for the purpose of obtaining the speed v – refer to (13). Hence the speed v is assigned to particular values of β and δ, dependent of course on the absolute thruster force. The higher is this force, the higher is the speed. If we plot the solved values of F'_T, β and δ versus the speed v for particular thruster force (e.g. 10 t or 50 t), we can state that the input thruster force is responsible for scaling the horizontal axis.

Simplifications and numerical results

Let's suppose the first possible simplification in that the hull hydrodynamic force is normal to the hull centre plane, i.e. the hull resistance (precisely the hull longitudinal force) is negligibly smaller than the lateral force. We are thus assuming:

$$c_{fxh}(\beta) = c'_{fxh}(\beta) \equiv 0 \tag{17}$$

This assumption $c'_{fxh} = 0$, which we call further the single simplification case, lead – see (16) and (14) – to the following final form:

$$\begin{cases} F'_{yT} = -\dfrac{\cos\delta}{\sin\beta} \\ F'_{yH} = -\left(\sin\delta + \cos\beta \cdot F'_{yT}\right) \\ \tan\delta = \dfrac{1 - 2 \cdot c'_{mzh}(\beta)}{-\tan\beta \cdot \left(1 + 2 \cdot c'_{mzh}(\beta)\right)} \end{cases} \tag{18}$$

For the assumption $c'_{mzh} = 0$ (theoretically justified for the needs of sensitivity analysis, but hardly proved in practice), we have:

$$\begin{cases} \tan\delta = \dfrac{1}{-\tan\beta + 2 \cdot c'_{fxh}(\beta)} \\ F'_{yH} = -\left(\sin\delta + \cos\beta \cdot F'_{yT}\right) \\ F'_{yT} = \dfrac{\sin\delta}{\cos\beta} \end{cases} \tag{19}$$

The relations (19) are however not considered later in detail and not simulated in this paper.

For both assumptions together: $c'_{fxh} = 0$ and $c'_{mzh} = 0$, which we will below refer to as the dual simplification case, one can read:

$$\begin{cases} \tan\delta = \dfrac{1}{-\tan\beta} \Rightarrow \delta = 90° + \beta \\ F'_{yH} = -2\cos\beta = -2\sin\delta \\ F'_{yT} = 1 \end{cases} \tag{20}$$

The performance of both simplifications – single (18) and dual (20) one – is presented in figures 4 and 5. The behaviour of the full model, through (11), (14), and (16), is demonstrated in the next figure 6. Thus figures 4 to 6 are arranged from the simplest to the most advanced instance of the model. In all these diagrams the usual range of escort speeds up to about 10 knots (5 m/s) is considered only.

The simplifications (18), (19), (20), and possible other more or less sophisticated approximations to the hydrodynamics of the hull and the thruster as well, are designed of course to provide the limits of operational control variables if the tug is subject to optimisation and innovations.

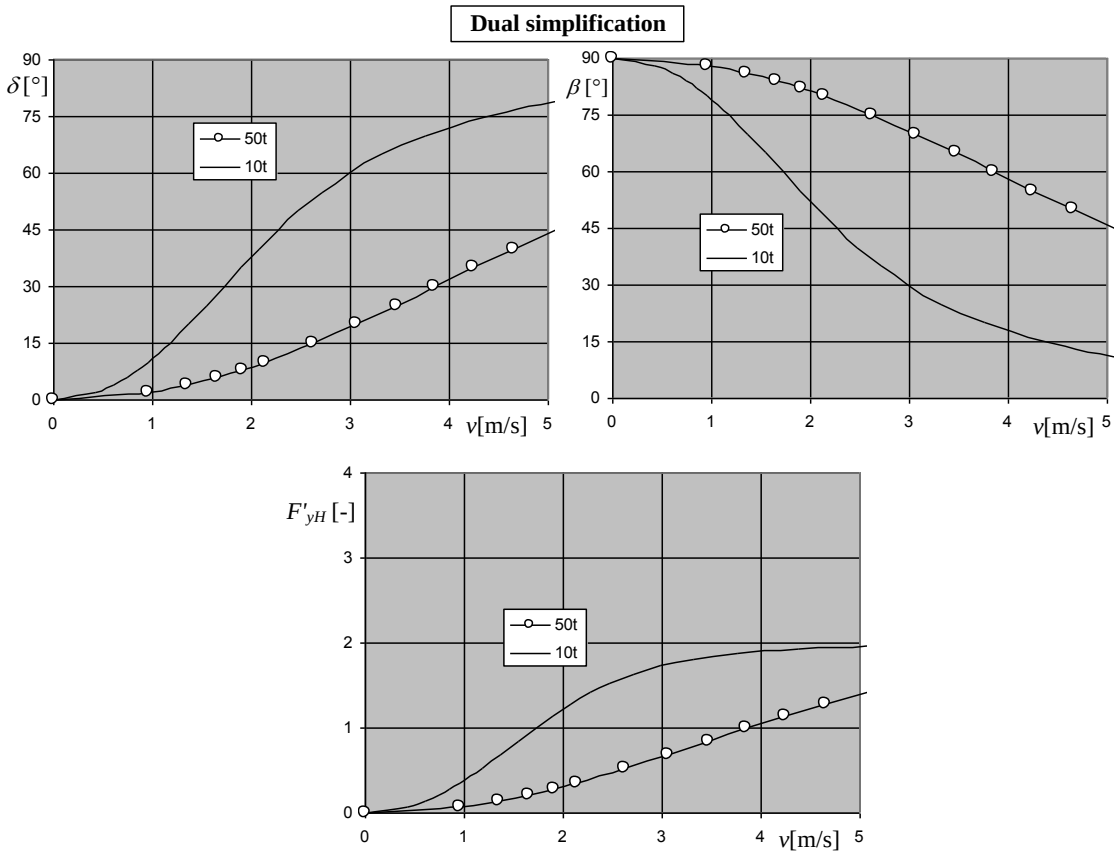

Fig. 4. Dual simplification model performance for practical escort speeds

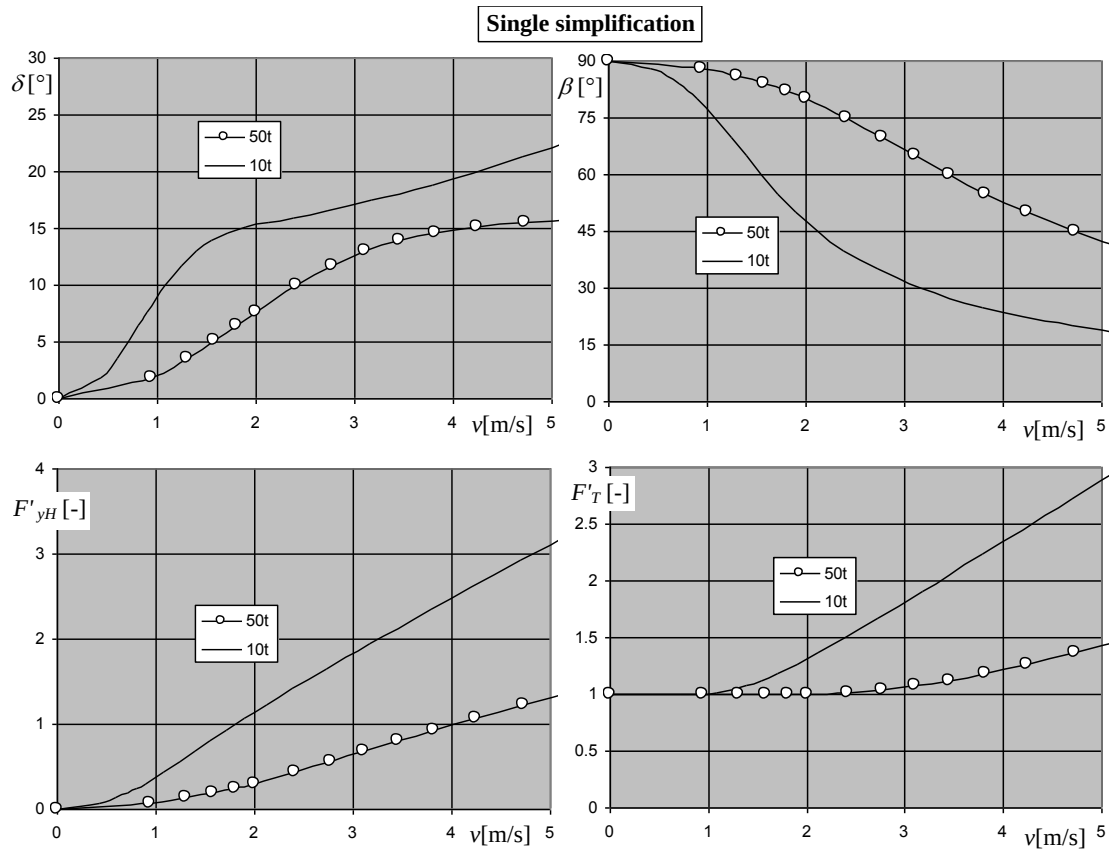

Fig. 5. Single simplification model performance for practical escort speeds

Figure 4 does not contain the relative tow force F'_T since it simply yields unity, i.e. there is no amplification of the propeller force. The efficiency of indirect mode of towing, through advantage of the hull hydrodynamic force for non-zero speed, gets essentially none. The hull lateral force, dominating

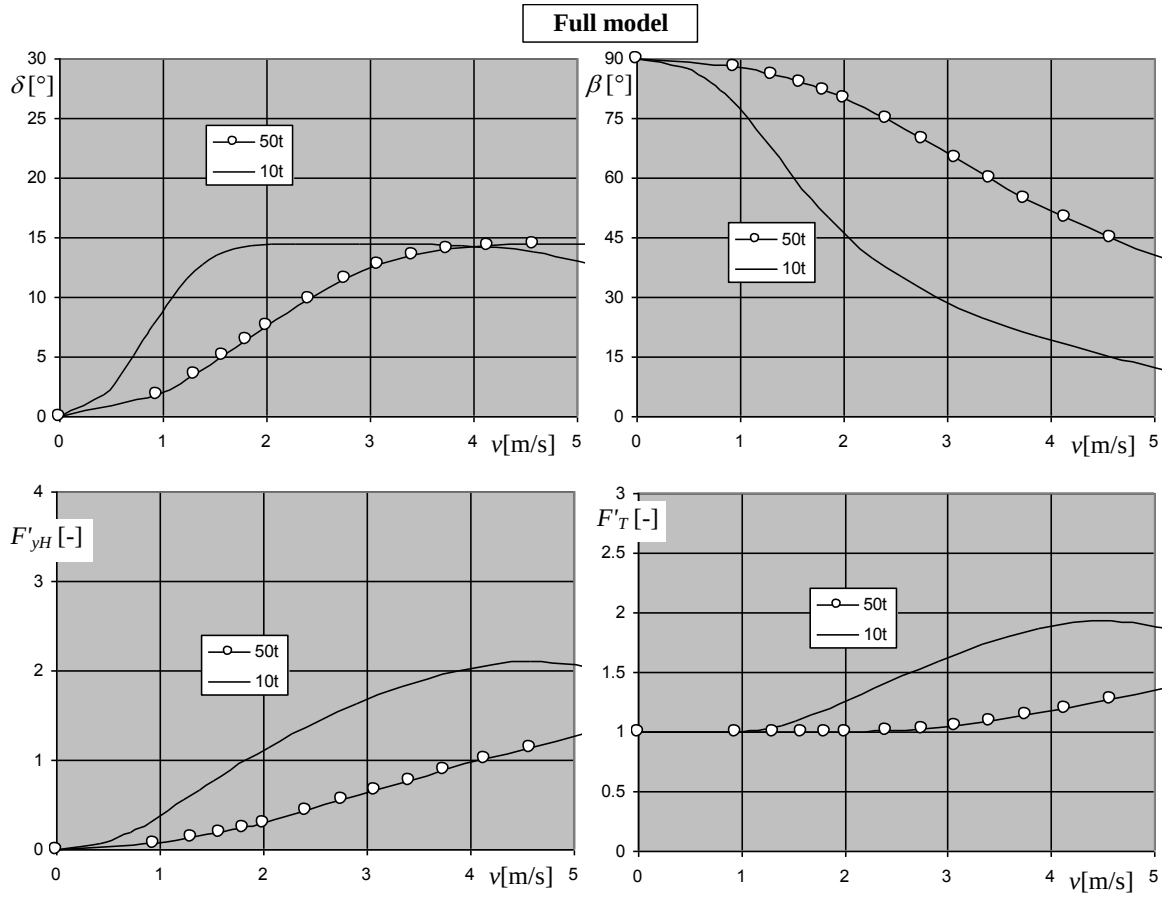

Fig. 6. Full model performance for practical escort speeds

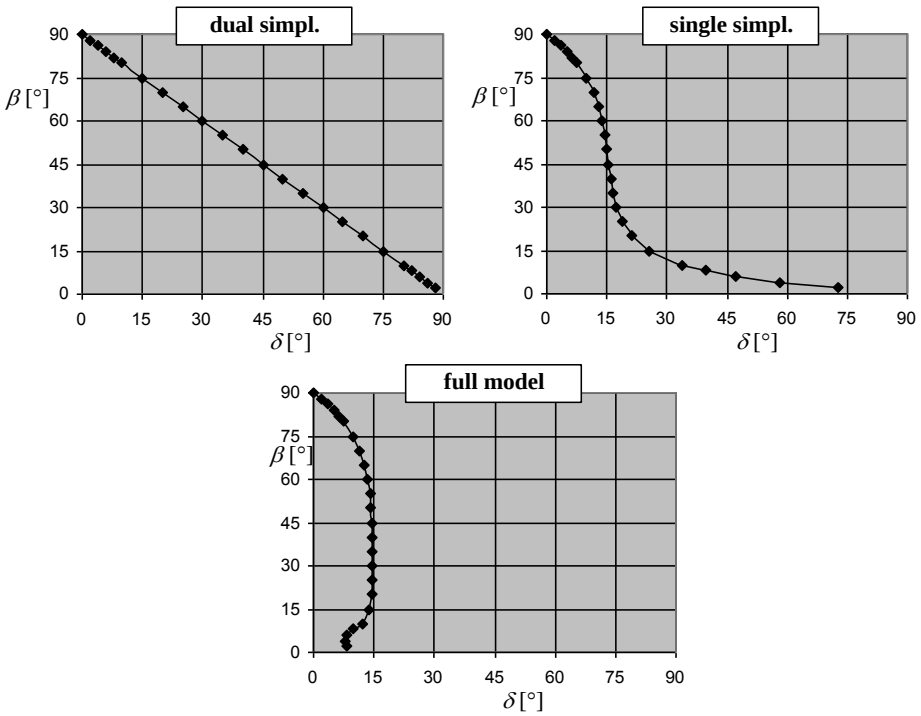

Fig. 7. Drift-thruster angle relation for whole range of drift angle

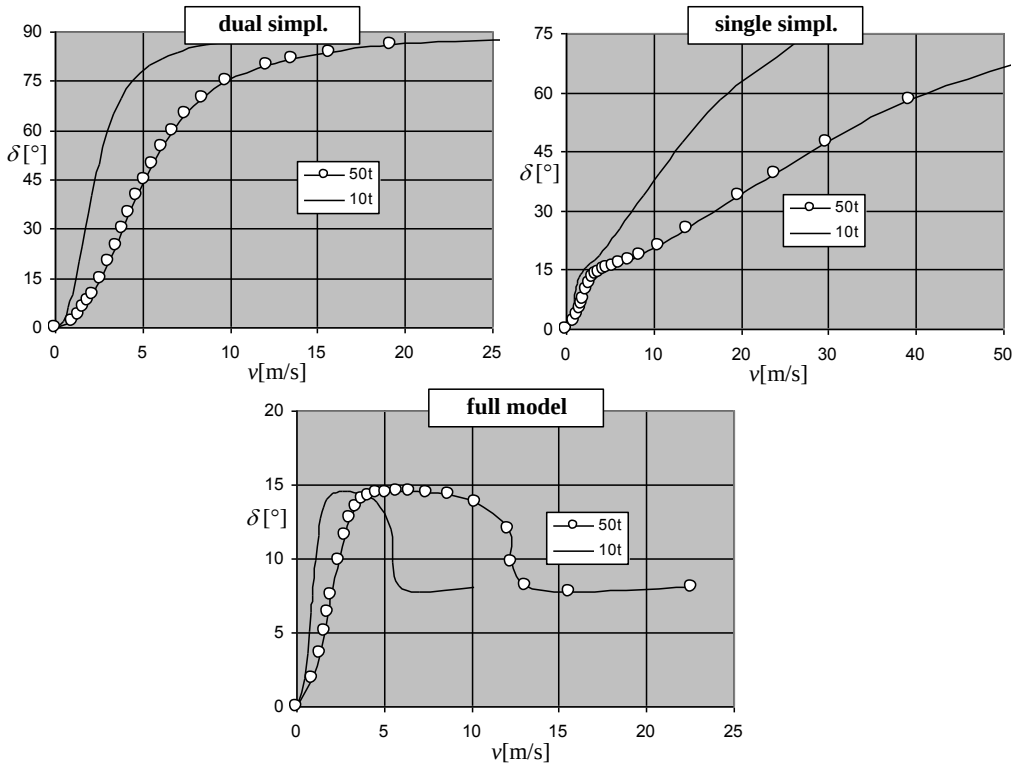

Fig. 8. Performance of all models within the whole range of speed

the hull total force (or contributing in 100% to the latter as in this case of dual simplification), and represented by F'_{yH}, assumes maximum value of 2.

For zero speed, the tug has to push normal to the hull (β±90°), i.e. in the "direct" way. The higher is the speed, the higher is the thruster angle and the lower the drift angle. However, this not specific to the dual simplification. Though there is no amplification of the thruster force for the dual simplification, if escort speed exists, the tug has to be less inclined to the ship's hull to "transfer 1:1" the thruster force to the push force. The thruster angle is surprisingly linearly dependent on the drift angle, which is graphically presented in figure 7, together with the output of other cases of the model.

However, the plots of figure 7 comprise the whole range of the drift angle in that the higher speeds (more than 5 m/s as adopted in figures 4 to 6) must be involved to get the equilibrium. Figure 8 gives the impression of the maximum speed in each case of simplification.

The largest differences between our instances of the model appear in the charts $\delta(v)$ – the top ones in figures 4 to 6, which is additionally confirmed in figure 7. For the dual simplification case the required δ is roughly twice as large as that in the other two cases. This curve shall be treated as the limiting range of the thruster angle.

For the single simplification (connected with rather weak assumption $c_{fxh} = 0$) and full model at speeds higher than 1 m/s (2 knots) we are able to develop nearly twice higher push force than the thruster force – refer to the last charts in figures 5 and 6. Thus the indirect mode has proved its excellence.

However, if the hull longitudinal resistance is omitted in the tug's hydrodynamic model (the single simplification case), the relative tow force F'_T can surprisingly go far beyond the value of 2, but this is coupled with very high speeds.

Both models, the single simplification and full ones, perform quite similarly within practical escort speeds.

Figure 7 proves that the full model is the only model that limits the thruster angle, which is remarkably below 15° in all operational situations. Of course, the full model is also based on some approximations to the tug's hydrodynamics.

Within practical escort speed range the drift-speed relation β–v is the least vulnerable to simplifications made to the model. However, the version of simplification is connected with completely a different speed range, leading even to an enormous speed – see figure 8 – though mathematically correct, rarely to be realised. This huge speed is related to small drift angles in the order of a few degrees.

For the full model, the thruster angle is the same for the wide range of speed, thus it is insensitive of the escort speed. This way some adjustments can be made only by means of the drift angle (the inclina-

tion angle to the ship's hull). This is of course a kind of unusual steering guidance for towmasters.

Conclusions

The obtained charts in the paper could serve as rough and clear guidance for towmasters.

Secondly, such data are also very useful for assessing and optimising more sophisticated models, where e.g. hull-thruster and thruster-thruster interactions are included, by providing a basis for further sensitivity analyses. In the latter context, one should be aware that incorporating some special hydrodynamic effects into the model would not always result in a significant change of a tug control parameters as essential from the viewpoint of a towmaster.

Thirdly, one can attempt to design the tug controllers both for fast- and real-time preliminary simulations, when the human input or interaction from a towmaster (to a tug simulator interconnected with the assisted ship simulator) is not yet necessary. In safety studies, this of course only concerns early stages of investigations, but is not so time and human resources consuming. Adequate tug automatic controllers guarantee proper "time constants" of tug response under various environmental and operational circumstances. This is much better than commonly adopted in simulators the so-called vector tugs (in terms of force and its direction, and their rates of change) as activated from the instructor's station by the instructor himself. While constructing control laws for the tug automatic controllers, the research on the steady-state manoeuvring conditions, including that undertaken in the present study, would certainly provide great help.

The presented model of tug's equilibrium of forces is really encouraging. It is worthwhile to next carry out investigations of the effects of the forward contact point abscissa and the thruster aft location. As mentioned before, they have been assumed equal in absolute magnitude – both are half the tug's length and set on both ends of the tug.

The algorithm is very general and the adopted simple formulas for tug's hull hydrodynamics provide exemplary numerical values. However, any definition, including the lookup-table stored data, can be easily linked to the algorithm. Thus the next valuable research steps could also be testing the model with real data of tug's hull hydrodynamic coefficients and improving the thruster submodel.

References

1. SLESINGER J.: ASD Tugs: Thrust and Azimuth. Learning to Drive a Z-Drive. Cornell Maritime Press/Schiffer Publishing, Atglen 2010.
2. HENSEN H.: Safe tug operation: who takes the lead? International Tug & OSV, Jul/Aug. 2012.
3. HENSEN H.: Tug Use in Port. A Practical Guide. The Nautical Institute, London 2003.
4. RENILSON M., TUITE A.: A Technique for Assessing the Difficulty of Ship Manoeuvring in Ports. International Pilotage Conference, Brisbane, Mar 11–13, 1998.
5. JURGENS D.: A Contribution to Safe Ship Assistance. International Tug & Salvage, Sep/Oct, 2009.
6. RENILSON M.R., BRANDNER P., TASKER R.L.: Realistic Simulation of Tug Forces on a Manoeuvring Vessel. 2nd Conference on Manoeuvring and Control of Marine Craft, MCMC'92, Southampton 1992.
7. ARTYSZUK J.: Ship Sway / Yaw Motions while Turning with Bow Lateral Thruster. 15th International Conference on Hydrodynamics in Ship Design, Safety and Operation, HYDRONAV'2003, Gdańsk, Oct 22–24, 2003.
8. STETTLER J.W., HOVER F.S., TRIANTAFYLLOU M.S.: Preliminary Results of Testing on the Dynamics of an Azimuthing Podded Propulsor Relating to Vehicle Manoeuvring. First International Conference on Technological Advances in Podded Propulsion, T-POD, Conference Proceedings (ed.: Atlar M.), Newcastle upon Tyne, Apr 14–16, 2004.
9. GRYGOROWICZ M., SZANTYR J.A.: Open Water Experiments with Two Pod Propulsor Models. First International Conference on Technological Advances in Podded Propulsion, T-POD, Conference Proceedings (ed.: Atlar M.), Newcastle upon Tyne, Apr 14–16, 2004.
10. AGDRUP K., OLSEN A.S., JURGENS D.: Development of a Mathematical Model of a Voith Schneider Tug and Experience from its Application in an Offshore Simulation Study. International Conference on Marine Simulation and Ship Manoeuvrability, MARSIM 2006, Paper No. M-21, Terschelling (NL), Jun 25–30, 2006.

Scientific Journals
Maritime University of Szczecin

Zeszyty Naukowe
Akademia Morska w Szczecinie

2013, 36(108) z. 1 pp. 15–21
ISSN 1733-8670

2013, 36(108) z. 1 s. 15–21

Automation of processes of identifying navigation situations requiring communication to be established by a sea-going vessel

Paweł Banaś, Zbigniew Pietrzykowski, Anna Wójcik, Piotr Wołejsza

Maritime University of Szczecin
70-500 Szczecin, ul. Wały Chrobrego 1–2
e-mail: {p.banas; z.pietrzykowski; a.wojcik; p.wolejsza}@am.szczecin.pl

Key words: communication, e-navigation, inference rules, navigation situations, automation

Abstract

One of the causes of ships' accidents are errors in the communication between navigators in charge of ships concerned. The most common causes include a lack of communication, misunderstanding of a received message, incorrect choice of the type of message or misinterpretation of the information exchanged. These errors can be significantly reduced by the automation of intership communication processes, in particular by a developed automatic maritime communication system. The decision to communicate is as essential as communication itself. This paper presents the problem of identifying situations requiring the establishing of communication by a sea-going vessel. A definition of the need to establish communication between the vessels is associated with the acquisition of data, analysis and evaluation of the navigational situation and the relevant inference process. Based on an analysis of the process of identifying navigation situations which require communication between proceeding ships, the model of automatic identification of such situations has been developed.

Introduction

Access to required up-to-date and reliable information is of primary importance for correct navigational decision making on ships and at land-based centres alike. Developed to this end by the IMO is the concept of e-navigation, based on an increasingly standardized form of navigational information and the standardization and automation of information exchange.

A complex character of a navigational situation may call for establishing communication between navigators steering their ships in vicinity of each other or between navigators and land-based centre personnel [1]. This refers to the need of ascertaining the actual situation, intentions of the ships involved or agreeing on manoeuvres to be performed. Hence we should expect that the next step will be taken towards the automation of communication processes taking place between navigators on board and land-based centre operators. Rapid advancements in IT and ICT technologies open possibilities for automated communications between shipboard and shore IT systems, and, in various combinations and proportions, between operators and IT systems. This will allow to restrict possibilities of human errors, such as failure to establish communication, misunderstanding of a received message, improper choice of a message or wrong interpretation of exchanged information. Such reduction will contribute to the enhancement of navigational safety.

The identification of the need of establishing communication between ships or between a ship and a land-based centre involves the acquisition of data, an analysis and assessment of a navigational situation and conducting the process of inference in this area.

Automation of communication processes in marine navigation

Communication processes in marine navigation

Participants of communication processes in maritime shipping are ship navigators, land-based

personnel of VTS and similar centres, shipowners, forwarders and others. The principles of communication between them are provided in relevant regulations, defining obligations resting on traffic participants. However, regulations do not eliminate possibilities of dangerous situations that may result, among others, from a failure to start communication or misunderstandings.

Correct and effective communication is of particular significance in situations threatening the safety of people, means of transport (ship), cargo or/and environment. Therefore, it seems purposeful, in defining areas of communication, to adopt the classification commonly used in the GMDSS system (Global Maritime Distress and Safety System) [2, 3] with strict rules and procedures for priority communications:

– distress communication (collisions, rescue of life and property);
– urgency communication (e.g. medical advice or assistance);
– safety communication (e.g. navigational and meteorological warnings).

Another mode in the GMDSS system is the so called routine communication. It is used, for instance, in situations where ships report their presence in traffic separation schemes or reporting systems. Routine messages, unlike the priority communication, do not have in the GMDSS a strictly defined procedure or circumstances that would make communication obligatory or recommended. This is due to a lack of legal measures that would regulate routine communication. The four aforesaid modes of communication (distress, urgency, safety and routine) define thematic areas of messages sent by participants of the transport process in marine shipping.

Communication processes in general comprise the transmission of information between a sender and a receiver. Taking into account the scope of conducted communications various aspects [3]:

– acquisition, processing, transmission and presentation of information, using standard navigational equipment and systems;
– selective acquisition of information (information needed in a given situation) for identification or more accurate description, interpretation, assessment of a present and/or predicted situation, intentions of traffic participants;
– mechanisms of co-operation and negotiations concerning safe ship conduct, avoidance of threats and the prevention and minimizing consequences of accidents.

Navigational information is nowadays acquired, integrated, processed, transmitted and presented to an increasingly wider extent. This is possible thanks to introduced standards of content and form of navigational information.

However, both navigators and shore operators of vessel traffic find it often necessary to obtain specific, i.e. selected information. This particularly refers to the acquisition of supplementary information and necessitates the establishment of communication for supplementing specific data through a dialog. This can be an oral exchange performed via a VHF radiotelephone.

Tasks of an automatic communication system in marine navigation

Tasks to be performed by the proposed system of automatic communication in marine navigation [4] correspond to the areas and ranges of communication processes taking place in maritime transport (see section *Communication processes in marine navigatio*). In a nutshell, they refer to:

1) acquisition and presentation of information,
2) mechanisms of communication and negotiations between ships and land-based centres.

The automation of communication in marine navigation at present refers to a typical exchange of data obtained from shipboard and shore navigational equipment and systems and addresses the former communication task area. Actually, the ongoing standardization of navigational or operational data scope and format goes in line and facilitates such automation. It seems particularly vital to broaden automatic communication to include selective acquisition of data needed in a given situation for identification or more accurate description, interpretation, assessment of a present and/or predicted situation, intentions of traffic participants.

Equally important in the system of automatic communication in marine navigation is the development and implementation of co-operation and negotiations mechanisms referring to safe conduct of the ship, avoidance of threats and the prevention and minimizing effects of accidents.

The mentioned mechanisms of selective information acquisition and mechanisms of co-operation and negotiations should take into account various forms of communication, resulting from the needs of users and from the transformation of communication processes:

- person – person, via a computer system (manual mode);
- person – computer system (in both directions, any range) (semi-automatic mode);
- computer system – computer system (automatic system).

The automation of both selective information acquisition and negotiation processes require the knowledge of inference rules for an analysis and interpretation of dialog contents. The rules refer to the identification of navigational situations requiring communication to be established by a ship or land-based centre, as well as the very mechanisms of communication and negotiations (form, area, range and time constraints / requirements).

Automatic execution of communication should also take into consideration the specific manner of verbal exchange by people. It should reflect and relevantly employ linguistic variables and values that people use.

For the automatic communication process to run correctly, the need for its initiation or continuation by an operator or system has to be first identified. This refers to both periodic stimuli (events at known time of occurrence) and non-periodic stimuli (events whose moment of occurrence is not known in advance).

Process of identifying navigational situations requiring communication to be established by a sea-going vessel

Priority communications

In an analysis of issues referring to the needs of communication for predefined areas of communication we examined navigational situations including cases of collision threats, and specific distress, safety and urgency message exchanges.

Collisions

Parameters that unequivocally indicate a risk of collision or close quarters situation are the Closest Point of Approach (CPA) and Time to Closest Point of Approach (TCPA). To calculate these parameters we have to know the positions and movement parameters of own and target ships (latitude and longitude, or possibly X/Y, course over the water and speed through water). Besides, when qualifying an encounter situation according to the Collision Regulations, we have to know true courses and navigational status of both ships. To determine whether a target ship is manoeuvring, its rate of turn has to be known, while the ship can be identified by its MMSI, call sign or name.

Limit (acceptable) values of CPA and TCPA, denoted as CPA_L and $TCPA_L$ – are specified for a given ship by its navigator (mostly instructed by the captain). The respective values in the open sea area are usually 1 Nm and 15 minutes. In a restricted area, the time is usually reduced to 10 minutes. The CPA value depends on ship size. The problem of determining CPA_L and $TCPA_L$ was examined in a number of real field, simulation and questionnair-based tests [5, 6].

Here is an example of a message sent in a collision risk situation from ship A to ship B:

A to B: ship B, CPA is 0 Nm, TCPA is 15 minute, you are a give-way vessel (Rule 15 – crossing courses), alter your course to starboard to pass astern of me.

The transmission of such message is preceded by an analysis of the relevant navigational situation and ascertaining the need for communication. This process is defined as identification of a navigational situation that necessitates establishment of communication by a vessel. The communication can be executed semi-automatically, using a message form filled out by the navigator, or automatically, where both the communication need identification and message preparation and sending are performed by a system of automatic communication.

Distress, urgency and safety communications

It seems that this type of communications should be executed semi-automatically, based on ready-made forms filled out by the navigator. On this basis, the system would generate an appropriate message. This actually means that the system does not establish communication with another ship or a centre automatically. Here is an example distress, urgency or safety communication where a form filled out by a navigator is used:

1. Priority: distress / urgency / safety;
2. In case of distress – type of danger: collision, abandon ship, grounding, fire, pirates etc.;
3. Ship position and time when obtained (acquired automatically);
4. Number of personnel, number of injured persons;
5. Required assistance;
6. Other information useful in rescue operation.

After the form is filled out, the system generates a message (it may also be a voice message), for instance this one:

MAYDAY
THIS IS vessel A
I am sinking in psn …… at …..UTC
20 persons on board, 2 badly injured
Required immediate assistance
Rough sea, wind NW 10B
OVER

Routine communications

Some navigational situations requiring routine communication have also been considered. They comprised navigation in areas where reporting systems and pilot navigation are in use.

VTS (reporting systems)

The reporting procedure is one of standard routine procedures performed by ships entering areas supervised by VTS centres. An example communication exchange between of ship A and a land-based centre can run like this:

A to VTS: VTS, this is ship A, I have crossed eastern boundary of the reporting system, my position is ….., course and speed ….. Over.
VTS to A: ship A, this is VTS, what was your last port of call, what is your destination? Over.
A to VTS: VTS, this is ship A, I am proceeding from …… to ……. Over.
VTS to A: ship A, this is VTS, are you carrying dangerous goods? Over.
A to VTS: VTS, this is ship A: Yes, dangerous goods class 1.4, 2, 3, 5, 8 and 9. Total weight 865 123 kg. Over.
VTS to A: ship A, this is VTS, thank you for the report, keep continuous watch on Channel .... during the passage. Out.

The amount of data and VTS enquiries may vary depending on a specific VTS centre, so that questions may refer to the port of departure, class and quantities of dangerous goods, number of crew members, number of passengers etc.

Communications of this type may be conducted in a semi-automatic mode, based on existing forms the navigator has to fill out, in a fully automatic mode.

The problem of communication need identification requires that a relevant VTS centre be identified, as it has its specific requirements for report form, scope and time of establishing communication.

VTS (pilotage)

Another procedure in routine communication is pilot boarding procedure. Here is an example communication between ship A and a VTS centre VTS:

A to VTS: VTS, this is ship A, I will be at pilot station in two hours, over.
VTS to A: ship A, this is VTS, what was your last port of call? What is your draft forward and aft? Over.
A to VTS: VTS, this is ship A, I am proceeding from Casablanca. My draft forward is 6 m, my draft aft is 6.2 m. Over.
VTS to A: ship A, this is VTS, are you carrying dangerous goods? Over.
A to VTS: VTS, this is ship A: Yes, class 1.4, 2, 3, 5, 8 and 9. Total weight is 865 123 kg. Over....

Further course of communication and scope of data required by a VTS operator depends on principles and regulations observed within a given area and its port/s (name of the agency, captain's name, last ten ports of call and days of departures etc.). The communication usually ends like this:

VTS to A: ship A, this is VTS, thank you for your report, pilot will be waiting for you on pilot station at …….., rig a pilot ladder on ..... side, …….. metres above water, keep continuous watch on Channel …

A model of automatic identification of navigational situations requiring communication to be established by a sea-going vessel

Algorithmization of the navigational situation identification

In the previous chapter we presented examples of identification of navigational situations for various events. As a step towards the automation of identification, it can be presented in a form of a checklist, whose fragment is given below:

1. Was there an external calling?
2. If NO: Go to DISTRESS COMMUNICATION.
3. Send a control to the reception module and message analysis

DISTRESS COMMUNICATION:

4. Is distress / urgency / safety communication required? (navigator's decision)
5. If NO: Go to RISK OF COLLISION
6. Select a proper message format (navigator's decision)
7. Fill out the form with information from shipboard systems
8. Fill out the form with information from external systems (done by the navigator)
9. Go to COMMUNICATION

RISK OF COLLISION:

10. Is there a risk of collision (based on CPA, TCPA and limit CPA and TCPA set by the navigator)?
11. If NO: Go to VTS
12. Am I a give-way vessel (due to reduced visibility or according to regulations)?
13. If NO: Go to COMMUNICATION
14. Inform the navigator on the obligation to give way

VTS:

15. Is the ship approaching the boundary of the reporting system or has it crossed the limit?
16. If NO: Go to END
17. Has a report been sent?
18. If YES: Go to PILOTAGE

19. Read out the list of information to be reported to VTS from the data base
20. Retrieve required information from shipboard systems, if not available, from the navigator
21. Go to COMMUNICATION

PILOTAGE:

22. Is pilot necessary in further manoeuvres?
23. If NO: Go to END
24. Is the time to reach the pilot station within limits set by the navigator?
25. If NO: Go to END
26. Read out from the data base a list of information items required by the VTS and pilot station
27. Retrieve required information from shipboard systems, if not available, from the navigator

COMMUNICATION:

28. Prepare information on the navigational situation and method of communication, then send a control to the communication system which will prepare and send a proper message

END:

29. No need to establish communication
30. Stop

The above algorithm should be regarded as a general form, a basis for creating an algorithm of the identification of a navigational situation involving own ship that will require communication to be established.

A generalized algorithm for the identification of communication need

If individual situations for which a decision to establish communication has to be made are independent, then appropriate rules can be developed for these situations. The process of automatic identification of a navigational situation requiring communication will be a sequence of launches of these rules for predetermined premises and checks of the conclusions resulting from them.

We resolved on considering situations separately for each of the objects (ships, land-based centres), as presented in figure 1. If there is a rule for which the premises are fulfilled, the set of parameters describing a given situation is memorized (memorizing the context), and the control variable NK that informs of the need to establish communication is defined. For a given object there exists a possibility for a given object to fulfil premises launching more than one rule. Then, as a result of algorithm operation, we obtain sets of parameters describing a situation (contexts) requiring to start communication.

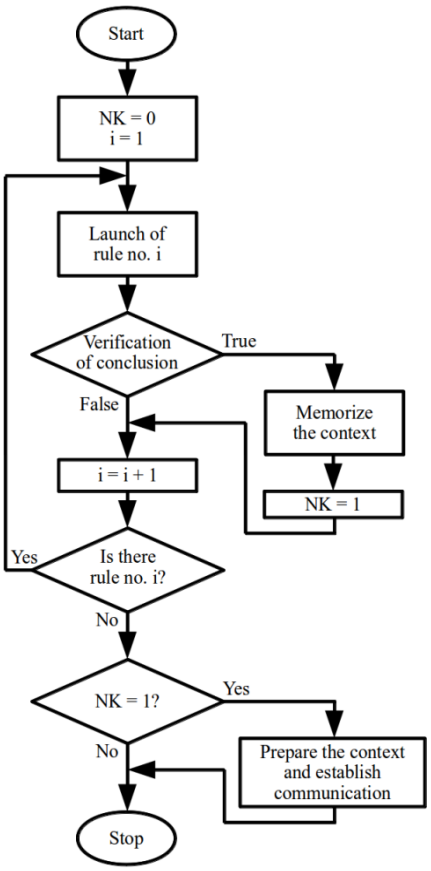

Fig. 1. An algorithm of the process of identifying navigational situations requiring communication to be established

Table 1. Examples of rules for the identification of navigational situations requiring communication to be established by a ship

No.	Premise	Conclusion	Remarks
1	External calling	Send a control to the received message analysis system	
2	Required distress OR urgency OR safety communication	Establish communication	Navigator's decision
3	Risk of collision exists AND I am NOT a give-way vessel	Establish communication	On the basis of CPA, TCPA and MPDM
4	Vessel is approaching the boundary of a reporting system or has crossed it	Establish communication	Boundary is set on the basis of a voyage plan or from information received from ECDIS system
5	Pilot is required for further manoeuvres	Establish communication	Based on voyage plan and navigator's decision

The algorithm shown in figure 1 is applicable to all objects that are essential for an analysis and assessment of own ship situation. That is why each rule can be launched many times. This refers to a situation when, for instance, there are two or more ships involved in a situation.

Individual rules are recorded in a knowledge base. Their form and order of launching may be adjusted so that the inference mechanism will be the same for various applications – the versions for ships and land-based centres differ only in the content of their respective knowledge bases. Presented in table 1 is a set of example rules intended for a ship.

Inference methods in a model of navigational situations identification

In the model of navigational situation identification, its inference module takes into account data (information) collected from available shipboard systems and information from the navigator, obtained after filling out of forms generated by the navigational situation identification system. These data are subject to formalization, using the computing with words. In the obtained form they make up premises in the process of inference. This, taking place at this stage, is restricted to inference with bivalent logic, that results in a message stating whether the existing navigational situation requires communication to take place.

The most frequently used rules of inference in the model are *modus ponens* and *modus tollens*, in which the implications used are derived from the knowledge base containing, among others, Collision Regulations [1] and values of parameters vital for safety (e.g. CPA_L and $TCPA_L$). One of the stages in navigational situation identification is an analysis of collision risk (compare section *Algorithmization of the navigational situation identification*). Based on the present values of CPA and TCPA and limit values CPA_L and $TCPA_L$ declared by the navigator, the system creates implications identifying situations, for which there is a risk of collision. On this basis a decision is generated through a subsequent implication on establishing communication or not. An example of inference scheme for point 10 of the checklist given in section *Algorithmization of the navigational situation identification* is as follows:

CPA, TCPA

If ($CPA < CPA_L$ and $TCPA < TCPA_L$ and $TCPA \geq 0$) Then A

If A Then B

B

where A denotes risk of collision, B denotes a need to establish communication. Similar schemes describe inference at other stages of the presented model of navigational situation identification.

The model of automatic navigational situation identification may be used in an automatic communication system in maritime shipping, exclusively for the identification of a situation that may require communication with another ship or a shore-based station, or for fully automatic execution of communication and negotiation mechanisms.

In the former case (identification), the module, made on the basis of the developed model, acquires and processes information needed for the assessment of a navigational situation, informing the navigator that communication has to be established and why. The latter case refers to automatic implementation of communication and negotiation mechanisms, for instance those in routine communication.

One example of the former case is when following the start-up of subsequent rules and conclusion verification, the outcome may be a message containing a notification on the need to establish communication due to a risk of collision. The notification might have this form:

ESTABLISH COMMUNICATION

RISK OF COLLISION with ship / object ....

CPA is .... (CPA_L=…), TCPA is … ($TCPA_L$=…)

The communication and negotiations are continued by the navigator, either orally or manually through a computer system.

The cause given in the example is *Risk of collision*, but it can be *Boundary of the reporting system*, *Distress or Urgency Communication.* Besides, a generated message may take a form of an instruction to fill out a form, e.g. data required by a VTS.

In the latter case the module executes the stage preceding automatic generation of messages (or their proposed texts), directed to external objects (ships, land-based centres). Then communication is performed in the semi-automatic or automatic mode, using the mechanisms of co-operation and negotiations concerning safe ship conduct. Based on the conclusions sent, the system generates and sends (automatically or when accepted by the navigator) a proper message to the other ship or shore station.

Conclusions

This article deals with a model of identifying navigational situations which require communica-

tion to be established between ships or a ship and a shore station. The model represents a system embedded in a larger system of automatic communication in maritime shipping and may have two functions: to identify a situation calling for communication with another ship or shore station, or to automatically implement mechanisms of communication and negotiations.

The automation of communication processes between ships and land-based centres may contribute to the limitation of human errors, such as failure to establish communication, misunderstanding a received message, improper choice of a message or wrong interpretation of exchanged information, thus it may contribute to enhancement of shipping safety.

The previously presented concept of marine automatic communication system and the herein presented model of identifying navigational situations requiring communication to be established by a ship fits into the concept of e-navigation, developed at the IMO forum. The concept includes standardization of navigational information and automation of information exchange processes.

References

1. COLREGs, Convention on the International Regulations for Preventing Collisions at Sea. International Maritime Organization 1972.
2. GMDSS Manual. IMO Publishing, London 2011.
3. PIETRZYKOWSKI Z., SZEWCZUK T., WÓJCIK A., BANAŚ P.: Reasoning Processes in Automatic Marine Communication System (in Polish). Scientific Papers of Warsaw University of Technology, Vol. 95 (Transport), Oficyna wydawnicza PW, Warszawa 2013 (in Polish), 421–431.
4. PIETRZYKOWSKI Z., HOŁOWIŃSKI G., MAGAJ J., CHOMSKI J.: Automation of Message Interchange Process in Maritime Transport. TransNav, the International Journal on Marine Navigation and Safety of Sea Transportation, Vol. 5, No. 2, 2011, 175–181.
5. ZHAO J., PRICE W.G., WILSON P.A. TAN M.: A statistical study of mariners behaviour in collision avoidance at sea. Marine Simulation and Ship Manoeuvrability, Balkema, Rotterdam 1996, 169–174.
6. PIETRZYKOWSKI Z., JUSZKIEWICZ W.: Analysis of navigators' decision processes in anti-collision manoeuvres in an open sea area. Scientific Papers Warsaw University of Technology, Faculty of Transport, No. 2/61, Technika komputerowa w systemach transportowych, Oficyna wydawnicza PW, Warszawa 2007, 109–120 (in Polish).
7. KACPRZYK J.: Fuzzy sets in system analysis (in Polish). Warszawa 1986, 213–215.

Scientific Journals
Maritime University of Szczecin

Zeszyty Naukowe
Akademia Morska w Szczecinie

2013, 36(108) z. 1 pp. 22–26
ISSN 1733-8670

2013, 36(108) z. 1 s. 22–26

Timestamp Discrepancies in Multisensor NMEA Environment during Survey Voyage

Paweł Banyś, Evelin Engler, Frank Heymann, Thoralf Noack

German Aerospace Center (DLR), Institute of Communication and Navigation Neustrelitz, DE

Key words: marine electronic devices, information, reliability of data, navigational data, survey voyage

Abstract

The standard for interfacing marine electronic devices (NMEA – National Marine Electronics Association), does not provide unambiguous information regarding the reliability of data and its timing. In this paper, time delays in navigational data are investigated. For this purpose AIS and navigational data collected offshore and onshore are used. The investigations are concentrated on lags among various NMEA sentences recorded in a relational database during the survey voyage. The analysis is based on standard elements of descriptive statistics.

Introduction

Digital technology has an impact on every sector of world economy. Maritime traffic systems are no exception. As the computerisation of vessels continues, operating a fleet nowadays is less of a slow and easy crossing the oceans and more of a managing data and racing against time. This has led the International Maritime Organization (IMO) to define the e-Navigation strategy. Its aim is "the harmonized collection, integration, exchange, presentation and analysis of marine information on board and ashore by electronic means to enhance berth to berth navigation and related services for safety and security at sea and protection of the marine environment" [1].

High level application user need recognised by this strategy is the provision of integrity information describing the current usability of sensors, services and data. Nowadays integrated navigation systems on board vessels operate in a multisensor environment. In case of a combined use of data coming from various sources, it is important to determine a temporal validity of data, in order to make it usable in data fusion processes applied to evaluate the integrity of data products, as well as navigational systems in real time.

For many years NMEA has been the standard for interfacing marine electronic devices. It has served its purpose well, because officers of the watch have worked with data on a visual perception basis. In the age of digital data processing the need for unambiguous information with assessed reliability grows. Furthermore, time attributes of data are often missing, and only their simple temporal synchronization is feasible. Therefore, it is important to investigate time delays in navigational data and to analyse their impact on surveying and assessment of the traffic situation. If lags among various NMEA sentences generated by the shipborne equipment are better understood, the most probable time delays can be applied during data fusion, thus helping the system reach proper synchronisation and error awareness.

Concept

Current research activities of DLR's Institute of Communication and Navigation concentrate on the development of algorithms and techniques, which are able to provide integrity information describing the current usability of sensors, services and data used in the maritime traffic system. In order to collect appropriate navigational data, which the integrity processors can be fed with, it is necessary to complete parts of the project under real world conditions at sea. So, a practical measurement concept is necessary to proceed with the investigation of

time delays in navigational data. All data streams available on the bridge conform to the NMEA standard. They form a data exchange network, which enables different sensors on board to share their readings.

By attaching our own voyage recording equipment to various output nodes of the bridge network, it is possible to use a chain of serial port converters and to acquire NMEA data over Ethernet. The live data storage is controlled by a piece of software interfacing with SQLite database management system. The data chunks are stored as database records and timestamped in nanosecond resolution. In order to maintain stable timing throughout the whole survey voyage, the recording system is synchronised over local area network with a GNSS receiver running a network time protocol (NTP) server. The following diagram shows the onboard setup of the voyage data acquisition.

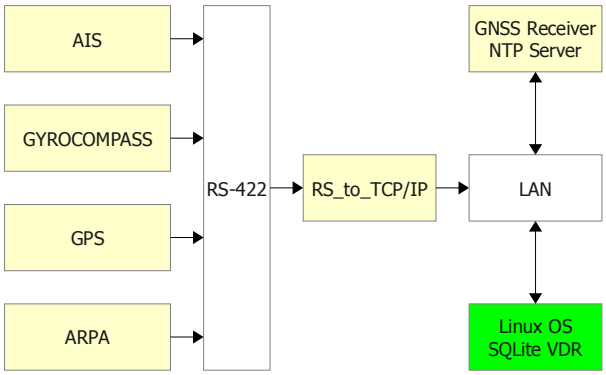

Fig. 1. The onboard setup of the voyage data acquisition

Besides assigned offshore data storage, it is necessary to have an insight into the overall traffic situation, with our survey vessel being one of the participants, as seen from onshore point of view. In order to accomplish this, similar data recording configuration is activated at the DLR onshore reference station in Rostock. It allows collecting and storing the AIS data transmitted by vessels operating in the Warnemünde VTS Area. The timestamp information is retrieved from a GNSS receiver running an NTP server. The following diagram shows

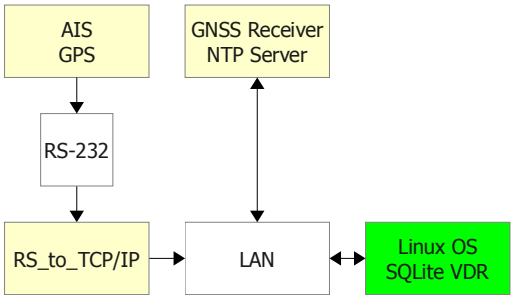

Fig. 2. The onshore station setup of the AIS traffic data acquisition

the station setup of the AIS traffic data acquisition.

With the above configuration it is possible to conduct a measurement campaign at sea and have a synchronised collection of data streams, which will serve as groundwork for analysis of timing discrepancies in multisensor NMEA environment.

Analysis

VDO versus VDM

A VDO sentence is a data package compliant with the NMEA standard and part of the Automatic Identification System. It contains a complete navigational dataset of own vessel, the copy of which is broadcast to other vessels over VHF by AIS transponder in form of a dynamic message packet. The data within VDO sentence is encapsulated according to the ITU R M.1371 specification. The VDO sentence is used internally and is output through a so-called pilot plug interface. It allows connecting an external chart plotter to the bridge network and visualisation of own position, course and speed.

A VDM sentence is identical to the VDO one in terms of data payload structure. The only difference is that VDM datagrams are output by an AIS receiver and contain dynamic navigational data of all vessels equipped with AIS transponders, which are within the radio range of the receiver.

During the survey voyage on board BALTIC TAUCHER II the VDO sentences generated by her AIS transponder were timestamped and recorded in the database. The same navigational content was broadcast over AIS link at the same time. The AIS receiver based at the onshore reference station in Rostock captured that data, timestamped and stored it in the local database in form of VDM sentences.

After joining both databases by using the values of time common to each, it was possible to find duplicates of dynamic data originating from our survey vessel and to query the timestamp differences between them. The following histogram shows the results of this analysis, computed with 5407 records.

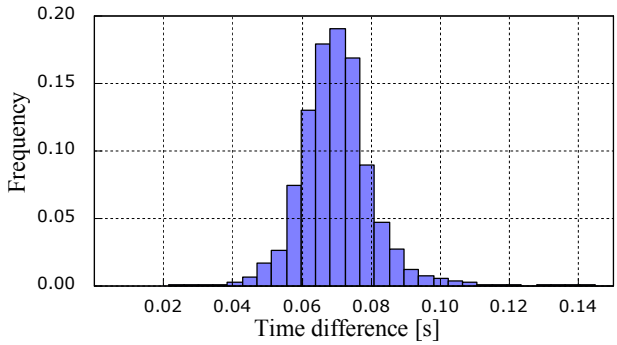

Fig. 3. Timestamp differences between the acquisition of VDO and VDM

As indicated on the chart, about 19% of all AIS dynamic messages from BALTIC TAUCHER II reaching the reference station in Rostock are delayed by 0.07 s, compared to the datagram creation timestamp on board. About 92% of observed time delays can be found in range between 0.05 s and 0.09 s. The rest of the cases are negligible due to their low occurrence. The delays around 0.07 s could be caused by the processing time needed to convert radio transmitted data into a usable NMEA compliant plain text format, as there is some computing power involved in the process. However, a precise assessment of the internal computation timing is beyond the scope of this research.

Acquisition of offshore VDM versus onshore VDM

During the survey voyage, the AIS data received from other vessels by onboard AIS transponder was timestamped and recorded. It led to creating a collection of VDM sentences describing the traffic situation in proximity of BALTIC TAUCHER II. At the same time the onshore reference station in Rostock acquired and timestamped the AIS data from the vessels navigating in the area of Warnemünde and approaches. As long as the radio ranges of both the survey vessel and the station overlapped, identical AIS dynamic messages could be obtained at both locations. Both databases were joined afterwards. The timestamps of duplicate VDM sentences were queried and their time differences were calculated. The following histogram shows the results of this analysis, computed with 103 337 records.

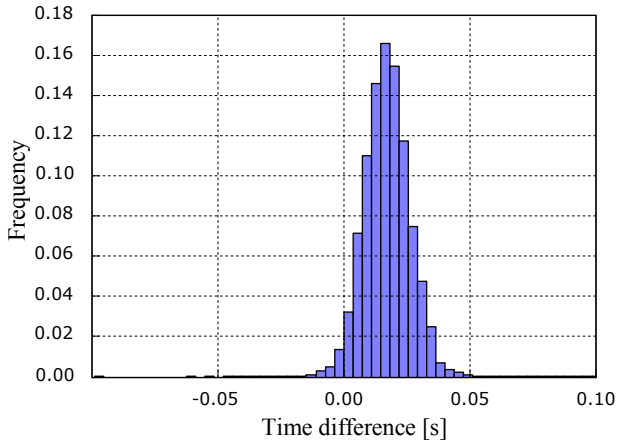

Fig. 4. Timestamp differences between the acquisitions of offshore VDM and onshore VDM

About 17% of VDM sentences received at the onshore reference station have a time delay of 0.016 s, compared to the shipborne acquisition of the same VDM data. In the majority of cases the time difference between the moments an AIS dynamic message reached the station in Rostock and the survey vessel is positive, because during a deep sea voyage BALTIC TAUCHER II had more vessels in her AIS vicinity than the number of vessels moored in Rostock, and could receive their data first due to shorter distances. Moreover, as it is possible to relay the AIS dynamic messages via base stations in order to artificially increase their range, the time they needed to reach Rostock might have slightly prolonged. As the histogram shows, only about 1.7% of VDM transmissions reached the onshore station earlier than the AIS sensor on board the survey vessel. This could also be explained by a smaller number of vessels made fast in Rostock, compared to the number of those at sea, and their proximity to the reference station.

RMC timestamp versus database timestamp

The data recording software running at the onshore reference station in Rostock was capable of storing not only AIS data in form of VDM sentences, but additional NMEA data, too. The AIS receiver, used there as a data source, had an internal GPS positioning module, which could output NMEA compatible RMC sentences. The RMC format contains position, course, speed, and additionally UTC date and time, all available in plain text. It is possible to compare the RMC timestamps originating from the GPS receiver with the NTP synchronised database timestamps indicating the moment RMC sentence was inserted as a new database record. The following histogram shows the results of this analysis, computed with 46 858 records.

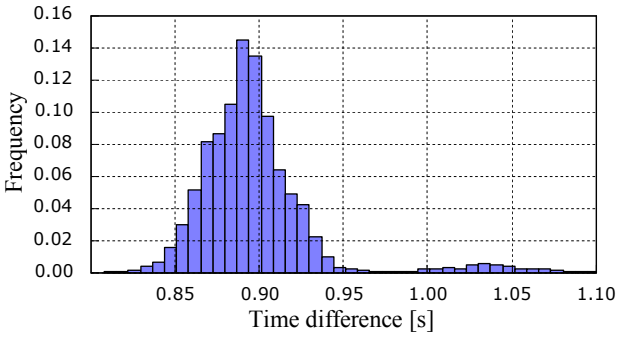

Fig. 5. Timestamp differences between the UTC of the RMC sentence and its database entry time

In about 14% of all cases, the RMC sentences were timestamped by the database time reference with a delay of about 0.89 s, compared to the time epoch indicated by the RMC time and date information. Another peak visible on the histogram marks all time delays of about 1.03 s. They occur within 1% of all analysed time differences. The

nature of the second delay cannot be explained straightforwardly. Since the AIS receiver processes and outputs a mixed set of NMEA and AIS data parallelly, it cannot be ruled out, that some elements of its internal software may contribute to interruptions of service, which could cause slightly longer time delays.

TTM timestamp versus database timestamp

One of the crucial tasks undertaken during the survey voyage on board BALTIC TAUCHER II was storage of TTM datagrams generated by her radar equipped with ARPA. The TTM stands for "tracked target message" and is used to output information about distance and bearing to an acquired radar echo. Every TTM sentence contains a UTC time, which indicates the moment, at which all data enclosed within a TTM datagram was calculated by the ARPA module. The TTM data is fed into ECDIS, which can overlay tracked radar targets on a nautical chart. Amid the measurement campaign the TTM data was timestamped and stored in the database aboard. Therefore, it was possible to compare the ARPA timestamps with the timestamps generated at the moment an end user received the data. The following histogram shows the results of this comparison, computed with 63 210 records.

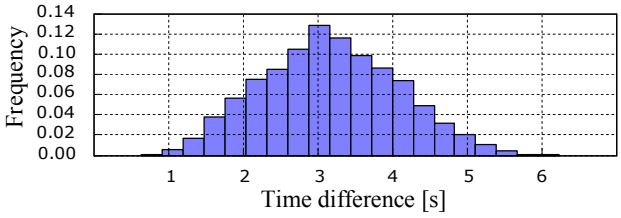

Fig. 6. Timestamp differences between the TTM sentence and its database time

In most cases the expected time delay of TTM data oscillates at around 3 s. However, this is represented by only 13% of all observed time differences, because they are triangularly spread over a time span of five seconds. Various reasons could have caused such distribution of time delays. In the course of the survey voyage two explanations are distinct enough to provide some interpretation of this histogram.

First, the onboard ARPA does not have its own source of time information, be it an internal GNSS receiver or any other suitable clock hardware. That is why it has to rely on an external timestamp feed, which is provided in form of an NMEA data stream wired to a GPS receiver. The time data transfer and its processing may introduce additional delays into the process of providing TTM data to other sensors. A good example of this type of GNSS timestamp deferral is the analysis of RMC message delays mentioned previously.

Second, as it is impossible to output the TTM data of all radar targets at once, the data has to be output stepwise in small groups of TTM sentences. Every TTM datagram contains the parameters of one single ARPA target. The number of tracked radar objects and the speed of serial data connection may contribute to a noticeable time delay, before all computed TTM sentences are transferred to an end user.

AIS base station timestamp versus database timestamp

The AIS equipment on board the survey vessel and at the onshore reference station in Rostock was capable of receiving the AIS base station reports. Those messages contain geographic position of the broadcaster, UTC date and time, as well as its current radio slot number. According to the ITU specification, "mobile stations, which are unable to attain direct or indirect UTC synchronisation, but are able to receive transmissions from base stations, should synchronise to the base station" [2]. The AIS base station reports, marked "ID 4" in the specification, were timestamped and inserted into the database both at sea during the survey voyage and ashore at the reference station in Rostock. It was possible to compare the timestamps encapsulated in the base station VDM message with the internal database time of the recording software. The following histogram shows the results of the time delay analysis of AIS base station data retrieved on board BALTIC TAUCHER II at sea, computed with 4103 records.

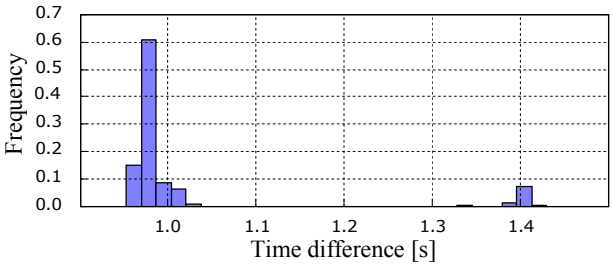

Fig. 7. Timestamp differences between AIS base station time and database time on board the survey vessel

The most frequent time delay occurs at 0.97 s and is common to about 61% of all analysed timestamp pairs. As the distribution shows, the prevailing part of time delays is shorter than 1 s. Another noticeable delay is located at 1.4 s, where about 9% of time delays are placed.

The histogram of time delays, which depicts the timing of AIS base station data recorded at the onshore reference station in Rostock and computed

with 7642 records, is similar to its offshore version above.

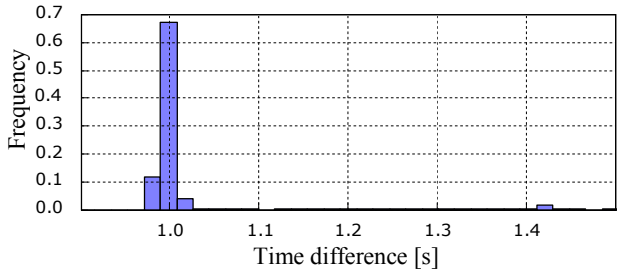

Fig. 8. Timestamp differences between AIS base station time and database time at the onshore reference station in Rostock

As the distribution plot indicates, about 67% of all recorded AIS base station reports are stored in the database with a delay of 1 s. In other words, a timestamp received from the AIS base station is one second old in reference to the NTP synchronised database time. Only 1% of all registered base station messages are delayed more than 1.4 s, which is less than the frequency of it observed at sea.

It is noticeable, that the distribution of delays computed both at sea and onshore has a significant degree of similarity. As the prevailing delay of 1 s seems to be reasonable, the second peak around 1.4 s occurred in both cases, although the AIS devices used on board BALTIC TAUCHER II and at the reference station in Rostock were not identical. This might suggest that the additional delay of 1.4 s may have been caused by the recording software or hardware, which was the same at both locations.

Conclusions

The time delays among various NMEA sentences were analysed, using a statistical approach. The data was collected on board the offshore supply vessel BALTIC TAUCHER II and at the onshore reference station at the Research Port of Rostock. In order to acquire the AIS data (VDO and VDM sentences), which were needed for the analysis, it was necessary to store the AIS transmissions both aboard and ashore. An experimental setup described in section *Concept* made it possible to store additional data, like navigational information, on the bridge. With the databases it was possible to compare time delays between the dataset pairs: offshore–onshore, offshore–offshore and onshore–onshore.

The data analysis in section *Analysis* has shown, that the lags observed in the NMEA data recordings follow statistical distributions, which contain distinguishable ranges of time delays marked with clearly discernible frequencies of occurrence. The time difference between the acquisition of the VDO message stored on board and the VDM message stored offshore is at the order of about 0.07 s. The analysis showed that the most probable time delay was approximately 0.016 s after it had been sent.

The timestamp of the AIS message received at the base station was delayed by about 1 s, when compared to its reception time. The above results confirm that the time delays of AIS data received offshore and onshore are small and have negligible influence on creating inconsistent assessment of the traffic situation.

In case of navigational data acquired on board BALTIC TAUCHER II, the time delays of TTM sentences generated by ARPA were analysed. The most frequent lag oscillated at about 3 s. Considering the inability of the radar software to output all tracked targets at once, especially in dense traffic areas, this time delay does not have negative effects on safety of navigation and should be expected in the majority of ARPA–to–ECDIS links.

Additionally, a mixed data output was analysed at the onshore reference station using AIS receiver with GPS positioning module, which could generate RMC sentences. The most frequent time delay of RMC timestamps measured at the station was about 0.89 s. The value is not significantly high, but systems using RMC as their source of UTC should be aware of the lag.

The results of this study will support further research activities related to the sensor data fusion. Determining the most probable time delays in NMEA data and identifying their patterns can improve overall synchronisation and error awareness of the fusion processes.

References

1. IMO NAV54/25 Annex 12.
2. ITU R M.1371 4.

Scientific Journals
Maritime University of Szczecin

Zeszyty Naukowe
Akademia Morska w Szczecinie

2013, 36(108) z. 1 pp. 27–31
ISSN 1733-8670

2013, 36(108) z. 1 s. 27–31

Improvement of oil spill fighting by using SAR satellite detection and e-navigation systems

Andrzej Bąk

Maritime University of Szczecin
70-500 Szczecin, ul. Wały Chrobrego 1–2, e-mail: a.bak@am.szczecin.pl

Key words: oil spill, satellite detection, e-navigation system, problem's identification, incidents

Abstract
The article presents the solution for improvement of oil spill fighting with utilization of synthetic aperture radar. The way of identification is presented as well as the treatment of obtained data in order to eliminated "looks like" objects. Such system will widely improve the oil spill fighting at a very early stage of incident.

System strategic objectives

The most important regulations for preventing pollution by oil from ships are contained in Annex I of the International Convention for the Prevention of Pollution from Ships, 1973, as modified by the Protocol of 1978 relating thereto (http://www.imo.org), The International Convention for the Safety of Life at Sea (SOLAS), 1974 also includes special requirements for tankers.

The crude oil is transported around the world by sea at any moment. The amount of oil is about 1.800 million tons per year. In most cases the oil is transported quietly and safely. But instead of measured introduced by IMO e.g. special tanker construction, the accidents with oil spill consequences still happen. Moreover, the guilty of large amount of oil spill incidents remain unfound. In effect oil is deposited on the bottom and along the coast destroying all living organisms. Very often it is too late for effective counteraction. The crucial thing in order to be able to react in time is detection in very early stage of incident [1].

Among few possibilities the satellite detection seems to be the proper one. Satellite observations offer the possibility of a frequent monitoring of wide areas. In SAR images, the brightness of the sea surface is a measure of the sea surface roughness. Smooth sea surface appears dark while the brightness increases as the sea surface becomes rougher. Oil films are very effective in damping wind-generated gravity capillary short waves on the sea surface and hence they appear dark against a brighter background in a SAR image [2]. However, there are other natural phenomena (e.g. biogenic slicks, ship wakes, low wind areas, etc.) which produce dark areas in SAR images. This class of phenomena is known as "look-alike" [3]. The figure 1 shows an example of a detected oil spill during the Event Horizon disaster. With red is marked the border of a detected oil spill.

Taking all above under consideration it seems that there is opportunity to create system responsible for detection of oil spill at very early stage of disaster.

The author proposed solution will be designed for:

- early oil pollution detection;
- evaluation of situation;
- planning antipollution action taking into account the rescue resources and other means located close to the incident area;
- contingency planning;
- analysis of situation;
- visualization in ECS/ECDIS system ashore and aboard;
- development of ECS / display applications for and integration on mobile devices (iPad, iPhone, Android tablets / smartphones etc.) (Fig. 2).

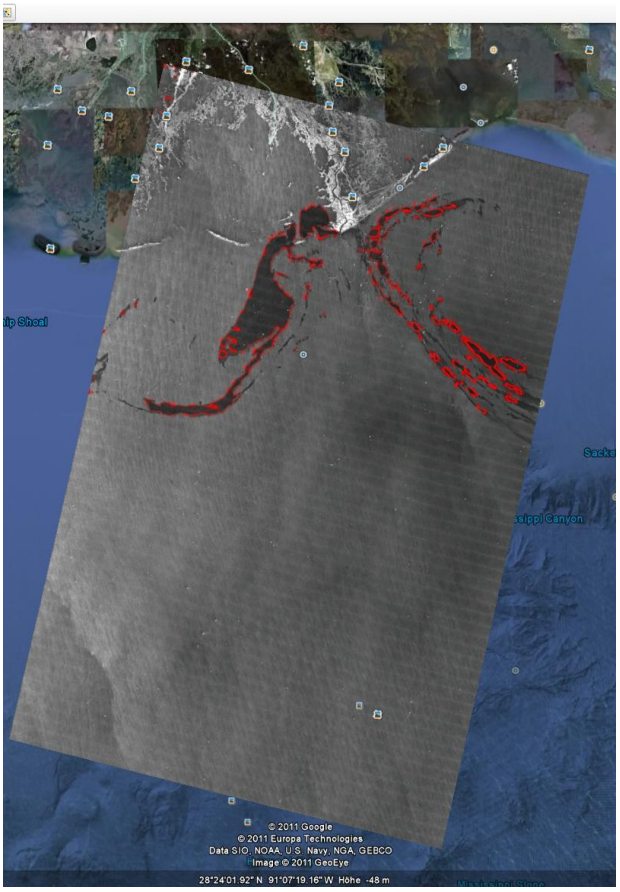

Fig. 1. Oil spill during the Event Horizon disaster within Google Earth

Scientific and technical aims of the proposed solution

Within proposed solution many other works must be performed and the following aims will be achieved:

- provision of algorithms and methodologies for decision support ensuring actions taken in case of oil spill are adequate in every stage;
- optimization of technical solutions under consideration of alternative approaches (gain compared to state of the art), complementary technologies (sensor and data fusion), and their ashore and onboard realization (sharing responsibilities) with the focus on sensor and system integrity;
- provision of sensor and data fusion based algorithms and methodologies ensuring specified integrity requirements during generation and dissemination of information used for comprehensive situation awareness;
- assumptions for visualization of navigational situation for presentation on board vessel, using criteria related to safe anti pollution operation;
- optimization of situational awareness visualization as one of problems in modern support system for aircrafts as well as vessels;
- development of optimal user interfaces for visualization on electronic chart (ECS and ECDIS);

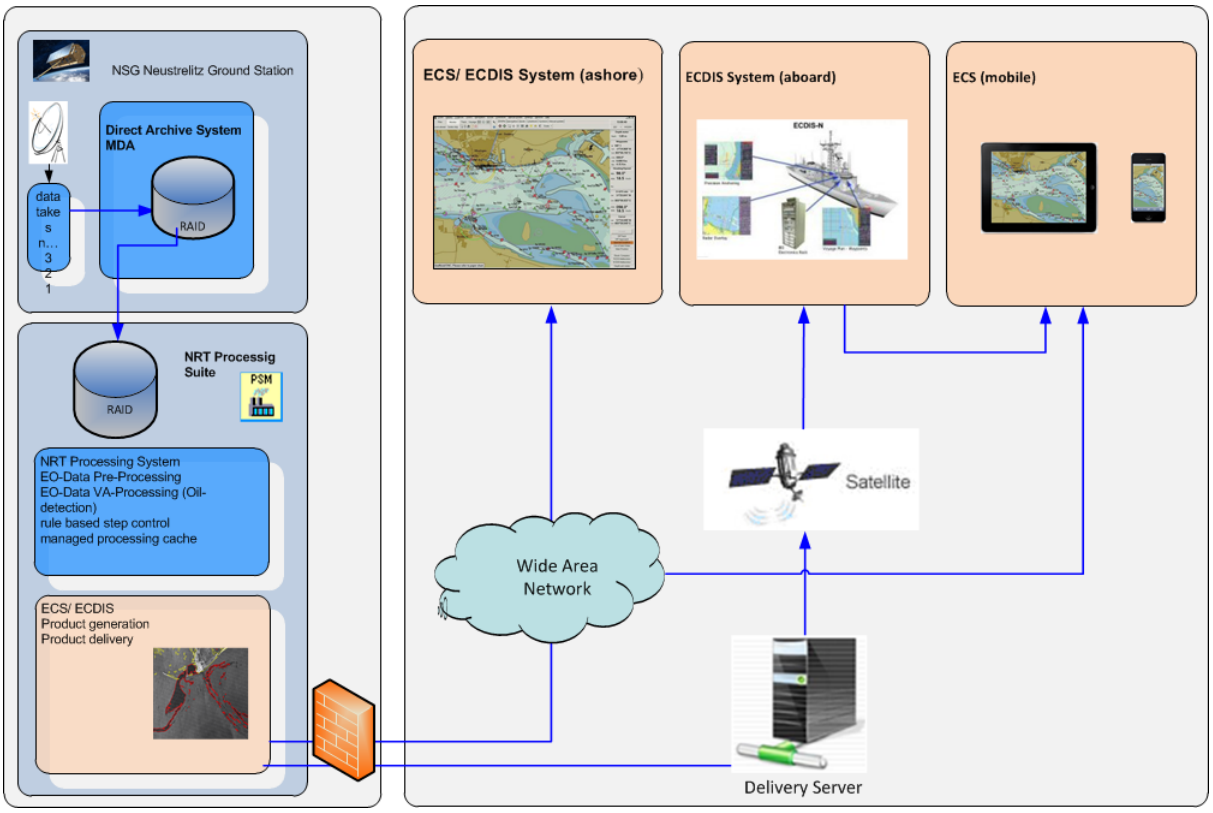

Fig. 2. Anti pollution detection system scheme

– development of optimal user interfaces for visualization on mobile devices;
– receiving current situation data on mobile devices;
– experimental and simulation based validation of technical solutions to develop and improve contingency planning in case of oil spill situations.

E-navigation and its relation with the solution

The most important challenge of IMO nowadays is to develop a framework which accommodates and builds on existing systems already furthering the concept of e-Navigation. Broadly used IALA definition of e-Navigation is as follows: "E-Navigation is the collection, integration and display of maritime information onboard and ashore by electronic means to enhance berth-to-berth navigation and related services, safety and security at sea and protection of the marine environment." At the 1st meeting of the IALA e-Navigation Committee, three fundamental elements were identified that should be in place before e-Navigation could be introduced. These are:

– electronic Navigation Chart (ENC) coverage of all navigational areas;
– robust electronic position-fixing system (with redundancy);
– standard infrastructure of communications to link ship and shore.

The most important projects in focused and related with e-Navigation are World Bank-funded Marine Electronic Highway (MEH) project in the Malacca Straits and the European Union's projects ATOMOS IV (Advanced Technology to Optimize Maritime Operational Safety – Intelligent Vessel) [4]. European Commission started working on e-Navigation in parallel with IALA funding the MarNIS (Maritime Navigation Information Services) project focused on developing e-Navigation.

ECDIS and ENC as the platform of shipborne system

ECDIS and ENC is very well defined standard. The delays in fully coverage by standard electronic charts (70% of coverage in medium and large scale charts today) and expected that coverage of all major international ports and international routes until 2012 will be at least comparable with existing paper chart coverage for those areas.

There are two types of onboard electronic chart systems, the first one is an Electronic Chart Display and Information System (ECDIS), which meets IMO / SOLAS chart carriage requirements. The second one an Electronic Chart System (ECS), which can be used to assist navigation, but does not meet IMO/SOLAS chart carriage requirements. As well as both of them can be used as stationary and mobile systems. For the cooperation with ECDIS there are two kinds of official digital charts commonly available:

– Electronic Navigational Charts (ENC);
– Raster Navigational Charts (RNC).

ENC means the database, standardized as to content, structure and format, issued for use with ECDIS on the authority of government-authorized Hydrographic Offices. The ENC contains all the chart information useful for safe navigation, and may contain supplementary information in addition to that contained in the paper, which may be considered necessary for safe navigation. Among all other available information there are that originated from satellites. At present such information is very rare in commercial systems used on the merchant vessels. In many cases data given by satellite means can give crucial information for safety of navigation, as well as environmental protection. The proposed solution focuses on the obtaining, selecting, adapting, sending and displaying additional information on the user layer in the commonly used ECDIS and ECS systems both, stationary and mobile ones [5].

Communication

The communication is most important issue of e-Navigation. Serious attempts are made to improve marine communication. The important one is MarCom (founded by Norwegian Administration) aimed towards creation of broad band marine communication networks. The interesting technique developed in the project is WiMax based and distributed mesh networks. Within the proposed solution different ways of communication will be utilized depend on the end user. In case of ashore systems, as well as mobile ones (tablest, smartphones etc.) combination of wide area network and Wireless Fidelity network will be used. For shipborne system the satellite communication will be established and utilized.

Integrated service platform

The DLR operated Ground Station at Neustrelitz is responsible for X-band data acquisition, as well as for NRT data processing and direct dissemination to users. Within proposed system the oil spill detection algorithm will be developed for TerraSAR-X/TanDEM-X SAR data. The operator complements the process of spill detection on

TerraSAR-X or TanDEM-X data. The table 1 gives an overview of TerraSAR or TanDEM-X modes used for planned oil spill monitoring in the DLR Service Chain (Table 1).

For monitoring of oil spills in near real time some dependencies have to be taken into account. With respect to the TerraSAR-X data policy only images with spatial resolution coarser than 2.5 m are available. For near real time application only single polarization data are up to now available. It is estimated that for the oil spill detection service less than 1 h including operator tasks is needed for delivering oil spill detection results to the user.

The remote sensing of oil slicks will be addressed in proposal by using single polarisation capability of TerraSAR-X. This sensor's high spatial resolution is of special importance, since the existing European oil spill detection service, EMSA's CleanSeaNet, is presently based on lower resolution images acquired by RADARSAT, CosmoSkyMed and ENVISAT satellites in conjunction with aerial and in situ observations in case of detection. Due to the recent anomaly of the Envisat satellite the revisit time for disaster monitoring will be reduced and could be improved by additional systems like TerraSAR-X and TanDEM-X. Moreover, it is expected that the incorporation of the higher spatial resolution of TerraSAR-X will offer the possibility to more accurately measure the width of discharges (being of the same dimension as the pixel size). Oil pollution at offshore platforms or due to illegal discharge from vessels, either in open sea or in coastal waters may have a severe impact on both, the flora and fauna of the polluted area (although small scale in comparison to tanker disasters). The environmental damages on the natural resources and on the economy of the area in distress are almost always uncountable. Thus, there is a need to rapidly and effectively detect and monitor such source of pollution, as well as predict oil spills drift. For this reason the solution also addresses the investigation of the possibility to measure the width of en route discharges. It should be investigated how oil spills will change

Table 1. TerraSAR-X Acquisition Modes for operational oil spill detection

	Stripmap (SM)	Spotlight (HS & SL) (NRT restriction)	ScanSAR (SC)
Swath width	30 km (single pol.) 15–30 km (dual pol.)	10 km, azimuth extend: 5 / 10 km (HS / SL)	100 km
Full performance incidence angle range	20°–45°	20°–55°	20°–45°
Azimuth resolution	3 m (single pol.) 6 m (dual pol.)	1 m / 2 m (HS, single / dual pol.) 2 m / 4 m (SL, single / dual pol.)	17 m (1 look, 4 beams)
Ground range resolution @ 150 MHz chirp BW	1.7–3.5 m (@ 45°..20°)	1.5–3.5 m (@ 55°..20°)	1.7–3.5 m (@ 45°..20°)

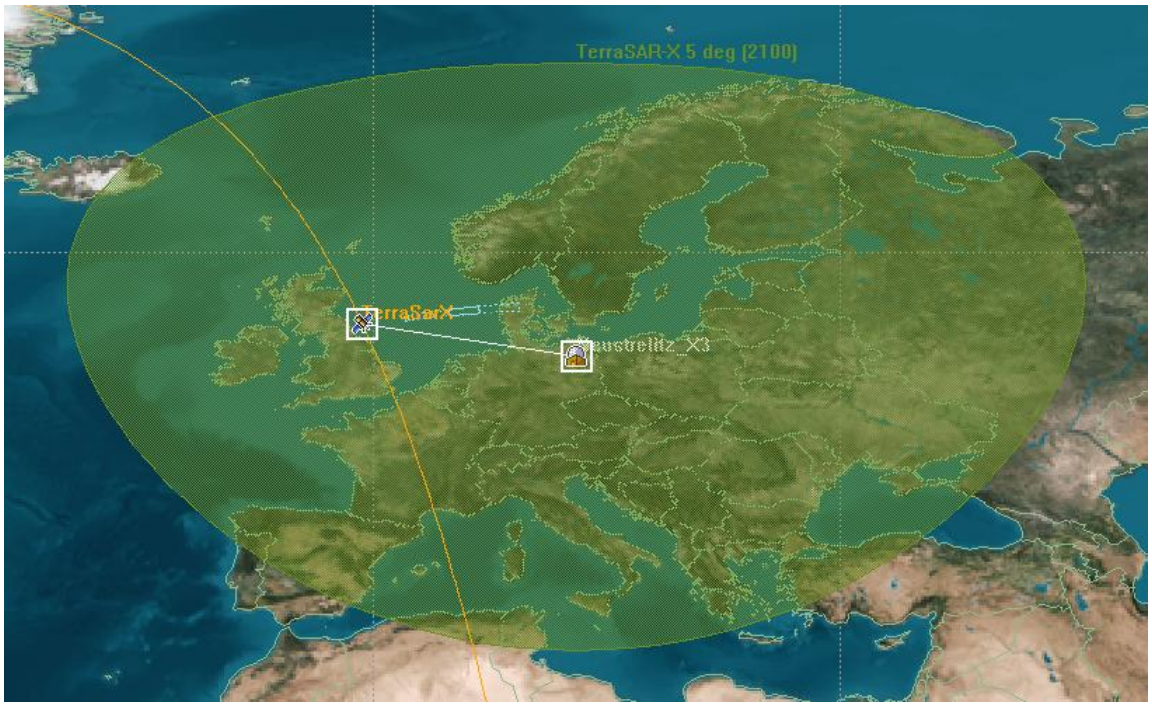

Fig. 3. Neustrelitz Horizon Mask 5 degree for TerraSAR-X

their characteristics (size, thickness, etc.) due to currents and winds.

One of the aims of the system is to analyse TerraSAR-X data in respect to its capability to improve the monitoring of oil pollution in the Baltic Sea. Improvements are envisaged regarding the algorithm performance related to near real time requirements including reduction of necessary operator interactions. Finally, the user-friendly dissemination of customised products by using new technologies will improve the availability and usage of earth observation products for oil spill fighting. It is expected that the scientific and technological achievements of this solution will be transferable to other seas (e.g. North Sea, Mediterranean) [6].

Conclusions

During the last years the possibilities and value of satellite based detection of oil spills could be impressively demonstrated. However, there are still open questions in research (algorithm development and validation), as well as in operational near real time processing and transmission of the satellite based results to the users on board vessels, ashore at e.g. coastal protection offices and further acting persons. The system is intended to close some important gaps presently still hampering the full exploitation of the available assets (SAR satellites, communication links, ECDIS, mobile systems) for oil spill fighting. Since the basic technologies are already developed at high level, the technological project risks are regarded as minor. Nevertheless, an unexpected malfunction of the TerraSAR-X satellite would cause the need to revise the remote sensing part of the proposal. However, needed SAR image data can also be acquired by a second, identically satellite TanDEM-X. It ist assumed, that the EO images needed for development and demonstration can provided by submitting a TerraSAR-X science proposal according to the innovative aim of this project.

References

1. BĄK A., LUDWICZAK K.: The Profile of Polish Oil Spill Fighting System. International Journal on Marine Navigation and Safety of Sea Transportation, Edit.: Adam Weintrit. Published by TransNav, Gdynia Maritime University. Vol. 6, No. 4 – December 2012.
2. VELOTT D., MIGLIACCIO M., NUNZIATA F., LEHNER S.: IEEE Transactions on geoscience and remote sensing. Vol. 49, No. 12, December 2011.
3. WILEY C.A.: Synthetic Aperture Radars: A Paradigm for Technology Evolution. IEEE Transactions on Aerospace and Electronic Systems, Vol. AES-21, No. 3, 1985.
4. GRAFF J.: E-Maritime: An Enabling Framework for Knowledge Transfer and Innovative Information Services Development Across the Waterborne Transport Sector. TransNav, the International Journal on Marine Navigation and Safety of Sea Transportation, Vol. 3, No. 2, 2009, 213–217.
5. WEINTRIT A.: Obsługa i wykorzystanie systemu ecdis. Akademia Morska w Gdyni, Gdynia 2007.
6. PERKOVIC M., SITKOV A.: Oil Spill Modeling and Combat. University of Ljubljana, Faculty of Maritime Studies and Transportation, Slovenia & A. Sitkov, Transas Technologies Ltd., Russia 2008.

Scientific Journals
Maritime University of Szczecin

Zeszyty Naukowe
Akademia Morska w Szczecinie

2013, 36(108) z. 1 pp. 32–37
ISSN 1733-8670

2013, 36(108) z. 1 s. 32–37

Determination of the inland units models parameters for short-term prediction

Mateusz Bilewski, Lucjan Gucma, Agnieszka Puszcz

Maritime University of Szczecin
70-500 Szczecin, ul. Wały Chrobrego 1–2, e-mail: {l.gucma; a.puszcz}@am.szczecin.pl

Key words: short term prediction, inland units, manoeuvring, hydrodynamics, navigation simulator

Abstract
Short-term prediction is a tool that helps to manoeuvre inland units, allows assessing the effect of the planned manoeuvre and reduces the probability of collision. Model of ships hydrodynamics is required to perform this task. In the paper simple to implement solution based on a Nomoto model is proposed. Method of determining the parameters of the model was presented. Researches were carried out with use of INSim Inland Navigation Simulator.

Introduction

For the purposes of ships position and state prediction [1] of any vessel it is usually necessary to create the hydrodynamic model. Such models could be adaptive [2] with constantly adjusting parameters. The most commonly used mathematical models are [3, 4, 5]:

– Norrbin model;
– de Witt-Oppe model;
– Nomoto model.

These models vary in complexity and a numbers of included physical phenomena. For the purpose of short-term prediction Nomoto model is adequate [1] because it allows calculating the individual model parameters. There are several methods of determining the parameters of Nomoto model. Two methods which use data from different types of tests are presented and compared. Researches were carried out on the INSim Inland Navigation Simulator (Fig. 1).

Methods of determining the Nomoto model parameters

Circulation data are used in the first method. Time measurements t_1 required for rudder angle inclination from zero to a predetermined rudder

Fig. 1. View of the INSim wheelhouse [2, 6]

position δ_r were performed. After reaching a constant rate of turn a record of two courses $\psi(t_2)$, $\psi(t_3)$ and time of manoeuvre is made. The model coefficients can be determined from these data as follows follows [7, 8]:

$$K = \frac{\frac{\psi(t_3)-\psi(t_2)}{t_3-t_2}}{\delta_r} \tag{1}$$

$$K = \frac{\psi(t_3)t_2-\psi(t_2)t_3}{\psi(t_3)-\psi(t_2)} - \frac{t_1}{2} \tag{2}$$

The second method uses the Z-Manoeuvre Test (Kempf). In this method we obtain an additional parameter correction angle δ_c [9]. The Z-manoeuvre test (Kempf, 1944) is used to express course changing (yaw checking) and course keeping qualities. Alternating changes of heading are performed. The following data are recorded:

- before heading change: the time t_i, heading ψ_i and rate of turn $\dot{\psi}_i$;
- for the maximum heading alternation form of the initial heading: time $t_{mi,}$ heading ψ_{mi}.

$$\frac{\int_0^{t_{mi}} \delta_r \,\mathrm{d}t}{\psi_{mi}} = \delta_c \frac{-t_{mi}}{\psi_{mi}} + \frac{1}{K} \tag{3}$$

To substitute:

$$y = \frac{\int_0^{t_{mi}} \delta_r \,\mathrm{d}t}{\psi_{mi}} \tag{4}$$

$$a = \delta_c \tag{5}$$

$$x = \frac{-t_{mi}}{\psi_{mi}} \tag{6}$$

$$b = \frac{1}{K} \tag{7}$$

Substituting further test parameters, pairs of values of x and y are obtained. Using the linear regression parameters a and b are determined. Two Nomoto parameters are obtained:

$$\delta_c = a \tag{8}$$

$$K = \frac{1}{b} \tag{9}$$

To obtain the last parameter for the next heading alternation:

$$T = \frac{\psi_{mi} - \psi_i - K\,\delta_c\,(t_{mi}-t_i) - K\int_{t_i}^{t_{mi}} \delta_r \,\mathrm{d}t}{\dot{\psi}_i} \tag{10}$$

The final model formula:

$$T\ddot{\psi} + \dot{\psi} = K(\delta_c + \delta_r) \tag{11}$$

Substitutes zero for δ_c for the previous method.

INSim Inland Navigation Simulator description

The INSim simulator allows for visualization of most navigation and manoeuvrability processes in a variety of inland waterway vessels (standard

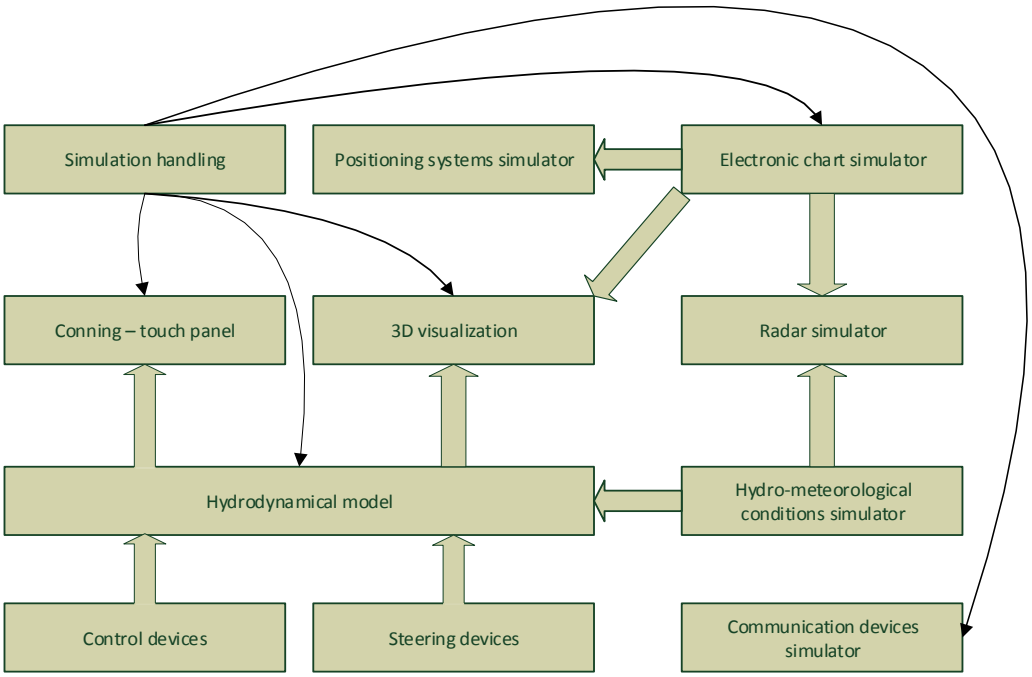

Fig. 2. Simplified block diagram of INSim simulator [11]

units) manoeuvring on various inland navigation waters (river, canal, lock, port and others). A simplified block diagram of a simulator is shown in figure 2. The hydrodynamic model is supplied with data from monitoring and steering devices and with hydro-meteorological conditions model [10]. Electronic charts are used by the simulator positioning systems, radar simulator (which also takes into account the hydro-meteorological conditions) and 3D visualization.

During construction of the conning panel two different visualizations were created:

a) for Astraada touch panel;
b) as a computer virtual panel.

For both connings types an innovative two-way operation mode was created. That allowed for precise operation of the most important controls from a single device. Such functionality is described in [11].

Two interfaces were created for the purpose of communication with both panels:

a) TCP/IP based, Modbus protocol, for communication between touch panel and virtual panel;
b) MDMB protocol for communication between virtual panel and other devices [12].

Virtual conning has the ability to save data (log) such as the telegraph and rudder settings, their current value, geographical coordinates, UTC time, meteorological conditions, rate of turn and the lights and sound signals status.

The mathematical model applied in INSim inland simulator is hydrodynamic model limited to 3DOFs (the horizontal planar motion) taking into account ship movement over the ground (thus the so-called dynamic effect of the water current is introduced) is given by Artyszuk [6] with following parameters ((12a) and (12b)):

$$\begin{cases} \left(m+m_{11}\right)\dfrac{\mathrm{d}v_x^g}{\mathrm{d}t}= \\ =\left(m+c_m m_{22}\right)v_y^g\omega_z+\left(m_{11}-c_m m_{22}\right)v_y^c\omega_z+F_x \\ \left(m+m_{22}\right)\dfrac{\mathrm{d}v_y^g}{\mathrm{d}t}= \\ =-\left(m+m_{11}\right)v_x^g\omega_z+\left(m_{11}-m_{22}\right)v_x^c\omega_z+F_y \end{cases} \quad (12a)$$

$$\begin{cases} \left(J_z+m_{66}\right)\dfrac{\mathrm{d}\omega_z}{\mathrm{d}t}= \\ =-\left(m_{22}-m_{11}\right)\left(v_x^g-v_x^c\right)\left(v_y^g-v_y^c\right)+M_z \end{cases} \quad (12b)$$

$$\frac{\mathrm{d}x_0}{\mathrm{d}t}=v_{NS}^g,\quad \frac{\mathrm{d}y_0}{\mathrm{d}t}=v_{EW}^g,\quad \frac{\mathrm{d}\psi}{\mathrm{d}t}=\omega_z \quad (13)$$

$$\begin{bmatrix} v_{NS}^g \\ v_{EW}^g \end{bmatrix}=\begin{bmatrix} \cos\psi & -\sin\psi \\ \sin\psi & \cos\psi \end{bmatrix}\cdot\begin{bmatrix} v_x^g \\ v_y^g \end{bmatrix} \quad (14)$$

where:

v_x^g, v_y^g, ω_z – ship surge, sway and yaw velocity over the ground;

x_0, y_0, ψ – position Cartesian coordinates and heading;

m – ship mass;

m_{11}, m_{22}, m_{66} – added masses;

c_m – empirical factor;

F_x, F_y, M_z – external excitations (resultant / total surge, sway force and yaw moment), generally consisting of the following items (denoted by additional subscripts) and being generally the functions of ship speed through the water ("v_w"):

$$\begin{cases} F_x=F_x\left(v_x^w,v_y^w,\omega_z\right) \\ F_y=F_y\left(v_x^w,v_y^w,\omega_z\right) \\ M_z=M_z\left(v_x^w,v_y^w,\omega_z\right) \end{cases} \quad (15)$$

$$v_x^w=v_x^g-v_x^c,\quad v_y^w=v_y^g-v_y^c \quad (16)$$

$$\begin{bmatrix} v_x^c \\ v_y^c \end{bmatrix}=\begin{bmatrix} \cos\psi & \sin\psi \\ -\sin\psi & \cos\psi \end{bmatrix}\cdot\begin{bmatrix} \left|\vec{v}^c\right|\cos\gamma_c \\ \left|\vec{v}^c\right|\sin\gamma_c \end{bmatrix} \quad (17)$$

where: $|\vec{v}^c|$ and γ_c represent the velocity and geographical direction of the water current (a uniform current by default).

Researches and results

The chosen parameters of analyzed types of inland vessels are presented in table 1 and figure 3.

Table 1. The parameters of analysed ships

Ships name	Luis Lynn	Chopin	BM600
Length overall [m]	78.81	83	70.7
Max width [m]	8	9.5	9
Engine power	360 HP	2×350 kW	2 × Sulzer-Cegielski, type 4BH22

Table 2. Determined Nomoto parameters and average error between the model and measurement

	Heading			COG		
	K	*T*	Mean Error	*K*	*T*	Mean Error
Luisa Lynn	0.069591	43.581930	2.15	0.069112	62.194846	2.30
BM600	0.090737	8.867580	1.32	0.090794	10.864230	1.27
Chopin	0.025780	2.460860	1.55	0.025796	9.461688	0.47

Fig. 3. Luisa Lynn (on the left) [13] BM 600 (right) [14]

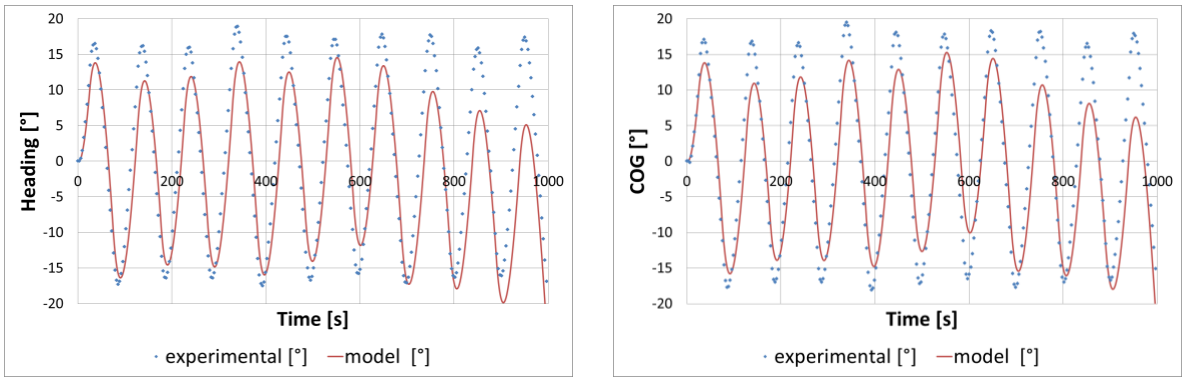

Fig. 4. Heading (T = 25.69685915, K = 0.133517128, δ_c = –0.079667512) and COG (T = 29.4517892, K = 0.141409932, δ_c = –0.070099909) for BM600

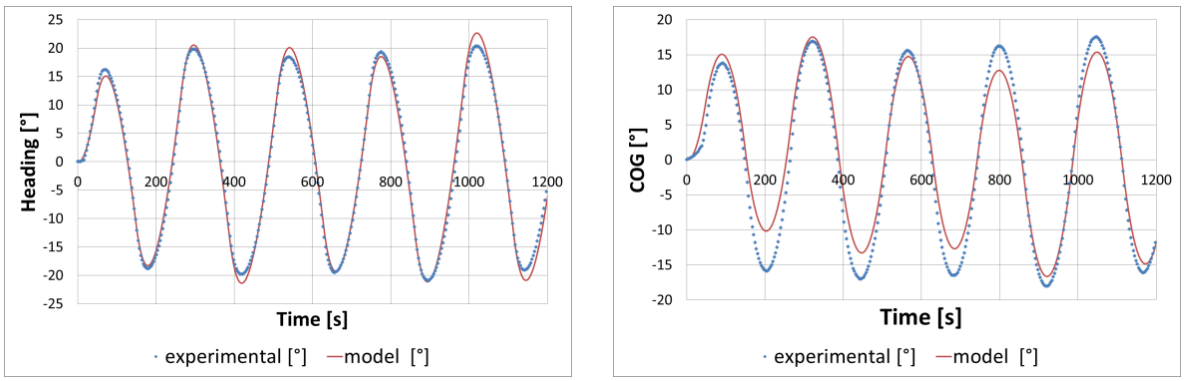

Fig. 5. Heading (T = 50.66497149, K = 0.070000817, δ_c = –0.015940908) and COG (T = 568.3399854, K = 0.448406806, δ_c = –0.01990968) for Luissa Lynn

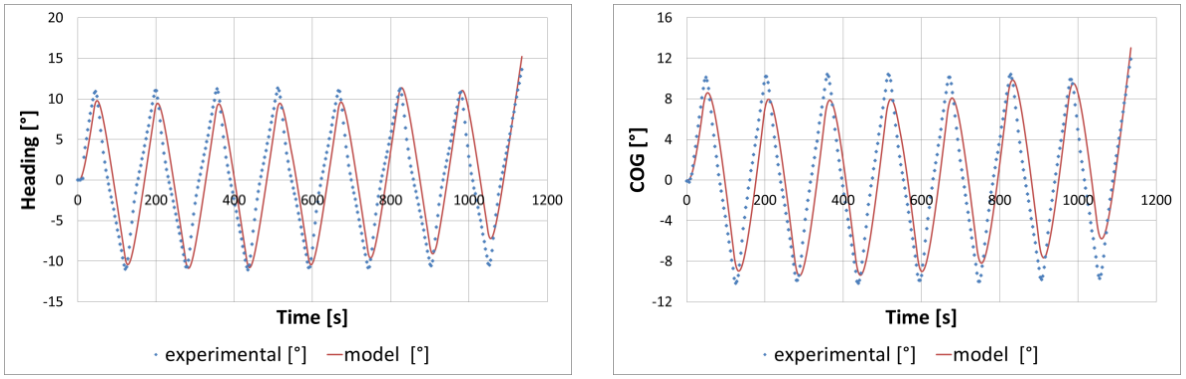

Fig. 6. Heading (T = 9.895612992, K = 0.032766704, δ_c = 0.198203792) and COG (T = 17.62053051, K = 0.0336303, δ_c = 0.194842589) for Chopin

On the basis of the circulation manoeuvre Nomoto model parameters were determined as shown in table 2.

Parameters T, K and δ_c for these three vessels were determined on the basis of the Z-Manoeuvre Test (Kempf). Simulated heading and COG for the same input parameters are presented in figures 4, 5 and 6.

Mean error value (the difference between the angle measured on the simulator and the angle at the same time in model during test) is shown in figure 7.

Conclusions

In this paper the determinations of simplify Nomoto model is presented and validated by INSim inland simulator model which incorporates multi parameters hydrodynamic model.

The achieved results proved that presented methods may be used to determine the simplified models parameters. Depending on the method of parameters determination the results are slightly different (Fig. 8). The method is more accurate with larger ships of less manoeuvrability. The potential of these methods depends on timing accuracy in relation to the speed manoeuvres. It was noted that model parameters which were determined on the basis of one or more tests are sufficient for a long time prediction. It should be remembered, however, that Nomoto model itself has several limitations and can be applied only to the rudder limits of 15–20 degrees.

Due to frequent changes of hydro-meteorological condition on rivers prediction on longer distances is not necessary. Short distances prediction with parameters adjustment for new conditions is sufficient. For the purpose of short-term prediction a simple hydrodynamic model for which parameters can be calculated in a simple and rapid method is needed. The presented method provides to achieve this result with an uncomplicated device

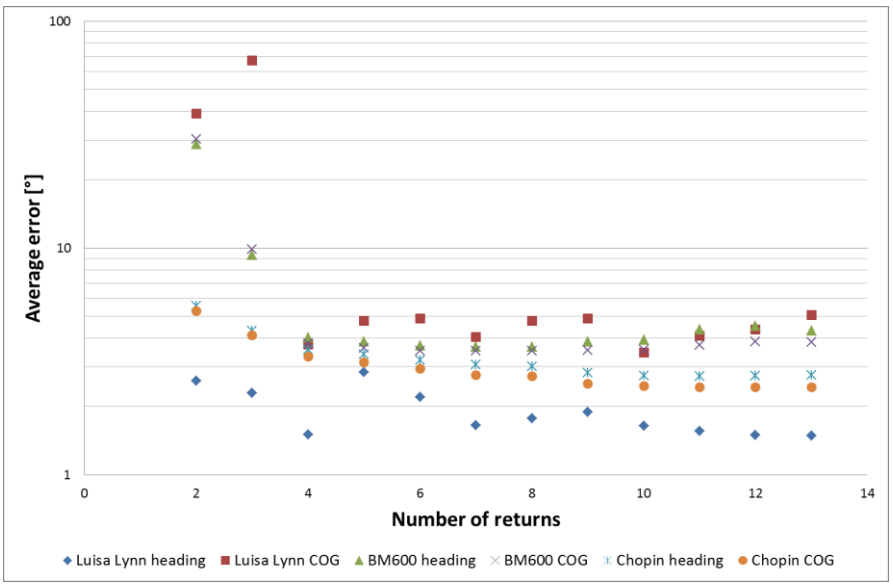

Fig. 7. The mean error value of depending on the amount of selected phrases in the calculation

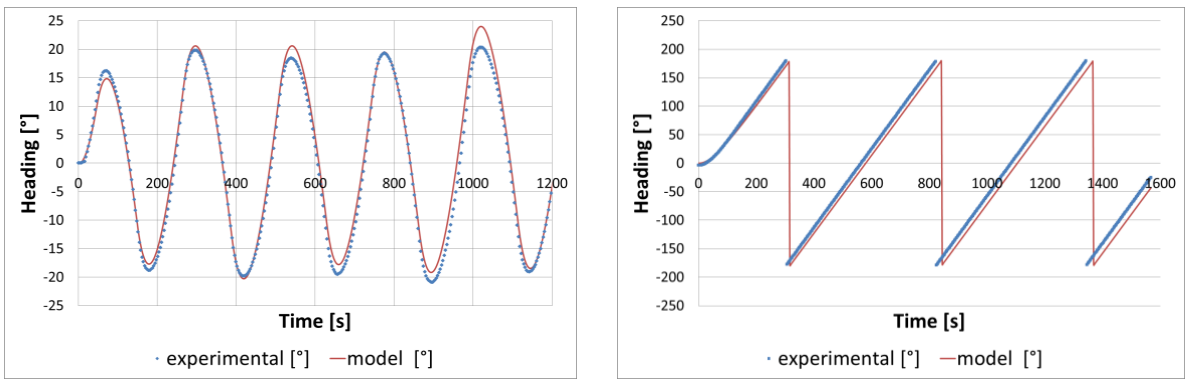

Fig. 8. Heading for Luisa Lynn: Z-Manoeuvre Test (Kempf) for parameters set in circulation (left); for circulation manoeuvre within the parameters of the Z-Manoeuvre Test

such as a microcontroller. Carried out tests were designed to check whether it is possible to have a reliable representation of a simplified model of the ship by Nomoto model. The positive results suggest that it is reasonable to use presented methods for inland vessels.

References

1. GUCMA L.: Predykcja w systemie map elektronicznych jako czynnik bezpieczeństwa manewru. Rozprawa doktorska obroniona przed Radą Wydziału Nawigacyjnego WSM w Szczecinie, WSM, Szczecin 1999.
2. AMERONGEN VAN J.: Adaptive steering of ships. PhD thesis, Delft University of Technology, 1982.
3. FOSSEN T.I.: Guidance and control of ocean vehicles. Willey and Sons Inc., New York 1994.
4. GUCMA L., KLIMKIEWICZ K.: Analysis of possible application of simplified hydrodynamic models in simulation methods of marine traffic engineering. MTE Conference, 2007.
5. NOMOTO K. et. al.: On the steering qualities of ships. International Shipbuilding Progress Information, Vol. 4, No. 35, 1975.
6. ARTYSZUK J.: Towards a Scaled Manoeuvring Mathematical Model for a Ship of Arbitrary Size. Scientific Bulletin, Maritime University of Szczecin, 2005.
7. JOURNÉE J.M., PINKSTER J.: Introduction in ship hydromechanics. Delft University of Technology, 2002.
8. NOMOTO K.: Analysis of Kempf's Standard Manoeuvre Test and Proposed Steering Quality Indices. First Symposium on Ship Manoeuvrability, DTRC Report 1461, 1960.
9. JOURNÉE J.M.: A Simple Method for Determining the Manoeuvring Indices K and T from Zigzag Trial. Data Report 267, Delft University of Technology, 1970.
10. JUSZKIEWICZ W, MUCZYŃSKI B, GUCMA M., BILEWSKI M.: Functionality of navigation systems interfaces in the integrated interactive simulator for inland ship navigation. Inland Shipping, Szczecin 2013.
11. BILEWSKI M., et. al.: Construction and functionality of integrated interactive simulator for inland ship navigation. Inland Shipping, Szczecin 2013.
12. BILEWSKI M., GUCMA M., DUCZKOWSKI M.: Consolidating navigational information for inland manoeuvre simulator purpose. ExploShip, Świnoujście 2012.
13. http://www.marinetraffic.com
14. http://www.zegluga.wroclawska.pl

Other

15. GUCMA L.: Modelowanie czynników ryzyka zderzenia jednostek pływających z konstrukcjami portowymi i pełnomorskimi. Wydawnictwo AM, Szczecin 2005.

Scientific Journals
Maritime University of Szczecin

Zeszyty Naukowe
Akademia Morska w Szczecinie

2013, 36(108) z. 1 pp. 38–41
ISSN 1733-8670

2013, 36(108) z. 1 s. 38–41

Identification of Water Traffic Black Spot

Houzhong Chen, Shanshan Du

School of Navigation, Wuhan University of Technology

Key words: water traffic, control methods, water area, traffic accidents, algorithms

Abstract

Through defining Water Traffic Black Spot and analyzing the advantages and disadvantages of identification methods of Road Traffic Black Spot, then choosing Quality Control Method to recognize water area of intensive traffic accidents and applying integrated influential intensity of accident rate based on Systematical Clustering Algorithm into defining the boundary of the area, an effective evaluation method of black spot identification that is established, which lays a foundation for the subsequent evaluation work.

Introduction

The distribution of water traffic accidents is both timeliness and spatiality. The spatiality of accidents could be divided into dispersing type and intensive type. In the study of road traffic accidents, the area of intensive accidents is always called "Black Spot". Domestic and overseas scholars have studied road traffic black spot from numerous aspects; however studying about water traffic black spot is deficient. Identification and preferential renovation sequence of water traffic black spots have a significant meaning to reduce water traffic accidents and improve the safety management of water traffic.

Definition of Water Traffic Black Spot

Ships will be affected by many factors when voyaging in the costal or inland, such as seamen, ship conditions, and environment etc. These factors work together caused the water traffic accidents which occur in a certain waters intensively, and then the intensive water area is called "Water Traffic Black Spot".

There is no related definition about water traffic black spot. The definition of water black spot in this paper is as follow: in a period of time, water traffic accidents occur in a water area intensively, the water area can be described quantitatively (length, width, diameter or area etc.), and the quantity and attribute of accidents and the risk feature of the water area is significantly different from other water areas.

Identification Methods Reviews

There are numerous studies about the identification of black spot in the field of road traffic. There are some similarities between road traffic and water traffic, so the identification of water traffic black spot can reference the research thoughts, methods and models of road traffic, then combining the reality of water traffic to establish the water traffic black spot identification model. The existing identification model of road traffic black spot can be divided into two parts, one is methods based on data statistics, such as accident frequency method, accident rate method, and matrix method etc.; the other is methods based on mathematical model, such as analytic hierarchy process (AHP), and fuzzy mathematics method etc.

Methods Based on Data Statistics

Accident Frequency Method

A typical definition of accident frequency method is as follow: "If a certain number of accidents happened in a fixed-length road in a period of time, then defining the fixed-road as road traffic black spot". This method is easy to understand and use, however it does not take traffic flow and road condition and the diathesis of drivers into considera-

tion, so it would misjudges a safe road which has a high traffic flow but low accident rate into a danger road [1, 2, 3].

Accident Rate Method

In this method, for road segment, the evaluation standard is the accident frequency of million vehicles kilometer per year. For intersections, the evaluation standard is the accident frequency of million vehicles per year. When the accident rates of a road segment or an intersection outweigh an acceptable critical value, then the road segment or intersection will be recognized as a black spot. Though this method takes traffic flow and the length of the road into consideration, however it is very easy to cause two situations: the road which has low traffic flow and accident frequency has a high accident rate; but the road which has high traffic flow and accident frequency has a low accident rate. If using this method to identify the black spot only, it also could lead to misjudging a safe road into a danger road, or even missing the more dangerous road [2, 3, 4].

Matrix Method

This method uses accident frequency method and accident rate method as a standard to identify black spot, the horizontal axis represents the accident frequency, and the vertical axis represents the accident rate. Each road is represented by a matrix unit, the position of a matrix unit represents the dangerous level of the road, the most dangerous road has highest accident frequency and accident rate which is situated in the bottom right corner in the matrix. The advantage of this method is the size of the matrix can be determined by the user according to the need. The disadvantage of it is that the method cannot distinguish the road which has a low accident frequency but a high accident rate from the road which has a high accident frequency but a low accident rate essentially; it also does not take into account the decisive effect of critical value and the severity of accident [1, 3, 4].

Equivalent Accident Frequency Method

If taking into account the accidents which have different severity in the same way, and accumulating the number of accidents simply, it will lead to misjudging. In order to identify the black spot accurately, the severity of accident should be taken into account, then the equivalent accident frequency method is proposed. This method distributes value to the injuries and deaths through calculating. However, this method does not take traffic flow and the length of road into consideration, so it has same defects with accident frequency method, and the result is affected by the value to injuries and deaths seriously [3, 4].

Method Based on Mathematical model

Analytic Hierarchy Process (AHP)

Analytic hierarchy process is an evaluation method which combines qualitative analysis with quantitative analysis. The character of this method is that it can make a complex process systematic and hierarchical and modeling. Through analyzing the factors and relation of each factor included in the complex problem, then hierarchy structure model could be established, then the influence degree of each factor to the complex problem could be determined. Therefore, using AHP to identify the factors of road black spot is good for distinguishing the preferential renovation sequence of road black spots, and it is also good for determining a reasonable improvement measures which has significant meaning for improving the traffic safety situation and preventing traffic accidents. However, when using AHP, the weight of each evaluation index is determined based on the experts' experience which has a great subjectivity and the weights also impact the evaluation result [3].

Fuzzy Mathematics Method

Because the understanding of road traffic safety is fuzzy, therefore the obtained evaluation indexes are some qualitative indexes. If using traditional method to identify black spot cannot ensure accuracy, however, fuzzy evaluation model can solve the problem. The specific ideas are as follow: according to the principle of fuzzy transform and maximum membership principle, confirming the factors which are related to the object evaluated, and then making a comprehensive evaluation and the most dangerous object is black spot. This method overcomes the defects of AHP that the indexes are quantitative indexes, the indexes are not considered comprehensively, this method also considers the fuzzy attribute of safety evaluation, and it need not change critical value, so this method is convenient in practical application. However, the evaluation result of the method is a fuzzy value, and there are also some other problems such as the subjectivity and randomness of the obtained indexes etc. [3].

Identification method based on experienced bayesian model

According to this method, the amount of expected accidents of a road is calculated based on the amount of historical accidents and the amount of widely expected accidents of the road.

The formula of experienced Bayesian is as follow:

$$E(\lambda / r) = v \cdot \lambda + (1 - v) \cdot r,\ v = 1/(1 + \lambda / k) \quad (1)$$

In the formula, $E(\lambda/r)$ represents the amount of expected accidents in a particular road; λ represents the amount of historical accidents of the road; v represents the reciprocal of over dispersion parameter.

The advantage of this method is that it discusses the fixed and random factors, but the general statistical data cannot support the method [2].

Through the above analysis, each identification method can identify black spot from different perspective, but they would ignore some factors in practical application, which could decline the accuracy of the identification result. Therefore, each identification method has a certain limitation when using.

Integration and innovation of identification method

Through analyzing the existing identification methods of Road Traffic Black Spot, combining the characteristics of water traffic, then choosing Quality Control Method to recognize water area of intensive traffic accidents and applying integrated influential intensity of accident rate based on Systematical Clustering Algorithm into defining the boundary of the area, an effective evaluation method of black spot identification is established.

Quality control method

When using quality control method to recognize water areas of intensive traffic accidents, assuming in any case, the probabilities of traffic accidents obey Poisson distribution of accident frequency, namely in a particular route, the accidents' probability in a certain time can be calculated as formula (2), then comparing the accident rate of the route with the average accident rate of the whole navigating zone. According to the significant level, confirming the bound of comprehensive accident rate of the intensive accident area.

$$P(n|\mu, t) = \frac{e^{-\mu t}}{n!}(\mu t)^n \quad (n \geq 0) \quad (2)$$

In the formula, t represents time, n represents the amount of accident, μ represents accident frequency of the route.

The mean value and variance of n are calculated as formula (3):

$$E(n) = \mu t,\quad \mathrm{var}(n) = \mu t \quad (3)$$

If the confidence level of the distribution is 95%, then the bound of accident rate is calculated as formula (4) and (5).

$$R^+ = \lambda + 1.96\sqrt{\frac{\lambda}{m_i}} + \frac{1}{2}m_i,\quad i = 1,2,3..n \quad (4)$$

$$R^- = \lambda - 1.96\sqrt{\frac{\lambda}{m_i}} - \frac{1}{2}m_i,\quad i = 1,2,3..n \quad (5)$$

In formula (4) and (5), λ represents the accident rate of the whole navigating zone, and $\lambda = \Sigma E(n)/\Sigma m_i$, m_i represents the accumulative standard ships in a certain route [5, 6].

Integrated influential intensity of accident rate based on systematical clustering algorithm

According to the identified intensive water area, using integrated influential intensity of accident rate based on systematical clustering algorithm to define the boundary of black spot.

(1) Numbering the identified intensive water areas and recording them as set $X = \{x_1\ x_2\ ...\ x_i\}$ (i represents the number of intensive water area, $i = 1,2,3..n$), then recording the accidents in x_i as set $G = (G_{i1}\ G_{i2}\ ...\ G_{im})$ and recording G_{ij} in x_i as a sample, calculating the distance of any two accidents and clustering the two samples that are near to each other, and the like until cannot cluster [7].

(2) Through analyzing the influence factors of water traffic safety, the water traffic safety influence factors index system is established.

(3) The grade of accidents and casualties and financial loss are different in different cluster, it is unable to compare the accidental severity in different cluster only using the amount of accidents. Therefore, it is necessary to standardize the amount of accidents to realize the comparability of accidental severity in different cluster. In this paper using synthetic weighted method to standardize the amount of accidents. The formula is as follow:

$$P = \sum_{i=1}^{n} f_i p_i \quad (6)$$

In the formula, p represents standardized amount of accidents; i represents the sequence number of different grade of accident; f_i represents the weight coefficient of different grade of accident; p_i represents the accident frequency of accident level i; n represents the amount of accident level.

Through calculating the ratio of financial loss and related grade of accident to confirm the value of f_i, regard the weight coefficient of small accident as 1, the weight coefficient of other grade of acci-

dent is confirmed by the ratio of unit accident direct financial loss and the unit accident direct financial loss of small accident.

(4) The standard accident rate is calculated by the formula as follow:

$$R = \frac{P}{Q} \tag{7}$$

In the formula, R represents standard accident rate, P represents standardized amount of accidents, Q represents the amount of standard ships.

(5) Confirming the influential intensity of factor K_{ij} to accident rate R_k is ρ_{kij}, dividing the accident rate R_k of the studying cluster by the accident rate R'_k of the similar cluster to the studying cluster which does not include factor K_{ij} to obtain the influential intensity ρ_{kij}, the formula is as follow:

$$\begin{aligned}\rho_{kij} = {} & \text{accident rate } R_k \text{ of factor } K_{ij} / \\ & \text{accident rate } R'_k \text{ of a similar cluster} \\ & \text{which does not include factor } K_{ij}\end{aligned} \tag{8}$$

In the formula, K_{ij} represents sub-factor j of factor i in cluster k, R_k represents standardized accident rate in cluster k, R'_k represents standardized accident rate in the cluster which is similar to cluster k.

(6) The influential intensities of factors in secondary index layer to accident rate are obtained by accumulated multiplying the influential intensities of the related evaluation factors, namely multiplying the influential intensity ρ_{kij} of each sub-factor in factor i of secondary index layer, then the sub influential intensity ρ_{ki} can be obtained, the formula is as follow:

$$\rho_{ki} = \Pi\rho_{kij} \tag{9}$$

(i represents the amount of sub factor in factor i).

(7) Multiplying the sub influential intensity ρ_{ki} of cluster k, the comprehensive influential intensity ρ_k can be obtained, the formula is as follow:

$$\rho_k = \Pi\rho_{ki} = \rho_{ki} \cdot \rho_{ki} \ldots \rho_{ki} \tag{10}$$

(8) The comprehensive influential intensity accident rate of cluster k is calculated as formula (10).

$$C'_k = \rho_k \cdot R_k \tag{11}$$

(9) Confirming the critical value of comprehensive influence intensity accident rate reference the Quality Control Method, the formula is as follow:

$$C_k^+ = A_k + \alpha\sqrt{\frac{A_k}{Q_k} + \frac{1}{2\overline{Q_k} \times 10}} \tag{12}$$

$$C_k^- = A_k - \alpha\sqrt{\frac{A_k}{Q_k} + \frac{1}{2\overline{Q_k} \times 10}} \tag{13}$$

In the formula, C_k represents the critical value of comprehensive influence intensity accident rate in cluster K, C_k^+ is the upper limit value and C_k^- is the lower limit value. A_k represents the comprehensive influence intensity accident rate in a cluster which is similar to cluster K. α represents an statistical constant, if the confidence coefficient is 95%, then the value of α is 1.96. $\overline{Q_k}$ represents the average traffic flow during investigating cluster K.

If the value of a comprehensive influence intensity of a cluster outweighs the upper limit value, then the cluster is confirmed as a black spot [8, 9].

Conclusions

Through analyzing the identification methods of road traffic black spot and combining the characteristics of water traffic, then innovating the existing identification methods and proposing new identification method to identify water traffic black spot which can precisely identify water traffic black spot and the preferential renovation sequence of water traffic black spots, providing a new basis to optimize water traffic environment and guarantee the safety of water traffic and also laying a foundation for the subsequent evaluation work.

References

1. SONG L., YINGJIE X.: Identification of Accident prone Route Segment in Ship Routing schemes. Navigation of China, 2010.
2. SHITING D., MANLI W.: Introduce on Identification Methods of Road Traffic Black Spot. Heilongjiang Science and Technology Information, 2009.
3. ZUFENG S.: Reviews on Identifying Methods of Traffic Accident Black Spot. Road Traffic and Safety, 2008.
4. ZUFENG S., JIANHU C.: Problems in Practice of Identifying Traffic Accident Macula and its Countermeasure. Journal of Hubei University of Police, 2009.
5. YULONG P.: Improvement in the Quality Control method to Distinguish the Black Spot of the Road. Journal of Harbin Institute of Technology, 2006.
6. MANQUAN G.: A comparative study of traffic accident black point identification method.Highway, 2009.
7. JIAN T., JIANG L., JIANFENG X., CHENGWU J.: Safety Evaluation of City Road Intersection Based on System Clustering. Journal of Wuhan University of Technology (Transportation Science & Engineering), 2006.
8. SHEN X., XIUCHENG G., JUNMIN S.: Road traffic accident black spots to identify method research. Technology of Highway and Transport, 2003.
9. SHEN X., XIUCHENG G., JUNMIN S.: Study on Road Traffic Accident Black Spot Identification Method. Journal of Highway and Transportation Research and Development, 2003.

Scientific Journals
Maritime University of Szczecin

Zeszyty Naukowe
Akademia Morska w Szczecinie

2013, 36(108) z. 1 pp. 42–48
ISSN 1733-8670

2013, 36(108) z. 1 s. 42–48

Position fixing and its accuracy evaluation

Włodzimierz Filipowicz

Gdynia Maritime University, Department of Navigation, Faculty of Navigation
81-345 Gdynia, al. Jana Pawła II/3

Key words: position fixing, accuracy, modeling, approach, measurment

Abstract
In traditional approach to position fixing navigator exploits mathematical apparatus based on probability theory. Series of assumptions are required in order to use the platform to draw final conclusions. Limited ability is available regarding fix accuracy a posteriori evaluation. In the paper Mathematical Theory of Evidence is exploited in order to introduce new foundations enabling modeling and solving problems with uncertainty. Modified scheme of approach towards making the fix delivers new standpoint for perceiving accuracy of the result.

Introduction

Imprecise and uncertain data dominate in maritime navigation. Imprecision results from wrong calibrated devices their natural limitation, as well as limitation in perceiving ability of an observer. Uncertainty is related to imprecision but also refers to quality of particular measurement. Observed object can be close and clear or far and vague, these two cases contributions to the fix should be differentiated. Positions indicated by various navigational aids are also of different quality. They are randomly distributed around the true place of the ship. Types of distributions of measurements and indications are assumed known although their parameters vary on real scale depending on many factors.

Hierarchy among available data is to be upgraded and included into computation scheme. Unfortunately in traditional approach possibility of doing so is rather limited.

Mathematical Theory of Evidence was proposed by Dempster [1] and Shafer [2], it extends probabilistic approach. Further extensions enabling processing imprecise data [3] create unique platform for modeling uncertain knowledge and ignorance. Evidence combination scheme as mechanism enabling enrichment combined data informative context is exploited in many applications [4, 5]. In nautical applications it can be useful in order to make position fixing and evaluate its accuracy [6, 7]. Scheme of combination is numerically complex; it is exponentially bounded on the number of observations [8]. Therefore, some effort must be done in order to reduce number of required iterations. Some improvement in the matter has already been achieved [9].

Mathematical Theory of Evidence enables upgrading models and solving crucial problems in many disciplines. The matter is rather hampered in traditional, probabilistic approach due to high level of uncertainty. MTE delivers new unique opportunity once possibilistic extension was adopted [10, 11, 12]. Approaches towards theoretical evaluation of tasks including nondeterministic ones and those with imprecise data are to be reconsidered. Despite obvious advantages significant interest in the new opportunity has not been observed so far. Publications devoted to nautical applications are rather scarce, those appeared are delivered by the author. Some of them considered evaluation of navigational situation within confined and congested areas of crossing routes [12]. In order to forecast and evaluate condition within confined region one has to engage possibilitic platform. Statement like: large vessels encounter at the crossing of heavy traffic routes create hazardous situation involves

fuzziness. Imprecision refers to classification of ships, sort of traffic and quality of condition. In another publication [13] uncertainty in floating objects detection ability by a group of monitoring stations was considered. Hereto synergetic effort is involved; cumulated ability of detection is of interest. Common ability of discovering floating object by all station covering considered region under certain sea surface conditions is sought, extrapolation, engaging approximate reasoning methods, for various conditions is required [14].

Uncertainty in available detections characteristics and measurements distribution is common feature for all presented problems. Shortcomings of traditional mathematical apparatus caused that this sort of tasks were solved mainly based on the skill and more often on intuition of engaged navigation experts.

Many tasks are realized under uncertainty resulted from variable natural condition of measurements or retrieving data from navigational aids. Variety of data quality can be subjectively classified, introducing this sort of hierarchy hardly matters since, there is not formal apparatus to include them into calculation scheme. Thus various quality data affects final solution in the same manner.

Mathematical Theory of Evidence exploits belief and plausibility measure and operates on belief functions. Belief function is a mapping that consists of pairs: vectors representing fuzzy locations of a set of points within sets related to each measurement – degrees of confidence assigned to these vectors. Degrees of confidence reflect probability that a line of position is being located within given strip area or, during processing, position being located inside two belts intersection region. Appropriate imprecise values are at disposal based upon statistical investigations of measurements distributions. In Mathematical Theory of Evidence belief structures combination is carried out [15, 16]. During combination all pairs of location vectors are associated and product of involved masses is assigned to the result set. Obtained assignment is supposed to increase informative context of the initial structures. Combination of structures embracing measurements data is assumed to result in position fixing. The goal can be achieved provided selection of common points is carried out during association. In navigation points situated within intersection of introduced ranges are to be selected. Selection is done thanks to T-form operations [14] used during association [17]. The simplest T-form results in smaller values being taken from consecutive pairs of associating elements.

Position fixing

Figure 1 shows traditional way of position fixing with three distances. Three circles intersect at three points in the vicinity of the fixed ship position. Assuming measured distances as mutually independent random variables, the true position is somewhere inside obtained triangle. It is up to navigator's knowledge and experience to estimate the fix. The more accurate the measured distances, the smaller is the triangle and thus the better is the estimation of the fixed position. Obviously an experienced navigator is able to verify acceptable dimensions of such triangle. Intersection area, greater than an average, results in rejection of the observations.

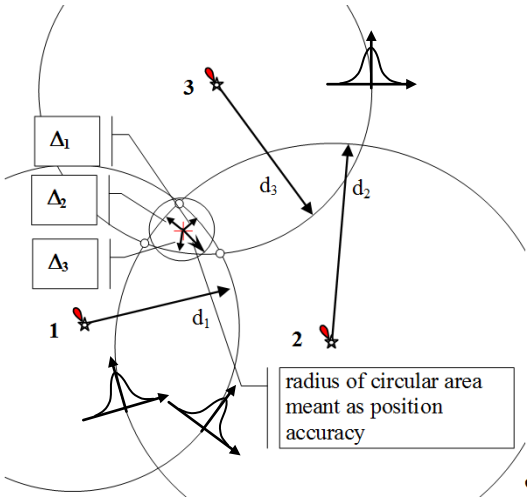

Fig. 1. Example of position fixing based on three imprecise distances

The most common approach to analytical way of position fixing exploits the least square adjustment method. One has to find a point for which expression $\Sigma_k w_k \cdot \Delta^2_k$ reaches its minimum. Sum of weighted squared deflections Δ_k from the measured isolines is calculated. Weights w_k introduce credibility masses attributed to each of the taken distance. Traditional way of position fixing engages:

1) available indications and/or measurements;
2) characteristics of the measured values and type of distribution are not important, although normal distribution is widely assumed and exploited in the least square adjustment method;
3) subjectively evaluated masses of credibility attributed to each of measurements included in analytical approach;
4) measured values as random variable governed by normal distributions, as well as constellation of observed objects are considered in the fix accuracy estimation.

The main disadvantage of traditional approach is the lack of inherited method evaluating quality of the obtained fix. Unfortunately, existing form of accuracy estimation appears to be inadequate in many practical cases.

In the previous papers [5, 18, 19] the author presented concept of engaging MTE extended for fuzzy environment to position fixing computation scheme. Possibilistic extension of the theory appeared to be flexible enough to be used for reasoning on the fix, provided imprecise measurements and/or indications are available. Contrary to the traditional approach it enables embracing knowledge and uncertainty into calculations. Knowledge regarding position fixing includes: characteristics of random distributions of measuring values, as well as ambiguity and imprecision in obtained parameters of such distributions. Moreover, observations can be differentiated by subjectively evaluated masses of confidence attributed to each of them.

The solution proposed and used herein is based on Mathematical Theory of Evidence (MTE), extended to fuzzy environment [12] is more flexible as it enables considering of the following:

1) available indications and/or measurements;
2) various characteristics of the measured values; kind of distribution is important and may affect final solution; empirical and theoretical distribution can be considered;
3) accuracy of measured distances, including ability of engaged aids, their lengths and characteristic of the referenced object;
4) imprecision in accuracy estimation[1];
5) subjectively evaluated masses of credibility attributed to each of measurement;
6) inconsistencies of the computation process;
7) fix adjustment in case of abnormal high inconsistency;
8) evaluation of selected position quality is embedded into computation scheme; plausibility, belief and inconsistency values enable direct assessment of the fix;
9) belief and plausibility measures instead of crisp valued probability are to be used once quality of the fix is evaluated;
10) plausibility of the fix being located within adjacent area is easily available, thus reasoning on the fix accuracy appears to be straightforward.

[1] In books devoted to navigation one can read that mean error attributed to measuring with particular aid is *x*, but reaching *y* ($y > x$) value is also possible.

Notes on the fix accuracy estimation

Traditional meaning of the fix accuracy is related to a regular area around the fixed position. Within the area the true position of the ship is located with certain and equal degree of credibility. It is assumed that the area is of circular or elliptical shape within which the fix is located with the same probability. The latest is widely assumed although it is known that condition (1), that contradicts the statement, is to be observed. The formula expresses probability of the fix being located in point (*x*, *y*) as a function of probabilities of all isolines embracing given point along with credibility attributed to each of the measurements.

$$p_{f|_{(x,y)}} = f\left(p_{o_i|_{(x,y)}}, \Omega_i \right) \tag{1}$$

where:

$p_{f|_{(x,y)}}$ – probability that the fix is located in (*x*, *y*) point;
$p_{o_i|_{(x,y)}}$ – probability that the point (*x*, *y*) is located at the isoline related to *i*-th observation;
Ω_i – credibility attributed to the *i*-th observation, subjectively evaluated quality of the measurement.

In traditional practical approach formulas enabling calculation of the radius or ellipse's parameters are derived for typical schemes of observations followed while a fix is being made [20, 21, 22]. Usually bearings and distances are taken. Two or three bearings combined with distances are often exploited for position fixing. Appropriate formula is to be engaged to evaluate mean error of the fix. Expression (2) (see [20]) is an example to be used when calculating mean error of the fix obtained with three distances. The formula engages mean errors of involved measurements and angles of intersection of lines of position.

$$m_f = \pm\sqrt{\frac{m_1^2 \cdot m_2^2 + m_2^2 \cdot m_3^2 + m_1^2 \cdot m_3^2}{m_1^2 \cdot \sin^2\Theta_2 + m_2^2 \cdot \sin^2(\Theta_1 + \Theta_2) + m_3^2 \cdot \sin^2\Theta_1}} \tag{2}$$

where:

m_i – mean error the the *i*-th observation;
Θ_1 – angle of intersection of the first and second isoline;
Θ_2 – angle of intersection of the second and third isoline.

Mean error of the fix is meant as circular area with the centre in the fix. Point representing fixed position is assumed to be located in geometric centre of a figure spanned over selected intersection

points of obtained isolines. The formula was derived based on normality of the measurement error distributions. It should be stressed that more observations engage even more complex formulas. For this reason expressions for greater number of measurements are impractical and usually not available in nautical publications.

There is yet another drawback related to traditional way of accuracy estimation. The approach does not correlate quality of observations and accuracy of the obtained fix consequently contradicts expression (1). Figure 2 presents two cases of fixed positions and their accuracy estimations. It should be noted that estimations are the same in both cases. Assuming the same scale and constellation of observed objects, as well as lack of constant errors in case a) quality of observations seems be poorer than in case b). Intersections of three isolines in case a) are spread over much larger area compared to right hand case. Thus accuracy of the fix b) seems be different than in case a). Unfortunately, in traditional approach accuracy estimation does not reflect real quality of the fix, although true the statement seems to be somewhat contradictory and illogic. Obviously supporters of the idea can claim that as long as measurements are random variables it may happen. Under this assumption accuracy estimations remain valid in both cases. Nonetheless allocation of isolines within area close to the fixed position seems important factor when accuracy is being a priori analyzed.

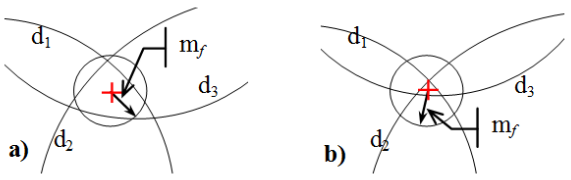

Fig. 2. Two cases of fixed positions and their accuracy estimations

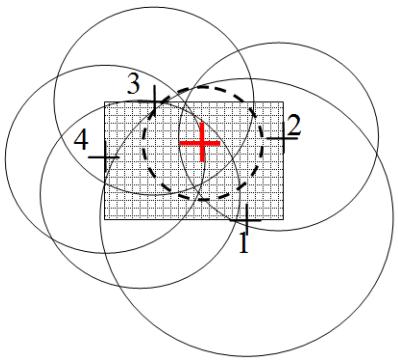

Fig. 3. Fixed position made with four indications delivered by various navigational aids

In monographs devoted to nautical science [21, 22] problem of making a fix based on indications delivered by various navigational aids (example shown in figure 3) is treated superficially, meaningless attention is devoted to accuracy of such fix. Authors suggest using Expression (3) to obtain hints on quality of the fix.

$$\sigma_w = \sqrt{\sigma_1^2 + \sigma_2^2 + ... + \sigma_n^2} \tag{3}$$

Formula (3) estimates mean error provided standard deviations of involved indications are known. Calculated value is a length of the radius defining circle within which the fix is located with probability of 0.68. Particular instance of constellation of indicated positions is not taken into account while estimating accuracy in this way.

Another view at the fix accuracy

In approach based upon MTE distribution of probabilities of the fix being located within explored area is embedded into methodology. Expression (1) is valid and engaged during calculation. Therefore, accuracy can be perceived as a cohesive area within which probability (plausibility) of the fix location is higher the required threshold value.

Using possibilistic concept that has been explained in previous papers [5, 19] software tools have been implemented. The software was used to make the fix with four distances. Presented in figure 4 illustration include probability distribution for the fix being located in adjacent area. Distributions of figures denote plausibility of the fix within hypothesis frame. Estimated mean errors of each observation [cables], as well as subjective evaluations of measurements are shown in the insertion. It was assumed that mean errors are interval valued. Presented error estimations should be treated as modal values of intervals $[\sigma_i - 0.1\cdot\sigma_i,\ \sigma_i + 0.1\cdot\sigma_i]$. Subjective assessments are modal for linguistic terms: “medium” and “very good” fuzzy values.

Iterative procedure was implemented to make the fix [23]. In consecutive iterations decreasing search area was explored. Explored area embraces all maxima points selected in previous iterations. Grid of 10×10 cells was spanned over the area in order to define hipothesis space. Distribution of the fix plausibility measures all over the area examined in the last iteration is shown in the centre part of figure. It should be noted that area within which probabilities reach their maxima is not a circular one. Instead irregular shape of cohesive area with highest plausibility measures represents the fix accuracy.

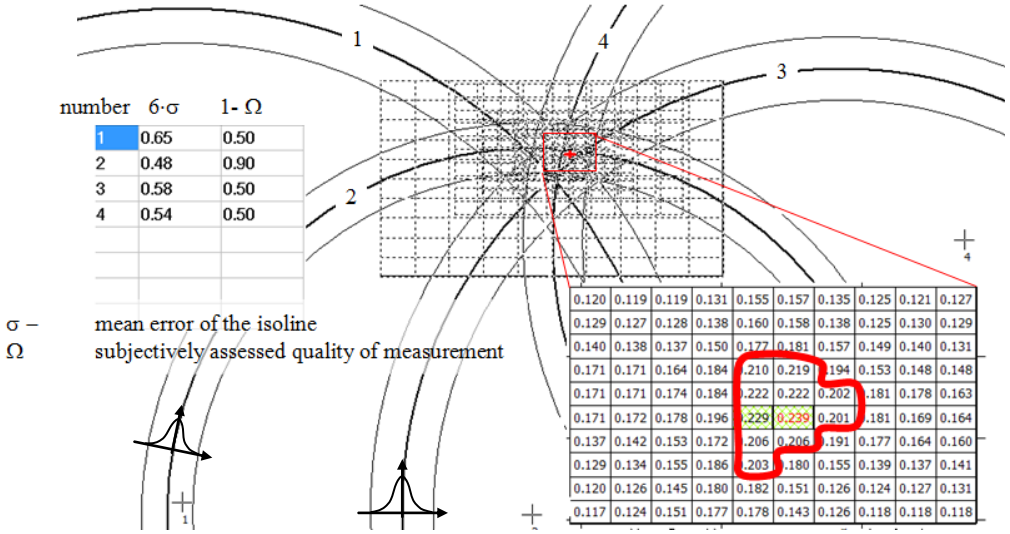

Fig. 4. Making the fix with four distances – output delivered by software implementing possibilistic approach towards position fixing

Representing uncertain evidence in nautical applications

In possibilistic approach uncertain evidence is represented using fuzzy sets. Each set has assigned mass of confidence. Relations between hypothesis and evidence spaces are encoded into evidence representation. Sets (usually fuzzy ones [23]) embrace grades expressing possibilities of belonging of consecutive hypothesis items to the sets related to each piece of evidence. As already mentioned each of the sets has credibility mass assigned. Thus evidence mapping consist of "fuzzy set – probability assigned to the set" pairs. Adequate mapping is expressed by Formula (4).

$$m(e_i) = \{(\mu_{i1}(x_k),\ f(e_i \to \mu_{i1}(x_k))), \cdots \\ \ldots, (\mu_{in}(x_k),\ f(e_i \to \mu_{in}(x_k)))\} \tag{4}$$

Herein in order to draw useful conclusions simplified evidence representation will be considered. Three distances measured to different objects will be taken into account (see Fig. 5). The drawing also shows example set of points treated as hypothesis frame or a search space. Hypothesis points locations will be encoded in binary terms: for situated within considered area value of 1 is used, for those outside the range 0 is applicable. It should be emphasized that such simplification does not affect generality of the rational in sense of usefulness of drawn conclusions.

Reducing scope of interest to measured distances sets related to each piece of evidence can be limited to the following items: $e_1 \to \{d_1\}$, $e_2 \to \{d_2\}$ and $e_3 \to \{d_3\}$. Thus membership function grades take the form of expression: $\mu_i(\{x_k\}) = g(\{x_k\} \to \{d_1, d_2, d_3\})$. The expression means that

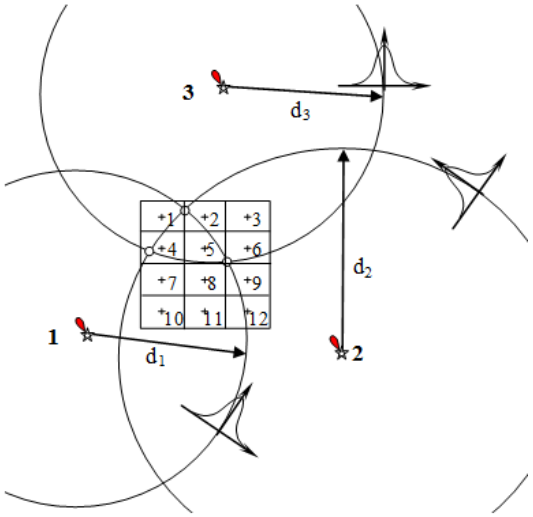

Fig. 5. Example of three distances and a set of hypothesis points

membership grades are degrees of inclusion of hypothesis points within evidence frames (in the example they refer to circles confined by appropriate distance). Grades identify whether respective point is located closer to observed objects than measured distance. Considering single grade $\mu_i\{x_k\}$ one can use formula (5) to obtain its binary value:

$$\mu_i(x_k) = \begin{cases} 1 & \text{if } d(x_k) \le d_i \\ 0 & \text{otherwise} \end{cases} \tag{5}$$

where: $d(x_k)$ is the distance between k-th point and i-th observed landmark.

Figure 4 presents example of distances taken to three different objects and a set of hypothesis points. Using formula (5) grades of sets related to taken distances were obtained and presented in table 1. Row headers named as: μ_1, μ_2, μ_3 show

locations hypothesis points within sets related to measured isolines. Vectors together with assigned, example masses presented in the last column are constituents of the evidence representation as specified by formula (4).

Table 1. Location vectors and results of their combinations

	1	2	3	4	5	6	7	8	9	10	11	12	*m*(..)
μ_1	{1	0	0	1	1	0	1	1	0	1	1	0}	0.6
μ_2	{0	1	1	1	1	1	1	1	1	1	1	1}	0.5
$\mu_1 \wedge \mu_2$	{0	0	0	1	1	0	0	1	0	1	1	0}	0.3
μ_3	{1	1	1	1	1	1	0	0	0	0	0	0}	0.7
$\mu_1 \wedge \mu_2 \wedge \mu_3$	{0	0	0	1	1	0	0	0	0	0	0	0}	0.21

Two evidence representations can be combined. Result grades of membership functions are selected using T-norm operation; for calculation details see previous publications [8, 23]. In the first step of combination data in row $\mu_1 \wedge \mu_2$ were obtained. Next the same procedure was used to associate row $\mu_1 \wedge \mu_2$ and row μ_3. Two steps combination yields data presented in row $\mu_1 \wedge \mu_2 \wedge \mu_3$. It should be noted that result set embraces two points situated within common area for three circles related to taken distances. It was achieved thanks to T-norm operation used during association.

Summary and conclusions

In the paper comparison of traditional way of position fixing and approach based on theory of evidence was presented. Main advantage of the proposed scheme of reasoning is that it engages possibilistic approach [24]. The approach is justified whenever insufficient data samples are available. It is quite often when dealing with estimations of measurements distributions. Possibilistic mechanisms engage belief and plausibility measures. Adequate formulas were derived based on exploration of knowledge base obtained as a result of evidence combination.

In proposed approach knowledge included into computational scheme is something what creates new opportunity. New standpoint for perceiving accuracy of the fix is possible when using reasoning mechanism. Traditional understanding and estimating of accuracy is inadequate in most cases. Appropriate formulas are intended for particular observations schemes that include at most three measurements. Although basic set of data (mean errors and constellation of observed objects) are included in accuracy estimation, applying the same mean error measure for different distributions of isolines seems unjustified. In the new approach accuracy estimation is embedded into reasoning scheme. Obtained results emphasize obvious shortcomings of the traditional approach.

References

1. DEMPSTER A.: A generalization of Bayesian inference. Journal of the Royal Statistical Society: Series B 30, 1968, 205–247.
2. SHAFER G.: A Mathematical Theory of Evidence. Princeton University Press, Princeton 1976.
3. YEN J.: Generalizing the Dempster-Shafer theory to fuzzy sets. IEEE Transactions on Systems, Man and Cybernetics 20/3, 1990, 559–570.
4. FILIPOWICZ W.: Mathematical Theory of Evidence in Maritime Traffic Engineering. Journal of KONES 15/3, 2008, 129–138.
5. FILIPOWICZ W.: Uncertainty Management In Maritime Applications. Communications in Computer and Information Science J. Mikulski (ed.), Springer-Verlag, Berlin – Heidelberg 2011, 17–27.
6. FILIPOWICZ W.: Application of Mathematical Theory of Evidence in Navigation. Marine Navigation and Safety of Sea Transportation, A. Weintrit (ed.), Gdynia 2009, 523–531.
7. FILIPOWICZ W.: Application of Theory of Evidence in Navigation. Knowledge Engineering and Export Systems, Academic Editorial Board EXIT, Warsaw 2009, 599–614.
8. FILIPOWICZ W.: Belief Structures and their Application in Navigation. Methods of Applied Informatics, 3, Szczecin 2009, 53–83.
9. FILIPOWICZ W.: Fuzzy Evidence in Terrestrial Navigation. Marine Navigation and Safety of Sea Transportation, A. Weintrit (ed.), CRC Press/Balkema, Leiden 2011, 65–73.
10. MIZUMOTO M.: Extended Fuzzy Reasoning. Approximate Reasoning in Decision Analysis, North-Holland, New York 1985, 71–85.
11. YAMADA K.: Uncertainty in Heuristic Knowledge and Reasoning. Management and Information Systems Science, Nagaoka University of Technology, 2004.
12. FILIPOWICZ W.: On Navigational Situation Evaluation under Ambiguity and Partial Evidence. Annual of Navigation, vol. 15, Gdynia 2009, 25–33.
13. FILIPOWICZ W., NEUMANN T.: (2008) Detection and Coverage Problems. Scientific Journals of Maritime University of Szczecin, 10–18.
14. RUTKOWSKI L.: (2009) Methods and Techniques of Artificial Intelligence. Scientific Editors PWN, Warszawa
15. LEE E., ZHU Q.: Fuzzy and Evidence Reasoning. Physica-Verlag, Heidelberg 1995.
16. LIU W., HUGHES J., MCTEAR F.: Representing Heuristic Knowledge in D-S Theory. In: UAI'92 Proceedings of the eighth conference on Uncertainty in Artificial Intelligence. Morgan Kaufmann Publishers Inc. San Francisco 1992.
17. YAGER R.: Reasoning with conjunctive knowledge. Fuzzy Sets and Systems 28, 1988, 69–83.
18. FILIPOWICZ W.: New Approach towards Position Fixing. Annual of Navigation, Vol. 16, 2010, 41–54.
19. FILIPOWICZ W.: Evidence Representation and Reasoning In Selected Applications. P. Jędrzejowicz, Ngoc Thanh Nguyen, Kiem Hoang (eds.), Lecture Notes in Artificial Intelligence, Springer-Verlag Berlin – Heidelberg 2011, 251–260.
20. GÓRSKI S. et. al.: Evaluation of Accuracy while Conducting Navigation. WSM, Gdynia 1990.
21. GUCMA S.: Principles of Theory of Lines of Position and Accuracy in Maritime Navigation. WSM, Szczecin 1995.

22. JURDZIŃSKI M.: Principles of Maritime Navigation. Scientific Editor of Gdynia Maritime University, Gdynia 2008.
23. FILIPOWICZ W.: Fuzzy Reasoning Algorithms for Position Fixing. Measurements, Automation and Control 12, 2010, 1491–1495.
24. PIEGAT A.: Fuzzy Modeling and Control. Academic Editorial Board EXIT, Warszawa 2003.

Others

25. DENOEUX T.: Allowing Imprecision in Belief Representation Using Fuzzy-valued Belief Structures. Proceedings of Information Processing and Management of Uncertainty, Paris 1998, 28–55.
26. DENOEUX T.: Reasoning with imprecise belief structures. Technical Report 97/44, Heudiasyc, Universite de Technologie de Compiegne, 1997.
27. DENOEUX T.: Modeling vague beliefs using fuzzy valued belief structures. Fuzzy Sets and Systems 116, 2000, 167–199.
28. FILIPOWICZ W.: On Normalization of Belief Structures. Communications in Computer and Information Science 104, 2010, 434–447.

Scientific Journals
Maritime University of Szczecin

Zeszyty Naukowe
Akademia Morska w Szczecinie

2013, 36(108) z. 1 pp. –
ISSN 1733-8670

2013, 36(108) z. 1 s. –

The influence of ship operational parameters on fuel consumption

Wojciech Górski[1], Teresa Abramowicz-Gerigk[2], Zbigniew Burciu[2]

[1] Ship Design and Research Centre, 80-392 Gdańsk, ul. Szczecińska 65
[2] Gdynia Maritime University, 81-225 Gdynia, ul. Morska 81–87

Key words: fuel consumption, vessel operational parameters, flow properties, hull geometry, legislative changes

Abstract
The paper discusses the influence of the main vessel operational parameters on fuel consumption. These parameters are the speed trough the water, mean draft and trim. The focus is set to the flow phenomena around certain elements of hull geometry as they are sensitive on the selection of discussed parameters. Therefore, the understanding of the flow properties and their impact on ship resistance thus the fuel consumption and emission is crucial taking into account legislative changes imposed by IMO with respect to carbon dioxide emissions from ships.

Introduction

Maritime transport is changing under the influence of external conditions related to the development of maritime technology, relocation of distribution centers and the quantity of cargo flow or the capacity of waterways and coastal infrastructure. An important factor in this transition is the growing awareness of the impact of transport on the environment, as reflected in legislative changes. Of particular importance in this regard is the reinforcement of the IMO provisions to limit carbon dioxide emissions from ships. The carbon dioxide emission quantity may be, assuming constant operational conditions, expressed as:

$$E_{CO2} = ZP \cdot C_F \tag{1}$$

where:

- E_{CO2} – quantity of emmited carbon dioxide expressed in *t*;
- ZP – fuel consumption expressed in *t*;
- C_F – non-dimensional fuel to CO_2 conversion coefficient.

Therefore, the fuel consumption optimisation results in lowering the carbon dioxide emissions.

Optimization of the ship's structure and systems for energy efficiency is important, but not the only factor limiting the negative impact on the environment. The use of appropriate solutions in the operation of the ship provides equal potential for reducing greenhouse gas emissions [1]. Among the elements influencing emissions reduction to the greatest extent is the selection of the favourable operating parameters (i.e. speed, draft and trim of the ship), both at the level of the fleet (fleet management and logistics) and individual ships (the route selection, optimization of load and water ballast) [2]. The solution of these tasks is based on the use of reliable, easy-to-application and universal models for prediction of fuel consumption and hence, emissions. An attempt to build such models must be based on sound understanding of the ship operational parameters' influence on fuel consumption. The present paper discusses the influence of most important parameters with respect to efficient ship operation.

Main ship parameters influencing fuel consumption and emission from ships

There are many factors influencing the energy efficiency of a ship (usually understood as amount of fuel consumed during the certain voyage with specific amount of cargo). Some of them are defined on ship design phase (e.g. hull form, propeller or main engine type) and can be hardly modified in

operation. Some others, although may change during ship operation, cannot be easily influenced by ship crew (e.g. hull and propeller fouling) or are totally beyond the crew control (weather conditions, presence of current or water depth). As far as the energy efficient ship operation is concerned there are few important parameters which, if properly adjusted, may benefit both in decrease of fuel consumption and low emissions. These ship's parameters are:

– speed trough the water;
– mean draft;
– trim.

Influence of ship speed

Vessel speed is the parameter mostly influencing the level of fuel consumption. This relation can be illustrated by Adirality Coefficient commonly used in shipbuilding. The formula originally was used to determine the relation between power, speed and the displacement of the ship. But can be also used to compare values correlated with the power, e.g. hull resistance or fuel consumption. Hence, the formula described in the literature as the fuel coefficient [3] can be written:

$$ZP_C = \frac{\Delta^{2/3} \cdot V^3}{ZP} \tag{2}$$

where:

ZP_C – fuel coefficient,
Δ – ship displacement,
V – ship speed,
ZP – main engine fuel consumption.

As indicated by analysis of the above formula, the speed of the ship, appearing in a third power, is the dominant factor. This conclusion is consistent with the experience derived from an analysis of both the ship model testing and measurement of fuel consumption during the operation of the vessels. Hence the speed reduction is the most common way to reduce fuel consumption. To a considerable simplification, one can assume that the speed decrease by 1% results in a decrease in fuel consumption by 2%. Nevertheless, it is worth noting that, according to recently published studies [4], speed reduction can lead to a number of adverse effects, often neglected when ship speed decrease is decided. Among these undesirable effects are:

– an increase of the rate of hull and propeller fouling;
– a decrease on the propeller efficiency due to operation under different conditions than assumed for the optimization of its design;
– prolongation of the voyage, i.e. the time the main systems of the ship are engaged;
– reduction of the efficiency of waste heat recovery systems and consequently higher fuel consumption by auxiliary engines.

So, the decision to reduce the speed may result in lower than expected fuel savings and also cause an increase in other operating costs of the ship (e.g.: cost of maintenance and repair of systems, the cost of maintaining the good condition of the hull and propeller).

Reduction in cruising speed resulting in main engine operation under low loading also affects the increase in NOx emissions. According to data published by Germanischer Lloyd [4], in the case of a large container ship with a capacity of 13,000 TEU and main engine power ~70 MW, reducing the speed of ~10% (assuming a 10,000 NM cruise), will cause an increase of NOx emissions by ~35 mt. Simplified calculations of fuel consumption and NOx emissions for the above case is shown in table 1.

As indicated by the above data, sailing at reduced speed allows for a significant reduction in fuel consumption. This implies, however, the consequences which, to some extent, reduce the expected benefits. For this reason, the shipbuilding industry, the trend to increase the main dimensions of the vessel. This procedure allows to keep a similar capacity (in terms of quantity of cargo per unit of time) while minimizing the crusing speed.

The examples of this concept are VLCC and ULCC vessels of more than 400 m length for the transport of crude oil. In addition to tankers, the use of which is controversial because of the significant threats to the environment (tanker accidents have

Table 1. Influence of engine load on ship speed, fuel consumption and emissions – 13,000 TEU container vessel on 10,000 NM voyage (own study based on [4])

Main engine load	Main engine power	Ship speed	Voyage duration	Fuel cons.	Fuel cons. reduction	NOx emission		Increase/decrease of NOx emission	
%MCR	kW	kn	days	t/voyage	%	t/day	t/voyage	t/voyage	%
100%	70000	25.0	16.6	5030	–	20.8	345.8	–	–
75%	52500	22.7	18.3	3930	22%	20.8	380.5	34.6	10%
50%	35000	19.8	21.0	3030	40%	16.8	352.8	7.0	2%
25%	17500	15.7	26.5	1990	60%	9.1	240.4	–105.4	–31%

caused major environmental disasters [5] e.g.: Tasman Spirit [2003, more than 12,000 t cargo], Prestige [2002 63,000 t cargo], Erika [1999 over 15,000 t cargo]), container ships with a capacity of several thousand TEUs gain increasing owners interest.

The flagship project of this type is a Triple E Class containership. Danish owner Maersk has ordered at the Korean group Daewoo 10 ships (with the option to build the further 10) of this type. Triple E class container ships have a capacity 18,000 TEU and a design speed 19 knots (about 24% lower than the typical ocean container vessel). Ships are designed to serve the Asia-Europe route. The first unit of this type entered service in July 2013.

Fig. 1. Visualisation of Ultra Large Container Vessel – Triple-E Class

Ships of this type are characterized by 50% reduction of CO2 emissions per unit of transported cargo (TEUs). Despite the benefits of economies of scale there is still an ongoing discussion about the impact of a massive flow of cargo on the functioning of the logistics chain. Service of such large vessels requires infrastructure changes in the ports with respect to e.g.: quays' preparation, installation of lifting equipment capable of handling 25 rows of containers, and setting up efficient transport channels to allow for the distribution of a large amount of cargo inland.

The industry magazines forecast that the increase in the size of container ships will cause marginalization or even elimination of the smaller ports which are unable to handle the largest ships.

In parallel to the changes in the infrastructure the change of the fleet structure takes place. The smallest container feeders will no longer work and their functions are taken over by container ships with a capacity of several thousand TEUs. Another important issue that remains poorly understood is the growing disparity between the performance of marine and land transport channels.

Oversupply of cargo in the ports may cause the traditional land transport channels (railway) reach their maximum capabilities, due to the conditions of infrastructure. This will force the launch of other transport channels whose environmental impact is greater (road transport). Thus, reduction of harmful emissions at sea achieved by employment of ultra large vessels may cause a significant increase of environmental pollution on land.

Influence of ship draft

Changing the draft is not effective in terms of fuel consumption control. Although the resistance of the ship hull and therefore fuel consumption decreases with decreasing draft as indicated by fuel coefficient formula, the same is not true in case of fuel consumption related to the transported cargo. Both, the design analysis and in-service experience, show that reduction of draft causes the ship capacity to decrease faster than fuel consumption. This is due to the geometric characteristics of the hull. Along with reduction of draft the block coefficient decreases due to slender fore and aft ends and bilge radius. Furthermore, usually the residual resistance coefficient increases at reduced draft due to non-optimum submergence of the bulbous bow. In addition, with the decrease of draft the share of deadweight in the displacements reduces.

On the other hand, one should be aware of the critical constraints on the maximum draft of the ship. Among them, the most important are the parameters of shipping routes which in areas close to ports, tight passages or channels, impose the maximum allowable draft. Draft is also an important parameter in view of the ship structure load. Along with the draft increase the hydrostatic pressure exposed on vessel plating increases. Therefore, the increase of draft above the level adopted for the dimensioning of the ship's structure can cause damage.

Influence of ship trim

Trim of the ship is a parameter that can significantly affect the level of fuel consumption in operation. Results of the onboard registrations presented in figure 2 indicate that for a fixed displacement and constant ship speed change of trim cause the differences in fuel consumption ranging from 3 to 7 percent. This change is important from the point of view of the operating costs. Unfortunately, the impact of trim can not be easily determined at the ship design stage.

The effect of trim on the fuel consumption varies significantly from both, the speed change and

the draft of the vessel. Qualitative determination of these relations requires multivariate numerical calculations.

Obtaining quantitative data requires the execution of resistance and propulsion tests for wide range of speeds, drafts and trims. Due to the costs and time constraints such tests are rearly performed. It is worth noting that the effect of trim on the fuel consumption is important for the operator, owner or charterer, who do not usually take an active role in the ship design cycle, in which the hydromechanics analyzes are carried out.

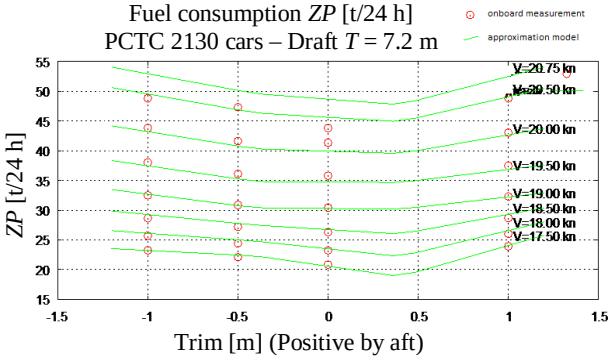

Fig. 2. Fuel consumption at different trim settings [own study based on data provided by CTO SA]

The difficulty in determining the trim effect on the fuel consumption is mainly due to the complexity of the hull geometry. Design practice shows that the hull form designed and optimized for parameters (speed and draft) defined in the contract retains its beneficial properties in a small range of variation of these parameters. Significant changes in navigational parameters (reduced draft or speed) cause that the hull optimized to ensure minimum losses in flow and thus resulting in low fuel consumption do not function properly.

Inflence of the bulbous bow immersion

A prime example of the above-mentioned phenomenon is the flow around a bulbous bow of the ship. Such bow is a typical element of the hull geometry of most cargo vessels operating at relative speeds (in terms of Froude number) above 0.2.

The main purpose of the application of bulb is a reduction of wave making component of the resistance by generating a high-pressure area in front of the stem and, consequently, an additional wave at the bow, which through favorable interference with the wave generated by a moving body, lowers the bow wave height.

Key parameters for the quality of fixed geometry bulb are its immersion below the free surface of the water and the speed of flow around it (the same as the speed of the ship). Bulb immersion must be adjusted to the actual speed of the vessel in order to ensure its proper functioning. Furthermore, it is necessary to take into account the phenomenon of dynamic trim and sinkage associated with the generation of the pressure field on the surface of the hull in motion. Changing ship trim allows customizing the bulb immersion to current speed.

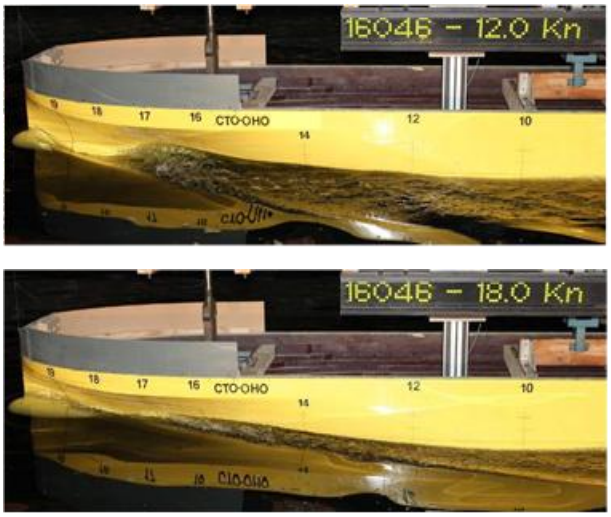

Fig. 3. Bulbous bow performance at non-optimum (upper) and optimum (lower) speed [CTO SA]

Figure 3 shows a view of the bow wave system generated by the hull moving at two speeds and the same initial draft. Despite significantly reduced speed the bow wave system is significantly more complex. In particular, for a speed of 12 knots with a short wave with a deep hollow appears in the area of theoretical frame 18 ½.

12 kn 17 kn 35 kn

Fig. 4. Transom wave system evolution – high speed displacement vessel [CTO SA]

This patern is typical for the flow around a bulb located too close to the free surface. In this case, change of the trim resulting in increased bulb immersion would result in less developed wave system and consequently lower total resistance of the hull and fuel consumption.

The choice of ship's trim with respect to proper immersion of bulbous bow does not automatically guarantee a reduction of fuel consumption. Beside the bulb there are other elements of the hull geometry around which the flow changes significantly with the trim and thus affects the hull resistance and fuel consumption.

Inflence of the transom immersion

Other key components with this respect are stern and transom. Resistence of the flow around the stern part of the ship depends, as in the case of bulb, both on the speed and the immersion. In the worst case, when the velocity of flow around submerged part of the transom is too low an area of strong turbulent flow, combined with a significant drop in pressure can be observed. Since the normal to the surface of the transom is approximately perpendicular to the direction of vessel motion, the pressure drop in this area greatly increases the resistance of the hull.

Phenomena associated with the flows around the transom observed in model tests are illustrated in figure 4. Initially, at low speeds, highly disturbed flow can be noted behind the transom, which, after reaching a sufficiently high speed, separates. Simulation using computational fluid dynamics tools allows for more precise understanding of this phenomenon.

Figure 5 shows the pressure field and streamlines for highly disturbed (top row) and detached (bottom row) flow behind the ship transom. Calculations were done at CTO SA with use of CFD code ANSYS STAR-CCM+ taking into account free surface deformation and dynamic trim and sinkage of the hull. Presented results are a part of the standard hull form optimisation process.

The occurrence of disturbed flow behind the transom causes a significant increase in resistance due to the presence of the vortex and resulting pressure drop. A reduced pressure acts on the wetted surface of the transom resulting in a force directed opposite to the direction of flow.

On the other hand, taking into account the horizontal run of the buttock in the stern area, a significant rise of the transom can cause a significant reduction of waterline and thus increase the Froude number characterizing flow around around the hull and the consequent increase in wave resistance.

Adjustment of the trim also affects, although to a lesser extent, other factors leading to the change of resistance of the hull and thus the change in fuel consumption. Although the following factors usually do not have a decisive impact in specific cases may affect the level of fuel consumption.

Due to the complex, asymmetric with respect to midship, shape of the hull, trim change, in spite of having the same displacement (i.e. realized by moving mass inside the hull of the ship), casues change of the wetted area. Since the frictional resistance is a linear function of the wetted surface, its significant changes affect the resistance and consequently the level of fuel consumption. In practice, as illustrated in figure 6, where the changes of the wetted surface for a bulk carrier in few operational conditions are presented, these changes are not significant.

In the case of a significant bow trim of the ship not only the loss of the positive impact of bulb on the wave system due to its deep immersion but also

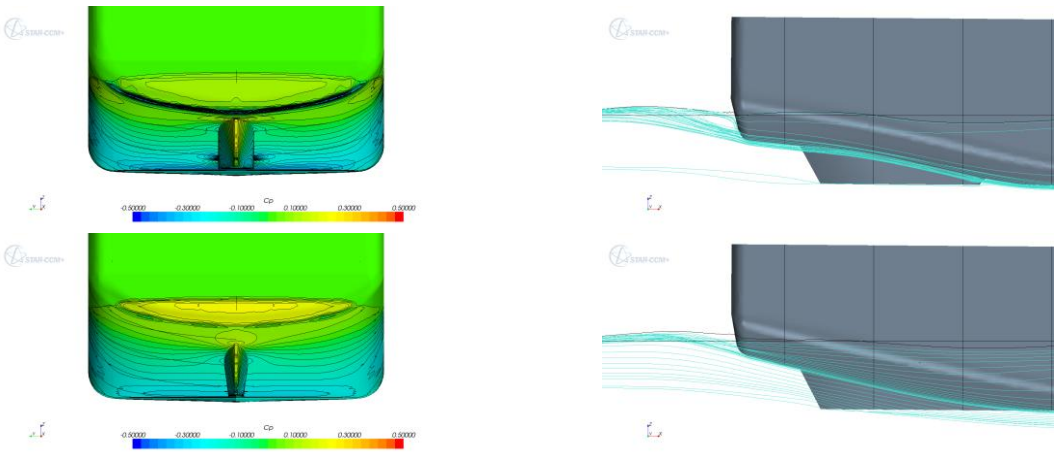

Fig. 5. Numerical flow analyses at stern area: left column – pressure field, right collumn – streamlines, upper row – disturbed flow, causing increase of resistance [CTO SA]

an additional resistance generated by the flow around the wider upper part of the stem should be expected.

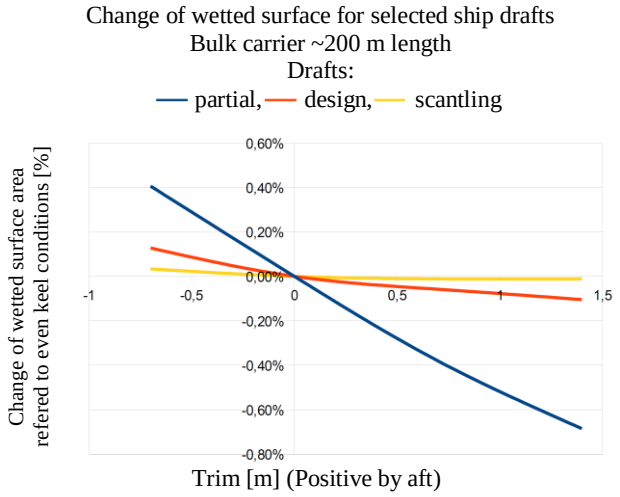

Fig. 6. Trim influence on ship wetted surface

The wave generated in such condition is shown in figure 7. Practice shows, however, that significant bow trim is not used, especially in bad weather conditions due to the reduction of freeboard and the risk of significant foredeck flooding.

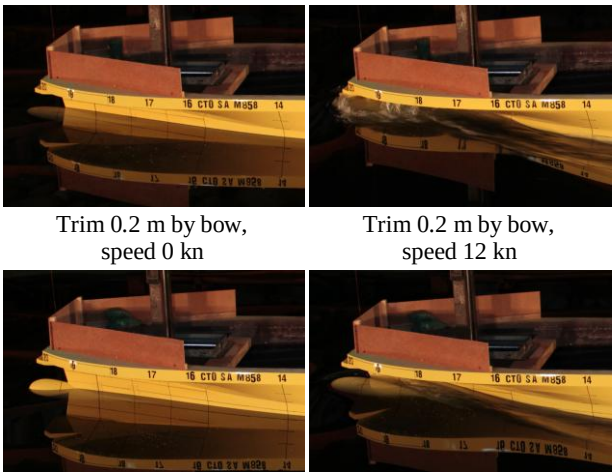

Trim 0.2 m by bow, speed 0 kn | Trim 0.2 m by bow, speed 12 kn

Trim 0.6 m by Stern, speed 0 kn | Trim 0.6 m by Stern, speed 12 kn

Fig. 7. Bow wave system for bow trim (upper) and aft trim (lower) [CTO SA]

Other trim dependent factors

Among the trim dependent factors which affect the ship resistance and thus fuel consumption, the flow around appendages should be considered. These elements are small compared to the size of the main hull and placed on the surface. Examples of common appendages are bilge keels, rudder consoles or shaft brackets. These elements are oriented in such a way that their position aligns with streamlines of the flow around the ship hull.

In this way, the pressure resistance is minimized and the total resistance of the appendage is approximately equal to the frictional resistance of the flat plate of the same area. In case of elements with small span in the flow direction, so called form factor, must be also taken into account. However, in the case the ship is operated in the conditions far different from those for which the position and alignment of the appendages have been designed, an increase in resistance can be expected.

Significant changes of the trim also affect, although slightly, the efficiency of the propeller. With the increase of trim the direction of water flow to the propeller changes causing an increase in the transverse velocity components of the flow. It may cause increased risk of cavitation. In addition, the direction of the force generated by the propeller is not parallel to the direction of ship motion and hence the effective thrust force is reduced.

Conclusions

The analysis of the examples presented above indicates that the effects of the ship operational parameters on fuel consumption can not be described by simple relations. Effects of trim change depend on the vessel speed and the mean draft. The most important factor with this regard is the hull form, especially in case of the presence of bulbous bow or stern transom. The determination of the conditions resulting in the reduction of fuel consumption requires the application of a computational model which properly reassembles these complex relationships and interactions of the various components of flow around the hull.

References

1. Second IMO GHG Study 2009. IMO, London 2009.
2. IMO, RESOLUTION MEPC.213(63), 2012 Guidelines for the Development of a Ship Energy Efficiency Management Plan (SEEMP), MEPC 63/23, Annex 9, Adopted on 2/03/2013.
3. MOLLAND A.F., TURNOCK S.R., HUDSON D.A.: Ship Resistance and Propulsion Practical Estimation of Ship Propulsive Power. Cambridge University Press, 2011.
4. Lloyd's Register, Container Ship Speed Matters, Marine Services, September 2008.
5. BURCIU Z.: Bezpieczeństwo w transporcie morskim i zarządzanie w akcji ratowniczej, Wydawnictwo AM, Gdynia, 2011 (in Polish).

Scientific Journals
Maritime University of Szczecin

Zeszyty Naukowe
Akademia Morska w Szczecinie

2013, 36(108) z. 1 pp. 55–58
ISSN 1733-8670

2013, 36(108) z. 1 s. 55–58

Conditions of safe ship operation in sea waterway systems

Stanisław Gucma

Maritime University of Szczecin, Marine Traffic Engineering Centre
70-500 Szczecin, ul. Wały Chrobrego 1–2, e-mail: s.gucma@am.szczecin.pl

Key words: marine traffic engineering, sea waterway systems, traffic control, safe ship operation, algorithm

Abstract
The article presents an algorithm developed for determining conditions of safe ship operation in a system of sea waterways consisting of three components, or subsystems: waterways, navigation and traffic control. A model of the optimization of sea waterway system parameters is described.

Introduction

For an analysis of sea waterway systems in view of safe ship operation, the following assumptions are made:

1. A system of sea waterways is composed of a number of distinct sections [1]. A waterway is divided into sections by using the following comparative criteria:
   – a manoeuvre being performed;
   – technical parameters of the waterway;
   – technical parameters of navigational systems used;
   – technical parameters of vessel traffic control system;
   – prevailing hydrometeorological conditions;
   – harbour regulations.
2. Each waterway section consists of three basic subsystems of:
   – waterway;
   – vessel position determination (navigational subsystem);
   – vessel traffic control.

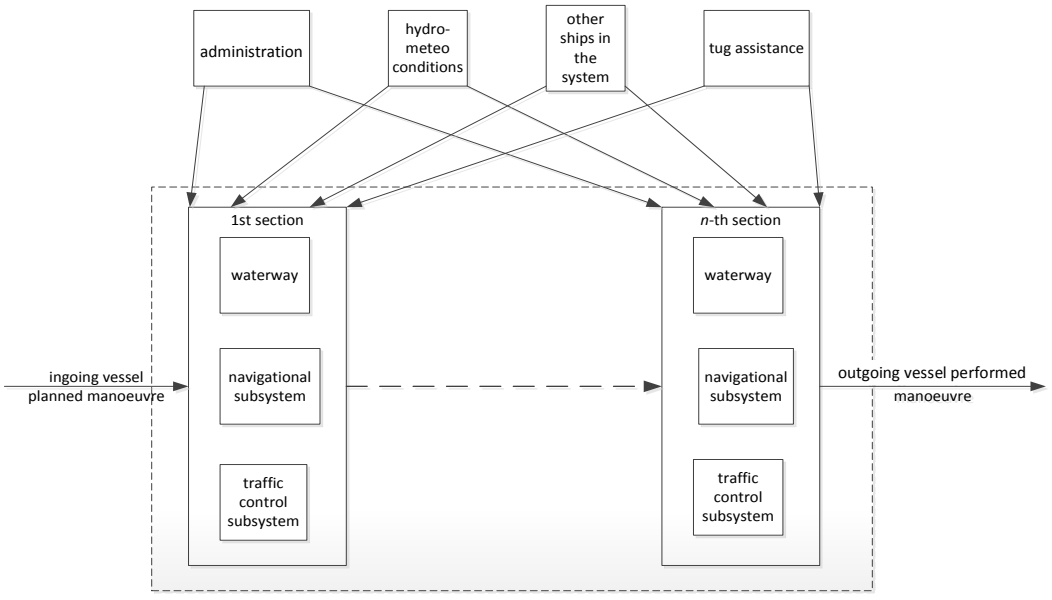

Fig. 1. A general model of waterway system with *n* sections

These elements interact with each other and significantly affect the properties of the system.

The function of a waterway system is to provide a ship with conditions for performing a planned manoeuvre by a ship of specific parameters. Therefore, the input quantity is a planned manoeuvre of a ship with specific parameters, the output quantity is a manoeuvre performed by that ship. A general model of waterway system is presented in figure 1.

The construction or change of waterway component parameters requires that conditions of safe ship operation in the system of sea waterways. Accurately developed conditions for safe ship operation allow to optimize parameters of particular elements of a given system of sea waterways.

Conditions of safe ship operation in a sea waterway system

Operational conditions of sea waterway systems are identified as conditions of safe ship operation on the waterway.

The construction and operation of sea waterway systems generates two basic research problems:

1. Determination of conditions of safe ship operation on the existing sea waterway.
2. Specification of sea waterway system parameters for assumed safe conditions of ship operation.

A system of sea waterways is defined by parameters of its elements (subsystems). Three elements of sea waterway system in each of the system sections are a function of conditions of safe ship operation. Therefore, the system of *i*-th section of sea waterway can be written in a matrix form as follows:

$$\begin{bmatrix} \mathbf{A^i} \\ \mathbf{N^i} \\ \mathbf{I^i} \end{bmatrix} = \boldsymbol{f}\left(L_c, B, T, V^i, C^i, \mathbf{H^i}\right)$$

Conditions of safe ship operation on a waterway are these:

L_c – length of a "characteristic ship";
B – breadth of a "characteristic ship";
T – draft of a "maximum ship";
V^i – allowable speed of a "maximum ship" in an *i*-th waterway section;
C^i – tug assistance in an *i*-th waterway section;
$\mathbf{H^i}$ – vector of hydrometeorological conditions acceptable for a "maximum ship" in an *i*-th waterway section.

$$\mathbf{H_i} = \left[d/n, \Delta^i, V_w^i, KR_w^i, V_p^i, h_f^i, KR_f^i\right]$$

where:

d/n – allowable time of day or night (daylight or no restrictions);
Δ^i – minimum underkeel clearance in an *i*-th section;
V_w^i – maximum wind speed in an *i*-th section;
KR_w^i – wind direction restrictions (if any);
V_p^i – maximum current speed in an *i*-th section;
h_f^i – maximum wave height in an *i*-th section;
KR_f^i – wave angle restrictions (if any).

The following matrix forms were adopted in describing the system components for *i*-th waterway section:

Waterway subsystem:

$$\mathbf{A^i} = \begin{bmatrix} l^i \\ D^i \\ h^i \end{bmatrix}$$

where:

l^i – length of an *i*-th waterway section;
D^i – width of a navigable area of an *i*-th waterway section;
h^i – minimum depth of an *i*-th waterway section.

Navigational subsystem:

$$\mathbf{N^i} = \begin{bmatrix} d_n^i \\ d_{on}^i \\ n_{en}^i \end{bmatrix}$$

where:

d_n^i – accuracy of an *n*-th navigational system in an *i*-th waterway section (standard deviation);
d_{on}^i – availability of an *n*-th navigational system in an *i*-th waterway section (dependent on time of day and visibility);
n_{en}^i – reliability of an *n*-th navigational system in an *i*-th waterway section (technical reliability).

Systems of position determination are designed for three types of visibility conditions:

– daytime (good visibility);
– night time (good visibility);
– poor visibility.

Operational guidelines of a waterway under consideration may restrict the number of design conditions for specified ship sizes, for instance:

– navigation of ships belonging to a specific size range is conducted only at daytime;

– navigation of ships on a given waterway is conducted only in good visibility.

Position determination systems for specific visibility conditions must be doubled, otherwise a failure of one position determination system creates a threat of navigational disaster (a series of accidents at the same time). For each of the three visibility conditions two navigational systems have to be designed:
– main system;
– additional system.

Vessel traffic control subsystem:

$$\mathbf{I}^{\mathbf{i}} = \begin{bmatrix} r_{sn}^{\ i} \\ o_{sm}^{\ i} \end{bmatrix}$$

where

$r_{sn}^{\ i}$ – type of an *n*-th traffic control system in an *i*-th waterway section,

$o_{sm}^{\ i}$ – type of an *m*-th hydrometeorological assistance system in an *i*-th waterway section.

There are four options in reference to traffic control systems:

1) lack of traffic control system;
2) waterway entry / exit control, information on waterway traffic;
3) control of entry/exit and of ship speed in each waterway section, information on vessel traffic on the waterway;
4) full waterway traffic control;

and the following types of hydrometeorological assistance:

1) information on hydrometeorological conditions prevailing on a waterway;
2) information on hydrometeorological conditions prevailing in each waterway section and operational system of dynamic underkeel clearance determination.

Determination and optimization of sea waterway parameters

Sea waterways are usually built for one-way or two-way traffic, the two cases featuring different conditions of safe ship operation. Safe ship operating conditions that determine parameters of sea waterway elements are specified separately for one-way and two-way traffic. Bearing this in mind, it can write:

– for one-way traffic:

$$\begin{bmatrix} \mathbf{A}_1^{\mathbf{i}} \\ \mathbf{N}_1^{\mathbf{i}} \\ \mathbf{I}_1^{\mathbf{i}} \end{bmatrix} = \boldsymbol{f}_1\left(L_{c_1}, B_1, T_1, V_1^i, C_1^i, \mathbf{H}_1^{\mathbf{i}}\right)$$

– for two-way traffic:

$$\begin{bmatrix} \mathbf{A}_2^{\mathbf{i}} \\ \mathbf{N}_2^{\mathbf{i}} \\ \mathbf{I}_2^{\mathbf{i}} \end{bmatrix} = \boldsymbol{f}_2\left(L_{c_2}, B_2, T_2, V_2^i, C_2^i, \mathbf{H}_2^{\mathbf{i}}\right)$$

When designing a sea waterway operated by one-way and two-way traffic, we choose a set of parameters that will satisfy conditions of safe ship operation for both types of traffic.

Parameters of waterway components for both, one-way and two-way traffic are determined by means of the optimization method where the objective function is the cost of construction and operation of sea waterway system, written down as follows [2]:

$$Z = (A1 + A2 + N1 + N2 + I1 + I2 + S) \rightarrow \min$$

with one of two constraints:

$$\left.\begin{array}{ll} 1) & \mathbf{d}_{\mathrm{ijk}}\,(1-\alpha) \subset \mathbf{D}(t) \\ & \bigwedge_{p(x,\,y)\in \mathbf{D}(t)} h_{xy}\,(t) \geq T_{xy}\,(t) + \Delta_{xy}\,(t) \\ 2) & R_l \leq R_{akc} \end{array}\right\}$$

where:

$\mathbf{D}(t)$ – navigable area (condition of safe depth at instant *t* is satisfied);

$\mathbf{d}_{\mathrm{ijk}}(1-\alpha)$ – safe manoeuvring area of *i*-th ship performing *j*-th manoeuvre in *k*-th navigational conditions, determined at a confidence level $1-\alpha$;

Z – cost of construction and operation of sea waterway system;

*A*1 – cost of construction (reconstruction) of a waterway;

*A*2 – cost of waterway operation;

*N*1 – cost of construction of ship position determination subsystem (navigational systems);

*N*2 – operating costs of navigational systems;

*I*1 – cost of construction of traffic control subsystem;

*I*2 – operating costs of traffic control subsystem;

S – ship operating costs related to waterway passage (pilotage, tug assistance, etc.);

R_l – navigational risk of passing *l*-th waterway section;

R_{akc} – acceptable navigational risk;

h_{xy} – depth of area at point *x*, *y*;

T_{xy} – ship draft at point *x*, *y*;

Δ_{xy} – underkeel clearance at point *x*, *y*.

Given that particular costs of construction and operation of the subsystems are a function of parameters of these subsystems, the objective function can have this form:

$$Z^i = \left(\mathbf{A}_{\mathbf{k}}^{\mathbf{i}}, \mathbf{N}_{\mathbf{k}}^{\mathbf{i}}, \mathbf{I}_{\mathbf{k}}^{\mathbf{i}}\right) \rightarrow \min$$

with constraints as above,
where:

$\mathbf{A}_k^i$ – matrix of costs of the construction and operation of waterway subsystem;

$\mathbf{N}_k^i$ – matrix of costs of the construction and operation of navigational subsystem;

$\mathbf{I}_k^i$ – matrix of costs of the construction and operation of traffic control subsystem.

The conditions of safe ship operation on an examined waterway for one- and two-way traffic are established following this algorithm:

1. Identify ports and terminals to which the examined waterway is leading.
2. Determine "maximum ships" characteristic of specific ports and terminals.
3. Classify characteristic "maximum ships" by type:
   - bulk carriers, tankers;
   - gas tankers;
   - container ships, refrigerated ships, general cargo vessels;
   - ferries, ro-ro ships;
   - cruise ships, passenger vessels;
   - other ships.
4. Taking into consideration traffic intensity for each group of vessels, we then define the relevant parameters of:
   - "maximum ship" in one-way traffic;
   - "maximum ship" in two-way traffic.
5. Based on marine traffic engineering methods, the following parameters are determined:
   - allowable speeds of "maximum ships" in each waterway section (V^i); ships proceed along waterways at varying allowable speeds that depend on the type of area and type of ship. On the one hand, these speeds are affected by operating factors, mainly time limits imposed on ships such as container carriers, Ro-Ro vessels, or gas tankers. On the other hand, there are restrictions resulting from the safety of navigation. Generally ships sail at "service speed in restricted areas" in remote roadsteads and anchorage approaches or a "reduced speed" developed on fairways. A service speed for restricted areas is not a maximum speed a ship can develop, it is a speed attained with the engines set for "full manoeuvring speed". A reduced speed, in turn, is used in approach channels and is developed by the engine set for "half ahead" [3];
   - allowable hydrometeorological conditions in each waterway section ($\mathbf{H}^i$); an example clearance for a minimum water level is specified for each ship type, minimum water level, probability of its occurrence and the period of designed waterway operation, for two groups of ships:
     – ships that cannot wait for a higher water level (ferries, gas tankers, etc.);
     – ships that can wait for a higher water level.

     A minimum water level assumed for the former group of vessels is the one occurring within a 20-year period of waterway operation (lifecycle period of this kind of project – construction of a waterway). For the latter group other values can be assumed (e.g. minimum water level occurring in a 5-year period). For the latter group of vessels in particular we should use the dynamic method of underkeel clearance determination.

Conclusions

The article presents a sea waterway system consisting of three elements (subsystems):

– waterway subsystem;
– navigational subsystem;
– traffic control subsystem.

A sea waterway system is defined with the use of conditions of safe ship operation on that waterway.

An algorithm has been developed for determining conditions of safe ship operation on the examined waterway. Besides, a model for the optimization of sea waterway system parameters is described.

The research results have been utilized in the design of approach channels leading to the outer port in Świnoujście, where an LNG terminal is located [4].

References

1. GUCMA S., ŚLĄCZKA W., ZALEWSKI P.: Parametry torów wodnych i systemów nawigacyjnych wyznaczane przy wykorzystaniu kryteriów bezpieczeństwa nawigacji. Wydawnictwo Naukowe Akademii Morskiej w Szczecinie, Szczecin 2013.
2. GUCMA S.: Optymalizacja parametrów systemu morskich dróg wodnych w ujęciu inżynierii ruchu morskiego. Materiały na Międzynarodową Konferencję Naukową „Transport XXI wieku". Ryn 16–19.09.2013.
3. GUCMA S., ŚLĄCZKA W.: Target development of the outer port in Świnoujście – optymalization of parameters and determination of operating conditions. 19th International Conference on Hydrodynamics in Ship Design – HYDRONAV 2012, Iława.
4. Projekt systemów zapewniających bezpieczną nawigację i obsługę statków LNG na podejściu i w porcie zewnętrznym w Świnoujściu. Praca naukowo-badawcza, Akademia Morska w Szczecinie, Szczecin 2012.

Scientific Journals
Maritime University of Szczecin

Zeszyty Naukowe
Akademia Morska w Szczecinie

2013, 36(108) z. 1 pp. 59–63
ISSN 1733-8670

2013, 36(108) z. 1 s. 59–63

Prospects for LNG in the South Baltic Sea Region

Stefan Jankowski

Maritime University of Szczecin
70-500 Szczecin, ul. Wały Chrobrego 1–2, e-mail: s.jankowski@am.szczecin.pl

Key words: LNG, environment protection, regulations, emission control, ship's fuel

Abstract
The global policy of protection environment enforces much more stringent regulations to reduce pollutants from exhaust gases. These requirements are being implemented gradually from 2010 and will have full force in 2015 and 2016. The shipping industry is facing a big challenge to meet these regulations, especially on ECA (emission control area). This paper describes the activities within project "MarTech LNG", that promotes the use of LNG as a ship's fuel on south Baltic Sea region.

Introduction

The worldwide policy is going towards environment protection and the limiting pollution in the seas, inland waters, grounds and the air. Therefore, the international organizations like IMO implements new, much tighter regulations.

The Annex VI "Regulations for the Prevention of Air Pollution from Ships" was added to the International Convention for the Prevention of Pollution from Ships (MARPOL) in 1997. The main aim of the annex is finding a solution to minimize emissions from ships oxides of sulfur (SO_x), particulate matter (PM), nitrogen oxides (NO_x), ozone depleting substances (ODS), volatile organic compounds (VOC) and their contribution to local and global air pollution and environmental problems. Annex VI entered into force in 2005, but in 2008 was revised. The significant tighten emissions limits adopted in 2008, were gradually introduced from 2010 and another milestones of limiting air pollutants are coming during next years which are shown on figures 1 and 2.

In addition IMO has adopted mandatory technical and operational energy efficiency measures which will significantly reduce the amount of CO_2 emissions from international shipping.

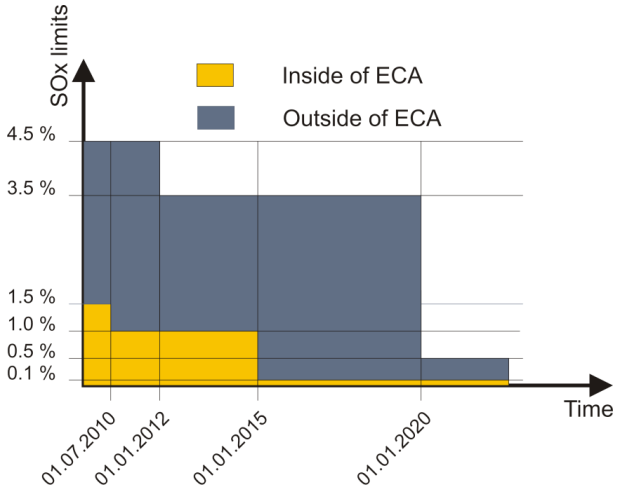

Fig. 1. The MARPOL Annex VI fuel oil sulphur limits [1]

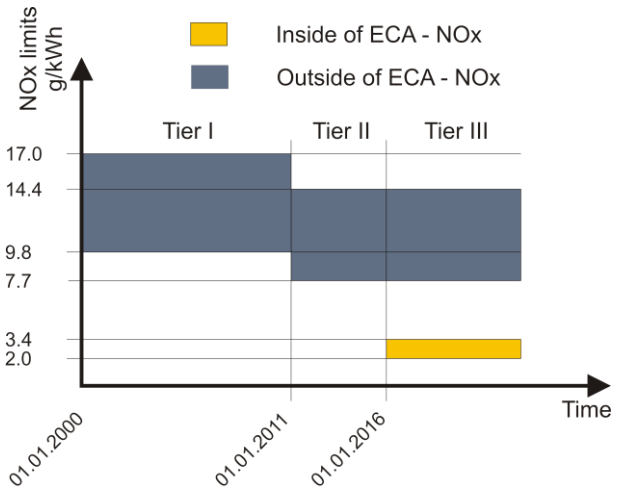

Fig. 2. The MARPOL Annex VI, emission limits for NOx [1]

Currently Baltic Sea and North Sea are established as an ECA only for SO_x, but everybody engaged in sea transport business should think perspectively. North America and from 1 January 2013 United States Caribbean Sea are SO_x, NO_x and PM ECA.

There is a high probability that new ECAs will be established (Fig. 3) or that the existing ones will be more restrictive.

Fig. 3. DNV's map of current and possible ECAs in the future [2]

Alternatives for heavy fuel oil (HFO)

The review of existing engine technology and its development indicates that currently only three solutions are in accordance with SOx regulations. If shipowners wish to continue sailing on Baltic Sea after 2015 they have to choose [3]:

– low sulphur fuel;
– an exhaust gas scrubber;
– LNG fuel (liquefied natural gas).

The first solution requires only minor modifications on vessel fuel systems. The content of sulphur in a fuel like MDO (marine Diesel oil) and MGO (marine gas oil) can be below 0.1%. The main disadvantage such a choice is limited availability of low sulphur fuel is that rising demand is expected to increase its price uncertainty.

The second solution requires installation of an exhaust gas scrubber to remove sulphur from the engine exhaust gas by using chemicals or seawater. This technology requires significant modifications on ship systems. Additional tanks, pipes, pumps, and a water treatment system. The sulphur-rich sludge produced is categorized as special waste, to be disposed of at dedicated facilities. Moreover, scrubbers increase the power consumption, thereby increasing its CO_2 emissions.

The third solution is using LNG (liquid natural gas) as a fuel. Natural gas is the cleanest form of fossil fuels available, and when fuelling a ship with LNG no additional abatement measures are required in order to meet the ECA requirements. However, an LNG-fuelled ship requires purpose-built or modified engines and a sophisticated system of special fuel tanks, a vapouriser, and double insulated piping. Available space for cylindrical LNG fuel tanks on board ships has been a key challenge, but new hull integrated tanks are expected to simplify this issue.

For new ships delivered after 1 January 2016, exhaust gas purification by Selective Catalytic Reduction (SCR) or LNG fuel are the only two currently available abatement measures to meet Tier III requirements.

LNG as a fuel

LNG means liquefied natural gas. The natural gas is temporarily converted to liquid form at –163°C, under atmospheric pressure. It takes up 600 times less space than as a gas, therefore, it is more efficient for storage and transport. LNG is currently tested as a fuel on more than 20 vessels sailing on Norwegian waters.

In addition, LNG is clean not only in aspect of exhaust gases, but also in case of spill. LNG does not cause environmental disaster because in such a case it will evaporate quite fast. The main hazard in case of LNG spill, are frostbites due to extremely low temperature.

Taking account above mentioned three solutions it should be said, that LNG is the best alternative in aspect of economic and environmental impact to Baltic Sea.

LNG as a fuel has the lowest emission of all three pollutants NO_x, SO_x, and particles, as well as the greenhouse gas CO_2 (GHG). SO_x and particles are reduced by close to 100%, NO_x emissions close to 85–90%, and net GHG emissions by 15–20% (Fig. 4). Below (Fig. 4) are presented emissions for typical Baltic Sea vessel.

The typical cargo vessel was determined as follows:

– gross tonnage: 2700;
– power of main engine: 3300 kW;
– yearly sailing hours: 5250.

Nowadays, the LNG trade market is large and flexible. The forecast developed by U.S. Energy Information Administration (EIA) in 2008 are optimistic and indicates an expanding gap between conventional fuel and LNG [4]. On the other hands the Lloyd's Register's forecasts of the fuel market indicate that demand of LNG as a fuel will depends on number of vessels fueled by LNG and its price [5].

The cost of a new vessel equipped with LNG propulsion is higher about 10–20% than conven-

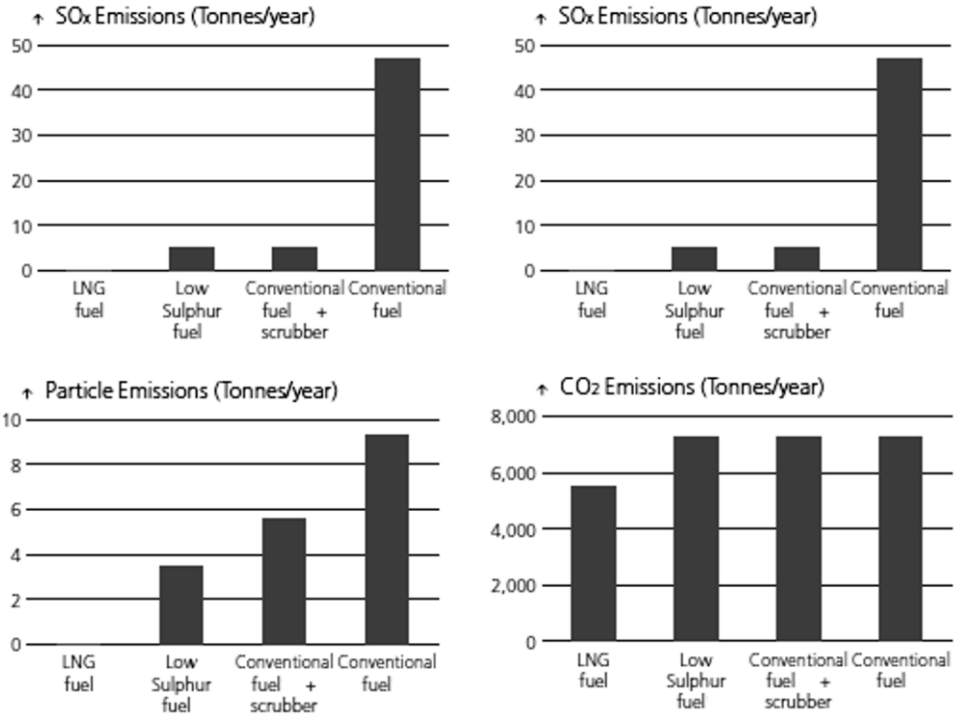

Fig. 4. The pollutants' emissions for typical Baltic Sea vessel [4]

tional vessel with similar gross tonnage. The additional cost is mainly due to the sophisticated LNG storage tanks, the fuel piping system and in some cases a slightly larger ship. Based on experience from ships built, the additional investment cost for the LNG fuelled typical Baltic Sea cargo vessel has been estimated to about 4 million USD. Estimated cost of scrubber installation should be around 1 million USD. Taking these assumptions into account and forecasting price of marine gas oil (MGO) in 20 years perspective the lowest exploitation cost are in case of LNG vessel (Fig. 5).

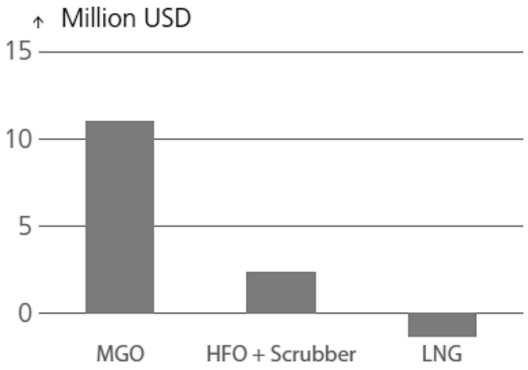

Fig. 5. Exploitation costs over 20 years related to conventional fuel (DNV 2010) [4]

The exploitation costs analysis indicates that fueling LNG is cheaper even in comparison to HFO, and differences between MGO option is up to 12 million USD.

Current status of LNG infrastructure on Baltic Sea

In order to enable navigation of vessels using LNG as a fuel, a grid of bunker stations is required. An average period between bunkering for the LNG vessels today is about one week, and vessels should have possibilities to obtain LNG in one of the ports during their trips. Currently, the LNG infrastructure on Baltic Sea is very weak (Fig. 6).

The number of import terminals is not enough to provide a supply of LNG for every route on Baltic Sea. They should operate rather as a hub of LNG and distribute it to small scale bunker stations.

In case of decision about building new import terminal, it belongs to government in order to securing energy independence of given country, but decisions about building small scale LNG terminals or bunker stations, depend on market. Currently, there is no LNG bunker stations on Baltic because there is a small number of LNG powered vessels, and lack such vessels is a result of lack of bunker stations. It seems correct that at least at the beginning, the bunker stations should also have a political support.

MarTech LNG – "Marine Competence, Technology and Knowledge Transfer for LNG in the South Baltic Sea Region (SBSR) is one of the projects which aims are dissemination of LNG technology by exchanging experiences, knowledge and competencies within SBSR. The project supports

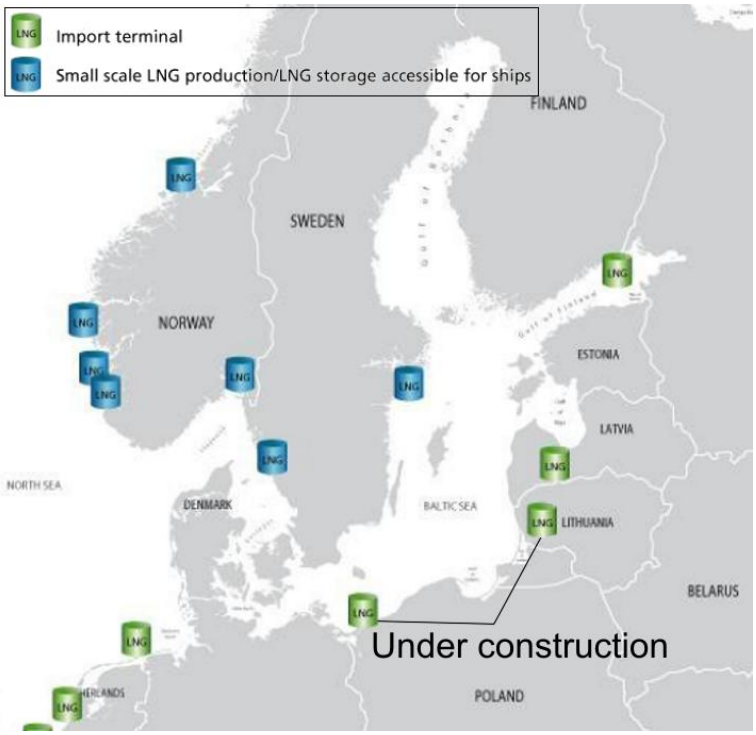

Fig. 6. LNG terminals on Baltic Sea [6]

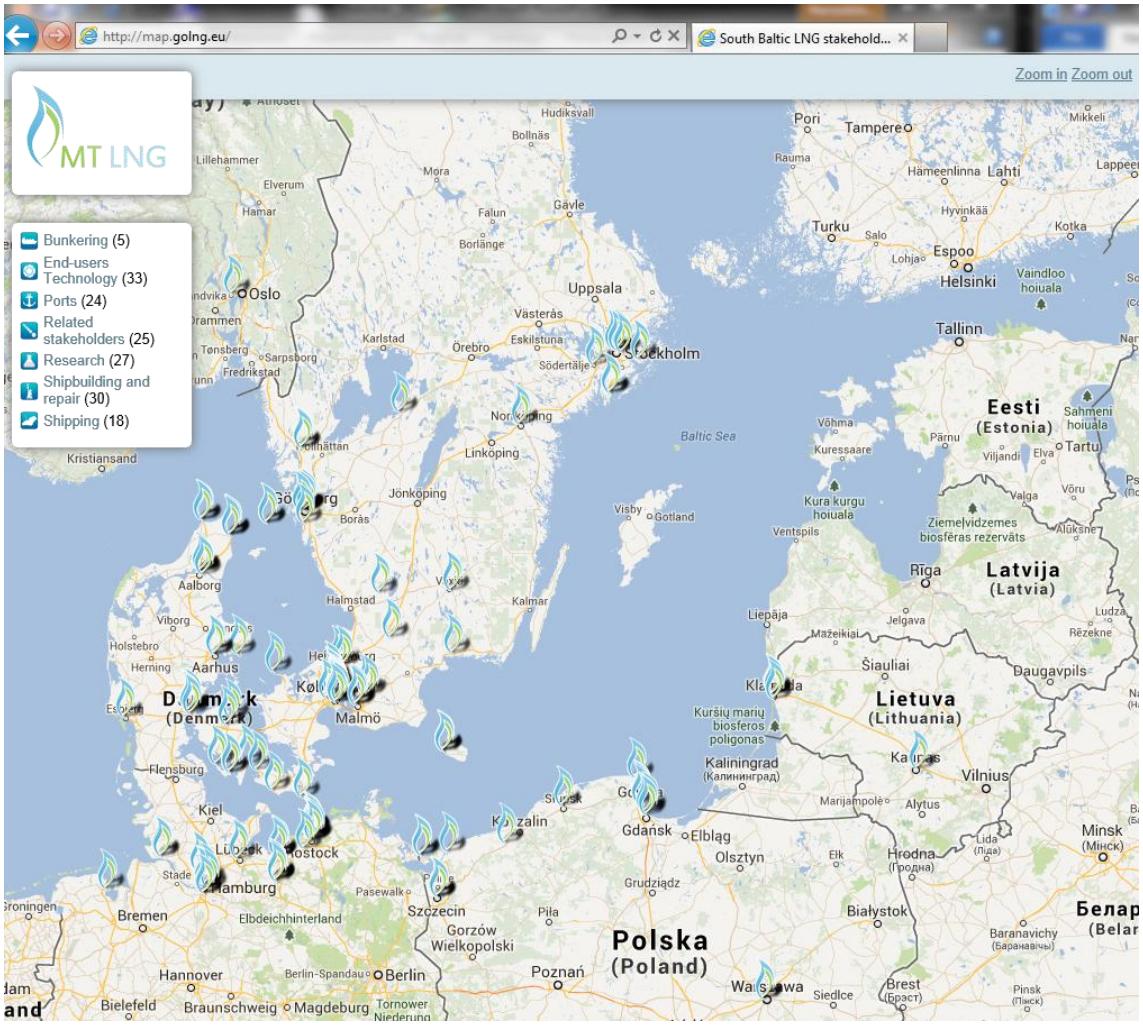

Fig. 7. LNG activities on Baltic Sea [6]

the activities related to LNG technology, promotes LNG as a green energy and the cleanest marine fuel. Main idea of the project is to create a better access to technology and knowledge on LNG related business activities to build up a better competences and specialization among the SBSR maritime business supply chain. The main idea will be achieved by realize following aims:

- develop the LNG related competences for the Maritime industries in SBSR;
- foster LNG targeted scientific research;
- create LNG supply / value chain in SBSR;
- support LNG development and operation processes in SBSR.

One of the first task of the project was region study in terms of existing education, research, training and consulting institutions providing activities related to LNG technology. Based on this analysis interactive map were created (Fig. 7).

The region was also analyzed in aspect of stakeholders dealing with LNG technology. The region LNG profile or joint study "Mapping LNG knowledge and competence in the SBSR" indicates on lack or too small amounts of LNG that could enable development of the LNG business. Cooperation between stakeholders and institutions is weak and really hard to find LNG supply chain. But LNG enterprises have a big potential which can be activated when LNG as a fuel will be available (MarTech LNG).

Conclusions

LNG is one of the best solutions for Baltic region to protect environment against pollution caused by conventional fuels. Now is the time for owners to decide which solution to choose to be in compliance with the MARPOL Convention. They will choose LNG, if on Baltic Sea the LNG infrastructure will exist. Unfortunately, it seems that without political support, building infrastructure may be difficult.

References

1. IMO, The Regulations for the Prevention of Air Pollution from Ships (Annex VI), 2008.
2. RYSST J.: DNV report on the potential of LNG shipping in the Baltic. 2011.
3. Danish Maritime Authority, North European LNG Infrastructure Project, 2012.
4. Det Norske Veritas, Greener shipping in the Baltic Sea, 2010.
5. Lloyd's Register, LNG-fuelled deep sea shipping, 2012.
6. Project MarTech LNG, Mapping LNG knowledge and competence in the SBSR – Joint Study, 2013.

Scientific Journals
Maritime University of Szczecin

Zeszyty Naukowe
Akademia Morska w Szczecinie

2013, 36(108) z. 1 pp. 64–69
ISSN 1733-8670

2013, 36(108) z. 1 s. 64–69

LNG supply chain in the SBSR

Stefan Jankowski, Marcin Przywarty

Maritime University of Szczecin
70-500 Szczecin, ul. Wały Chrobrego 1–2, e-mail: {s.jankowski; m.przywarty}@am.szczecin.pl

Key words: LNG, transfering, supply chain, structural delineation, end-user technologies

Abstract
The paper presents the LNG-related supply chain in the South Baltic Sea Region which was specified as a result of the MarTech LNG Project. First part of the paper presents specification of technologies and technical solutions. Then it turns to the LNG-related stakeholders, i.e. all actors involved into LNG supply, delivery as well as end-user technologies. Aspects of LNG-related infrastructure accomplish the presentation of the SBSR supply chains. The paper is concluded by structural delineation of the supply chains in the SBSR.

Introduction

The MarTech LNG Project aims at transferring tested and proven LNG knowledge and technology to implement into the South Baltic countries. LNG building and operation knowledge will allow the local maritime industries to benefit from the investments and support the development of new products and services that are demanded in the global market thus strengthening the Baltic maritime Sector. Furthermore, the creation of a Baltic supply chain will establish cooperation between regional maritime industries and scientific institutions locally, nationally and internationally, and support the creation of cluster development, able to respond to international tenders in the future. Presented paper describes the LNG-related supply chain in the South Baltic Sea Region which was specified as a one of the results of the MarTech LNG Project.

Technological capabilities

Technological capabilities of the SBSR are presented by the overview of the key current LNG-related devices and inventions:

- Biggest LNG ferries (129.9 m long, 19.2 m wide with capacity for 242 passenger cars and 600 passengers, gas-electric system with 3 large LNG gas motors and alternators, thus enabling a speed of approx. 20 knots) [1];
- Terminal LNG cargo tanks made by using a slip-form construction method [2];
- Methods of regasification (evaporators heated by fuel itself – Submersible Combustion Vaporizer (SCV) and Evaporators heated by air or sea – Open Rack Vaporizer (ORV)) [3];
- Pilot navigation and docking system for LNG carriers to increase of safety of berthing ships by the construction and implementation of innovative information and telecommunication system [4];
- LNG-powered ships, i.e. cruise ferries with engine compartments enable to run them on LNG [5];
- WS1 LNG / FO Bunker vessel with a 1400 DWT, equipped with flexible cargo configuration (3 configurations possible) combining traditional HFO and MDO fuels with LNG and possessing a capacity for LNG between 700–1400 m^3 [6];
- LNG Hybrid Barge as electricity supplier to the AIDA cruise ships with year-round utilization of the system by feeding the produced energy in the cruise-off season into the municipal grid, thus supplying electricity and heat to approx. 11,000 households [7];
- LNG Hybrid Ferries Watten Link for use in the North Sea equipped with 3 proven LNG Gen sets, 2 electrical drive motors and 1 hybrid

battery pack with LNG (only one fuel on board) supply for ferry service up to 4 days [8];
– LNG fuel tank containers [9];
– New generation passenger and car ferry powered by LNG – Viking Grace [10];
– Cruise ferries run by LNG [11];
– Focus on investments into smaller ships with reduced emissions as a result.

LNG-related stakeholders and players

Potential stakeholders and players located in the SBSR, can be found among companies, associations, authorities, consultants, classification societies, ports, producers, distributors, ship-owners, storage and bunkering companies, system operators, end-user technologies, as well as further organisations and institutions. On the basis of the data gathered following stakeholders and players portfolio for the SBSR was generated (Fig. 1). It is noteworthy that only key stakeholders and players are listed here. Stakeholders and players presented in the portfolio refer to the following main categories:

– bunkering;
– shipbuilding & repair;
– ports;
– shipping;
– end-user technologies.

Beyond this, for the purpose of this study, it has been decided to incorporate such stakeholders and players groups as regulators (including authorities, classification societies and other relevant organisations and associations), storage stakeholders, distributing stakeholders and consultants.

Taking into account this breakdown of all relevant stakeholders across the SBSR, it is first important to accentuate stakeholders that are already equipped with LNG technological solutions, products and services, or do record LNG-related young or mature existing activities that have been mapped in the maritime industry discourses. In this respect, the table below presents key stakeholders that due

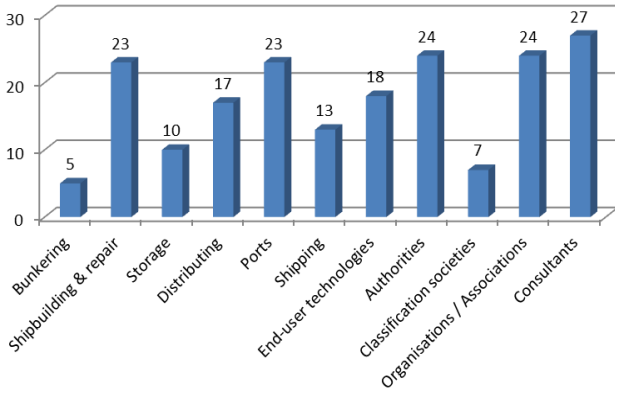

Fig. 1. Profile of stakeholders in the SBSR

to their activities can be referred to as LNG stakeholders (Table 1).

One of the largest group of stakeholders behind the regulation and framework conditions providing stakeholders such as authorities, classification societies can be located in the shipbuilding-related industry. In this context, naval architects should be also allocated to this group of stakeholders, since they are involved into design, construction and repair of marine onshore and offshore infrastructure and related structures. The following shipbuilding and repair industry-related stakeholders are present in the SBSR (Table 2).

When taking into account shipping companies and related stakeholders, in some cases it is hard to allocate them distinctly to the shipping stakeholders category. In fact, these can be in some cases placed either in shipbuilding & repair or shipping-related group. Nevertheless, this study made an attempt to identity key shipping stakeholders in the SBSR (Table 3).

Turning towards stakeholders capable to distribute or storage gas, especially with the focus on LNG, there are located over 20 companies able to provide demanded services currently and in the future. As a result of the data, the following constellation of the distributing and storage companies has been generated (Table 4).

Table 1. LNG stakeholders

Company	Activity
Fjord Line AS	Cruise ferries powered by LNG (DK)
Man Diesel & Turbo	LNG fuelled two-stroke engines (DK)
Rolls Royce Marine AS	LNG carriers (DK)
Wärtsilä	LNG systems (DK)
Viking Line	LNG ferry Viking Grace (SE)
White Smoke Shipping	LNG Bunkering solutions & STS Bunkering (SE)
Cryo AB	LNG bunker tanks and systems (SE)
Nordic Yards GmbH	LNG tank systems for arctic use (DE)
Marine Sevice GmbH	LNG fuel tank container (DE)
KAEFER	Marine & Offshore Cryogenic insulation solutions for LNG tank and cargo systems (DE)

Table 2. Shipbuilding and repair industry-related stakeholders

Company	Company
Søby Yard (DK)	Muehlhan Rostock GmbH (DE)
Marstal Yard (DK)	R & M Ship Technologies GmbH (DE)
Fayard Yard (DK)	KAEFER Marine & Offshore (DE)
Man Diesel & Turbo (DK)	Neptun Ship Design GmbH Rostock (DE)
RollsRoyce Marine AS (DK)	IMAVIS Maritime Wirtschafts- und Schiffbauforschung GmbH (DE)
Wartsila (DK)	BaltiCo GmbH bei Rostock (DE)
ABB (DK)	Marine- und Automatisierungstechnik GmbH Rostock-Warnemünde (DE)
OSK Ship-Tech (DK)	SDC SHIP Design & Consult GmbH (DE)
Schottel GmbH Wismar (DE)	SC "Western Shipyard" (LT)
Nordic Yards GmbH (DE)	Gdansk Shiprepair Yard Remontowa (PL)
Becker Marine Systems Hamburg (DE)	White Smoke Shipping (SE)
Frauenhofer Anwendungszentrum Rostock (DE)	Cryo AB (SE)
Ingenieurtechnik und Maschinenbau GmbH (DE)	

Table 3. Shipping stakeholders

Company	Company
Lauritzen Kosan (DK)	Rederiet færgen (DK)
Mæersk LNG (DK)	Nordic Yards GmbH (DE)
Evergas (DK)	SDC SHIP Design & Consult GmbH (DE)
Clipper Group (DK)	DFDS Seaways (LT)
Fjord Line Denmark AS (DK)	Swedish Marine Forum (SE)
Mæersk Line Ltd (DK)	Stena (SE)
Mols linien AS (DK)	

Table 4. Distributing and storage stakeholders

Company	Company
Dong gas Distribution / Dong Storage (DK)	PL Energia (PL)
EnergiDK (DK)	Polskie LNG (PL)
Energinet DK Gaslager (DK)	PGNiG (PL)
Aalborg gasforsyning (DK)	Swedish Gas Association (SE)
Naturgas fyn (DK)	Stockholm liquefied methane gas station (SE)
HNM Naturgas (DK)	Enagas SA (SE)
EON (DE)	EON (SE)
Klaipedos Nafta (LT)	Marine Service GmbH Hamburg (DE)
Gaz-System (PL)	JSC Klaipedos Nafta (LT)
Budnaft (PL)	AGA AB in Nynäshamn port (SE)
Petrolinvest (PL)	Royal Vopak in Gothenburg port (SE)

Dovetailed with the storage companies are bunkering companies that are of paramount importance when dealing with LNG-related issues. However, bearing in mind the bunkering solutions landscape in the SBSR it appears to be scarce with a record of only 5 bunkering service providing companies:

- Dan-Bunkering Ltd (DK);
- OW Bunker & Trading (DK);
- White Smoke (SE);
- Swedish Marine Technology Forum (SE);
- SSPA Sweden AB and ÅF AB (SE).

Distributing, storage, shipbuilding & repair, as well as shipping stakeholders are significant only in a case, where there exists respective LNG-related sufficient "room" to operate for the identified stakeholders. Here, this particular room or space to operate has to be understood as infrastructure. Coming back to the LNG-related discourse, usually the infrastructure is located in ports, and often, in the immediate proximity. Taking the SBSR into account against this background, the SBSR possess a series of ports that are relevant for LNG-activities. At the second glance, however, 23 identified ports along the SBSR manifest different degree of relevance for the LNG-activities and infrastructure. In order to provide a clear insight into the significance of the identified ports, it was decided to build the following discussion concerning the ports upon a proposed classification of these particular ports. After having studied the information on the ports, there was made an observation that SBSR can be divided into some groups in terms of their current participation into LNG activities. The proposed classification is as follows: ports currently involved into LNG activities (1), future participation into LNG activities (2), high level of maturity / potential for LNG activities (3) and having potential, but necessary to undergo further development (4).

By bearing on the potential stakeholders identified so far, the potential for the LNG development in the SBSR appears of solid nature. However, solid supply chain is ground not only on the private sector stakeholders, but involves actors from the public sphere that may be crucial in changing, for instance, the perception of the development of LNG

Table 5. Ports involved and potentially involved in LNG activities

Ports currently involved into LNG activities	Nynäshamn Port (SE)	
Ports involved into LNG activities in the near future	Gothenburg Port (SE)	
	Port of Klaipeda (LT)	
	Port of Świnoujście (PL)	
Mature Ports and/or ports of high potential for LNG activities Location in the SBSR	Hirtshals Port (DK)	Port of Wilhelmshafen (DE)
	Port of Hamburg (DE)	Port of Brunsbüttel (DE)
	Rostock Port (DE)	Port of Lübeck (DE)
Ports having potential for LNG activities but requiring certain modifications	Esbjerg Port (DK)	Helsingor Port (DK)
	Rønne Harbour (DK)	Spodsbjerg Port (DK)
	Aarus Harbour (DK)	Tårs Port (DK)
	Port of Copenhagen and Malmö (DK)	Port of Gdynia (PL)
	Port of Sjællands Odde (DK)	Port of Gdańsk (PL)
	Rødby Færgehavn (DK)	Port of Szczecin (PL)
	Gedser Port (DK)	

in the SBSR. Hence, stakeholders that take significant decisions are involved into relevant ruling procedures, or outlines, e.g. regulations pertaining to maritime industry etc., such as standards etc., provide normative grounds that in the particular context of LNG development shows up as significant. This study reveals that there are a number of such "regulators" involved into respective processes. As key authorities can be listed (Table 6).

Table 6. Authorities related to LNG

Denmark	**Lithuania**
Danish Maritime Authority	Lithuanian Ministry of Energy
Danish Ministry of Business and Growth	Lithuanian Ministry of Transport and Communications
Danish Ministry of Transport	Lithuanian Ministry of Finance
Danish Ministry of Climate, Environment and Building	Lithuanian Ministry of Environment
Germany	Lithuanian Ministry of Foreign Affairs
BSH – Federal Maritime and Hydrographic Agency	SE Klaipeda State Seaport Authority
Federal State of Mecklenburg-Vorpommern	**Sweden**
German Ministry of Transport (federal and/or regional)	Swedish Ministry of Defence
German Ministry of Environment (federal and/or regional)	Swedish Ministry of Transport
German Ministry of Regional Planning (federal and/or regional)	Swedish Ministry of Enterprise
Poland	Swedish Ministry of Energy and Communications
Maritime Office Szczecin	Swedish Ministry of Environment
Maritime Office Gdynia	Swedish Maritime Administration
Maritime Office Słupsk	Swedish Ministry of Defence

Key identified authorities (alongside a large number of regional municipalities and regional authorities) are accompanied by the relevant organisations and/or associations, which may have an important impact when developing LNG in the SBSR (Table 7).

Table 7. Organisations and associations related to LNG

Danish Ship-owners Association	Lithuanian Ship-owners Association
Danish Maritime	Association of Polish Maritime Industries
Danish Gas Association	Polish Ship-owners Association
Danske Havne	Swedish Maritime Administration
Society for Naval Architecture and Marine Engineering	Swedish Ship-owners Association
DTL	Swedish Gas Association
German Association for Positioning and Navigation (DGON) e.V.	Swedish Transport Agency
German Ship-owners Association	Gothenburg Transport Agency
Association of Lithuanian Stevedoring Companies	

The last group of "regulators" refer to classification societies. When overviewing these ones in the SBSR, the distribution of them tends to be equal. However, most of them refer to the same organisations, but have a status of branch or are established in the particular region. There can be listed following classification societies in the SBSR:

- Bureau Veritas (DK), (DE), (LT);
- DNV (DK), (DE), (LT), (PL), (SE);
- Germanischer Lloyd (DK), (DE);
- Lloyds Register (DK), (PL);
- Polish Register of Ships (PL);
- SIS (SE);
- CIMET (SE).

Beside the regulation institutions providing with the norms and normative information, there can be

Table 8. Consulting companies, organisations and associations

Danish Gas Technology Centre (DK)	Sweco Lietuva (LT)
Rambøll Oil & Gas (DK)	DNV Poland (PL)
Grontmij (DK)	Polish Register of Ships (PL)
Force Technology (DK)	AGA AB (SE)
IMAVIS – Maritime Wirtschafts- und Schiffbauforschung GmbH (DE)	CRYO AB (SE)
Marinesoft – Entwicklungs- und Logistikgesellschaft mbH (DE)	Skangass AS (SE)
ATI erc GmbH (DE)	White Smoke Consulting (SE)
ATI Küste GmbH (DE)	Frederiet AB (SE)
FGW – Forschungs-GmbH Wismar (DE)	FKAB Marine Design (SE)
DNV Lithuania (LT)	Samson (SE)
Klaipeda Science and Technology Park (LT)	Mann-Teknik AB (SE)
Novikontas SCM, UAB (LT)	CIMET (SE)
Association "Baltic Valley" (LT)	DNV (SE)
NPPE Klaipeda Shipping Research Centre (LT)	

consulting companies, organisations or associations that may assist in LNG-related issues. To the key consultants in the SBSR can be ascribed (Table 8).

To finalise the stakeholder profile, it is inevitable to look at the end-users that will be approached in terms of LNG products, services etc. and thus are regarded of paramount importance for demanding and absorbing the knowledge and competence accumulated in the SBSR. Relevant for identification of end-users are, first, end-user technologies stakeholders that are already available in the SBSR. As end-user related technologies are understood technologies that refer to ship-owners and ship operators, land infrastructure (e.g. trucks, cars), industry power generation and gas grid (Table 9).

Table 9. End users of LNG

Østkraft produktion A/S (DK)	Marine Service GmbH Hamburg (DE)
Dong Energy A/S (DK)	Energobaltic (PL)
Clipper Group (DK)	AGA AB (SE)
FjordLine A/S (DK)	ETG (SE)
Lauritzen Kosan A/S (DK)	Volvo AB (SE)
Maersk Line Ltd (DK)	Wayne (SE)
Maersk LNG (DK)	Alfa Laval (SE)
Mols linien AS (DK)	AGA Gas AB (SE)
Rederiet færgen (DK)	AGA / Volvo Trucks (SE)

Bearing in mind the overview of the main stakeholders and players within the SBSR, it is, however, apparent that some of the identified actors across the SBSR can be ascribed to more than one type of the stakeholders and players, since some of them are simultaneously involved into more activities. Therefore, overlappings cannot be excluded. Nevertheless, when making a comparison of the key stakeholders pinpointed, it is evident that the highest proportion of the stakeholders and players consists of companies, where most of them are involved into maritime-related activities, i.e. shipping, ship repair and construction, as well as gas and oil supply. What appears to be at stake at the moment is the involvement of the authorities and public institutions into LNG activities and infrastructure. Hence, the promotion of LNG and awareness of LNG advantages might be limited to the business sector, thus gaining little consent in the public sphere and political support. Furthermore, when it comes to the assessment of the stakeholders and players, it can be argued that also the SBSR in general has available stakeholders and players relevant for the LNG supply chain, the bottlenecks tend to lie in LNG itself as a primary resource and its

Table 10. Matrix of LNG supply chain in the SBSR

Segment of the Supply chain	Short specification of the capabilities	Distribution of capabilities along the SBSR	Evaluation criteria	
			Existing	++
			Developing	+
			Planned	0
			Missing	–
Shipping	LNG feeder vessels		–	
	LNG bunker vessels	SE	++	
	Ship-to-ship bunkering (STS)	SE	++	
LNG Terminals	LNG Import terminal	SE / LT & PL	++ / +	
LNG onshore infrastructure	Small-scale export / bunker facilities	DE, DK, LT, PL	0	
	LNG bunker stations	DE, DK	0	
	LNG filling stations	DE	0	
	LNG fuel tank containers	DE	++	
	LNG trucks	SE	++	
End-users	Tank & bunkering solutions	SE, DK	++	
	Shipping	SE, DK	++ / +	

supply or export. On the contrary, when it comes to those components of the LNG supply chain that refer to LNG shipping, potential locations for LNG importing (terminals), regasification, its storage, distribution and marketing, the region seems to reveal a sound potential for the utilisation of LNG in the future. From the data gathered it is apparent that there are actors capable of taking over the particular LNG activities within the LNG supply chain, for instance, ports, manufacturers, shipyards, consultants etc.

Conclusions

To anchor the capabilities presented in the region concerned, the following matrix was delineated. On the one hand, this matrix embraces the information reflecting what parts of the supply chain and to what extent entail developed knowledge and competence portfolio, which, in turn, is capable to support businesses to with the LNG-related knowledge and technologies. On the other hand, the matrix unveils the capabilities of the SBSR supply chain more specific how LNG-related infrastructure has been handled at present and will be dealt with in the next future.

References

1. MF Boknafjord – the world's largest gas ferry, 2012, http://www.dnv.com/industry/maritime/publicationsanddownloads/publications/updates/ferry/2012/01_2012/mf_boknafjord__theworldslargest_gas_ferry.asp, accessed on 20 March 2012.
2. Polskie LNG: Works on Second Swinoujscie LNG Tank Progressing Well, 2011, http://www.lngworldnews.com/polskie-lng-works-on-second-swinoujscie-lng-tank-progressing-well/, accessed on 9 July 2012.
3. Polskie LNG – LNG Re-gasification Methods, http://en.polskielng.pl/lng/re-gasification-methods/, accessed on 9 July 2012.
4. GUCMA L., GUCMA M., BAK A.: Pilot Docking System – New Tool for Safe Maritime Operation. 2012, 1–11.
5. Poland at Sea – Review of Polish Maritime Industry, 2012, http://www.portalmorski.pl/resources/poland-atsea/poland_at_sea_2012.pdf, accessed on 9 July 2012.
6. http://whitesmoke.se/files/WS1%20web.pdf, accessed on 19 November 2012.
7. LNG Hybrid Barge, http://www.lng-hybrid.com/2_projects/barge_intro.html, accessed on 19 November 2012.
8. LNG Hybrid Ferry WattenLink, http://www.lng-hybrid.com/2_projects/fering_data.html, accessed on 19 November 2012.
9. LNG fuel tank containers, 2013, http://www.marine-service-gmbh.de/content.php?seitenid=5, accessed 12 January 2013.
10. Viking Grace, 2013, http://www.vikingline.com/en/Investors-and-the-Group/Safety-environment/Environment/Viking-Grace/, accessed on 11 January 2013.
11. Fjord Line LNG cruise ferries, 2013, http://www.fjordline.com/Our-ships/Our-new-ships/Environmental-profile, accessed on 11 January 2013.

Scientific Journals
Maritime University of Szczecin

Zeszyty Naukowe
Akademia Morska w Szczecinie

2013, 36(108) z. 1 pp. 70–75
ISSN 1733-8670

2013, 36(108) z. 1 s. 70–75

Satellite navigation systems applications, the main utilization limits for maritime users

Jacek Januszewski

Gdynia Maritime University, Navigation Department
81-345 Gdynia, al. Jana Pawła II 3, e-mail: jacekjot@am.gdynia.pl

Key words: satellite navigation, positioning systems, ship's position, maritime users, limits

Abstract
Nowadays (October 2013) information about ship's position is obtained generally from specialized electronic positioning systems, in particular, at present functionally satellite navigation systems (SNS) as GPS and GLONASS, and satellite based augmentation systems (SBAS) as EGNOS, WAAS and MSAS. Two next SNS, Galileo and BeiDou, and two next SBAS, GAGAN and SDCM, are under construction. After all the user of these systems, the maritime user also, continually meets and will meet with numerous different limitations of SNS coverage in restricted area, SBAS and DGPS reference stations coverage area, the lack of integrity information about the systems, and of many charts referred to WGS–84 datum, with problem of position fix in restricted area, etc.

Introduction

Nowadays information about ship's position is obtained generally from specialized electronic positioning systems, in particular, at present functionally global satellite navigation systems (SNS) as the GPS and the GLONASS, and satellite based augmentation systems (SBAS) as EGNOS, WAAS and MSAS. Next SNS and next SBAS are under construction [1, 2, 3, 4, 5, 6]. SNS and SBAS are being developed and deployed by governments, international consortia and commercial interests. The generic name given to all these systems is Global Navigation Satellite Systems – GNSS.

The accuracy of all SNS has improved continually over the last years. However, the accuracy which can be expected today (October 2013) remains in the order of several meters (95% confidence level), which can prove inadequate for certain applications. IMO A.915(23) summarizes requirements on GNSS based on the specification of several horizontal position errors taking into account operation areas and applications. Other main utilization limits in SNS and SBAS applications concern the lack of full information about all details of these systems, the lack of many charts referred to WGS–84 datum, the availability of SNS in restricted area and SBAS at high latitudes, local interference, sensitivity to ionospheric effects and scrambling.

Information about satellite and based augmentation systems

As performance parameters and operation capability of GPS and GLONASS change permanently the user must have access to information about current status of these SNS. The information can be found in Internet but at sea in many cases this medium is not available for navigator. SNS status, which satellites are healthy and which unhealthy, theirs azimuths and elevation angles etc. can be known by the user only if the ship's receiver is professional. However, the knowledge of these parameters can be very helpful for the accuracy and reliability estimation.

Information about current status of SBAS must be taken into account if on the ship's the navigator uses integrated, SNS, and one, two or three SBAS, receiver, but at the time of this writing the number of these receivers is on the ship's bridges small still. On the contrary many GPS receivers installed

on the ships have the possibility to work in differential mode also, in this case the use of volume 2 of Admiralty List of Radio Signals (ALRS) is indispensable [7].

Since 2010 the edition of volume 2 (NP282) only lists the details of known operational radiobeacons used to transmit DGPS and DGLONASS corrections. Information about several dozen radiobeacons with status on trial or planned are now not published [7]. This change is very inconvenient for all DGPS users, maritime navigator, in particular. Volume 2 of ALRS should only be used once fully updated by Section VI Weekly Notices to Mariners [8]. As these Notices can be obtained from authorized Admiralty Distributors (in ports, but no all), or from the United Kingdom Hydrographic Office Website [8] and continually approximately only 50% of the ships has access to Internet at sea it means that many SNS and SBAS users during several weeks of the voyages can be deprived of current information about these systems.

The distribution in the world of more than 280 currently operational radiobeacons, with the information about theirs details (8 parameters) and integrity monitoring is showed in the table 1. The greatest and the lowest number of these radiobeacons are in Asia & Europe (both 95) and in Africa (6) & South America (13), respectively. In the case of some number of radiobeacons (59) this information is incomplete, in particular it concerns 40 radiobeacons without information about integrity monitoring, especially in Europe and North America. The most of radiobeacons (82%) provides integrity monitoring [7]. The IALA recommendation R-121 summarizes requirements on maritime differential GNSS (DGNSS) services in the MW frequency band. Though integrity aspects are mentioned, there doesn't exist a clear specification of integrity requirements and implementation guidelines.

Coverage, range and accuracy limitations

Currently, only SNSs have global coverage, but user's position with nominal accuracy can be obtained in open area solely. All SBAS and DGPS reference stations have limited coverage or range, respectively. Additionally, the users of these systems meet some limitations in restricted area, i.e. the area where because of the obstacles some satellites above horizon or masking elevation angle of the receiver cannot be visible by the observer.

Global satellite navigation systems in restricted area

Actually two SNS, GPS (American) and GLONASS (Russian) are fully operational, two next, Galileo (European) and BeiDou (Chinese) are under construction. All these systems assure or will assure the nominal accuracy but in open area only. However, considering the opportunity of dual frequency positioning in combination with an increased number of available GNSS signals, the position's accuracies in the order of several meters could meet the requirements for some coastal areas.

In restricted area the position accuracy can be decreased when the masking elevation angle causing by the obstacles is greater than masking angle of observer's receiver. The diminution of GPS position accuracy in restricted area is currently less than still few years ago because of the actual number of fully operational satellites, at least 30, is greater considerably than this number in nominal constellation (24 only).

This limitation concerns car navigation in urban canyon mainly, but in some cases maritime navigation also, e.g. ship sailing in the narrow strait or along the height coast. The increasing of dilution of precision (DOP) coefficients values depends then on the height of the coast, the distance between the observer and the coast, the ship course and the ship antenna height. The calculations of these coefficients and the study of the possibility of

Table 1. Distribution in the world of the radiobeacons transmitting DGPS and DGLONASS corrections, information about details of services and integrity monitoring [7]

Continent	Number of radiobeacons								
	Total	All details of services known		Integrity monitoring					
				Yes		No		No information	
		Number	%	Number	%	Number	%	Number	%
Africa	6	6	100	6	100	0	0	0	0
Asia	95	87	92	91	96	0	0	4	4
Australia	16	0	0	16	100	0	0	0	0
Europe	95	74	78	73	77	0	0	22	23
North America	58	45	78	44	76	0	0	14	24
South America	13	12	92	2	15	11	85	0	0
Total	283	224	79	232	82	11	4	40	14

position determination were made among others by author for different values of all mentioned above parameters [9, 10].

As in restricted area (e.g. on the ship's bridge), the accuracy of the user's position obtained with GNSS can be less than in open area, considerably, and in some cases cannot be obtained, additional provision of navigational data and correction to existing GNSS must be used. Actually one of these methods is Assisted-GPS (A-GPS), a support given to stand-alone GNSS receiver, new technology that uses an assistance server to cut down the time needed to determine a location using GPS (Time To First Fix – TTFF). With unassisted SNS TTFF including the process of locating the satellites, receiving the data and achieving a position fix, can take several minutes. A-GPS can be used in all SNS today and in the future. It can be defined as a system where outside sources, such as an assistance server and reference network, help a GPS receiver perform the tasks required to make range measurements and position solutions [11, 12].

Radiobeacons transmitting DGPS and DGLONASS corrections

One of the most important parameter of the radiobeacons transmitting DGPS and DGLONASS corrections is an approximate indication of the range in nautical miles within these corrections may be received. The range of 270 operational radiobeacons is presented in the table 2.

The range of the majority of radiobeacons (51.2%) is less than 150 Nm, range 250 Nm or greater has 5.3% of radiobeacons only (Table 2). In the case of 13 radiobeacons (4.6%), all 11 in Australia, in particular, information about range is not provided. The greatest (300 Nm) and the lowest (60 Nm) range has Kokole Point, Hawaii and Robinson Point, Washington, respectively, both in United States. Two polish radiobeacons have the same range 80 Nm [7].

Table 2. Range [Nm] of 283 radiobeacons transmitting DGPS and DGLONASS corrections [7]

Range [Nm]	50–99	100–149	150–199	200–249	250–299	≥ 300	No information	Total
Number	13	132	77	33	14	1	13	283
Percentage	4.6	46.6	27.2	11.7	4.9	0.4	4.6	100

The range of radiobeacons is limited because of the effect called "spatial decorrelation". With increasing distance of the user's receiver to the reference station, the atmospheric influences on the satellite signals get more different and the correction get less and less accurate. Even worse, due to the large distance the user's receiver may receive information about Pseudo Range Correction (PRC) from completely different satellite where no correctional information are provided in the correctional data.

Geostationary satellites transmitting SBAS messages

Actually, three SBAS, EGNOS (Europe and North Africa), WAAS (North America) and MSAS (Japan), are operational, two next, GAGAN (India) and SDCM (Russia), are under construction. The numbers of monitoring, master and land uplink stations for five SBAS are presented in the table 3 [2, 4, 5].

The area covered by SBAS depends on where monitoring stations are located and if signals from geostationary satellites are being received. These satellites positioned in the equatorial plane are vertically above a user located at the Equator. Therefore, the further a user travels towards the north or south pole, towards high latitudes, the more the satellite is too close to the horizon, it is no longer usable. At latitude 70° GEO satellite is visible at about 10° above horizon in open area, at latitude 75° this angle is 5° only. As 5 degrees is the most frequently used in the receivers masking elevation angle value, it means that beyond latitude 75° SBAS service becomes barely usable. Additionally, the user must take into account that if his longitude differs from GEO satellite longitude the highest latitude at which this satellite can be visible is less. The characteristic orbit of the GEO satellites may be degraded, and in consequence some far North regions of the service area may be covered with only one GEO satellite during some periods of the day and may experience some degradations in availability performance [13].

Currently, the coverage area of three operational mentioned above SBAS is limited to north hemisphere only, since there are no possibility to calculate corrections because of no sufficient number of monitoring stations in south hemisphere. Only then new additional stations in south hemisphere will be operational all three currently used SBAS will cover all continents (except for Arctic and Antarctica) as well as all principal offshore tracks.

At middle latitudes (40–60)° satellites GEO are visible by the user at angle 40° or lower. It means that in these areas, in urban canyons and mountains regions, in particular, SBAS cannot be used because its satellites are invisible to users. That's why Japan decided to create new augmentation system

Table 3. The ground segment of different Satellite Based Augmentation Systems SBAS, currently and in the future [2, 5, 6, 14]

System	Number of stations, regions			
	monitoring		Master (control)	Land (Earth) Uplink
	current	future		
EGNOS	39 29 – Europe, 1– Algeria, 1 – Israel, 2 – Egypt, 1 – Canada, 1 – RPA, 1 – Jordan, 1 – Tunisia, 1– Morocco, 1 – Mauretania	7 5 – South Africa, 2 – Madagascar	4 Europe	6 Europe
WAAS	38 20 – USA (CONUS), 7 – Alaska, 1 – Hawaii, 1 – Puerto Rico, 4 – Canada, 5 – Mexico	13 10 – South America (coast), 2 – Brazil (interior), 1 – Middle America	3 USA	4 USA
MSAS	6 Japan	9 6 – Australia, 2 – New Zealand, 1 – Indonesia	2 Japan	2 Japan
GAGAN	15 India	0	1 India	1 India
SDCM	21 19 – Russia, 2 – Antarctica	6 2 – Russia, 1 – Australia, 1 – Brazil, 1 – Indonesia, 1 – Nicaragua	1 Russia	1 Russia

QZSS (Quasi Zenith Satellite System) which will provide positioning services primarily to the users of urban transport, a GPS differential corrections service to a higher resolution than Japanese SBAS, MSAS, in particular. The QZSS constellation will comprise three satellites in separate geosynchronous orbits, inclined to the equator at 45°, there is always at least one satellite over Japan at a high elevation angle, 70° or more [15, 16]. QZSS is expected to improve positioning availability from 90% to 98%. This system will not improve positioning in the Asia-Pacific region, also at sea for maritime users, but is expected to improve the capacity to respond to natural disasters [5].

The main limitations

Each user of SNS and SBAS must take into account the different kinds of limits from the lack or incomplete integrity to the problem of receiver's antenna installation on the ship.

Problem of integrity

In the literature various definitions of integrity exist. According to [8] integrity can be defined as the ability of a system, SNS also, (structure and user) to provide positioning with an associated level of confidence. As today integrity is not available within all currently SNS (GPS and GLONASS), GPS is planning to implement it within the third generation of this system, the GPS III, in the case of Galileo system integrity will be assured by one from services, Integrity Monitoring Service. The former Safety of Life service is being re-profiled. SBAS have been developed with two main goals: accuracy improvements and requirements for integrity. The second is clearly identified as the most important and has been the main guide for system definition. As SBAS provides integrity externally the user is provided with differential corrections of known quality, and does not need to perform checks to mitigate the effect of large satellite biases. SBAS is enable to detect and estimate receiver errors at the user side [18]. It means that currently SBAS integrity is assured in these regions of north hemisphere only where the user can receive the corrections from GEO satellites. The integrity information but only about selected satellites and no about whole system can be provided by radiobeacons transmitting DGPS and DGLONASS corrections. Currently 82% of them has ability to provide timely warnings to users when it should not be used for navigation and also to verify the validity of the DGPS broadcast (Table 1). However, the timely warnings are generated on methods differing on the applied algorithms and used threshold.

Local interference, breakdown and malfunction

All SNS and SBAS use a frequency band, 1.1–1.6 GHz, that is protected by the International Telecommunication Union (ITU). It is possible that during some period in some specific locations, spurious transmissions from services operating in adjacent or more remote frequency bands could cause harmful interference to the signals of just used SNS and SBAS. Depending on the level of this interference, the effect on the user receiver may be a degradation of the position accuracy or a total loss of the navigation service in case the interfering signals preclude the tracking of navigation signals [13].

In the event of system breakdown or malfunction, e.g. clock drift, broadcasting of erroneous

data, the pseudorange measurement can be biased by anything from a few meters to a few kilometres. Due to the system architecture, and specifically the limited number of SNS ground stations, these errors may impact the user for several hours (6 hours maximum) [19].

Sensitivity to ionospheric effects and to scrambling

Under some circumstances due to solar activity and in some specific regions of the Earth, for boreal and subtropical latitudes, in particular, ionospheric disturbances, called also scintillation, will affect the SNS and SBAS signals and may cause the complete loss of these signals for a short period time. It means that the position solution may be affected by sudden jumps when satellite signals are lost due to scintillation. If the number of tracked satellites drops seriously, the position accuracy decreases considerably, if this number is less than 4, a 3-dimensional position may not be available [13, 20]. It depends on HW and SW receiver design, some professional receivers have e.g. the capability to overbridge short term disturbances on single signals.

The physical parameters of ionosphere have a direct influence on propagation delay, therefore, they cause significant user's position error. That's why to eliminate ionospheric error single frequency GPS receivers get correction data from satellite message or, if it is possible, apply SBAS or DGPS ionospheric corrections, while dual frequency SNS receivers use the measurements on two transmitted satellite frequencies [21].

As all SNS and all SBAS signals are received on the ground at very low power levels, they are relatively susceptible to scrambling, deliberate or otherwise [19]. In the case of GPS system when the satellite signal reaches the user's receiver on the Earth, the received signal power is about 100 attowatts only, 1 atto means 10^{-18}. This power is when the receiver is outdoors; when this receiver moves indoors, the signals rapidly get weaker, by 10–100 times in a house, and by 100–1000 times or more in a large building. The weak signal is a problem outdoors, also, the standard GPS receivers have trouble acquiring satellites with even the slightest interference or blockage [12].

Horizontal datums on maritime charts and satellite-derived positions notes

World Geodetic System 1984 (WGS84) is applied for GPS system. The most frequently used charts, in particular in Europe, are published by United Kingdom Hydrographic Office. On ship's bridge there are several hundred charts at least, often several thousand, but many chart are not yet referred to WGS-84 geodetic datum (also known as horizontal datum). That's more a problem of provided charts and data fusion on screens, ECDIS and INS.

Currently, the total number of charts published by UKHO is greater than 8000; almost 3000 (37%) are referred to WGS84, in this case position obtained from GPS receiver can be directly plotting on the chart. However, about 3400 (43%) charts are referred to several dozen local datums, the user must now select in the receiver the datum of the chart. If this datum is not available the user must search for Satellite Derived Positions Notes showed on the chart and take it into account. If these notes are not available the user must know that this effect may be significant to navigation. Positions referred to different datums can differ by several hundred metres or even more. The same consequences are in the case of about 1600 (20%) charts referred to unknown datum [7, 22].

Installation marine satellite navigation system antenna and screen unit on the ships

In order for the SNS unit to function as expected, the antenna must be mounted properly and the position of the SNS screen unit suitable. That's why the SNS user's receiver should be a minimum of a meter away from any obstruction that may interfere with maintaining line-of-sight to the satellite. Radio whips, radar arrays and any metal assemblies on the roof of the ship must be accommodated. The receiver cable should be routed to pass through a vertical surface on the pilothouse if it is not being used on an "open" boat. The receiver cable cannot be spliced or extended, making if the most critical consideration. The user must keep the SNS screen unit out of direct sunlight will maximize screen visibility and prevent ultra-violet (UV) degradation of the screen [23].

Conclusions

- Differential mode of SNS have been developed in response to inherent and previously imposed limitations of SNS;
- SNS and SBAS users meet different kinds of limitations, some of them, e.g. propagation conditions are independent of the users, some depend on theirs decision, e.g. receiver's parameters. DGPS users meet apart from restricted range of reference station often limitations concerning the lack complete information, integrity monitoring, in particular;

- The lack integrity is one of the most important weakness and at the same time limitation of the current stand–alone GPS system, which is a paramount requirement for safety critical applications. Missing integrity information will be a problem, if it is needed but not provide. The next generation of this system, GPS III, will have very good accuracy and integrity, good enough for most navigation, maritime, in particular;
- Assisted-GPS technology offers significant performance advantages over either stand-alone GPS or mobile-station-based, particularly at low power levels often associated with consumer applications, as accuracy, availability, and coverage at a reasonable cost;
- The most frequently used SNS receivers are single-frequency receivers, all SBASs has been designed to operate in single-frequency mode; this can give rise to degraded service availability in the event of very strong ionospheric turbulence;
- SNS receiver designed for the ship navigating around the world must have in its software all datums on which the charts of navigation bridge, often several thousand, were published;
- SNS errors or breakdown can have serious repercussions for user safety if not detected in time and have the effect of restricting the number of possible applications. In particular, they make the system unsuitable for some applications, e.g. maritime navigation in restricted area.

References

1. BENEDICTO J.: Galileo Programme Status. Satellite Navigation Summit, Munich 2011.
2. JANUSZEWSKI J.: New Satellite Navigation Systems and modernization of current systems, why and for whom? Scientific Journals Maritime University of Szczecin 32(104) z. 2, 2012, 58–64.
3. www.glonass-ianc.rsa.ru
4. www.gps.gov
5. www.gpsworld.com
6. www.insidegnss.com
7. Admiralty List of Radio Signals. (2011/2012) vol. 2, NP 282 The United Kingdom Hydrographic Office, Tauton.
8. www.ukho.gov.uk
9. CALINI G.G.: Emerging challenges for GNSS in Maritime Transport. Munich Satellite Navigation Summit, 2012.
10. JANUSZEWSKI J.: Satellite navigation systems in coastal navigation. Scientific Journals Maritime University of Szczecin 29(101), 2012, 45–52.
11. JANUSZEWSKI J.: (2010) Assisted-GNSS, why, where and for whom? Communications in Computer and Information Science 104, 2010, 142–151.
12. VAN DIGGELEN F.: A-GPS: Assisted GPS, GNSS, and SBAS. Artech House, Boston/London 2009.
13. EGNOS Open Service, Service Definition Document V. 2.0, 2013.
14. www.navcen.uscg.gov
15. HOFMANN-WELLENHOF B. et al.: GNSS Global Navigation Satellite Systems GPS, GLONASS, Galileo & more. Springer, Wien, NewYork 2008.
16. www.qz-vision.jaxa.jp
17. SAMAMA N.: Global Technologies Technologies and Performance. John Viley & Sons, New Jersey 2008.
18. JANUSZEWSKI J.: Satellite navigation systems integrity today and in the future. Monograph "Advances in Transport Systems Telematics", Edited by Jerzy Mikulski, Wydawnictwa Komunikacji i Łączności, Warszawa 2009, 123−132.
19. www.ec.europe.eu
20. KAPLAN E.D., HEGARTY C.J.: Understanding GPS Principles and Applications. Artech House, Boston/London 2006.
21. JANUSZEWSKI J.: How the ionosphere affects positioning solution using terrestrial and satellite navigation systems. Communication in Computer and Information Science, Telematics in the Transport Environments 329, 2012, 249–257.
22. JANUSZEWSKI J.: The problem of compatibility and interoperability of satellite navigation systems in computation of user's position. pp. Artificial Satellites, Journal of Planetary Geodesy 3, Vol. 46, 2011, 92–103.
23. www.ehow.com

Other

24. JANUSZEWSKI J.: Comparison of Geometry of Galileo and GPS in maritime and urban restricted area. Annual of Navigation 6, 2003, 37–48.

Scientific Journals
Maritime University of Szczecin

Zeszyty Naukowe
Akademia Morska w Szczecinie

2013, 36(108) z. 1 pp. 76–79
ISSN 1733-8670

2013, 36(108) z. 1 s. 76–79

LNG market trends

Wiesław Juszkiewicz

Maritime University of Szczecin, Faculty of Navigation, Institute of Marine Traffic Engineering
70-500 Szczecin, ul. Wały Chrobrego 1–2, e-mail: w.juszkiewicz@am.szczecin.pl

Key words: LNG market, natural gas, marine market trends, LNG carriers, transport of gas

Abstract

Natural gas, being the cleanest burning fossil fuel, will play a key role in the future. Liquefying natural gas lets moving it to regions where pipeline transport is not possible, allowing end-use markets access to natural gas. LNG is more energy dense than gaseous natural gas, so there using fields are still increasing in end-use applications, e.g. different types of transportation (heavy duty vehicles, marine or rail applications). Global LNG demand is expected to grow, mostly because of new economic markets from Asia and Middle East.

Introduction

Natural gas is mainly composed of methane, but it can also contain traces of ethane, propane and other heavier hydrocarbons and small quantities other components. The liquefaction process to obtain LNG requires separation of some of its components, and then the gas is cooled to –163ºC.

The LNG value chain consists of the processes and stages of liquefied natural gas from the reservoir to end consumers and is represented by four stages [1]:

– exploration and production (15–20% of costs);
– liquefaction (30–45% of costs);
– maritime transport (10–30% of costs);
– storage-regasification (15–25% of costs).

The LNG carriers transport the LNG from the liquefaction plant to the regasification terminal, which is located in the destination country near to end consumers. These carriers are designed to transport the LNG under cryogenic conditions, thus reducing the volume of the gas by a factor of around 600 and providing the consequent cost savings.

The LNG trade

Based on a geographical classification of the LNG markets, the following regions could be highlighted due to their importance: Asia-Pacific, Europe and North America (Fig. 1). But another possible classification could be the differentiation between the Atlantic Basin and the Pacific Basin. However, it is important to distinguish separately (due to its characteristics) the North American market: East and West Coast.

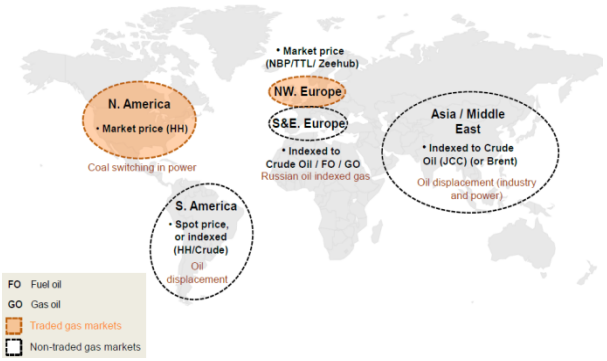

Fig. 1. Gas pricing mechanisms by region [2]

The main gas hubs of both LNG and pipeline gas are:

– United States (Henry Hub);
– The United Kingdom (NBP);
– Europe (Zeebrugge in Belgium).

Because historical and geographical separation it should be understanding that LNG markets are sensible independent and LNG prices are different in each hub (Fig. 2).

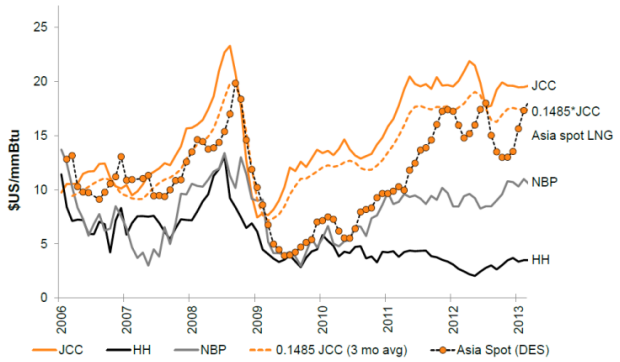

Fig. 2. Global LNG price divergence [2]

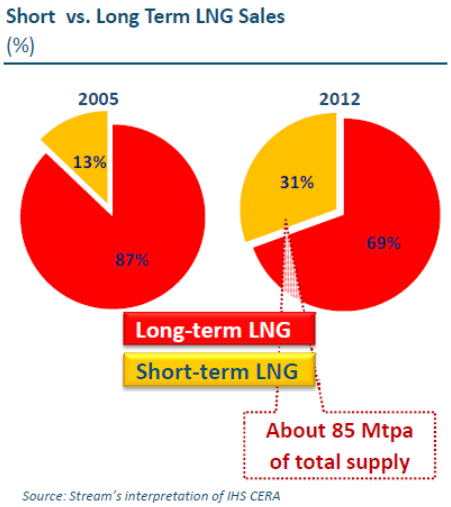

Fig. 3. Global LNG price divergence [2]

Another important change in LNG market are contracts. At the beginning almost all contracts were long terms agreements but in the last years short terms start be more popular (Fig. 3) and represent almost 1/3 LNG demand.

But it should be taken into consideration that long term contract are still the main way of LNG contracting and hasn't changed in essence. Short term contracts are the second market which make LNG market more flexible. This part of LNG market could balance expected supply gap within next years. According to Stream Repsol-Natural Gas LNG forecast in 2015 non contracted LNG gap (due to demand increase and contract expiration) will be about 180 Mtpa (Fig. 4).

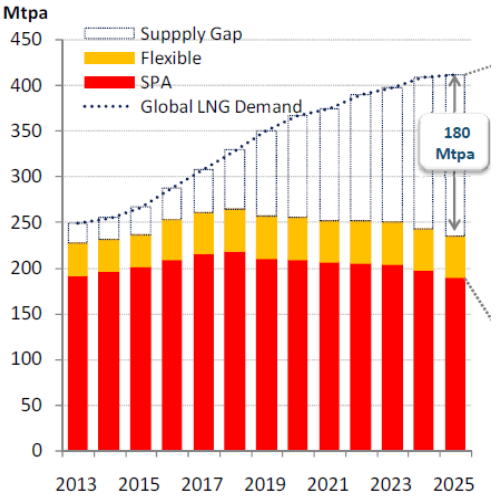

Fig. 4. Non contracted LNG Supply gap [3]

An increase in future flexibility (in terms of volumes and pricing) will depend strictly on the evolution of new and present LNG exporter projects.

Fig. 5. Current and planned LNG importing countries [1]

The LNG market trends

The LNG market has doubled every 10 years in the last two decades from some 50 mt in 1990 to over 240 by 2011. In 2001, the world had 40 LNG regasification terminals in 11 countries. By the end of 2011 there were 89 regasification terminals in 25 countries, more than doubling in the space of a decade [4].

All LNG market analysis lead to conclusion that global gas demand is projected to grow up to 2–2.6% per year [4, 5]. Main reasons of this trend are:

– predicted strong economic growth;
– energy regions or countries policies;
– other energy sources influence.

Of course there are some unexpected influencing factors (shorter or longer time of influence) as Fukushima case or seasonal weather anomalies but for long-range prospects they are not so important.

At the same time LNG demand is expected to grow at 5% per year so total gas demand by 2030 will represent 16–17% of total demand [2, 5] but of course there are some regions where LNG demands will increase more rapidly in comparison with another.

Natural gas is the only fossil fuel for which global demand grows in all scenarios, showing that it fares well under different policy conditions; but the outlook varies by region. Two thirds of the growth in LNG demand is expected to come from Asia (China, India) and the Middle East but gas market in Europe will see relatively minor growth (Fig. 6).

Demand growth in China, India and the Middle East is strong. Active policy support and regulatory reforms push China's consumption up from around

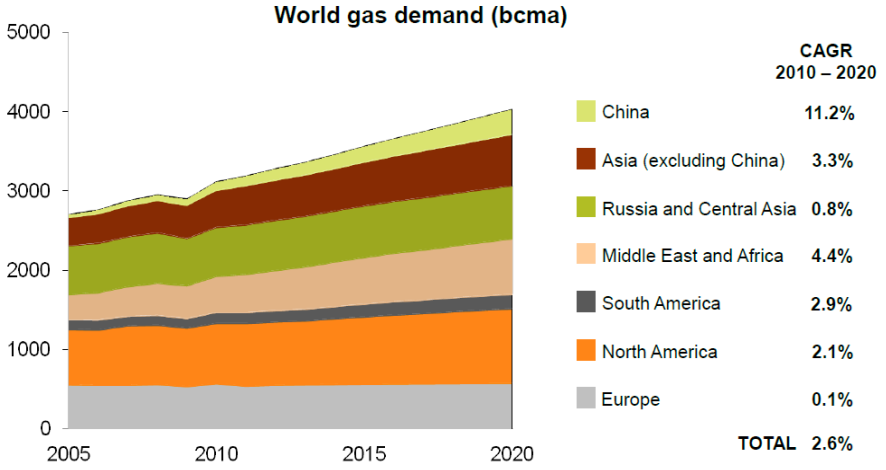

Fig. 6. An example of the prognossis of natural gas demand growth [2]

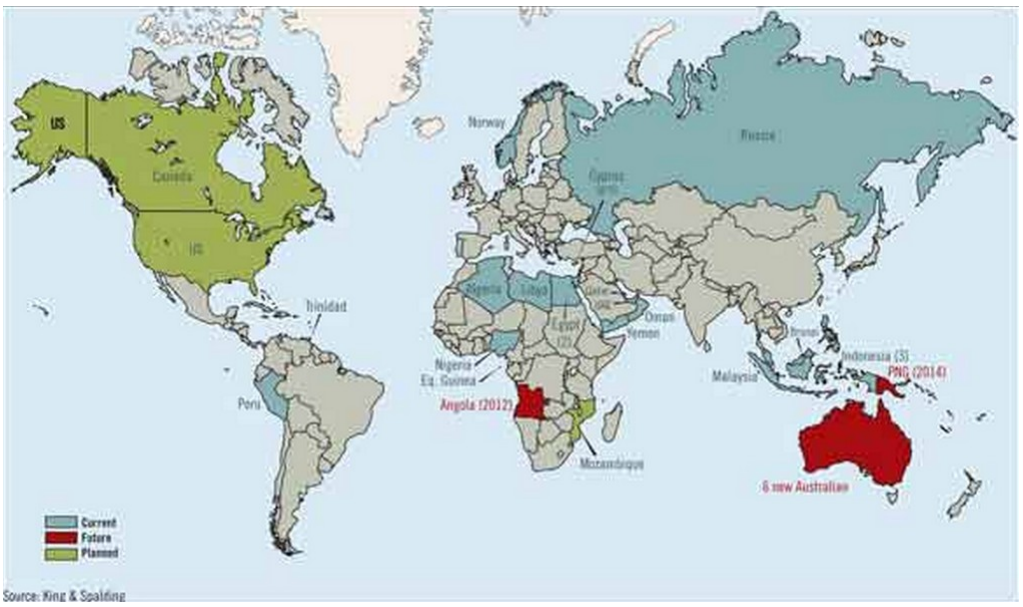

Fig. 7. Current and planned LNG exporting countries [6]

130 billion cubic metres (bcm) in 2011 to 545 bcm in 2035. In the United States, low prices and abundant supply see gas overtake oil around 2030 to become the largest fuel in the energy mix. Europe takes almost a decade to get back to 2010 levels of gas demand: the growth in Japan is similarly limited by higher gas prices and a policy emphasis on renewables and energy efficiency [7].

Parallel to LNG importers market changes the global LNG market is changing. New LNG industry projects are planned both by actual and new LNG exporters. Further changes could be seen as unconventional LNG export projects. The rapid developments in unconventional natural gas (especially North American shale gas and Australian coalseam gas – CSG) have changed the LNG market. New discoveries off East Africa should introduce Mozambique and perhaps Tanzania into the top ranks of the world's LNG exporters. Australia is currently forecast to become the world's largest LNG exporter, surpassing Qatar by 2020 [6] (Fig. 7).

Conclusions

Gas and especially LNG (because of it transportation flexibility) will still play very important role in the global energetistic politics. The growth in gas demand will require investments, innovation, and interdependency between the supply and demand countries.

It is very important that gas and LNG demand could have good influence to the environmental emissions reduction and promote renewable energies sources. The development of floating liquefaction and regasification technologies, which include small and medium scale projects may promote the development of new reserves and markets.

References

1. LEROY P.A.: History, trends and prospects for LNG shipping. International Seminar "Energy and Shipping", IENE, Athens 2012.
2. SPOMER B.: Natural gas challenges and drivers for the future. Energy Institute's IP Week, London 2013.
3. AGUIRRE I.: New trends in LNG contracts. http://www.streamlng.com
4. STINIS H.: LNG trade flows. 17th International Conference & Exhibition on Liquefied Natural Gas (LNG 17), Houston 2013.
5. ROGERS H.: Globalising gas markets – is convergence in prospects?
6. WEEMS P.R., SALO M.: Global LNG 2012 and beyond must address many questions. http://www.ogj.com
7. World Energy Outlook 2012 (Released on 12 November 2012).

Others

8. BRATHWAITE L.D., DEAVER P., JONES M., KENNEDY R., MILLER R., PUGLIA P. WOOD W.: 2012 Natural gas market trends.
9. TOCA A.: Characteristics and evolution of the main LNG markets. Cuadernos de Energía – Club Español de la Energía, October 2010.

Scientific Journals
Maritime University of Szczecin

Zeszyty Naukowe
Akademia Morska w Szczecinie

2013, 36(108) z. 1 pp. 80–84
ISSN 1733-8670

2013, 36(108) z. 1 s. 80–84

Characteristics of vessel traffic monitoring functions in the Navi-Harbour 5000 system

Wiesław Juszkiewicz, Diana Kotkowska

Maritime University of Szczecin, Faculty of Navigation, Institute of Marine Traffic Engineering
70-500 Szczecin, ul. Wały Chrobrego 1–2, e-mail: {w.juszkiewicz; d.kotkowska}@am.szczecin.pl

Key words: VTS, VTS operator, traffic monitoring, traffic areas, navigation safety

Abstract

Increasing of the navigation safety level, especially in difficult and heavy traffic areas, is the main reason of VTS creation. The Navi-Harbour 5000 is the one of the newest systems created for VTS system management and it fulfils requirements included in IMO Resolution A.857(20). Main system functions of the vessels traffic movement monitoring are characterized in this article. The effectiveness of the VTS operator work should be increased by proper configuration and use these functions in everyday service.

Introduction

Vessel Traffic Service (VTS) can be defined as *"a service implemented by a competent authority, designed to improve safety and to improve vessel traffic and the protection of the environment. The service should be able to interact with the traffic and to respond to situations developed in the VTS area"* [1].

According to many papers and documents (including SOLAS chapter V rule 12) properly designed VTS should contribute to the level of safety of life at sea, safety and efficiency of navigation, the effective protection of the marine environment in the vicinity of the coastal zone and offshore installations increasing. It should prevent possible negative effects resulting from the traffic of the sea. The basic principles of the introduction and implementation of VTS systems were also defined in SOLAS Convention. Vessel traffic control system and VTS operating procedures should comply with guidelines of the International Maritime Organization (IMO) and the International Association of Marine Aids to Navigation and Lighthouse Authorities (IALA). Detailed guidance on the implementation of traffic control systems gives IALA Recommendation V-119, and the IALA Recommendation V-128 (IALA Recommendation V-128 Operational and Technical Performance Requirements for VTS Equipment) which refers to the operational and technical requirements of VTS equipment.

Depending on the operating range of the system the protection, terminal, route or sea VTS can be distinguished. Of course, the range of services provided by the system is the result of the area characteristics and desirable function to fulfill during supervision. An important component of any system are VTS operators. Only professionally qualified and competent staff properly equipped can provide a high level service.

The solution proposed by the Transas regarding VTS systems fully meets these requirements. The Navi-Harbour 5000 is one of the better-designed systems which let to create and manage vessel traffic services (VTS) at any area. It is designed to improve the safety of navigation and planning of traffic in coastal waters. This system meets the basic functions recommended by the IMO and has additional features (e.g., SAR, Special Operations on Zones).

In recommendations of IALA V-128 (IALA Recommendation V-128 Operational and Technical Performance Requirements for VTS Equipment) basic operational requirements of the VTS system are discussed, which include [2]:

– VTS radar system;
– Automatic Identification System (AIS);
– communication system;
– closed-circuit television (CCTV);
– hydro-meteorological monitoring devices;
– VTS database system.

The authorities while planning areas under the supervision of the VTS are required to establish a system of administrative management, which is responsible for the preparation of local regulations regarding the traffic control system (not conflicting with the provisions of A.857 (20) Resolution).

Characteristics of Navi-Harbour of Transas 5000 System

The Navi-Harbour system made by Transas allows to carry out all VTS functions, receive information about navigational situation and all tracked objects (in tabular or graphic form) and enable vessel traffic monitoring along the ability areas including the targets movement planning and appropriate alarms generating (according to the criteria set by the operator). The system also allows digital recording of all navigational situation data and thus the possibility of later retrieval and these situations analysis (which is particularly important in the event of failure or while vessels violate regulations in force in the waters covered by the system).

Main window of the system with data structures and system alarms tables is shown in figure 1.

The main menu contains a full list of functions to enable the user the proper execution of their duties. The acquisition of objects (with a choice of sources of information on the subject), the identification and implementation of data units, cargo, destination port and other relevant information, the ability to display data in tabular and graphical form (on a chart), their analysis in general terms of traffic and mutual threats occurring between the selected targets may be included to the basic functions of the system.

Since an operator must know and take into account existing regulations on areas under VTS surveillance it is also a great help, to configure the operating alarms available.

The most significant are:

- CPA / TCPA limits exceeded alarm;
- target manual / automatic acquisition;
- target manual / automatic drop from tracking;
- loss of sensor alarm due to lack of proper input signals;
- Zone Alarm – an alarm in special target zones;
- grounding on route alert when the vessel's grounding;
- XTE out on a route – established recommended route cross track error alert;
- course out of route alert when ship deviates from the recommended course;
- speed limit breach on route alarm when target exceeded recommended speed limits;

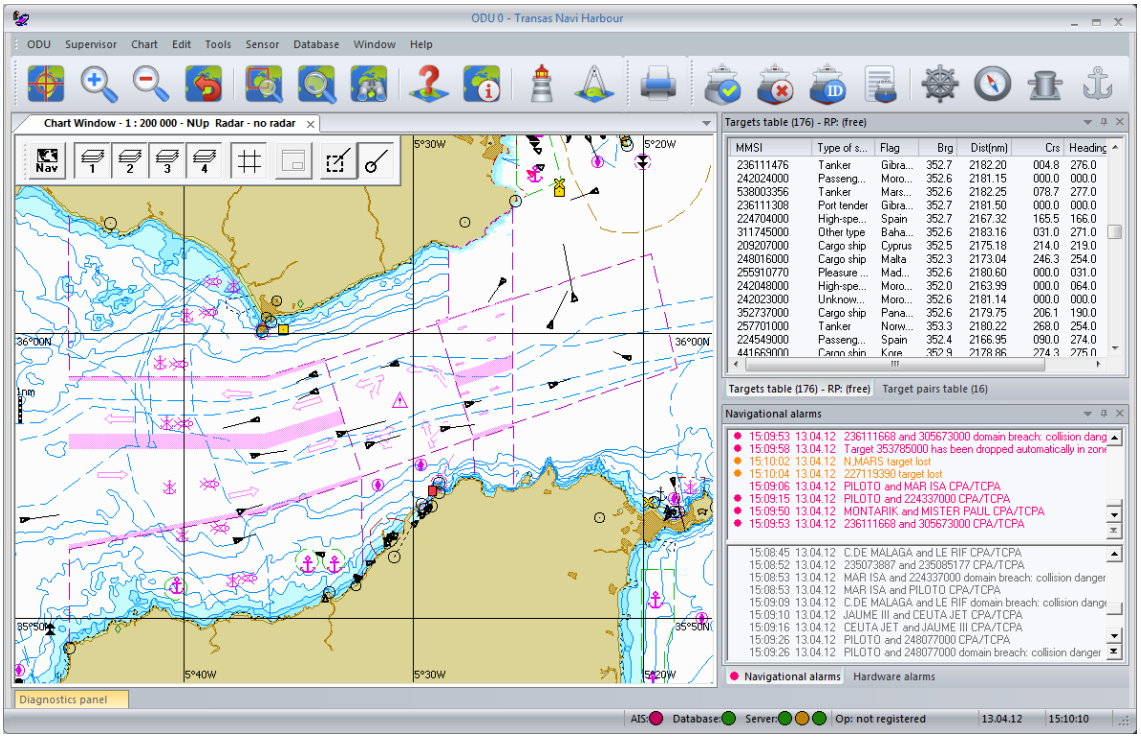

Fig. 1. Navi-Harbour 5000 – the main window of the system [3]

- enter / leave route line alarm when target exit / enter the recommended specified route;
- dangerous DTE alarm on exceeding the minimum distance to the edge of the fairway.

Effective use of the system, especially when service covers restricted water areas with diverse characteristics and where occurs heavy ship traffic, can't be limited only to the use of a basic set of functions. VTS operators knowing the capabilities of the system should also properly use additional functions that, when properly configured (taking into account the characteristics of the area and the operator's own needs) will be a significant help in supervision over the ships movement. The designation of special zones, routes or areas with recommended speed limits or traffic intensity, should ensure strict compliance with the local regulations and help to create standard procedure (using the same criteria) in case they are exceeded.

Characteristics of the vessel traffic monitoring functions available in the Navi-Harbour 5000

Recommended routes

The Navi-Harbour system allows you to create so-called designated/recommended routes (*Route Profile*). This function is particularly useful for systems to monitor the vessels traffic consisting mainly in canals, rivers or fairways and let to define a certain safe lane width. These are exactly the traffic lanes and consist of some segments of a certain adjustable width. The area of each segment is determined by crossing the centre line and determining an acceptable deviation of the vessel from the axis. In addition, you can specify the maximum and minimum speed limit on the selected section of route (Fig. 2).

Created route consists of a single lines so that ships are moving from one to the next waypoint. Each route has its own name and can contain any number of waypoints. The start and the end of the line are treated as reference points of the route. One line of the route may consist of several segments. Each of the recommended route has a set of individual parameters, the operator adapts to the requirements applicable to the area.

The use of recommended routes that were created involves assigment of moving ships to selected route. From that moment, the system monitors the positions of assignated targets in relation to the axis of created route and their speed. Of course, when the limits imposed by the operator are exceeded, corresponding alarm will be generated to turn operators attention to the incident. Alarm acknowledgment by the operator will automatically display on the screen the position of the offending vessel. Another advantage of the recommended routes is the ability to use them in the prediction of the expected vessels positions and to determine their potential passing positions with other vessels. The operator is able to determine the change in the speed of ships in order to obtain the correct passing positions. For this purpose operator should use the diagram *Route profile* (Fig. 3). In practice, it is used to determine the safety place of vessels passing positions on the fairways and channels. In the diagram, there are points that are essential for the system operator for the correct assessment of the situation on the fairway.

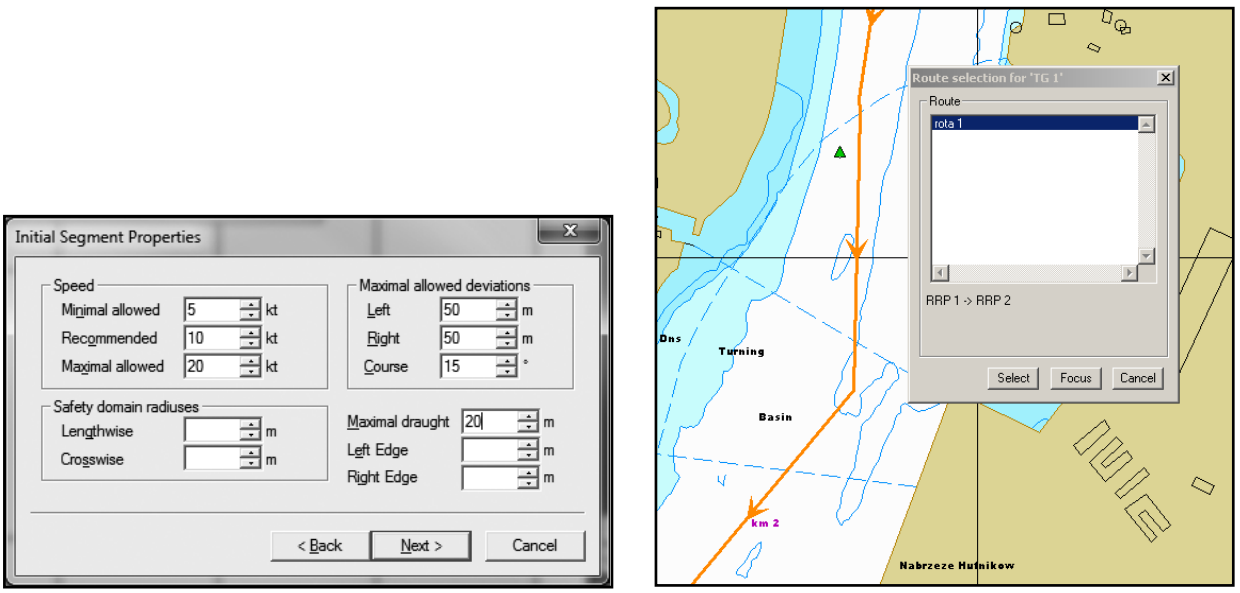

Fig. 2. The initial parameters and presentation of recommended route created on the chart [3]

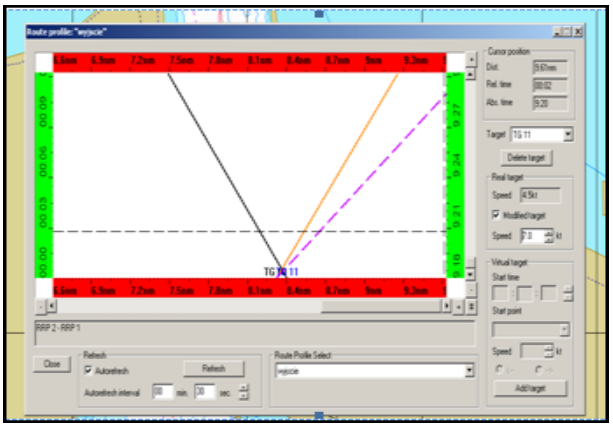

Fig. 3. Diagram *Route profile* for a selected recommended route

Additional possibility of using the diagram *Route profile* it is to generate virtual objects (Fig. 4), allowing the operator to plan the traffic planning on a given sector of the route for example when deciding whether to add new units to the traffic (leaving the berth, entering the fairway by units waiting at anchor).

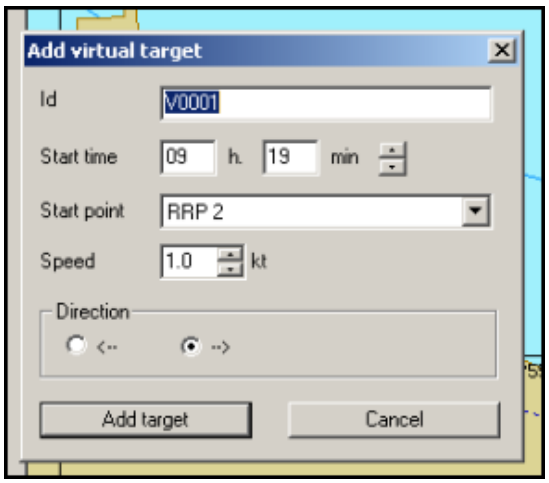

Fig. 4. Window to create a virtual object in the Diagram *Route profile*

Simulated echoes

In Navi-Harbour 5000 system, you can create so-called simulated echoes (Fig. 5). These are the objects artificially generated by the operator by entering information about the position, course and speed that can be obtained for example by direct radio communication with the ship, which the operator is not directly monitoring. This function allows you to enter information about ships that are on the radar, for which the information is also available in the AIS. This makes it possible to monitor the vessel presence until that echo appear on the radar screen and allows to acquire the object manually.

Before that happens, the operator can analyze the motion of the ship surrounded by other ships and (in the event of an emergency situation) to take appropriate action.

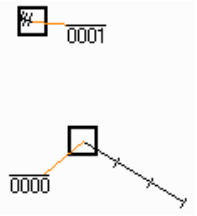

Fig. 5. Echoes simulated by the operator – Navi-Harbour 5000

Special areas of the Navi-Harbour system

The system allows the VTS operator to create special areas in which automatic tracking control is conducted. These areas are designated as special zones and can be identified as:

– traffic zone;
– auto acquisition zone;
– drop zone;
– responsibility zone;
– guard zone;
– zone special tracking mode.

The operator for each of these zones can set individual alarms generated only when a particular situation occurs in a specific part of the monitored area. This allows a better fit of alerting function to the specifications of the type of area, which can eliminate unnecessary alarms, useless for safety. This has an important impact on the way the operators response to the generated alarms, because too many unimportant or even unnecessary alarms may decrease his watchfulness and provoke automatic alarms reset without proper analysis.

The parameters of each alarm can be adjusted by setting the alarm status and determine its type (info, notice, warning or alarm). In the alarm parameters setting it is also possible to choose the alarm sound, the alarm text (text message alert) and the alarm delay. When alarm limits are exceeded selected zone alarm is generated and it can be found in the navigation alarms table.

With Traffic zone the user can create lines in vicinity of which the speed limit, the number of ships, banned sectors etc. can be generated. Designating the maximum or minimum speed on the fairway provides a necessary information for the operator about the traffic flow (no alarm) or breach of the rules (for example, the possibility of causing damage to jetty or vessels moored in the harbor). Exceeding any set value is indicated by the appropriate alarm and by showing the location of an alerted situation.

Depending on the operator's needs automatic acquisition zone could be created. In these areas,

objects start be tracked automatically. The system Navi-Harbour target acquisition object can be performed by radar or by using AIS data. The operator in a very simple manner may set automatic acquisition area. In this case the operator is notified by an alarm that a new object had been added to acquisition by automatic acquisition zone (Fig. 6).

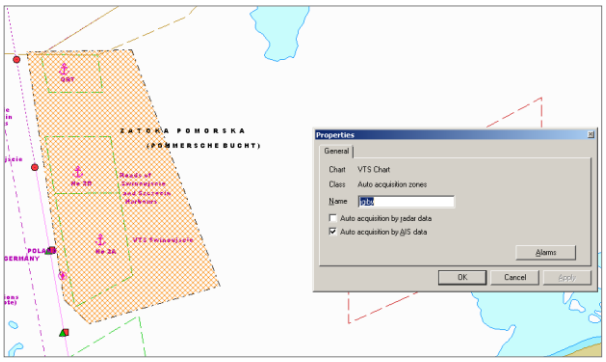

Fig. 6. Example of Nav-Harbour automatic acquisition zone

It is also possible to create zones where objects are automatically removed from tracking (Drop zones). There are two types of that type zone. The first type is a zone in which only lost objects are removed (Free zone). In this area, the operator also has the ability to set preferences so that the lost objects are not removed (keep), or objects would be deleted after a chosen time (after drop). There is also a possibility to enter a function "*always keep Identified*", which will cause that all lost objects will be deleted except identified ones. If operator selects "*continue moving after lost*", the movement of the lost object will be calculated according to the data available prior to disposal.

The second type of such zones (*No service*) are areas in which all objects will be removed. For such a zone it is only possible to set the parameters described above (*keep* and *drop after*).

Another important for the VTS operator areas are a safety zones (guard zones) designed to generate alarms when the object approaches the zones border (or exceeds it). Guard zones area settings enable the operator to make a decision for moving targets regarding to next manoeuvres without undue delay, which could arise as a result of an oversight of a particular ships position.

An area of responsibility (responsibility zones) is also worth mentioning which is meant to distribute the responsibility on selected operator stations, as well as very useful in the traffic monitoring function (reporting lines), which are set to generate a message about exceeding ship position with necessary contact with VTS center for relevant reports sending.

The system allows the creation of special tracking mode zones for automatic tracking mode choose (data from radar or AIS).

Conclusions

An overview of the basic set of traffic monitoring functions of Navi-Harbour 5000 system is described in this paper. These functions are designed to facilitate the VTS operator work by faster his reaction for potentially dangerous situation. Thanks to NH5000 incidents are reported quickly and automatically in the form of information, warnings or alarms. Especially important for VTS operators is the possibility to create all kinds of special zones (with individual alarm system) and the recommended route (with a large number of options available that describe the sections of the route). These capabilities give the operators of specific VTS system's ability to match the individual needs and take into account both the specific characteristics of the area, as well as local regulations.

However, it is also noted that the benefits may bring only the functions that will be used in a proper manner by properly trained personnel. Therefore, attention should be paid to the adequate training methods, both at the basic and advanced level.

It is also very important that operators should work properly supervised and, therefore, they couldn't give up an adequate possibilities to set up and operate the system fully and properly. They work couldn't base only to their own intuition and routine behavior, which may lead to the level of safety reduction.

References

1. IMO Resolution A.857(20).
2. IALA Recommendation V-128 Operational and Technical Performance Requirements for VTS Equipment.
3. Navi-Harbour UserManual volume 4.

Others

4. JAGNISZCZAK I.: Systemy sterowania i Zarządzania Ruchem Statków. AM, Szczecin 2001.

Scientific Journals
Maritime University of Szczecin

Zeszyty Naukowe
Akademia Morska w Szczecinie

2013, 36(108) z. 1 pp. 85–89
ISSN 1733-8670

2013, 36(108) z. 1 s. 85–89

Gumbel distribution in analysis of vessel speed on the Świnoujście–Szczecin fairway

Lech Kasyk, Monika Kijewska

Maritime University of Szczecin, Department of Mathematics
70-500 Szczecin, ul. Wały Chrobrego 1–2, e-mail: {l.kasyk; m.kijewska}@am.szczecin.pl

Key words: vessel speed, restricted area, vessel traffic flow, probability, Gumbel distribution

Abstract
The present article concerns a problem of vessel speed modeling in restricted areas, where vessel traffic flow is disturbed. In analysis of vessel speed on the Świnoujście–Szczecin fairway, division into the particular ship types has been made. Probability distributions describing speed of different ship groups have been analysed. Using the chi-square goodness-of-fit test it has been showed that the best distribution describing vessel speed of the most ship groups, is the Gumbel distribution.

Introduction

The vessel speed in restricted areas, where a vessel traffic flow isn't too much disturbed, may be described and modeled by normal and lognormal distribution [1, 2]. Whereas the growing disturbances the bigger difference between the speed distribution and the normal distribution [2, 3]. Additionally, the vessel traffic flow isn't homogeneous. Different groups of ships have their own distributions. So, in this article the data set of vessel speed has been divided into 7 types:

– barges;
– tankers;
– containers;
– cargo;
– general cargo;
– carriers;
– other ships.

For particular ship groups, a vessel speed has been analysed on different section of Świnoujście–Szczecin fairway. Data from VTS Szczecin have been used.

Vessel speed distribution on the section 11 km – I Brama Torowa

The section *11 km – I Brama Torowa* is a part of the Świnoujście–Szczecin fairway 5.2 km long. In first half 2009, in the direction north-south, 1034 ships were registered on this section. The following table presents the division of this set into 7 groups.

Table 1. The vessel number of different types on the section *11 km – I Brama Torowa*

No.	Vessel type	Number of vessels
1	Barges	30
2	Tankers	140
3	Containers	73
4	Cargo	500
5	General cargo	184
6	Carriers	69
7	Other ships	38

Speed distribution of barges

Figure 1 presents the frequency histogram and the graph of Gumbel probability density function, fitted to data for barges.

In the chi-square goodness-of-fit test [4], the test statistic is equal to 0.96 alongside the critical value 3.84 (at the 0.05 level of significance). So, we are unable to reject the hypothesis that the speed of barges between reporting points *11 km* and *I Brama Torowa* has a Gumbel distribution. In this case location parameter $\alpha = 9.1$ and scale parameter $\beta = 0.65$.

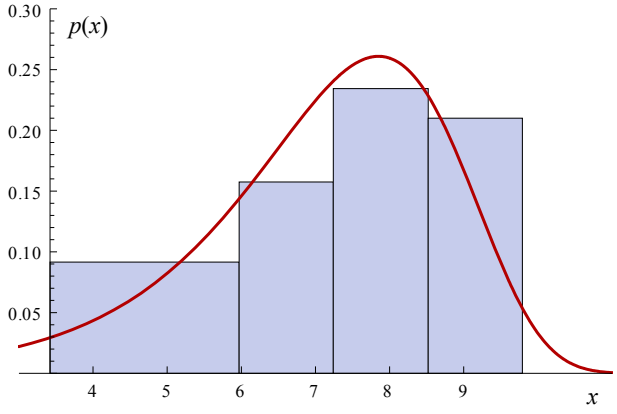

Fig. 1. Frequency histogram of vessel speed for barges

Speed distribution of tankers

Figure 2 presents the frequency histogram of data connected with tankers speeds.

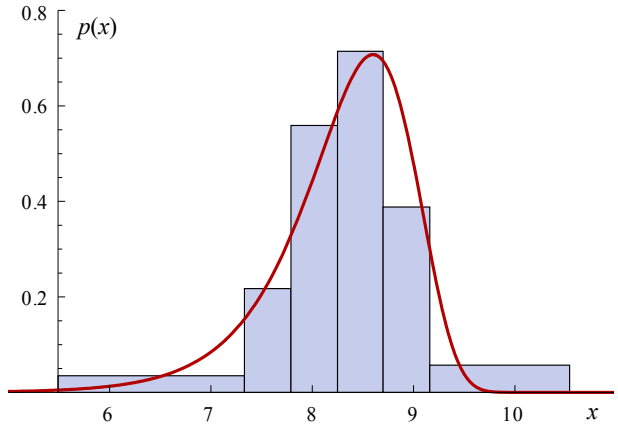

Fig. 2. Frequency histogram of vessel speed for tankers

Using the chi-square goodness-of-fit test we find that the test statistic is equal to 6.53 alongside the critical value 7.8 (at the 0.95 confidence level). So, we are unable to reject the hypothesis that the speed of tankers has a Gumbel distribution. In this case location parameter $\alpha = 8.6$ and scale parameter $\beta = 0.52$.

Speed distribution of containers

Figure 3 presents the histogram and the graph of Gumbel probability density function, fitted to data for containers.

In the chi-square goodness-of-fit test, the test statistic is equal to 6.96 and the test probability $p = 0.03$. So, at the 0.05 level of significance, we must to reject the hypothesis that the speed of containers has a Gumbel distribution. But at the lower significance level we can describe the speed of containers between reporting points *11 km* and *I Brama Torowa* by the Gumbel distribution with parameters $\alpha = 8.8$ and $\beta = 0.54$.

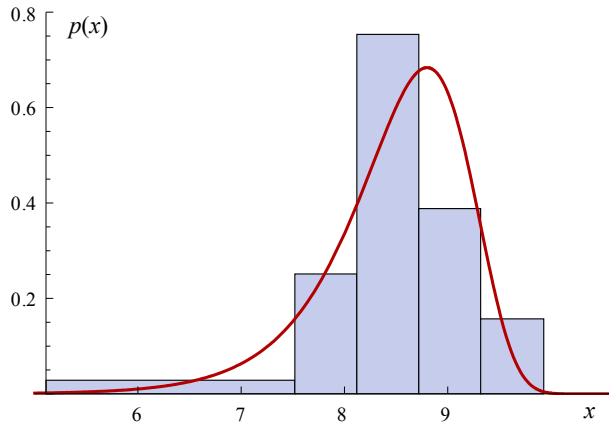

Fig. 3. Frequency histogram of vessel speed for containers

Speed distribution of cargo ships

On the base of chi-square goodness-of-fit test we must to reject the hypothesis that the speed of cargo ships has a Gumbel distribution. Because the test statistic is equal to 33.8 alongside the critical value 14.1 (at the 0.05 level of significance). But using mixed distribution [2, 3], the hypothesis about Gumbel – Uniform distribution of cargo ships speed can be tested. Probability density function in the form presented below describes good speed distribution of cargo ships. In the chi-square goodness-of-fit test, the test statistic is equal to 8.53. This function is the following:

$$f(x) = 0.93\,pdfG(8.72, 0.46) + \\ + 0.07\,pdfU(6.54, 10.55) \tag{1}$$

where

pdfG(*a*, *b*) – probability density function of Gumbel distribution with parameters *a* and *b*;

pdfU(*c*, *d*) – probability density function of Uniform distribution giving values between *c* and *d*.

Figure 4 presents the frequency histogram of data connected with cargo ship speeds and fitted pdf of mixed distribution.

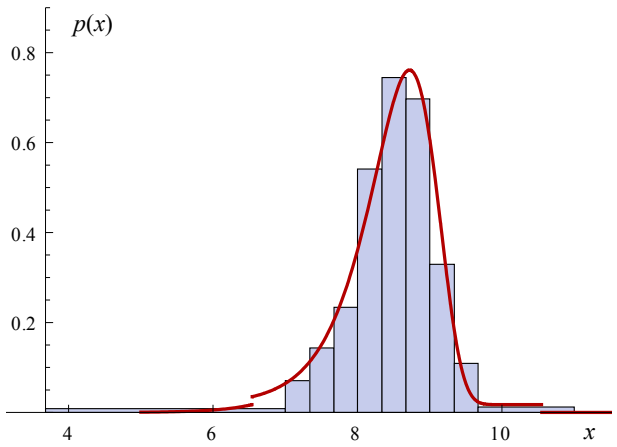

Fig. 4. Frequency histogram of vessel speed for cargo ships

Speed distribution of general cargo ships

Figure 5 presents the frequency histogram and the graph of Gumbel probability density function, fitted to data for general cargo ships.

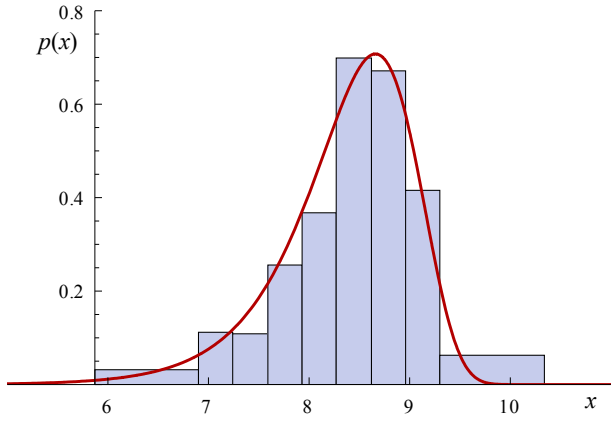

Fig. 5. Frequency histogram of vessel speed for cargo ships

In the chi-square goodness-of-fit test, the test statistic is equal to 9.4 alongside critical value 12.6 (at the 0.95 confidence level). So, we are unable to reject the hypothesis that the speed of general cargo ships between reporting points *11 km* and *I Brama Torowa* has a Gumbel distribution. In this case location parameter $\alpha = 8.66$ and scale parameter $\beta = 0.52$.

Speed distribution of carriers

Figure 6 presents the histogram and the graph of Gumbel probability density function, fitted to data for carriers.

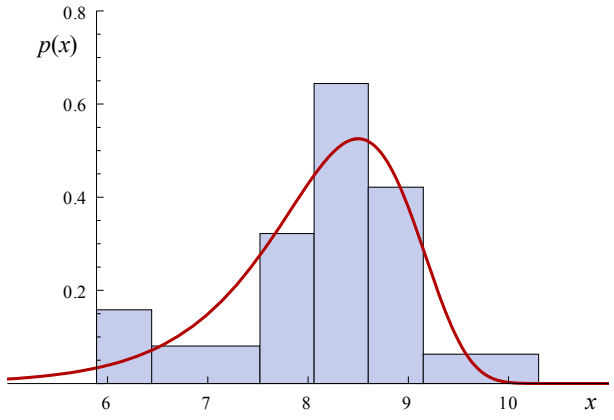

Fig. 6. Frequency histogram of vessel speed for carriers

Using the chi-square goodness-of-fit test we find that the test statistic is equal to 6.06 and test probability $p = 0.11$. So, we are unable to reject the hypothesis that the speed of tankers has a Gumbel distribution. In this case location parameter $\alpha = 8.5$ and scale parameter $\beta = 0.7$.

Speed distribution of other ships

Tugs, factory trawler, research / survey vessel, suction dredger, diving support vessel, ro-ro / passenger ship, fishing vessel and offshore supply ship formed a group called “other ships”.

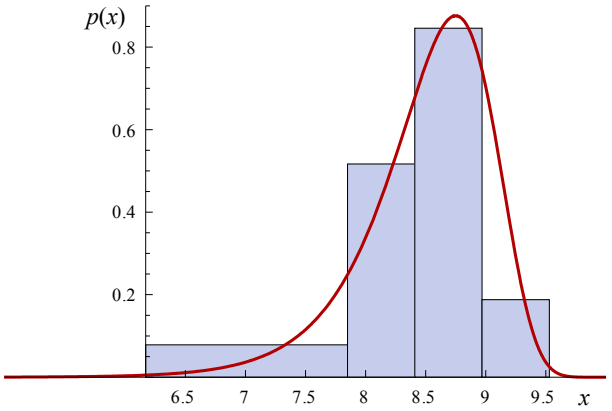

Fig. 7. Histogram of data for other ships

In the chi-square goodness-of-fit test, the test statistic is equal to 1.73 alongside the critical value 3.84 (at the 0.95 confidence level). So, we are unable to reject the hypothesis that the speed of “other ships” between reporting points *11 km* and *I Brama Torowa* has a Gumbel distribution. In this case location parameter $\alpha = 8.75$ and scale parameter $\beta = 0.42$.

Vessel Speed Distribution on other sections

Section Karsibor – Dok5

The section *Karsibor – Dok5* is a part of the Świnoujście–Szczecin fairway 53.7 km long. In first half 2009, in the direction north-south, 752 ships were registered on this section. But 13 vessels had different stoppages on this section. So, the data set used to analyse, had 739 elements. The table 2 presents the division of this set into 7 groups.

Table 2. The vessel number of different types on the section Karsibor – Dok5

No.	Vessel type	Number of vessels
1	Barges	27
2	Tankers	67
3	Containers	69
4	Cargo	366
5	General cargo	134
6	Carriers	49
7	Other ships	27

Like in chapter *Vessel Speed Distribution on the section 11 km – I Brama Torowa*, the testing

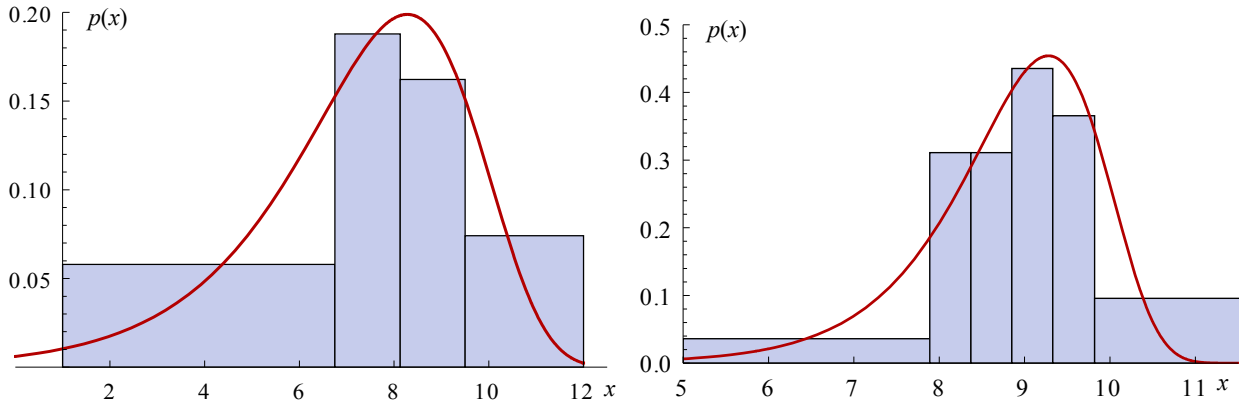

Fig. 8. Frequency histogram of vessel speed for barges and tankers

hypothesis about Gumbel distribution of the vessel speed for separate types of ships has been made. For groups: barges, tankers, containers, general cargo and other ships, we can accept that the vessel speed between reporting points *Karsibor* and *Dok5* has a Gumbel distribution. In figure 8 are presented demonstration histograms with fitted Gumbel pdf.

For cargo ships and carriers mixed distributions have been used.

Section Plawy 13–14 – Krepa Dolna

The section *Plawy13–14 – Krepa Dolna* is a part of the Świnoujście–Szczecin fairway 8.3 km long. On this section, in first half 2009, in the direction north-south 1004 ships were registered and in the opposite direction 1012 ships were registered. For almost all ship types, the hypothesis about a Gumbel distribution of vessel speed has been proved. Below demonstration histograms with fitted Gumbel pdf are presented.

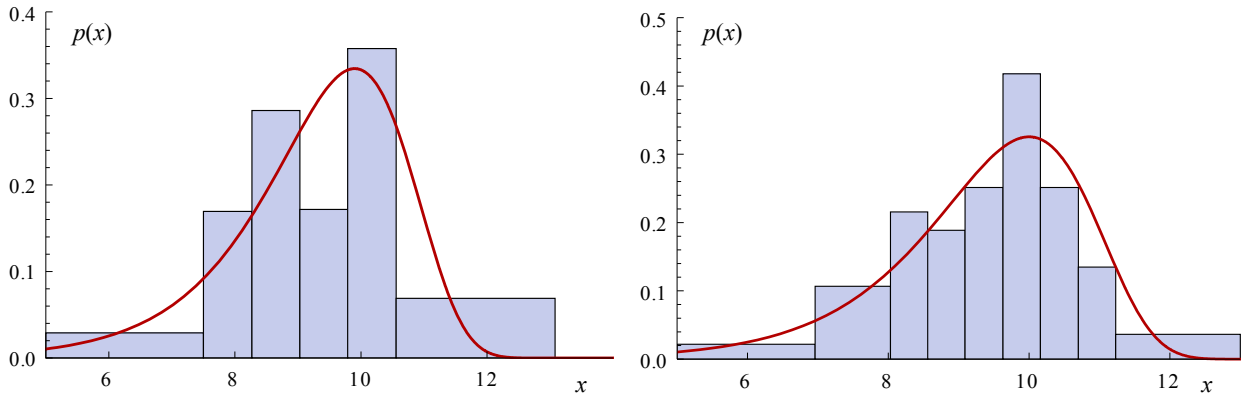

Fig. 9. Frequency histograms of vessel speed for carriers and tankers, direction Świnoujście–Szczecin

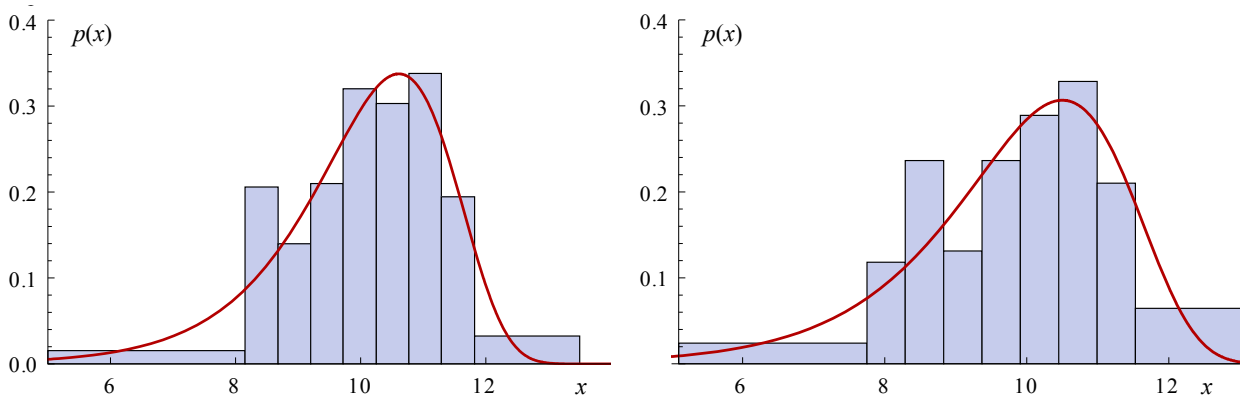

Fig. 10. Frequency histograms of vessel speed for general cargo and tankers, direction Szczecin–Świnoujście

For the vessel speed in opposite direction the hypothesis about a Gumbel distribution was true, too (Fig. 10).

Conclusions

All frequency histograms aren't symmetrical and all have negative coefficients of skewness (a long left tail). The cause of that is the speed limit, what is one of the most important factors disturbing vessel traffic on the Świnoujście–Szczecin fairway. So, the most of presented vessel speed distributions are in accordance with Gumbel distribution. But disagreement with this distribution of some groups (especially cargo ships) results probably from a big diversity inside these groups. And necessary is to do further research on this diversity. Other reasons of this disagreement are other than speed limit restrictions of vessel traffic on the fairway.

References

1. GUCMA L., SCHEFS S.: Studium prędkości statków na torze wodnym Świnoujście–Szczecin. Wydawnictwo AM, Szczecin 2007.
2. KASYK L.: Probabilistyczne metody modelowania parametrów strumienia ruchu statków na akwenach ograniczonych. Wydawnictwo UTH, Radom 2012.
3. KASYK L.: Rozkład prędkości statków na torze wodnym Szczecin–Świnoujście. Logistyka 3, 2012, 971–976.
4. SOBCZYK M.: Statystyka. Wydawnictwo Naukowe PWN, Warszawa 2004.

Scientific Journals
Maritime University of Szczecin

Zeszyty Naukowe
Akademia Morska w Szczecinie

2013, 36(108) z. 1 pp. 90–93
ISSN 1733-8670

2013, 36(108) z. 1 s. 90–93

The use of Pareto-Lorenz analysis for the determination of faults in fishing vessel refrigerating systems

Waldemar Kostrzewa, Katarzyna Gawdzińska, Artur Bejger

Maritime University of Szczecin
70-205 Szczecin, ul. Podgórna 52/53, e-mail: {w.kostrzewa; k.gawdzinska; a.bejger}@am.szczecin.pl

Key words: faults diagnosis, fishing vessels, Pareto-Lorentz analysis, refrigerating system, determination of faults

Abstract
This study is aimed at the determination of the significance of faults diagnosed in refrigerating plant components of fishing vessels. The problem is described by the Pareto-Lorenz analysis. The field work covers vessels of the Polish fishing fleet. Ships under examination are typical of the Polish fishing vessels operating at sea. The research has been based on data gathered in 2007–2011, consisting of 235 faults, detected and estimated for refrigerating systems of 25 small vessels of the Polish fishing fleet. Taking the refrigerant as a criterion of division, we have analyzed two types of vessels.

Introduction

Polish fishing fleet operating on the Baltic Sea from Polish ports consists of a variety of vessels and boats of different age. At some point of their long operation, these vessels were modernized, which comprised refrigerating installations. The operation of outdated and worn refrigerating systems in fishing vessels often affects frequent faults resulting from untight installations and resultant leaks of the refrigerant, faults of refrigerating units, condensers, evaporators, fans etc. [1, 2, 3]. The multitude of refrigerating equipment used in Poland and all over the world adversely affects the ozone layer and adds to the greenhouse effect. Ozone in the upper stratum of the atmosphere (ozonosphere) protects people from harmful ultraviolet radiation. In refrigerating practice ozoning has been used to prevent the development of microorganisms in refrigerating chambers [3]. For decades, a dramatic drop of ozone content in the Earth's protective layer of the atmosphere has been observed. The main reason for this phenomenon is appearance in the atmosphere of large amounts of CFCs (chloroflourocarbons) and nitrogen compounds (greenhouse gases) [1, 2]. On the one hand, the presence of greenhouse gases in the atmosphere enables life on our planet (without them, the temperature would have dropped much below zero). On the other hand, leaking refrigerants and wrong energy management are among factors contributing to the melting of glaciers due to growing temperature of the atmosphere. As a result, the level of the seas may rise, leading to flooding of many areas located low above the sea level, some of them being most densely populated places on Earth.

Other effects of the depleted ozone layer include enhanced ultraviolet radiation, adverse impact on physiological and developmental processes of plants, climatic changes, limited development of phytoplankton in the oceans, increase in skin cancer and eye diseases in people and animals.

For these reasons it is important to forecast and limit faults of fishing vessel refrigerating systems, to prevent such faults by continuous monitoring, and the determination of likelihood of most frequent failures and their causes. These measures are necessary for the protection of marine environment in which fishing vessels operate, and to avoid situations in which such a failure might stop operation of the vessel, creating a threat to other vessels in vicinity [2].

The research

On the basis of [1, 2, 3] and data gathered during this study we found that the most frequent reasons of cooling system component faults include damage to:

1) sealings in refrigerating installations and related refrigerant leaks (Fig. 1a);
2) refrigerating compressors (Fig. 1b);
3) heat exchangers (condensers and evaporators);
4) control systems;
5) fans (Fig. 1c);
6) water, brine and oil pumps;
7) defrosting systems.

a)

b)

c)

Fig. 1. Examples of refrigerating system component faults: a) refrigerant leaking from a refrigerating installation, b) damage to a compressor, c) damage to a condenser fan [4]

The faults were divided into seven main categories (as points 1–7 above) and related research was done exploring data gathered in the years 2007–2011. 235 faults of refrigerating systems were gathered and evaluated from 25 vessels of Polish fishing fleet, distributed in ports on westerns, central and eastern coasts (Table 1).

The analysis focused on two groups of fishing vessels, divided by the type of refrigerant:

1) Vessels herein marked **X** – those using an old type of refrigerant belonging to the group of hydrochlorofluorocarbons (HCFC) (16 such vessels were examined);
2) Vessels herein marked **Y** – those with modernized refrigerating equipment (or having it originally installed), using refrigerants that replace HCFCs and clorofluorocarbons or CFCs (9 such vessels were examined).

Table 1. Data on refrigerating system component faults, with a division into two groups of vessels X and Y, from 2007–2011

X	2007	2008	2009	2010	2011
1	6	6	7	10	10
2	3	4	6	8	8
3	3	3	3	3	3
4	5	2	4	5	7
5	2	1	3	3	2
6	0	1	2	1	0
7	0	1	1	0	0

Y	2007	2008	2009	2010	2011
1	3	1	1	2	2
2	6	5	5	6	7
3	3	4	4	2	5
4	8	8	6	7	7
5	2	4	2	3	2
6	0	2	1	0	1
7	0	1	1	1	0

We have analyzed the recorded faults of refrigerating systems in fishing vessels by the Pareto-Lorenz method [5]. The diagram, an effect of the analysis, is based on the empirically observed regularity that in engineering generally 20–30% of causes (factors) contributes to 70–80% of effects (Fig. 2).

The diagram is constructed in the following phases [5, 6]:

– gathering data on the examined object that are related to a given problem;
– determination of the quantity to be used for measuring the process outcome in reference to

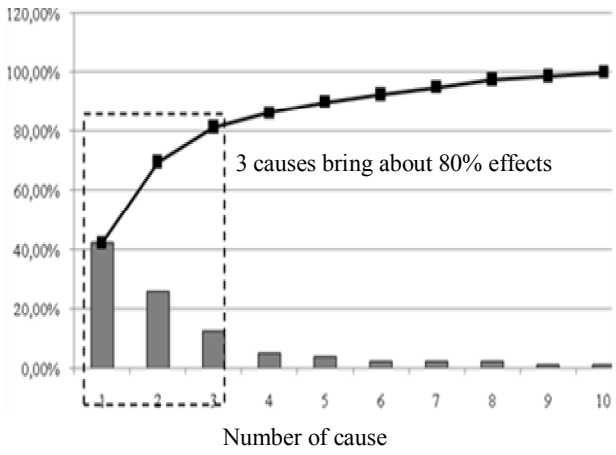

Fig. 2. Pareto-Lorenz diagram illustrating unequal cause-effect distribution: relatively few causes account for many effects

the problem under consideration. In the case herein described the determination of the quantity was based on seven categories of faults selected during analyses, in the course of acquiring data from 25 vessels in all. The sample of 25 vessels under examination is a sufficient and representative sample while using tools for the description of the problem according to the specialized literature [7];

- putting faults in order (on the basis of information gathered and knowledge) due to the force with which they affect the fault outcome;
- determination of cumulative percentage values of each fault;
- drawing a line through points corresponding to the cumulative values;
- analyzing the diagram to identify a group of faults that are mostly responsible for affecting the object under consideration.

From the data included in control sheets, the faults of fishing vessel refrigerating installations were segregated by the number of occurrences in the descending order. The faults are given in table 2 for vessels of group X and in table 3 for vessels of group Y. The tables, in respective columns, contain cumulative values needed to draw up a Pareto-Lorenz diagram. The diagrams, a graphic result of the analysis, are shown in figures 3 and 4.

Table 2. Classification of faults identified in refrigerating systems of fishing vessels by the frequency of occurrence in fishing vessels of group X

No.	Type / location of fault	Number of faults	Relative number (%)	Cumulative number of faults	Relative cumulative number (%)
1	Untight refrigerating installation and related leaks of refrigerant	39	31.70	39	31.70
2	Refrigerating compressors	29	23.58	68	55.28
3	Control system	23	18.70	91	73.98
4	Heat exchangers (condensers and evaporators)	15	12.20	106	86.18
5	Fans	11	8.94	117	95.15
6	Water, brine and oil pumps	4	3.23	121	98.37
7	Defrosting systems	2	1.63	123	100
	Total	123			

Table 3. Classification of faults identified in refrigerating systems of fishing vessels by the frequency of occurrence in fishing vessels of group Y

No.	Type / location of fault	Number of faults	Relative number (%)	Cumulative number of faults	Relative cumulative number (%)
1	Control systems	36	32.14	36	32.14
2	Refrigerating compressors	29	25.89	65	58.03
3	Heat exchangers (condensers and evaporators)	18	16.07	83	74.01
4	Fans	13	11.61	96	85.71
5	Untight refrigerating installation and related leaks of refrigerant	9	9.04	105	93.75
6	Water, brine and oil pumps	4	3.57	109	97.32
7	Defrosting systems	3	2.68	112	100
	Total	112			

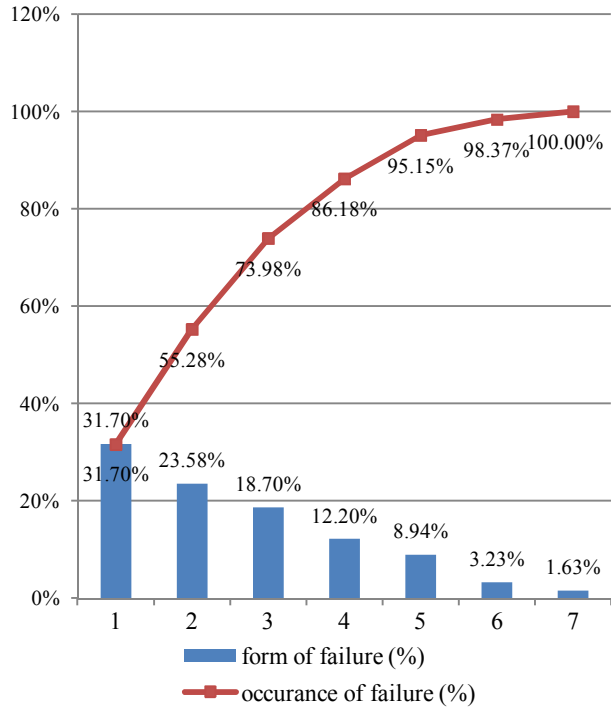

Fig. 3. Pareto-Lorenz diagram for refrigerating system faults in fishing vessels of group X – based on table 2

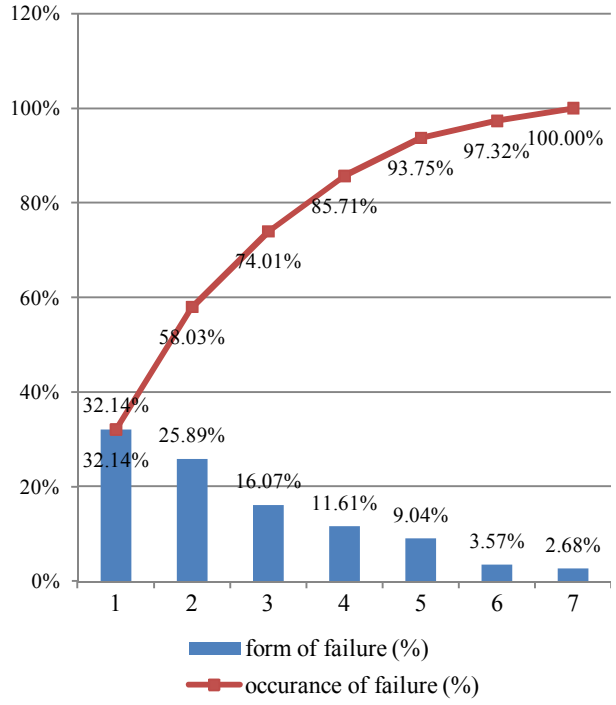

Fig. 4. Pareto-Lorenz diagram for refrigerating system faults in fishing vessels of group Y – based on table 3

Conclusions

The Pareto-Lorenz diagram presents in the descending order a relative share of each factor in the overall effect of operation [6]. It puts in order the faults of refrigerating systems in two groups of fishing vessels defining their significance for the operation of such vessels. In case of fishing vessels of X type – untight refrigerating installation and related leaks of refrigerant, refrigerating compressors, control system is 73.98% of this group and according to the Pareto-Lorenz rule, has main influence on its failure. In case of fishing vessels of Y type – damages of control systems, refrigeration compressors and heat exchangers (condensers and evaporators) the importance of interaction is 74.1%.

The presented analysis has shown a large diversity of faults occurring in fishing vessel refrigerating installations of two, previously defined types: older X type and new Y type. The outcome allows to quickly and effectively assess the profitability of the vessels. It is also a valuable tool describing the probability of fault occurrence. Identification of these causes in the assessment of faults of refrigerating systems in fishing vessels permits to determine directions of actions to be taken to effectively contribute to better and smooth operation of vessels under consideration, or to gather and store onboard a vessel necessary spare parts.

References

1. BEJGER A.: An Analysis of chosen engine failures of the Seismic Research Type Ships, Journal of Polish CIMAC 2, Vol. 6, Gdańsk 2011.
2. ZAKRZEWSKI B.: Z doświadczeń praktyków: czy amoniak, jako czynnik chłodniczy jest bezpieczny? Chłodnictwo 11, Tom 35, 2004, 20–23.
3. BEJGER A.: Zużycie i możliwość diagnozowania wybranych elementów układu wtryskowego silników okrętowych. Diagnostyka 4(40), 2006, 47–50.
4. KĘDZIERSKA K., ZAKRZEWSKI B.: Analiza wycieków czynnika podczas eksploatacji okrętowych urządzeń chłodniczych (Analysis of refrigerant's leakage during the use of refrigeratetion equipment for ships). Chłodnictwo 8, tom XLV, 2010.
5. HAMROL A.: Zarządzanie jakością z przykładami. PWN, Warszawa 2008.
6. HAMROL A., MANTURA W.: Zarządzanie jakością. Teoria i praktyka. PWN, Warszawa 2006.
7. MONTGOMERY D.C.: Statistical Quality Control. Wyd. Wiley, 2011.

Scientific Journals
Maritime University of Szczecin

Zeszyty Naukowe
Akademia Morska w Szczecinie

2013, 36(108) z. 1 pp. 94–99
ISSN 1733-8670

2013, 36(108) z. 1 s. 94–99

Cost optimization of marine fuels consumption as important factor of control ship's sulfur and nitrogen oxides emissions

Adam Kowalski

Polish Steamship Company
70-419 Szczecin, Plac Rodła 8

Key words: cost optimization, fuel costs, fuel consumption, data collection, determination

Abstract

This paper proposes an efficient, objective method of optimizing fuel costs during the sea passage. The presented method based on data collection and calculations can be used in daily practice for masters of vessels and by ship's management divisions. The paper presents not only the use of the method for newly constructed but also for ships already in service. The biggest advantage of this method is that it does not need extra expenses to determine the fuel effectiveness in a changeable marine fuel market.

Introduction

Cost of marine fuels dominate over the other maritime transport expenses. This is due to, among other things, the introduction of requirements for Sulphur Oxide Emission Control Areas (SECA) and Nitrogen Oxides Emission Control Areas (NECA). IMO Resolution MEPC.203 (62) requires to introduce Marine Energy Efficiency Management Plans since January 1st. One of the most effective ways for existing ships to meet all of these requirements is the optimal use of fuel on board. In practice, this would mean for a shipping, inter alia, to determine the vessel's economy speed.

The world market of ships fuels based on the processing of crude oil forecasts a continuous increase in the price of bunker in relation to other costs incurred in shipping. The increase of bunker costs is also due to the implementation of international regulations limiting the sulfur content of marine fuels. In this case, there is an essential link – the price increases with a decrease in the sulfur content of marine fuel. The 3.5% standard of maximum sulfur content in the fuel binding in the past is gradually moving in the Baltic Sea Area to 0.1% standard on January 1, 2015. It means a surge in the cost of business for shipping in this region since that date.

For the operation of a ship the aim is to enlarge the profit level by reaching the highest freight with the lowest operational costs. Commercial success of the transport projects require to reduce important operating costs, especially in times of global crisis when shipping freight rates drop considerably on the market. Regardless of the operation costs of ships, the shipping company should always look for cost savings resulting from the "shore" part of their business. However, the ships expenses will be an essential component of the operating costs. Then, the next main component of the cost will be the charges for fuel used by the ship. In this situation, for the success of the business it is particularly important ship's captain cooperation with the owner or charterer. The method described in this article allows to optimize ship's fuel consumption by a fast, low cost and efficient way and to ensure the economic success of the transport task.

Assumption of the method

On the one hand seagoing vessels are running at sea passages with two speed ranges corresponding with main engine settings:

1. Sea speed, usually a range of most likely used speed of the ship. The engine is running at optimal range of the load curve. Ship speed adjust-

ment in addition to the change of the main engine revolutions may also concern setting of variable pitch propeller.
2. Range of speeds less than the sea speed, so-called manoeuvre speed. At this range the set of the main engine will be reduced – lower setting of propeller's revolutions will be used and alternative lower angles of pitch propeller. Manoeuvring ship requires the activation of additional mechanisms in the engine room, needs additional power requirement. Ship energy security needs starting additional generator sets. Manoeuvring setting of the main engine causes the increase of the total consumption of marine fuels in spite of reduced speed.

On the other hand, there are several classifications of navigable waters. For the purposes of this paper, it is advisable to adopt the division of navigable waters as a non restricted and restricted areas [1]:

1. Non restricted areas (open waters) where the vessel is able to fairly freely choose its speed. The only significant external factors affecting the speed of the vessel are hydro and meteorological conditions. The capability of decision on the ship's speed on open waters can be an effective solution to the problem of optimization of fuel consumption.
2. Restricted areas where vessels usually navigate close to land. Ships traffic is regulated by a number of local and international rules, including those that affect the speed of the vessel. In such areas ships are forced to perform frequent by changing both manoeuvres the speed and the course. Other phenomena limiting propeller efficiency can be observed, among other things additional resistance to motion caused by shallow water effect [2]. Captain decisions during navigation in restricted areas are mainly motivated by safety of navigation. Economic considerations come therefore in the second place.

The presented classification of settings of the main engine and navigational areas allow to draw a conclusion that the area on which the ship's captain can have effective influence on the economical success is non restricted area where a ship is sailing with a sea speed. The conclusion drawn for this case can also be used for some parts of the sea passage on the restricted areas.

Object of research

The conditions presented in the paper occurs when a ship is operated directly by a Shipping Company. The owner can always specify fixed daily costs of the vessel, described for the purpose of this paper as day costs. They include, among other things, technical costs, crew and any additional costs directly related to the transport of cargo (port charges, pilots, tugs etc.). It is necessary to take into consideration that some of the technical costs are not exactly fixed. For example running of the main engine on the low revolutions generate some cost of additional maintenance. Lower revolutions cause lower burning temperature at the cylinder and in consequence raise the quantity of not burned hydrocarbons accumulating on internal parts of the main engine. The result is for example the increased wear of piston rings. There are also shorten periods of routine maintenance and increase in costs. There are no major obstacles for the owner to estimate the rising cost of the main engine maintenance based on computerized maintenance and purchase systems like SpecTec's AMOS. But for the purpose of this article it has been assumed that daily costs are fixed, independent of the setting of the main engine revolutions. Daily costs should also include appropriate part of on shore owner activities.

In addition to these generally considered fixed daily costs of the ship, there is a group of costs related to the amount of fuel burned. There is no doubt that there is a strong correlation between the speed of the vessel and the daily amount of fuel burned. This correlation is valid also for speed and the daily cost of fuel burned.

Knowledge of the daily cost of the ship and the daily cost of fuel burned allow for the best affreightment decision. Estimated daily profit achieved in the carriage of cargo cannot be less than the sum of the daily cost of the vessel and cost of burned fuel. On the basis of the knowledge of the total daily cost of the vessel, the decision to hire a ship to the Time Charters may be taken. The difference between the daily cost and the daily charter rate will be a profit for the owner.

The calculations presented in this article have been done for universal bulk carrier with a deadweight of 38 thousand tons, the length of 190 m and the width of 29 m.

Experimental model of ship's fuel daily consumption

The ship's captain in every sea passage situation has the ability to take a decision on the ship's speed. The theoretical analysis shows that daily consumption increases with the propeller revolutions to the third power. Then the ship's speed should increase in the proportion to the increase of screw turns. Therefore, in order to describe the

daily consumption and speed of the vessel, binominal power model should be applied:

$$\text{consME}(V) = a\,V^b + \varepsilon \qquad (1)$$

where:

consME – daily fuel consumption of the main engine for speed V [t];
V – speed of the vessel for which consME is determined [kts];
a, b – parameters of the model;
ε – the error of term power regression function.

For the previously presented theoretical considerations, exponent b should be set to three. Because of mechanical losses and due the propeller slip, vessel speed increases more slowly than the screw revolutions. Practical dependence of binding daily consumption speed of the vessel will have an exponent value slightly greater than three. To recapitulate, the value of the parameter b of the power regression functions should be in the range from 3 to 4. Regression parameters a and b can be determined by known methods using a widely available statistical analysis software.

Acquisition of data and determination of the fuel consumption curve

In order to create a model based on the power regression method of least squares, it is necessary to meet the assumptions of the random component ε of equation (1). The values of each error ε should be independent random variables having a normal distribution with mean 0, or the expected value of 0, and a constant variance, independent of the value of the variable V measurement [3]. In order to establish normal distribution of ε, it is necessary to obtain a large number of data pairs consME – V. As mentioned previously, the vessel speed is carried on the sea passages in the optimum range of the main engine load curve. For most of the ship, speed range will be between 10 to 15 knots for the engine load between 30 to 75 percent. In sea practice, due to the limited duration of the experiment and in order to avoid the additional cost, it is difficult to get more than 4 to 5 measuring connecting ship speed V and fuel consumption consME. Typically, data at intervals of about 1 knots of value V are recorded.

In view of this fact, the regression equation based on a built achievable in practice, four or five pairs of data, the regression model cannot be built. Determined equation can be used for descriptive purposes only. Such an approach is sufficient to draw practical conclusions. Generally, available computer's spreadsheets allow to easily determine the equation describing the relationship consME as a function of the ship's speed V. As it has previously been demonstrated, the regression of two-dimensional power law must be used for the description.

However, nothing stands in the way as far as completion of data collection over a long period of time is concerned, to build and analyze models of fuel consumption as a function of speed. But the long-term change which disturbances of the model has to be taken into consideration. Among other things, the influence on the model has the main engine efficiency change due to aging and interval between inspections. Deformation and fouling of the submerged part of the ship's hull are also significant factors. In practice, it turns out that it is better to build the current descriptive equations instead of determining the not always valid and current model.

Due to hydrodynamics, ship speed strongly depends on the load condition. The consequence of mean draft increasing and simultaneously maintaining the same ship's speed is always the increase of daily consumption. For example, the differences between the main engine daily consumption for the fully loaded and the ship at ballast condition reach 30 percent.

This article presents the calculations carried out for the loaded ship. Similar considerations, made by the same algorithms can be carried out not only for ship at ballast but also for other intermediate loading conditions.

Graph and analytical formula describing consME depending on V for modeled ship at full loading condition is shown on figure 1.

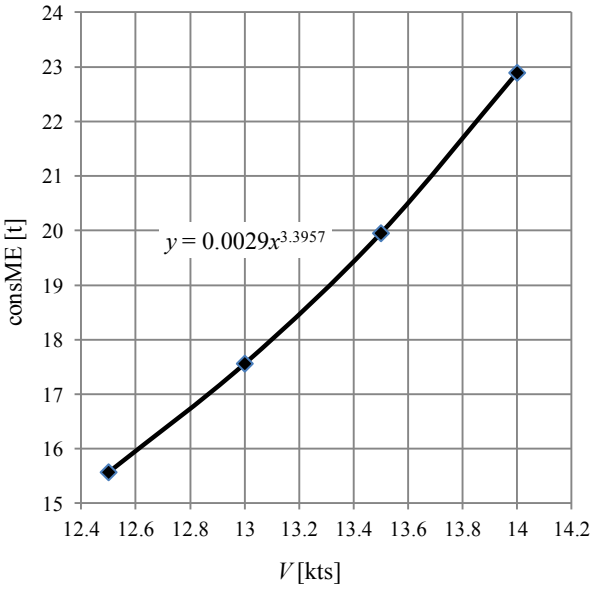

Fig. 1. Function consME(V) of fully loaded vessel

In practice V values can be obtained from the log, or in the absence of the currents also from the satellite receiver GPS. The value of consME can be obtained from counters of the fuel flow transported to the main engine. Typically, these data are available only for the engine crew. The appliance solutions available also enable to read the parameters directly on the bridge. The figure 2 shows an example of a device installed in the ship's engine control room, where it is possible to read the amount of fuel supplied to the main engine.

Fig. 2. Fuel flow meter showing current fuel consumption of 1.06 m^3/h

During the voyages such favorable hydro and meteorological conditions can be found that enable reading of not deformatted parameters of consME and V. However, such experiments are performed only when a vessel does not bear additional costs resulting from the extension of the route or the longer voyage time. Particularly favorable circumstances are when the ship accelerates to the speed at sea after leaving the port or slows before entrance to the port. Then for some intermediate speeds between manoeuvring speed to sea speed, it is necessary to write down two pairs of parameters: speed V and the main engine fuel consumption consME. To minimize errors an experiment both for the acceleration and deceleration phases has been conducted.

Optimizing the cost of ship's fuel during a sea voyage

In order to present the method to optimize the cost of ship's fuel it is necessary to define the cost of one nautical mile passage which borne by the owner – mileCost(V). This relation is represented by the formula:

$$\text{mileCost}(V) = \frac{\text{consME}\cdot\text{priceHFO}}{24\cdot V} + \frac{\text{consAE}\cdot\text{priceMGO}}{24\cdot V} + \frac{\text{dayCost}}{24\cdot V} \quad (2)$$

where:

consME – daily fuel consumption of the main engine for ship speed V [t];

priceHFO – the price of heavy fuel oil for main engine [USD / t];

consAE – daily fuel consumption of the auxiliary engines (power generators) [t];

priceMGO – the price of marine gas oil for the auxiliary engines [USD/ t];

V – speed of the vessel for which it is determined consME [kts];

dayCost – the owner's daily cost [USD].

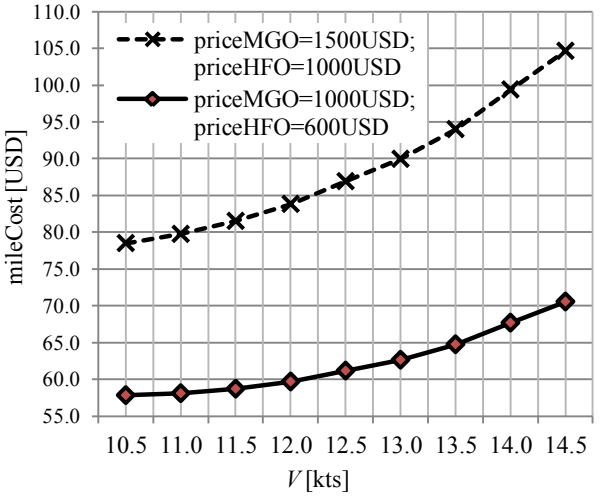

Fig. 3. Cost of one nautical mile passage as function of ship's speed, owner's dayCost 6000 USD

From figure 3 the effects of irrational decisions of ship's management can be directly read off. For lower fuel prices and the low owner's daily cost 6000 USD, forced by fleet management high value of sea speed ship costs abt. $ 10 by every nautical mile of the passage. This seemingly small amount can no longer be underestimated, taking into consideration several thousand miles of sea passages. There are two positive effects, the costs are minimized and the consumption of fuel is reduced.

Figures 3, 4 and 5 show the graphic description of the equation (2) obtained for the modeled ship. Four pairs of input data consME – V on board the full loaded vessel after leaving the port are recorded. The calculations were performed for two samples of data sets:

1) priceHFO – 600 USD / t, consAE – 3 t, priceMGO – 1000 USD / t,
2) priceHFO – 1000 USD / t, consAE – 3 t, priceMGO – 1500 USD / t.

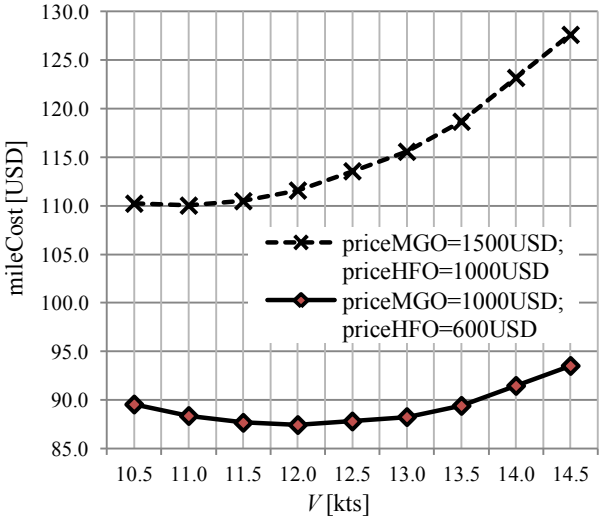

Fig. 4. Cost of one nautical mile passage as function of ship's speed, owner's *dayCost* 14000 USD

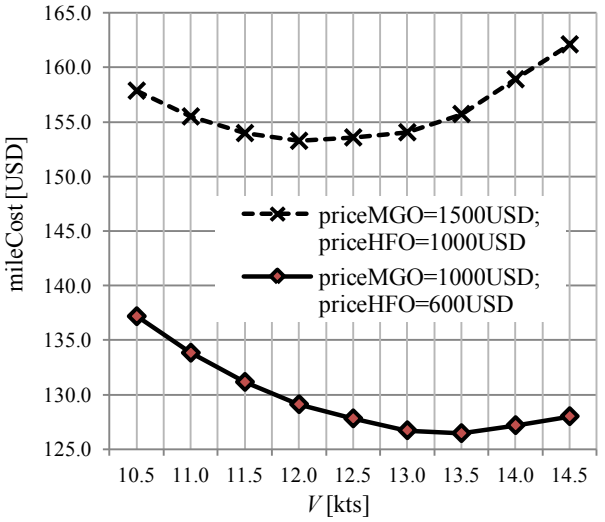

Fig. 5. Cost of one nautical mile passage as function of ship's speed, owner's *dayCost* 26000 USD

From the graphs presented on figures 3, 4, 5 optimum ship's speed can be read, where the cost of one nautical mile reaches minimum value. For example, at low owner's daily cost 6000 USD it is effective to plan the possible minimum ship's speed. Optimum ship's speed is going up parallel to increasing the value of owner's daily cost.

Broken white line on the figures present fuel price increase as an effect of introduce of new both Emission Control Areas. In this condition ship has to use mostly minimum sea speed to minimize cost of one mile passage. Presented bunker prices are not showing economic prediction, are used only for method's presentation.

The above calculation confirms the shipping company Maersk strategy called "slow steaming" – reducing the ships speed to minimum reasonable value. Based on paper presented method the analysis of the optimization of fuel is available not only for shipping giants but also for small owner's companies.

One additional advantage of this method is the ability to optimize the costs of ships still in their construction stage. But it is necessary to obtain theoretical determination of the relation consME(V) for the designed ship. The method to determine this relation is suggested in unpublished studies by MSc. Janusz Falkiewicz, an employee of Polish Steam Company Investment Department. For one of the ships in a design stage consME(V) functions calculated theoretically were confirmed experimentally on ship leaving the building shipyard.

Conclusions

Simplicity, speed and flexibility of the proposed cost optimization method give great profits in terms of the continuous increase in the price of marine fuels. Without any real expenses, it is possible tracing nonstop of current function consME(V), which is the base of the proposed method. This is particularly important, because the conditions of the ship are changing constantly and rapidly. As an example is fouling of underwater part of ship's hull on freshwater navigable areas, especially in tropical rivers or lakes connected to the ocean waters. Fouling due to a long layover may cause a decrease in vessel speed by up to ten percent. The method of optimizing the cost of fuel can also be used to demonstrate the economic sense of cleaning the underwater part of the hull of the ship.

Another problem of efficiency may also be solved by proposed method. The underwater part of hull is affected by continuous deformation which systematically increases hydro resistance. Also long-term aging of the main and auxiliary engines is not without effect on the ratio of fuel consumption and due to this fact decreases the effectiveness of ship's gears.

To ensure an economic success, it is essential that the owner should define operating speed and corresponding reverse per minutes of the main engine revolutions or pitch propeller setting. Optimal speed value should be calculated on the shore, on the basis of data obtained from the vessel and trade secret and not data available on board of the ship. On board of the ship captain will be obliged to continuously update pairs of data consME – V. It should be done in all conditions not generating additional expenses. The presented method of optimizing fuel costs allows the shipping company to adapt to the rapidly changing economic conditions in the shipping market.

The optimization of the consumption of fuels on board usually requires the lowest possible speed. That means less fuel consumption. This will be particularly important from January 1, 2015. From this date the use of expensive distillate fuels with a sulfur content less than 0.1% in Sulphur Oxide Emission Control Area is mandatory.

Annex VI of the MARPOL Convention in 2016 introduces emission control areas of nitrogen oxide. The presented method allows optimization of the fuel quantity based on the ship's speed. Main conclusions concerning high bunker prices is movement of the ship with minimum speed means lower main engine load. The lower engine load entails lower combustion temperature. Such situation could result in lower emissions of nitrogen oxides in relation to the power obtained on board – ratio of gNO_2/kWh.

The approach proposed in the paper allows the owner not only to optimize the economic analysis of the project but also allows to make the initial calculation on how the ship may meet requirements of Nitrogen Oxide Emission Control Area in 2016.

References

1. GUCMA S.: Inżynieria ruchu morskiego. Okrętownictwo i Żegluga Sp. z o.o., Gdańsk 2001.
2. KOWALSKI A.: Traffic engineering methods solutions of problems concerning ship's manoeuvres and sailing on the large rivers of Central America. Scientific Journals Maritime University of Szczecin 33(105), 2013, 57–61.
3. WIECZORKIEWICZ G.: Badania sondażowe i eksperymentalne. Wydawnictwo Naukowe Wydziału Zarządzania Uniwersytetu Warszawskiego, Warszawa 2005.

Scientific Journals
Maritime University of Szczecin

Zeszyty Naukowe
Akademia Morska w Szczecinie

2013, 36(108) z. 1 pp. 100–104
ISSN 1733-8670

2013, 36(108) z. 1 s. 100–104

Reliability analysis of a system subjected to two-state operation process

Ewa Kuligowska

Gdynia Maritime University
81-225 Gdynia, ul. Morska 81–87, e-mail: e.kuligowska@wn.am.gdynia.pl

Key words: reliability analysis, simulation methods, operation states, a semi-Markov process, modeling

Abstract

The paper presents analytical and Monte Carlo simulation methods applied to the reliability evaluation of a system operating at two different operation states. A semi-Markov process is applied to construct the system operation model and its main characteristics are determined. Analytical linking of this operation model with the system reliability model is proposed to get a general reliability model of the system operating at two varying operation conditions and to find its reliability characteristics. The application of Monte Carlo simulation based on this general model to the reliability evaluation of this system is proposed as well. The results obtained from those two considered methods are evaluated.

Introduction

The reliability analysis of a system subjected to varying in time its operation process very often leads to complicated calculations and, therefore, it is difficult to implement analytical modeling, prediction and optimization, especially in the case when we assume the system multistate reliability model and the multistate model of its operation process [1, 2, 3, 4, 5]. On the other hand, the complexity of the systems' operation processes and their influence on changing in time the systems' reliability parameters are very often met in real practice [3, 6, 7, 8]. Thus, the practical importance of an approach linking the system reliability models and the system operation processes models into an integrated general model in reliability assessment of real technical systems is evident. The Monte Carlo simulation method [5, 9] is a tool that sometimes allows to simplify solving this problem [4, 10, 11]. All cited here publications presents general results obtained under a strong assumption that the system components have exponential conditional reliability functions at different operation states. To omit this assumption that narrows the investigation down and to get general solutions of the problem, at the beginning, we deal with the two-state reliability model of the system and two-state model of its operation process. The analytical approach to the reliability analysis of two-state systems subjected to two-state operation processes is presented and next the computer simulation modeling method for such systems reliability assessment is proposed.

System operation process

We assume that a system during its operation at the fixed moment t, $t \in \langle 0, +\infty \rangle$, may be at one of two different operations states z_b, $b = 1,2$. Consequently, we mark by $Z(t)$, $t \in \langle 0,+\infty \rangle$, the system operation process, that is a function of a continuous variable t, taking discrete values at the set $\{z_1, z_2\}$ of the system operation states. We assume a semi-Markov model [2, 3] of the system operation process $Z(t)$ and we mark by θ_{bl} its random conditional sojourn times at the operation states z_b, when its next operation state is z_l, $b,l = 1,2$, $b \neq l$. The exemplary realizations of the considered system operation process are presented in figure 1.

Consequently, the operation process may be described by the following parameters [4]:

– the vector $[p_b(0)]_{1\times 2}$, $b = 1,2$, of the initial probabilities of the system operation process $Z(t)$

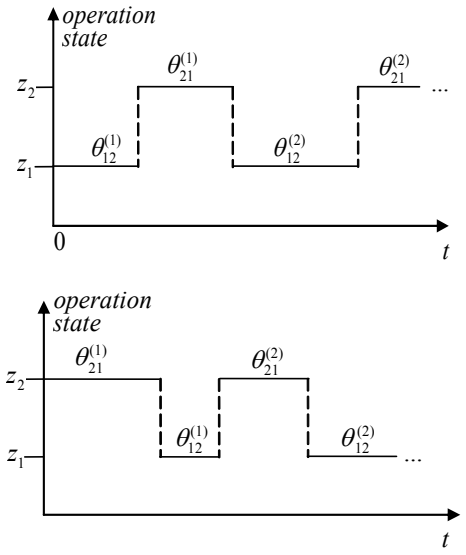

Fig. 1. The exemplary realizations of the system operation process

staying at the particular operation states at the moment $t = 0$;

- the matrix $[p_{bl}]_{2\times 2}$ of the probabilities of the system operation process $Z(t)$ transitions between the operation states z_b and z_l, $b,l = 1,2$, $b \neq l$;
- the matrix $[H_{bl}(t)]_{2\times 2}$ of the conditional distribution functions of the system operation process $Z(t)$ conditional sojourn times θ_{bl} at the operation states, $b,l = 1,2$, $b \neq l$.

We mark by:

$$\phi_1^{(n)}(t) = P(\theta_1^{(n)} < t),\ t \in \langle 0,\infty),\ n = 1,2,...,$$

the distribution functions of the random variables:

$$\theta_1^{(n)} = \theta_{12}^{(1)} + \theta_{12}^{(2)} + ... + \theta_{12}^{(n)},\ n = 1,2,...,$$

where the variables $\theta_{12}^{(i)}, i = 1,2,...,n,$ are independent random variables having identical distribution functions with the distribution of the sojourn time θ_{12}, i.e.:

$$P(\theta_{12}^{(i)} < t) = P(\theta_{12} < t) = H_{12}(t),\ i = 1,2,...,n,$$

and by:

$$\phi_2^{(n)}(t) = P(\theta_2^{(n)} < t),\ t \in \langle 0,\infty),\ n = 1,2,...,$$

the distribution functions of the random variables:

$$\theta_2^{(n)} = \theta_{21}^{(1)} + \theta_{21}^{(2)} + ... + \theta_{21}^{(n)},\ n = 1,2,...,$$

where the variables $\theta_{21}^{(i)}, i = 1,2,...,n,$ are independent random variables having identical distribution functions with the distribution of the sojourn time θ_{21}, i.e.:

$$P(\theta_{21}^{(i)} < t) = P(\theta_{21} < t) = H_{21}(t),\ i = 1,2,...,n.$$

Realizations $\theta_{12}^{(i)}$ and $\theta_{21}^{(i)}$ of the random variables $\theta_{12}^{(i)}$ and $\theta_{21}^{(i)}, i = 1,2,...,$ are illustrated in figure 1.

Consequently, we get:

$$\phi_1^{(1)}(t) = H_{12}(t),$$

$$\phi_1^{(n)}(t) = \int_0^t \phi_1^{(n-1)}(t-u)\,\mathrm{d}H_{12}(u),\ n = 2,3,...,$$

$$\phi_2^{(1)}(t) = H_{21}(t),$$

$$\phi_2^{(n)}(t) = \int_0^t \phi_2^{(n-1)}(t-u)\,\mathrm{d}H_{21}(u),\ n = 2,3,....$$

Moreover, we mark by:

$$\psi^{(n)}(t) = P(\theta^{(n)} < t),\ t \in \langle 0,\infty),\ n = 1,2,...,$$

the distribution functions of the random variables:

$$\theta^{(n)} = \theta_1^{(n)} + \theta_2^{(n)},\ n = 1,2,...,$$

and we have:

$$\psi^{(n)}(t) = \int_0^t \phi_1^{(n)}(t-u)\,\mathrm{d}\phi_2^{(n)}(u)$$
$$t \in \langle 0,\infty),\ n = 1,2,..., \qquad (1)$$

If we denote by $N(t)$ the number of changes of the system operation process' states before the moment t, by $N_b(t)$, $b = 1,2$, the number of changes of the system operation process' states before the moment t when its operation process at the initial moment $t = 0$ was at the operation state z_b, $b = 1,2$, for $t \in \langle 0,+\infty)$, we immediately get the following results [5].

Proposition 1

The distribution of the number $N(t)$ of changes of the system operation process' states before the moment t, $t \in \langle 0,+\infty)$, are given by:

$$P(N(t) = 2n) =$$
$$= \psi^{(n)}(t)\left[p_1(0)\left(1 - \int_0^t \psi^{(n)}(t-u)\,\mathrm{d}H_{12}(u)\right) + \right. \qquad (2)$$
$$\left. + p_2(0)\cdot\left(1 - \int_0^t \psi^{(n)}(t-u)\,\mathrm{d}H_{21}(u)\right)\right]$$

$$P(N(t) = 2n+1) = p_1(0)\cdot\int_0^t \psi^{(n)}(t-u)\,\mathrm{d}H_{12}(u)\cdot$$
$$\cdot\left(1 - \int_0^t \psi^{(n+1)}(t-u)\,\mathrm{d}H_{21}(u)\right) +$$
$$+ p_2(0)\cdot\int_0^t \psi^{(n)}(t-u)\,\mathrm{d}H_{21}(u)\cdot \qquad (3)$$
$$\cdot\left(1 - \int_0^t \psi^{(n+1)}(t-u)\,\mathrm{d}H_{12}(u)\right)$$

for $t \in \langle 0,+\infty)$, $n = 0,1,2,...,$ where $\psi^{(0)}(t) = 1$ and $\psi^{(n)}(t)$ for $n = 1,2,...,$ are determined by (1).

System reliability subjected to two-state operation process

We assume that the considered two-state system reliability depends on its operation state it is operating and on the number of changes of the operation process states. We define the system conditional reliability function at the operation state z_b, $b = 1,2$, after k, $k = 0,1,...$, changes of its operation process states:

$$R_k^{(b)}(t) = P(T_k^{(b)} > t)$$
$$t \in \langle 0,\infty), \quad b = 1,2, \; k = 0,1,..., \tag{4}$$

where $T_k^{(b)}$, $b = 1,2$, $k = 0,1,...$, is the lifetimes of the system at the operation state z_b, $b = 1,2$, after k, $k = 0,1,...$, changes of its operation process states with the conditional distribution functions:

$$F_k^{(b)}(t) = P(T_k^{(b)} \le t) = 1 - R_k^{(b)}(t)$$
$$t \in \langle 0,\infty), \quad b = 1.2, \; k = 0,1,....$$

Under those assumptions, we want to find the unconditional reliability function of the system subjected to two-state operation process:

$$\boldsymbol{R}(t) = P(T > t), \; t \in \langle 0,\infty),$$

where T is the unconditional lifetime of the system with the unconditional distribution function:

$$\boldsymbol{F}(t) = P(T \le t), \; t \in \langle 0,\infty).$$

Analytical approach to system reliability evaluation

The application of Proposition 1 results in the following proposition.

Proposition 2

The unconditional reliability function of the system subjected to two-state operation process is given by:

$$\boldsymbol{R}(t) = \sum_{k=0}^{\infty} P(N(t) = k) R_k^{(b)}(t), \; t \in \langle 0,\infty),$$

where the distribution $P(N(t) = k)$, $t \in \langle 0, \infty)$, $k = 0,1,...$, is determined by (2)–(3) and $R_k^{(b)}(t)$, $t \in \langle 0, \infty)$, $b = 1,2$, $k = 0,1,...$, are the conditional reliability functions of the system determined by (4).

Its particular case for the Weibull conditional reliability functions is as follows.

Corollary 1

If the conditional reliability functions of the system subjected to two-state operation process are:

$$R_k^{(b)}(t) = \exp[-\alpha_k^{(b)} t^{\beta_k^{(b)}}]$$
$$t \in \langle 0, \infty), \; k = 0,1,..., \; b = 1,2,... \tag{5}$$

Then, the unconditional reliability function of the system subjected to two-state operation process is given by:

$$\boldsymbol{R}(t) = \sum_{k=0}^{\infty} P(N(t) = k) \exp[-\alpha_k^{(b)} t^{\beta_k^{(b)}}], \; t \in \langle 0,\infty),$$

where the distribution $P(N(t) = k)$, $t \in \langle 0, \infty)$, $k = 0,1,...$, is determined by (2)–(3). Unfortunately, the fixed analytical results are complex and difficult to apply practically. The problem can also be analyzed by Monte Carlo simulation method.

Monte Carlo approach to system reliability evaluation

We can apply the Monte Carlo simulation method based on the result of Corollary 1, according to a general Monte Carlo simulation scheme presented in figure 2.

At the beginning, we fix the following parameters:

- the number $N \in \boldsymbol{N} \setminus \{0\}$ of iterations (runs of the simulation) equal to the number of the system lifetime realizations;
- the vector of the initial probabilities $[p_b(0)]$, $b = 1,2$, of the system operation process $Z(t)$ states at the moment $t = 0$ defined in Section 2;
- the matrix of the probabilities $[p_{bl}]$, $b,l = 1,2$, $b \ne l$, of the system operation process $Z(t)$ transitions between the various system operation states defined in Section 2.

Next, we generate the realizations of the conditional sojourn times $\theta_{bl}^{(i)}$, $b,l = 1,2$, $b \ne l$, $i = 1,2,...,n$, of the system operation process at the operation states defined in Section 2.

Further, we generate the realizations of the system conditional lifetimes $T_k^{(b)}$, $b = 1,2$, $k = 0,1,...$, according to the formula (4).

In the next step we introduce:

- $k \in \boldsymbol{N}$ as the number of system operation process states changes;
- $j \in \boldsymbol{N} \setminus \{0\}$ as the subsequent iteration in the main loop and set $j = 1$;
- $t_j \in \langle 0,\infty)$, $j = 1,2,...,N$ as the system unconditional lifetime realization and set $t_j = 0$.

As the algorithm progresses, we draw a random number q from the uniform distribution on the interval $\langle 0,1 \rangle$. Based on this random value, the realization $z_b(q)$, $b = 1,2$, of the system operation process initial operation state at the moment $t = 0$ is generated according to the formula:

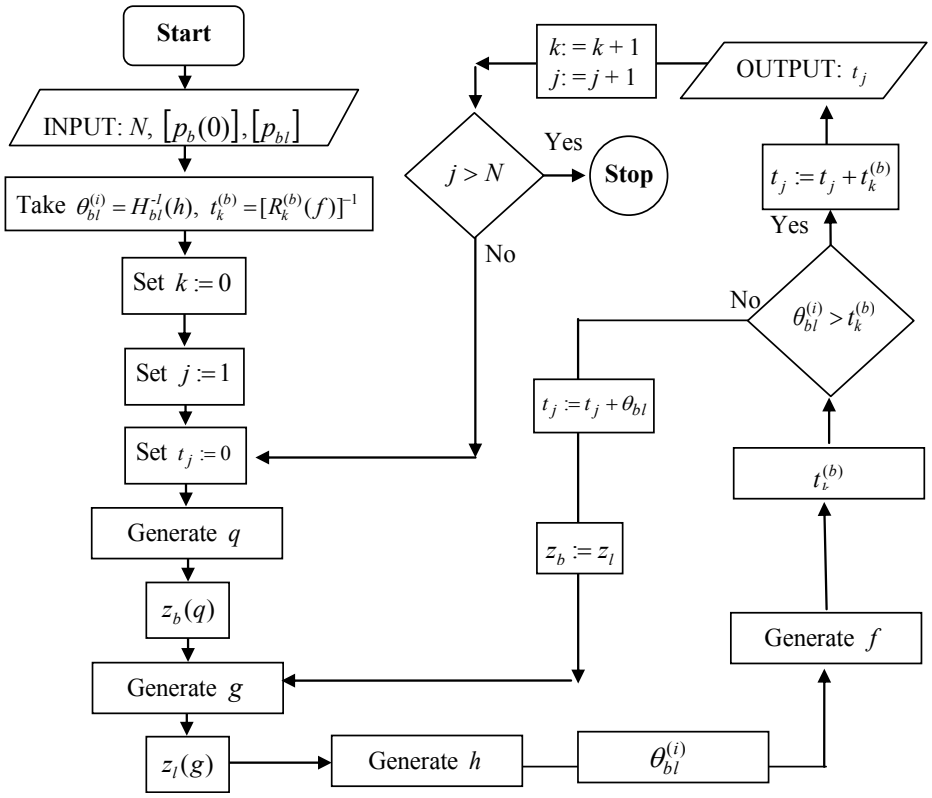

Fig. 2. Monte Carlo algorithm for a system reliability evaluation

$$z_b(q) = \begin{cases} z_1, & 0 \le q < p_1(0), \\ z_2, & p_1(0) \le q < 1. \end{cases}$$

Next, we draw a random number g uniformly distributed on the unit interval. Concerning this random value, the realization $z_l(g)$, $l = 1,2$, $l \neq b$, of the system operation process consecutive operation state is generated according to the formulas:

$$z_{1l}(g) = z_2,$$
$$z_{2l}(g) = z_1.$$

Further, we generate a random number h from the uniform distribution on the interval $\langle 0,1 \rangle$, which we put into the formula $H_{bl}^{-1}(t)$, $b,l = 1,2$, $b \neq l$ obtaining the realization $\theta_{bl}^{(i)}$, $b,l = 1,2$, $b \neq l$, $i = 1,2,...,n$. Subsequently, we generate a random number f uniformly distributed on the unit interval, which we put into the formula (5) obtaining the realization $t_k^{(b)}$, $b = 1,2$. If the realization of the empirical conditional sojourn time is not greater than the realization of the system conditional lifetime, we add to the system unconditional lifetime realization t_j the value $\theta_{bl}^{(i)}$. The realization t_j is recorded and z_l is set as the initial operation state.

We generate another random numbers g, h, f from the uniform distribution on the interval $\langle 0,1 \rangle$ obtaining the realizations $z_l(g)$, $\theta_{bl}^{(i)}$ and $t_k^{(b)}$, $b,l = 1,2$, $b \neq l$. Each time we compare the realization of the conditional sojourn time $\theta_{bl}^{(i)}$ with the realization of the system conditional lifetime $t_k^{(b)}$. If $\theta_{bl}^{(i)}$ is greater than $t_k^{(b)}$, we add to the sum of the realizations of the conditional sojourn times $\theta_{bl}^{(i)}$ the realization $t_k^{(b)}$ and we obtain and record an system unconditional lifetime realization t_j. Thus, we can proceed replacing j with $j + 1$ and shift into the next iteration in the loop if $j < N$. In the other case, we stop the procedure.

Example 1

The input data for the system operation process are:

– the vector of the initial probabilities of the system operation process $Z(t)$ staying at the particular operation states at the moment $t = 0$:

$$[p_b(0)]_{1\times 2} = [0.4, 0.6];$$

– the matrix of the probabilities of the system operation process $Z(t)$ transitions between the operation states:

$$[p_{bl}]_{2\times 2} = \begin{bmatrix} 0 & 1 \\ 1 & 0 \end{bmatrix};$$

– the matrix of the conditional distribution functions of the system operation process $Z(t)$ sojourn times $\theta_{bl}^{(i)}$, $b,l = 1,2,\ b \neq l,\ i = 1,2,...,n$ at the operation states:

$$H_{12}(t) = F_{N(m_{12},\sigma_{12})}(t),\ H_{21}(t) = F_{N(m_{21},\sigma_{21})}(t),$$

where:

$$m_{12} = 290,\ \sigma_{12} = 10,\ m_{21} = 70,\ \sigma_{21} = 5.$$

The input data for the system reliability are:

$$R_k^{(1)}(t) = \exp[-0.0000033 5\frac{2k+1}{k+1}t^2],$$

$$R_k^{(2)}(t) = \exp[-0.0000016 3\frac{2k+1}{k+1}t^2],$$

$$t \in \langle 0,\infty),\ \ k = 0,1,2,.... \qquad (6)$$

The results of simulation calculated for $N = 1{,}000{,}000$ realizations are:

– the mean value of the system unconditional lifetime $\overline{T} \approx 820$ days;
– the standard deviation $\sigma \approx 676$ days.

Conclusions

The discussed problem seems to be very interesting in practice because of the natural omitting the assumption on exponentiality of the system reliability functions at operation states. Both, the analytical method and the simulation method, should be modified and developed to get results better fitting to real technical systems.

References

1. GRABSKI F., JAŹWIŃSKI J.: Funkcje o losowych argumentach w zagadnieniach niezawodności, bezpieczeństwa i logistyki. Wydawnictwa Komunikacji i Łączności, Warszawa 2009.
2. GRABSKI F.: Semi-Markowskie modele niezawodności i eksploatacji. System Research Institute, Polish Academy of Science, Warszawa 2002.
3. KOŁOWROCKI K., SOSZYŃSKA-BUDNY J.: Reliability and Safety of Complex Technical Systems and Processes: Modeling – Identification – Prediction – Optimization. Springer, London-Dordrecht-Heidelberg-New York 2011.
4. KULIGOWSKA E.: Preliminary Monte Carlo approach to complex system reliability analysis. Journal of Polish Safety and Reliability Association, Summer Safety and Reliability Seminars, Vol. 3, 2012, 59–71.
5. KULIGOWSKA E.: Monte Carlo simulation analysis of complex technical system reliability. Report, Gdynia Maritime University, 2013.
6. KOŁOWROCKI K., SOSZYŃSKA J.: Reliability modeling of a port oil transportation system's operation processes. International Journal of Performability Engineering, Vol. 6, No. 1, 2010, 77–87.
7. SOSZYŃSKA J.: Systems reliability analysis in variable operation conditions. International Journal of Reliability, Quality and Safety Engineering. Special Issue: System Reliability and Safety, Vol. 14, No. 6, 2007, 617–634.
8. SOSZYŃSKA J.: Reliability and risk evaluation of a port oil pipeline transportation system in variable operation conditions. International Journal of Pressure Vessels and Piping Vol. 87, No. 2–3, 2010, 81–87.
9. ZIO E., MARSEGUERRA M.: Basics of the Monte Carlo Method with Application to System Reliability. LiLoLe, Hagen 2002.
10. KOŁOWROCKI K, KULIGOWSKA E.: Monte Carlo simulation application to reliability evaluation of port grain transportation system operating at variable conditions. Journal of Polish Safety and Reliability Association, Summer Safety and Reliability Seminars, Vol. 4, No. 1, 2013, 73–81.
11. KULIGOWSKA E.: Monte Carlo simulation for reliability assessment and optimization of an system to varying operation conditions. Journal of Polish Safety and Reliability Association, Summer Safety and Reliability Seminars, Vol. 4, No. 2, 2013, 205–218.

Scientific Journals
Maritime University of Szczecin

Zeszyty Naukowe
Akademia Morska w Szczecinie

2013, 36(108) z. 1 pp. 105–109
ISSN 1733-8670

2013, 36(108) z. 1 s. 105–109

Theoretical and experimental methods for prediction the propeller jet hydrodynamic loads

Łukasz Lewczuk, Teresa Abramowicz-Gerigk, Zbigniew Burciu

Gdynia Maritime University
81-225 Gdynia, ul. Morska 81–87

Key words: prediction, hydrotechnical construction, propeller, thruster, manoeuvring procedures

Abstract
The paper presents the theoretical and experimental methods used in scientific and operational practice to predict the hydrodynamic loads generated by propellers and thrusters on the hydrotechnical constructions. The influence of different parameters: pitch and rotational speed of the propeller, aft body form of the ship hull and shallow water effect on the velocity field are discussed.

Introduction

Prediction of the hydrodynamic loads generated by propellers and thrusters on the quays or seabed protection in ports is the case of still growing importance due to the increase of short sea shipping and number of high powered self-manoeuvring vessels. The main objectives in this case are the accurate data to design well protected hydrotechnical constructions and develop safe manoeuvring procedures [1, 2].

In the calculations of the propeller wash only 20–25% of the maximum installed engine power used per propeller is assumed with respect to operational restrictions in ports. In practice, the amount of power in different weather or ice conditions, used during manoeuvres, can be much greater [3].

The empirical formulae developed on the basis of the theoretical and experimental studies are used to predict the maximum design loads and distribution of the loads in time and space domains to determine reliability or safety functions for the port structures [4, 5, 6, 7]. They can be used for water depth optimization in berthing areas [8] and prediction of boundary weather conditions for the particular manoeuvers.

The major concern is the downstream propeller jet flow which lasts for the distance of several propeller diameters and has the axial velocity components whose magnitudes can exceed 10 m/s [9, 10]. In shallow water conditions the tangential and vertical velocity components can be the reason of propeller scouring under the vessel in the propeller plane [3]. The axial velocity distribution is different compared to the common design methods. The velocities are overestimated using the "Dutch method" and even more overestimated with the "German method" [11].

The results of the calculations based on two formulae proposed by and Blaauw and Van De Kaa [12] and Lam [13] in for efflux velocity for the open water propeller are compared with the measurements of mean jet velocities on the appended hull just behind the rudder.

Theoretical methods for prediction of hydrodynamic loads from propeller jet

PIANC [6] recommends Dutch and German methods for jet induced flow prediction for design of sea bed protection. These methods are valid only for a non-ducted propeller jets. They represent two different ways of computing the required flow velocities and are based on the axial momentum theory. However, both methods are based on the similar principles, the different empirical constants are used in them, therefore, mixing these two methods could lead to inaccurate results. The principles of

Dutch and German methods are presented in figure 1.

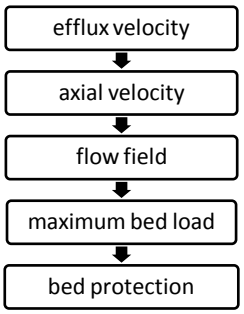

Fig. 1. Dutch and German method principles

There are serious limitations of the axial momentum theory regarding to propeller jets:

- the theory includes axial flow directions but omits the tangential and radial velocity which also occur;
- the velocities on each side of the propeller are not equal;
- the maximum axial velocity does not occur at any lateral section at the rotation axis.

The main parameters used in both, theoretical and experimental methods, for prediction of hydrodynamic loads from propeller jet cited in the paper are presented in table 1.

Dutch method for prediction of hydrodynamic loads from propeller jet

Blaauw and Van De Kaa [12] derived an equation for the estimated value of the efflux velocity. The flow directly behind the propeller is defined as a relation between rotational speed of the propeller, propeller diameter and propeller thrust coefficient. This equation is used in both Dutch and German method:

$$U_0 = 1.60\, n_p\, D_p \sqrt{K_t} \tag{1}$$

In some cases the propeller thrust coefficient is not known. For that reason, Blaauw and Van De Kaa [12] created another equation which includes engine power of the vessel, density of water and diameter of the jet just behind the propeller:

$$U_0 = 1.15\left(\frac{P}{\rho_w D_0^2}\right)^{1/3} \tag{2}$$

The equation for the flow velocity along the jet axis depends on flow behind the propeller, located at maximal contraction of the jet, distance in axial direction from propeller and propeller diameter:

$$U_{x,\mathrm{axis}} = 2.8\, U_0\, \frac{D_p}{X} \tag{3}$$

Table 1. Main parameters used in theoretical and experimental methods

Parameter	Description	Units
a	coefficient = 2.8	–
A	1.88·exp(–0.092 H_{pb}/D_p) – no rudder, for ($0.9 \le H_{pb}/D_p \le 9$) 1.88·exp(–0.092 H_{pb}/D_p) – with central rudder, for ($0.9 \le H_{pb}/D_p \le 8$) 2.6 – unobstructed jets	–
C_4	0.25 – two propellers 0.30 – restriction by a transverse wall 1.62 – jet reflected at a quay wall 0.60 – with a restriction from bed and water level 1.00 – no restrictions	–
D_0	diameter of the jet just behind the propeller, located at the point of maximal contraction $D_0 = D/\sqrt{2} \approx 0.71\, D_p$ – applied to thrusters without tunnel $D_0 = 0.85 \cdot D_p$ – applied to propeller jet in a tunnel $D_0 = 1.00 \cdot D_p$ _ applied to ducted thrusters	m
D_p	propeller diameter	m
E	0.71 – for sea going vessels equipped with a rudder 0.42 – for sea going vessels not equipped with a rudder 0.25 – for inland vessels with a tunnel stern and twin rudder configuration	–
H_{pb}	distance between the bed and the propeller axis	m
K_t	propeller thrust coefficient	–
n_L	scale factor for length	–
n_p	rotational speed of the propeller	s^{-1}
n_u	scale factor for flow velocity	
r	radial distance from the propeller axis	m
P	engine power	W
R_m	radius of the maximum axial velocity	m
R_p	propeller radius	m
R_h	propeller hub radius	m
ρ_w	density of water	kg/m³
U_0	flow directly behind the propeller, situated on the maximal contraction of the jet	m/s
$U_{b,\max}$	maximum flow velocity along horizontal bed	m/s
$U_{x,\mathrm{axis}}$	axial flow velocity in the centre of a free non ducted jet	m/s
$U_{x,\max}$	maximum axial flow velocity	m/s
$U_{x,r}$	axial flow velocity at radius r from the axis	m/s
X	axial distance	m

The equation for flow velocity distribution includes flow velocity along jet axis, distance in axial direction from the propeller and radial distance to the propeller axis:

$$U_{x,r} = U_{x,\mathrm{axis}} \exp\left[-15.4(r/X)^2\right] \tag{4}$$

The values between 0.1–0.25 obtained by Verheij [11] results in:

$$U_{b,\max} = 0.3\,U_0\,\frac{D_0}{H_{pb}} \tag{5}$$

German method for prediction of hydrodynamic loads from propeller jet

This method is established by Fuehrer, Römisch and Engelke [5]. The basic assumptions are exactly the same as in the Dutch method. Flow directly behind the propeller, situated on the maximal contraction of the jet, is calculated using equation (1) or (2).

The equation for flow velocity along jet axis in comparison to Dutch method uses values of constant A and exponent *a*:

$$U_{x,\text{axis}} = A\,U_0\left(\frac{D_p}{X}\right)^a \tag{6}$$

The flow velocity distribution equation:

$$U_{x,r} = U_{x,\text{axis}}\exp\left[-22.2\left(\frac{r}{X}\right)^2\right] \tag{7}$$

In the equation for maximum flow velocity constant values and C_4 are used:

$$U_{x,\max} = U_0\,A\left(\frac{X}{D_p}\right)^{-C_4} \tag{8}$$

The formula for the maximum velocity at the bed (9) is developed for the different types of ships: sea going vessels equipped with a rudder, sea going vessels not equipped with a rudder, inland vessels with a tunnel stern and twin rudder configuration, expressed in the form of constant *E* values given in table 1.

$$U_{b,\max} = E\,U_0\left(\frac{h_{pb}}{D_p}\right)^{-1} \tag{9}$$

Experimental methods for prediction of hydrodynamic loads from propeller jet

The experimental methods for prediction of hydrodynamic loads from propeller jet are mostly based on physical scale model tests which include average flow velocities and turbulence.

One of the major limitations of the model tests is the scale effect due to the difficulties in obtaining accurately dynamic and geometrical similarity of fluid flow. Mainly due to the influence of viscosity scale effect it is not possible to obtain proper scaling of all dynamic forces which act on the real seagoing vessel and transfer it to the physical scale model.

The Froude criterion with a high Reynolds number is used to obtain dynamic similarity and minimizing viscous scale effects. The gravity acceleration is exactly the same in the prototype and model for the Froude number $n_u = (n_L)^{1/2}$ and the Reynolds number $n_u = n_L^2$.

Reynolds number for a physical model is about 100 times smaller than it is for real ships [2]. It is recommended by the ITTC'78 (International Towing Tank Conference) to input empirical amendments which include viscosity. For the power-propulsion research, the extrapolation methods can

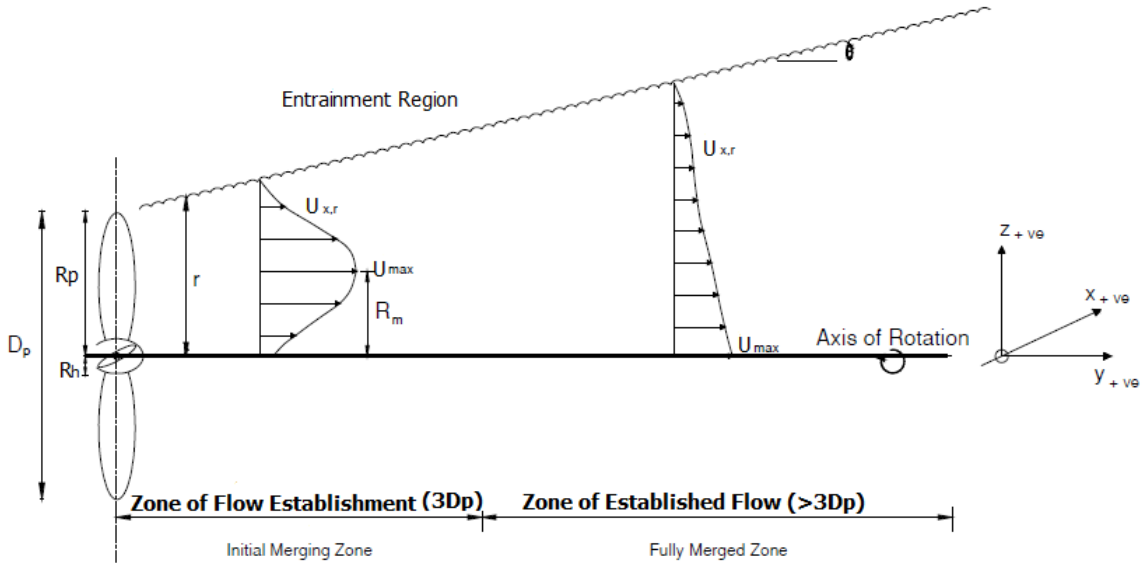

Fig. 2. Distribution of the axial velocity by Lam

be used. The Reynolds number for physical model of the propeller should be larger than the critical Reynolds number.

The experiments are conducted to establish equations for efflux velocity, maximum flow velocity, flow velocity distribution and maximum velocity over the sea bed. Lam et al. [14] presented a maximum tangential velocity which stands for 82% of the maximum axial velocity. The tangential velocity has two peaks lying in between the rotation axis and the jet boundary, at the efflux plane. Additionally, he showed that the contraction at the efflux plane is trifling.

Figure 2 [14] illustrates that the position of the maximum velocity within the zone of flow establishment remains at the constant location r/R_p = 0.53 from the rotation axis and for the zone of established flow remains at the rotation axis $r/R_p = 0$.

The distribution of the axial velocity is not axisymmetric. It is influenced by the rudder, aft body shape, free surface and seabed [2, 3, 15].

The flow in the stern region of a fully appended hull was analyzed by Muscari et al. [15] by both computational and experimental fluid dynamics. The study was focused on the velocity field induced by the rotating propellers. Measurements have been performed by laser Doppler velocimetry (LDV) on the vertical midplane of the rudder and in two transversal planes behind the propeller and behind the rudder.

The mean axial velocity U measured for deep and shallow water on the appended physical model, in geometrical scale 1:16, just after the rudder, $0.18D_p$ (D_p = 0.319 m) from the propeller plane has been presented in [3].

The result of the measurements behind the rudder compared with efflux velocity values calculated using the semi-empirical equation based on the actuator disc theory proposed by Blaauw and Van De Kaa – efflux velocity U_0 (1) [12] and equation proposed by Hamil – efflux velocity U_{01} (9), refined through several experimental investigations [13] are presented in table 2.

$$U_{01} = 1.33\, n_p\, D_p \sqrt{K_T} \tag{9}$$

Table 2. Mean axial velocities

Propeller settings			U [m/s]		Open water propeller	
θ [°]	n_p [1/s]	K_T	$h/T = 3$	$h/T = 1.2$	U_0 [m/s]	U_{01} [m/s]
5	13.63	0.012	0.284	0.307	0.633474	0.762074
10	15.88	0.032	0.444	0.616	1.205224	1.449894
15	17.08	0.079	0.725	0.907	2.036778	2.450259
19	17.08	0.114	0.917	0.992	2.446711	2.943411

The mean velocity results from the integration of flow speed over the circle area of 0.304 m in diameter, equal to the maximum range of the pressure probe used for the measurements.

The calculated values are over twice greater than the measured mean values. However, the presented mean values are about 50% less than the maximum measured axial velocities.

The thrust coefficient K_T for the corresponding propeller pitch angle θ, propeller rotational speed n_p was calculated using equation (10).

$$K_T = \frac{T}{\rho \cdot n_p^2 \cdot D_p^4} \tag{10}$$

The velocity field was measured behind the port rudder, for the propeller settings presented in table 2, for rudder angle 0° and two depth to draft ratios, $h/T = 1.2$ for shallow water and $h/T = 3$ for deep water.

Conclusions

The knowledge of hydrodynamic loads is essential for better understanding of the forces affecting the hydrotechnical structures. In spite of many investigations there are still some areas in design and experimental methods which should be improved for better protection of quay and bed constructions.

Coefficients in the German method include restrictions of walls, seabed and water level. The German method used in the Hamburg harbour resulted in heavier bed protection, compared to the Dutch method in the Rotterdam harbour, although in the Rotterdam harbour occurs no extensive damage level to bed protection [11].

The Dutch method is still considered leading, however, the results of model tests performed on the appended physical models show the underestimated initial jet velocity, more than twice less than the calculated on the basis of the axial momentum theory. The proper prediction of the initial velocity is the most important problem as it is a basic variable used in design methods.

References

1. ABRAMOWICZ-GERIGK T.: Comprehensive safety analysis of ship – port system with respect to ferry manoeuvring operations. Logistyka 4/2010.
2. ABRAMOWICZ-GERIGK T.: Bezpieczeństwo manewrów krytycznych statków w systemie transportowym autostrady morskiej. Transport 83, 2012.
3. ABRAMOWICZ-GERIGK T.: 3D measurements of the effective propeller jet flow behind the rudder. Sustainable Maritime Transportation and Exploitation of Sea Resource's. Rizzuto & Guedes Soares (eds.). Taylor and Francis Group/Balkema, London 2011.

4. FUEHRER M., RÖMISH K.: Effects of modern ship traffic on islands and ocean waterways and their structures. Proceedings 24th PIANC Congress, Leningrad 1977, 187–198.
5. FUEHRER M., RÖMISCH K., ENGELKE G.: Criteria for dimensioning the bottom and slope protection and for applying the new methods of protecting navigation canals. 25th International Navigation Congress, Permanent International Association of Navigation Congresses, 1981.
6. Guidelines for berthing structures related to thrusters. PIANC, Brussels 2012.
7. RÖMISCH K.: Erosion potential of bow thrusters on canal banks (in German). Binnenschifffahrt-ZfB 11, 2006.
8. GUCMA S., JANKOWSKI S.: Depth Optimization of Designed New Ferry Berth. 7th International Symposium on Marine Navigation and Safety of Sea Transportation TransNav'2007, Gdynia 2007.
9. LAM W., HAMILL G.A., SONG Y.C., ROBINSON D.J., RAGHUNATHAN S.: Experimental investigation of the decay from a ship's propeller. China Ocean Engineering 25(2), 2011, 265–284.
10. WILSON P.R., HAMILL G.A. JOHNSTON H.T., KEE C.: Influence of a Horizontal Boundary on a Marine Propeller Wash. Proc. of the Sixteenth International Offshore and Polar Engineering Conference, San Francisco, California, USA, The International Society of Offshore and Polar Engineers, 2006.
11. VAN DOORN D.: Bow Thruster Currents at Open Quay Constructions on Piles M. Sc. Thesis Delft University of Technology. Delft 2012.
12. BLAAUW H.B., VAN DE KAA E.J.: Erosion of the bottom and sloping banks caused by the screw race of maneuvering ships. Publication 202, Delft 1978, The Netherlands.
13. KEE C., HAMILL G, LAM W., WILSON P.: Investigation of the Velocity Distributions within a Ship's Propeller Wash. Proc. of the Sixteenth Int. Offshore and Polar Engineering Conference, San Francisco, California 2006, 451–456.
14. LAM W., HAMILL G.A., ROBINSON D.J., RAGHUNATHAN S.: Observations of the initial 3d flow from a ship's propeller. Ocean Engineering 37(14–15), 2010, 1380–1388.
15. MUSCARI R., DI MASCIO A.: Numerical simulation of the flow past a rotating propeller behind a hull. Second International Symposium on Marine Propulsors smp'11, Hamburg 2011.

Others

16. FUEHRER M., RÖMISCH K., ENGELKE G.: Criteria for dimensioning the bottom and slope protection and for applying the new methods of protecting navigation canals. 25th International Navigation Congress, Permanent International Association of Navigation Congresses, 1981.
17. VERHEIJ H.J.: The stability of bottom and banks subjected to the velocities in the propeller jet behind ships. Proceedings 8th Int. Harbour Congress, 1983.

Scientific Journals
Maritime University of Szczecin

Zeszyty Naukowe
Akademia Morska w Szczecinie

2013, 36(108) z. 1 pp. 110–115
ISSN 1733-8670

2013, 36(108) z. 1 s. 110–115

M/t "Baltic Carrier" accident. The reconstruction of oil spill with PISCES II simulator application

Kinga Łazuga[1], Lucjan Gucma[1], Marco Perkovic[2]

[1] Maritime University of Szczecin
70-500 Szczecin, ul. Wały Chrobrego 1–2, e-mail: {k.lazuga;l.gucma}@am.szczecin.pl
[2] University of Lubljana

Key words: oil spill, accident, PISCES II simulator, safety, mathematical models

Abstract
This paper presents reconstruction of the oil spill that occurred as result of an m/t "Baltic Carrier" accident. This reconstruction was carried out with use PISCES II simulator. The result of several simulations could be the step to usability and validation of PISCESS II simulator and as a guideline for setting up this kind of simulations.

Introduction

Problems related to oil spills are still actual [1] especially on sea areas of high sensitivity like Baltic Sea qualified by IMO to PSSA (Particularly Sensitive Sea Areas) [2]. However, the safety on the Baltic Sea is relatively high comparing to other regions [3]. All possible efforts have to be taken to increase its level.

Such aims were set up to the Baltic Master I and II project where Maritime University of Szczecin took part as partner conducting several studies in field of oil spill at sea.

The research area with highest importance is using mathematical models and simulators for prediction of accidental situations, response planning and training. The paper presents the biggest oil spill on the Baltic Sea reconstructed with used of PISCES II simulator for validation purposes.

M/t "Baltic Carrier" accident

In the morning of the 29th of March 2001 at 0015 (L.T.), the vessel "Tern" and the oil tanker "Baltic Carrier" (Table 1) collided on the Baltic Sea in the position 54°43'N and 012°35'E, east of the Danish Falster Island. "Tern" was the bulk carrier carrying sugar from Cuba to Latvia. "Tern" ran into the tanker "Baltic Carrier", which was carrying 30,000 tons of heavy fuel oil of 380 type from Estonia to Sweden [4]. Parameters of collided ships are presented in table 1.

Table 1. Particular of the vessels [4]

Name of ship	BALTIC CARRIER	TERN
Registration No.	V7CC4	P3Q02
Home Port	Majuro	Limassol
Flag	Marshall Island	Cyprus
IMO No.	9208124	7327603
Type of ship	Chemical / Oil Tanker	Bulk Carrier
Construction year	2000	1973
Tonnage	22500 BT	20362 BT
Length / breadth / draft (in meters)	182.2/27.3/10.9	185.5/26.0/11.1
Engine Power	12 871 kW	8496 kW
Crew	19	22
Owner	Interorient Nav, Hamburg	Ranger Marine SA, Piraeus
Classification Society	Det Norske Veritas	American Bureau of Shipping

After collision heavy fuel oil from tank No. 6 began to release. Sea conditions at that time didn't allow the controlling of leakage and oil slick started to drift towards Danish islands.

Despite the implementation of the contingency plan for a couple hours after the accident, the operation at sea was limited only to observe the

leakage from the air. Sea operations were difficult to organize due to waves of two meters height. About 0530 p.m. the oil slick reached the coast of Bogø, Møn and Falster islands.

Fig. 1. ‘Baltic Carrier’ after the collision [4]

On March 30th the Danish Environmental Protection Agency prepared the Task Force mission to collect the oil settled on beaches. About 50 km of beach was polluted by oil. There was no time left because the highly polluted coastline which consisted mainly on very sensitive wet, shingle and gravel beaches. Also disturbing was the fact that much of the oil had settled on the shore overgrown with reeds.

Due to the inconvenient weather conditions oil recovering was not performed at the sea. About 16 km of the coast was polluted by oil. The area of pollution was divided into 8 zones to make the oil clearance operation more efficient. There were 220 civilians who helped with oil cleaning and 15 vessels involved.

Fig. 2. Localization of the sites of oil recovering [4]

In total from 2700 tons released, 2135 tons of oil was recovered on the coast.

PISCES II Simulator

The Potential Incident Simulation, Control and Evaluation System (PISCES II) is a response simulator that helps with preparing and conducting command centre exercises and area drills in oil spill response. Simulator PISCES II is one of the most effective tools to control and predict the propagation of oil spills.

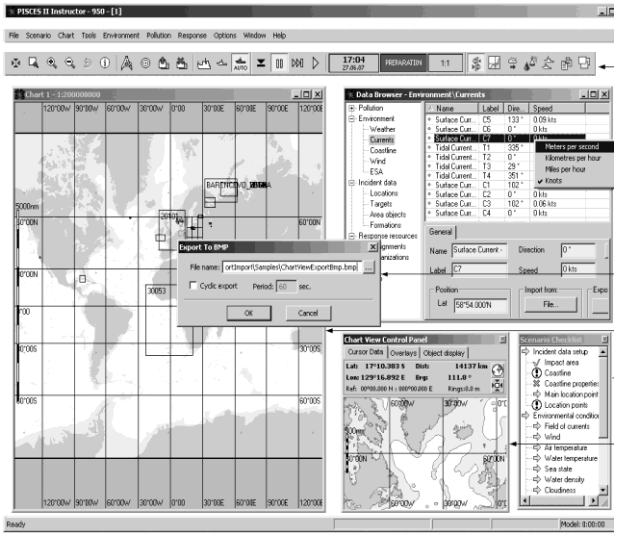

Fig. 3. PISCES II graphical interface layout

The PISCES II (Fig. 3) spill model simulates processes in an oil spill on the water surface: transport by currents and wind, spreading, evaporation, dispersion, emulsification, viscosity variation, burning, and interaction with booms, skimmers, and the coastline (stranding or beaching). The following factors are taken into consideration in the math model [5, 6]:

– environmental parameters: coastline, field of currents, weather, wave height and water density;
– physical properties of spilled oil: specific gravity, surface tension, viscosity, distillation curve and emulsification characteristics;
– properties of spill sources;
– human response actions: booming, on-water recovery, application of chemical dispersants.

Reconstruction of oil spills by PISCES II with use of “Baltic Carrier” case

To check if reconstruction in PISCES II simulator is possible, the case of “Baltic Carrier” has been chosen. Two scenarios were performed on the basis of the real data. Both of them were simulated to evaluate if the oil slick movement is similar to the real scenario.

Scenario 1

In the first scenario the information obtained from the "Baltic Carrier" report provided by Denmark Authorities was applied. In this report there were only general hydrometeorological data, given for the moment of collision. There was no detailed information about its temporal changes.

The simulation was performed on the following data:

Date of accident:

29^{th} of March 2001, 0015 LT.

Accident position:

$\varphi = 54°43.33'N$, $\lambda = 012°35.12'E$.

Spill:

- type of oil: IFO 300 (similar particulars to 380 UK Texaco);
- amount of spill: 2700 tons.

Hydrometeorological conditions:

- wind: direction S-SE, speed 15–18 m/s;
- height of waves: 2.5 m;
- water temperature: 2°C;
- air temperature: 3°C;
- current: direction 315°, speed 5 knots;
- coastland type: sands.

The above conditions were not changed during the simulation as the accident report contained any information about it.

In the first scenario any response resources were used. Oil slick movement in this case was much different than in real case. The probability of reaching the coastline near the real positions was 0 and continuing simulation was abandoned after five hours and 20 minutes (Fig. 4).

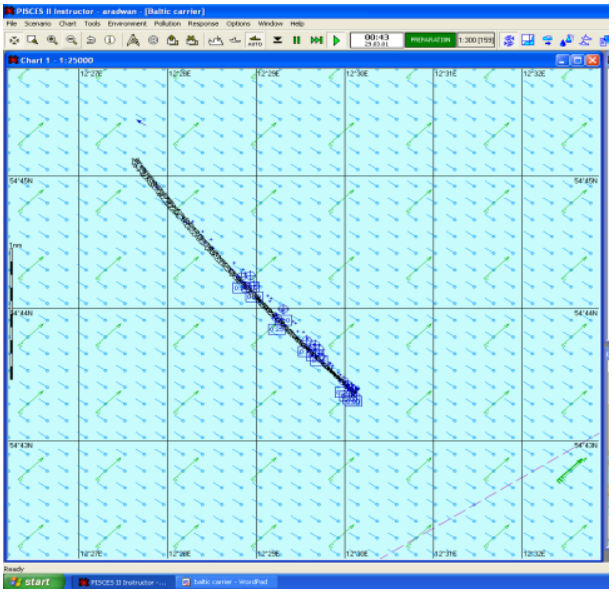

Fig. 4. Movement of the oil slick half an hour after collision

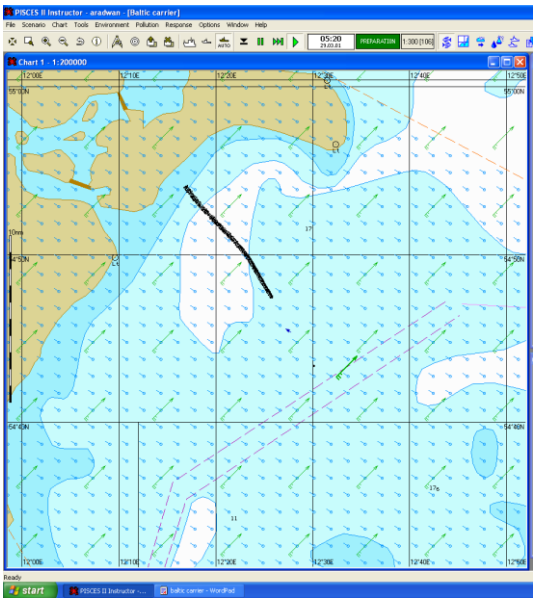

Fig. 5. Position of the oil slick five hours after simulated spill in Scenario 1

Scenario 2

In the second scenario the input data were the same as in the first scenario. Only difference was that now current data are changed during simulation.

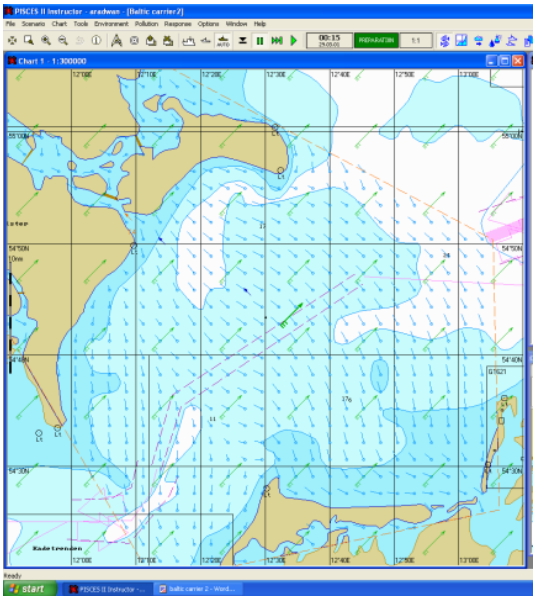

Fig. 6. The beginning of the simulation in Scenario 2

During the simulation the most important data to change were tidal current speed and direction. One hour fifteen minutes after starting the scenario, to increase probability of reaching the coast, current parameters were changed to: direction 295°, speed 2 knots, which is presented in the figure 6. A parameter change has been made in order to fit the simulated trajectory to the real trajectory of the slick.

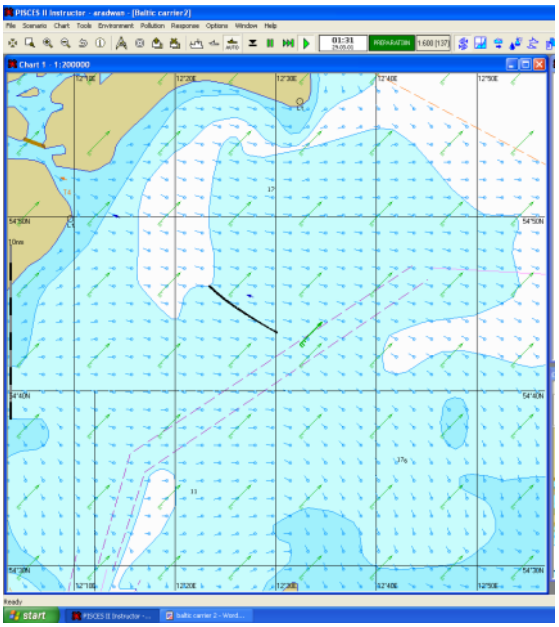

Fig. 7. Movement of the oil slick during changing current parameters

The current speed was reduced to two knots and direction was stated as 290°. The wind speed through the all simulation was not changed. At 0543 a.m. the following data of oil slick were obtained (Fig. 8):

– area of pollution: 3,622,866 m^2;
– maximum thickness: 5.1 mm;
– floating amount: 2645 t;
– stranded amount: 0.0 t.

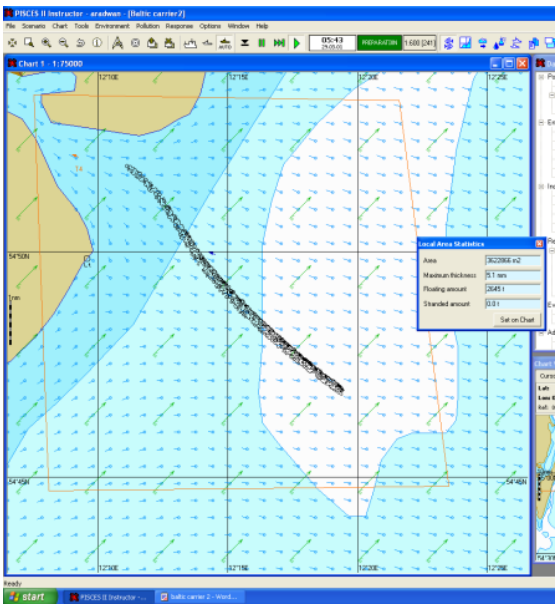

Fig. 8. Movement of the oil slick during changing current parameters 2

In the figure 8 it is precisely presented that the oil will reach the coast on Møn Island. It happened at 0618 a.m. and program showed the information “Oil impact the land” in the information window (Fig. 9). Oil slick parameters at those moments were as follows:

– area of pollution: 3625,501 m^2;
– maximum thickness: 5.7 mm;
– floating amount: 2627 t;
– stranded amount: 8.6 t.

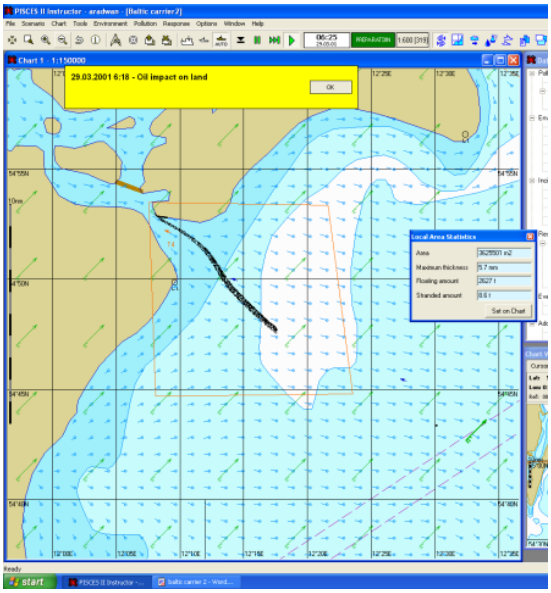

Fig. 9. Oil slick while impact the coast

In the figure 10 it is presented two booms, used in simulation, in “U” shape which were placed at 0700 AM between Bogø and Møn Islands in positions:

– boom formation 2: $\varphi = 54°54.377'N$, $\lambda = 012°05.794'E$;
– boom formation 3: $\varphi = 54°54.251'N$, $\lambda = 012°06.194'E$.

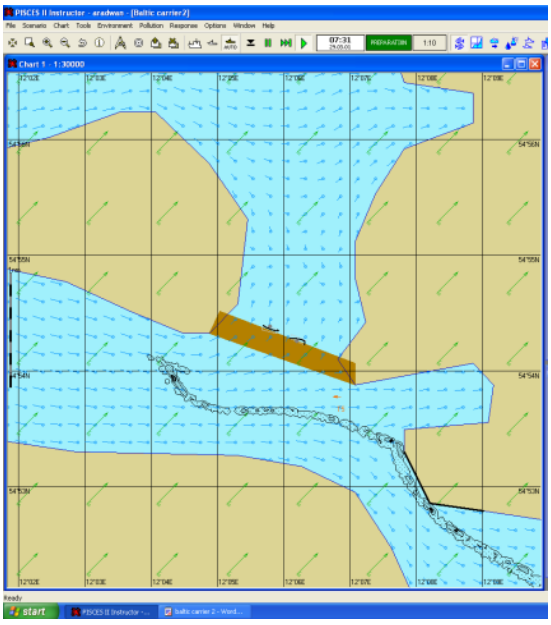

Fig. 10. Booms formation positions

The direction of the tidal current was changed to 270° at about 0800 am. The oil impacted the Bogø Island. The slick was still moving north-east and three more boom formations were set in positions:

– boom formation 4: $\varphi = 54°56.694'N$, $\lambda = 011°58.804'E$;
– boom formation 5: $\varphi = 54°56.557'N$, $\lambda = 011°59.066'E$;
– boom formation 6: $\varphi = 54°55.889'N$, $\lambda = 011°59.881'E$.

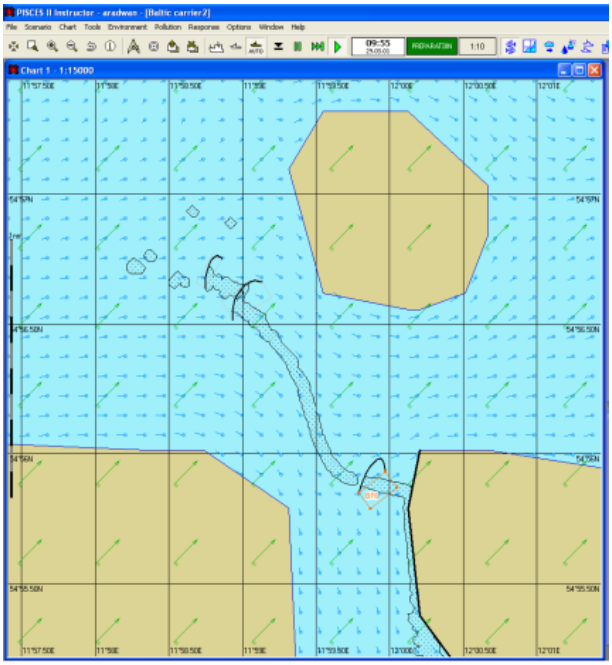

Fig. 11. Oil spill reaches the coast of Bogø Island and goes through the booms

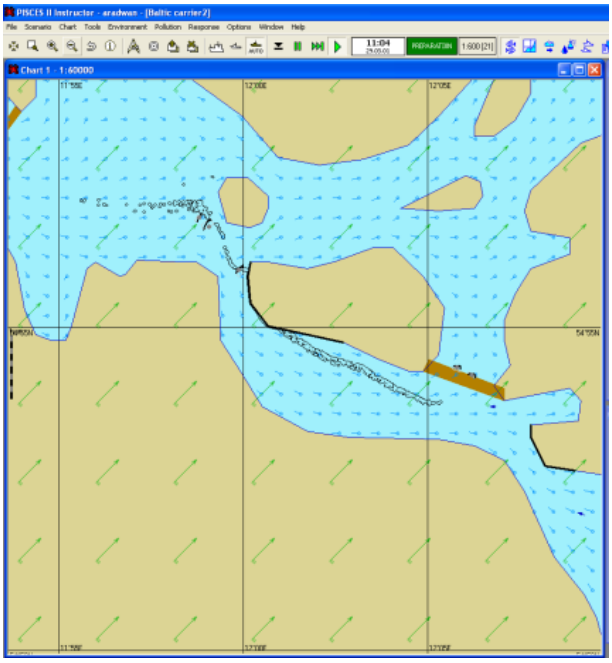

Fig. 12. Booms formation in positions 1

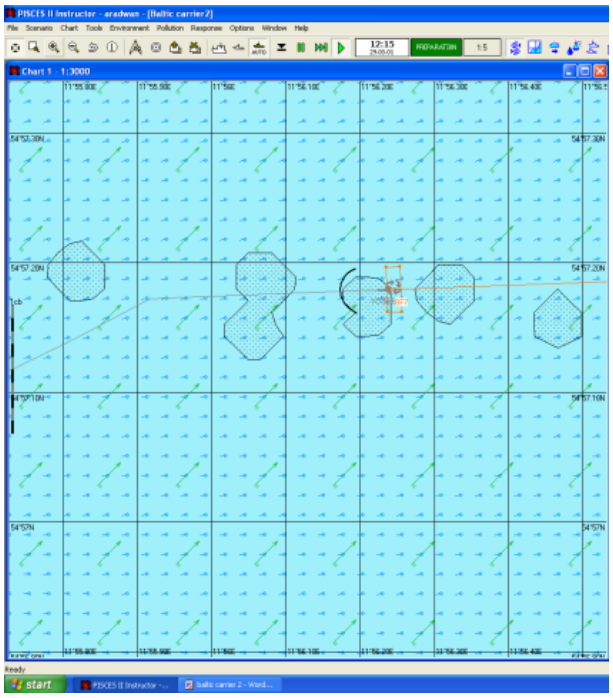

Fig. 13. Booms formation in positions 2

The oil could not be stopped integrally by those three booms, as it is shown in figure 12, so for the thickest and the smallest groups of oil there was located one more boom formation at 1148 a.m. in position $\varphi = 54°57.172'N$, $\lambda = 011°55.916'E$ (Fig. 13).

The boom formation No. 7 was also "U" shape 20 meters length device as the previous booms. But in the opposite it was moving in direction of 88° with speed of 5 knots. Such data were adopted because of tidal current speed and direction. The last boom collected final groups of oil. Only small part of the slick was moving on but it evaporated very quickly not impacting other coasts. After one hour of using boom formation No. 7, which was at 1250 p.m. the simulation was finished.

Conclusions

The aim of this study was to prove that the oil spill reconstruction with use PISCES II simulator is possible. Several limitations, however, have been observed during realization of experiments. The crucial for oil behavior at sea are meteorological conditions which rarely are known. Especially the currents are affecting oil spills. The currents are nor recorded and in many cases only information from accident reports could be used for its determination in past.

The PISCES II simulator showed good correlation with real data especially in case of amount of oil which polluted the beach.

The main advantage of using such tools is possibility to test several scenario of response action with application of scenarios.

As a result of conducted simulations the guidelines could be developed for performing this type of research on the simulator PISCES II. These guidelines relate mainly to the quality and quantity of information to be provided in order to efficiently and accurately simulate. This includes detailed data on every possible change of direction and strength of the wind and current at a given area, type and physical and chemical properties of spilled substance and hydrometeorological conditions.

References

1. PERKOVIC M., PETELIN S., HARSCH R.: Hindcast simulation and data fusion: satellite technology applied to illicit pollution at sea. Scientific Journals Maritime University of Szczecin 20(92), 2010, 107–113.
2. LUDWICZAK K., JUSZKIWICZ W.: The probability of coast pollution – accident simulation in the PISCES II Simulator. 8th International Probabilistic workshop, Szczecin 2010.
3. GUCMA L., PRZYWARTY M.: The Model of Oil Spills Due to Ships Collisions in Southern Baltic Area. Conference proceedings TRANS'NAV 2007. Advances in Marine Navigation and safety of sea transportation, The Nautical Institute, Gdynia 2007.
4. Accident of the oil tanker "Baltic Carrier" off the Danish coastline final report European Task Force in Denmark from 1st to 5th April, 2001.
5. PISCES2 – Potential Incident Simulation, Control & Evaluation System, Transas Marine International.
6. Transas Pisces II Specification, July 2007.

Others

7. GALT J.A.: The Integration of Trajectory Models and Analysis Into Spill Response Information Systems: the Need for a Standard. Second International Oil Spill Research and Development Forum, May 1995.
8. PERKOVIC M., SITKOV A.: Oil Spill Modeling and Combat. University of Ljubljana, Faculty of Maritime Studies and Transportation, Slovenia & Transas Technologies Ltd., Russia.
9. Transas Pisces II What's New, July 2007.

Scientific Journals
Maritime University of Szczecin

Zeszyty Naukowe
Akademia Morska w Szczecinie

2013, 36(108) z. 1 pp. 116–120
ISSN 1733-8670

2013, 36(108) z. 1 s. 116–120

Application of eye-tracking techniques in human factor research in marine operations. Challenges and methodology

Bartosz Muczyński, Maciej Gucma

Maritime University of Szczecin
70-500 Szczecin, ul. Wały Chrobrego 1–2, e-mail: m.gucma@am.szczecin.pl

Key words: eye-tracking, technique methodology, maritime operations, human factor research, data analysis

Abstract
The following paper provides information about eye-tracking techniques and methodology. It is focused on introducing eye movement metrics in human factor research in maritime domain, explaining basic methodology and describing the types of data analysis, thus providing the background and guidelines for simple eye-tracking studies.

Introduction

In the recent years, the human factor has become increasingly important in many different areas, including shipping. Although there is a set of methods successfully used in this field, eye-trackers are rarely used to measure and evaluate bridge environment and officer's behaviour.

The following paper presents how the video-based eye-trackers can be used for improving the safety of navigation, and introduces the basics of eye-tracking methodology.

Eye-trackers

Eye-tracking, as the name suggests, focuses on tracking the position and movement of an eye. In general, we can distinguish two types of eye movement monitoring techniques: those that measure the position of the eye relative to the head; and those that measure the orientation of the eye in space (or *Point of Regard*, POR). For human factor studies, it is very important to understand the connection between eye movement and the visual scene, which allows to measure where, and for how long, the subject was focusing his/her attention, and how often certain areas in visual field were revisited, etc. Such an approach is widely used in usability studies, interface design, marketing, ergonomic evaluation of a workspace and in many other fields where subjects need to acquire information from specific areas in the visual field.

Video based eye-trackers

This type of eye-trackers uses video camera that constantly records the eye to provide information about the eye's position and movement. The most common method to estimate the point of regard (or point of gaze) is based on pupil and corneal reflection tracking.

Pupil is the most distinguishing feature of a human eye and it is relatively easy to extract from the recorded image information about its size and the location of its centre. The corneal reflections of the light source (typically infrared) are known as the Purkinje reflections, or images [1]. Four such images are formed on a human eye, each one on a different layer. Most of the modern eye-trackers determine the location of the first Purkinje image; the one that is formed directly on the outer surface of the cornea, relatively to the pupil centre. Technically, it is possible to use only the pupil-tracking but information about corneal reflection offers an additional reference point that allows for the compensation for the smaller head movements.

A crucial part of every eye-tracking system is the software used. It is directly responsible for the pupil and corneal reflection detection, for calculating the point of regard, and, most importantly,

for the proper identification and classification of the recorded eye movement events. The quality of the gathered data highly depends on the type of algorithm used for raw data processing and it is advised to know the general characteristics and the limitations of the algorithm used for data analysis. More information about the most common algorithms can be found in [2, 3].

Stationary eye-trackers

This type of eye-tracker is perfect for working with a single monitor screen. Most often, it is a small piece of equipment with infrared light source and a camera that is attached below the screen. It is very easy to set up and does not require any additional equipment to be worn by the subject. Its calibration procedure is also fairly easy and reliable. Such eye-trackers are used in studies where stimuli are displayed directly on the screen, and it is very simple to map recorded events on the stimuli picture. From the point of view of the navigator, such an eye-tracker can only be used in a situation, where a subject remains stationary and works on a single screen. For this reason, it is highly difficult to introduce this type of equipment on the navigation bridge, or anywhere else, where the subject is moving. Still, it can be very useful in studies of a single interface, like, for example, a radar screen, ECDIS or for VTS operators.

Mobile eye-trackers

Modern mobile eye-trackers are pieces of head-mounted equipment with two cameras that record eye movements, and one additional camera that records the visual scene in front of the subject. In the most advanced solutions, such an eye-tracker has a form of lightweight glasses that are comfortable to wear and do not restrict head movements. It is widely used in studies where the subject is not stationary. It has already proven useful in studies on a navigation bridge simulator [4, 5]. Its main disadvantage is the time consuming and laborious analysis that requires mapping of every fixation from a video recording onto a static image of the stimulus.

Fig. 1. Example of mobile (left picture) and stationary (right picture) eye-trackers [6]

Eye movement events and their values in human factor researches

From several types of eye movement events (Table 1), two are the most common in human factor studies: the fixations and the saccades. The most recent studies suggest that also microsaccades can be used as a measure for mental workload [7] but to detect microsaccades, which have the duration of 10–20 milliseconds, an eye-tracker with very high sampling rate needs to be used. Most mobile eye-trackers, which are the only practical option to use on-board, have a sampling rate of not more than 30 Hz (with the exception of SMI eye-tracking glasses 2.0, which were presented in September 2013 and have the sampling rate of 60 Hz) and are simply not capable of detecting microsaccades.

Table 1. Types of eye movements and their characteristics

Type	Duration [ms]	Amplitude	Velocity
Fixation	200–300	–	–
Saccade	30–80	4–20°	30–500°/s
Glissade	10–40	0.5–2°	20–140°/s
Smooth pursuit	–	–	10–30°/s
Microsaccade	10–30	10–40'	15–50°/s
Tremor	–	< 1'	20'/s
Drift	200–1000	1–60'	6–25'

Fixations

A fixation is one of the most basic events related to movement of the eye and it occurs when the eye remains still over a period of time (it is fixating on a specific point in the visual field). During a fixation, three distinct types of eye movements occur: tremor, microsaccades and drifts [8] but those are mainly used in studies of human neurology and have not yet found any application in human factor research. Fixation itself, as an event during which visual information is acquired, is strongly connected to cognitive processing. Thus, the distribution of fixations in space: shows the main sources of navigation information for an officer; allows for identification of the main distractors, both on the bridge and in the manoeuvring area; helps to understand how the navigational and the hydrometeorological situations influence the behaviour of an officer; and shows differences in the decision-making process between experienced and inexperienced crew [4].

The duration of fixations is directly related to mental workload. Subjects tend to fixate longer on the areas that are critical for a given task but also when the visual information is more complex or requires additional mental tasks (e.g. calculations). Also, experienced subjects show shorter fixations in

the same task, compared to novices. Initial studies showed the same relation between captains, junior officers, and students [4].

Some researchers point out that shorter fixations can also indicate high mental workload, due to the stress level and the complexity of the task [2].

Saccades

A saccade is a rapid motion of an eye between one fixation and another one. It is the fastest movement that the body can produce and it is assumed that visual information is not acquired during this movement.

Since a saccade takes place between two fixations, the number and proportions of both events are strictly connected. Saccadic measures are widely used, mainly in the studies with a static stimuli. It is unclear, how exactly saccadic rate should be interpreted for a mixed stimuli (i.e. stimuli with both static and dynamic items, e.g. real world) [2].

A visualization of saccades and fixations on a stimuli picture creates the so called *scanpath*, which helps to identify information-seeking patterns and is very useful for the initial inspection of data. Observing a dynamic *scanpath* from a recording with a mobile eye-tracker, allows for quick evaluation of an officer and his performance, for example by showing when exactly and basing on which information, a risk of collision situation has been identified properly.

Pupil diameter

The changes in pupil diameter are a very popular measure for a variety of cognitive and emotional states. Increased pupil dilatation is positively correlated with difficulty level of a given task. Both complex calculations and tasks that require memorizing a large quantity of data result in significant increase of pupil diameter when compared to basic tasks. Additionally, pupil diameter is reported to decrease with increased drowsiness and fatigue.

At the same time, the pupil is highly sensitive to any changes in the luminance level. Even during studies in a closed simulator, with constant lightning conditions, radar, conning, and radar screens, introduced enough luminance changes to make pupil dilatation an unrealizable measure [4].

Blink rate and duration

Blink rate, defined as a number of blinks per second or minute, has proven to be a reliable measure of mental workload. Studies of drivers and air traffic controllers have shown an increased blink rate during more complex tasks [9, 10]. However, it is crucial to remember that there are many factors that can influence this measure as well, e.g. air pollutants, dry eye, time of day or age [2].

At the same time, the duration of a single blink is reported to be positively correlated with drowsiness and loss of vigilance [11, 12]. That can potentially help to identify moments during navigational watch when officer's level of concentration is the lowest.

Data analysis

When dealing with eye-tracking data, it is important to consider both, statistical analysis and visualisation of the data. It poses a problem when a dynamic scene is studied, if a mobile eye-tracker is used and the subject is not stationary.

Semantic gaze mapping

A function called *semantic gaze mapping*, offered by one of the manufacturers, allows mapping (transfer) every single fixation from a video recording acquired with mobile eye-tracker, onto a prepared static stimuli. Video stops automatically on every fixation and waits until a point is selected on static stimuli area and proceeds to next fixation (Fig. 2). It is reported that this piece of software can increase the efficiency of analysis by factor 10–50, compared to conventional frame-by-frame coding [13].

Having in mind that the average number of fixations for an 11 minutes-long simulator trial is around 1000 [4], it results in over 1000 mouse clicks for a single subject. Such approach would make an analysis of a full 4-hour navigational watch extremely time-consuming. This is one of the reasons why automated data analysis is so important for future eye-tracking studies.

Graphic visualizations

The two most commonly used methods for graphic representation of the eye-tracking data are focus maps and heat maps. A focus map alters transparency of the image basing on the amount of attention paid – the number and the time of fixations. It shows in the simplest way which areas have drawn the subject's attention and which were omitted. Heat maps use colour coding to add information about the number of fixations on the stimuli (Fig. 3). Both functions allow for a quick evaluation of the subject's performance, showing information that was missed; how the subject's attention was distracted; and what the preferred sources of information were.

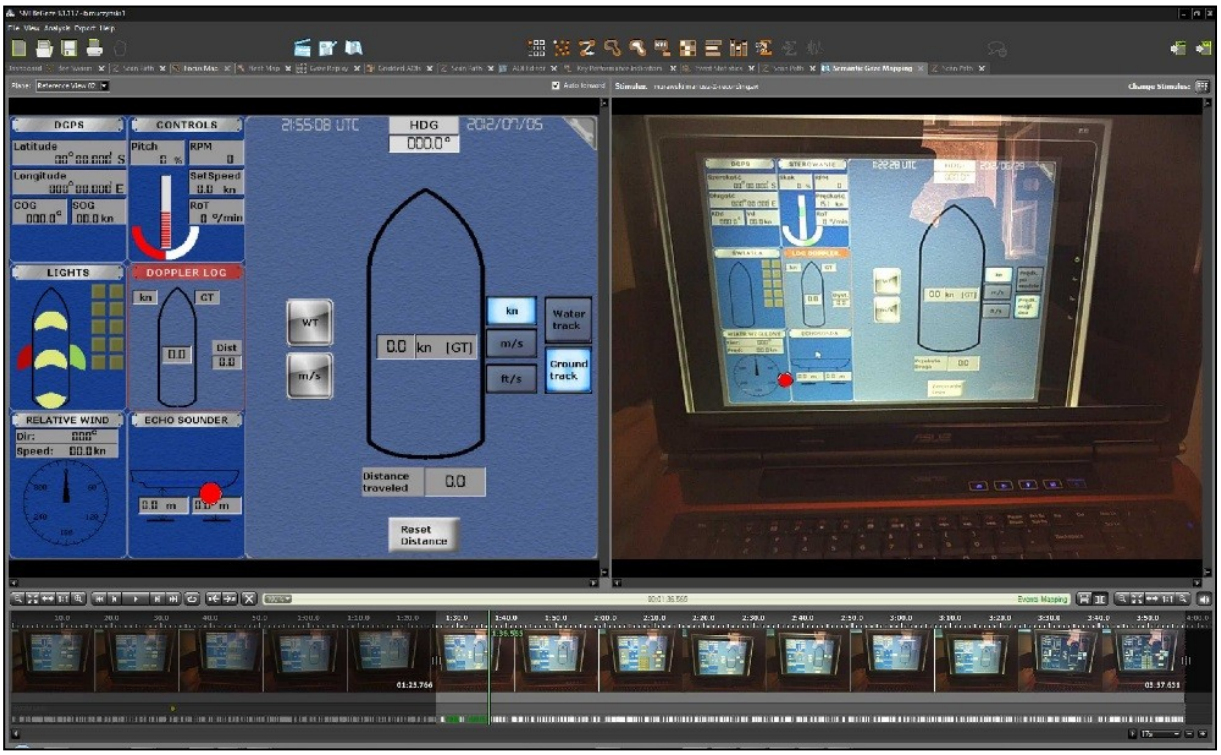

Fig. 2. Sematic Gaze Mapping function. The right side shows a recorded video stimulus; the left side shows static stimulus – image of tested interface. The red dot on both sides is the recorded fixation point

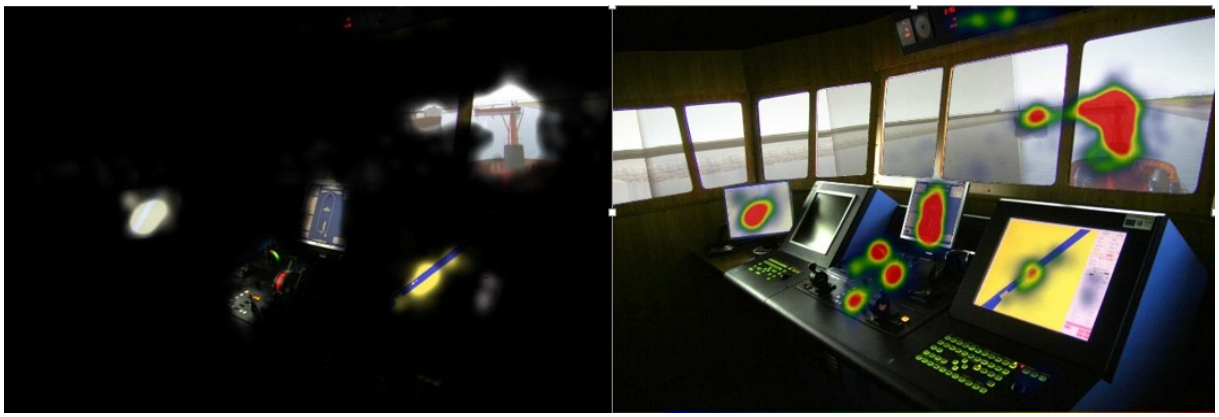

Fig. 3. Focus map (left) and heat map (right) created from eye-tracker data

Fig. 4. Defined (left image) and gridded (right image) Areas of Interests

Data distribution: Areas of Interests

Focus and heat maps give a very general overview of the subject's performance. Analysing the behaviour of an officer of the watch can show how long it took to acquire relevant information from navigational equipment; what the primary sources of information were; how often certain data was compared between different sources; how much the officers relayed on their own observations; how long it took to notice events relevant to safety of navigation, etc. To obtain such information, it is necessary to define those areas in the visual scene, for which additional analysis is made. In the eye-tracking studies they are generally called *Areas of Interests* – AOIs. On a navigational bridge we can, for example, define separate areas for ECDIS, radar, conning display, controls, GPS unit or specific ships in the visual field. For each one of such AOI, a set of eye-tracking metrics, like: the number of fixations; the dwell time; the per cent of all fixations; the average fixation time, is calculated separately. Additionally, gridded AOIs that divide whole stimuli evenly into small rectangle areas can be used (Fig. 4).

Conclusions

Eye-tracking techniques are widely used in many fields and have proven to be valuable in studies focused on usability, ergonomics and human factor [7, 14]. So far, very a few studies focused on measuring the eye movements of an officer of the watch. Additional research could help to improve both, the bridge design and the usability of ECDIS and radar interfaces contributing to safer navigation. Solving the problem of automated data analysis would provide a chance for a wide study of officers on different types of vessels and in different bridge layouts.

References

1. CRANE H.D.: The Purkinje Image Eyetracker, Image Stabilization, and Related Forms of Stimulus Manipulation. Visual Science and Engineering: Models and Applications, 1994, 13–89.
2. HOLMQVIST K., NYSTROM M., ANDERSSON R., DEWHURST R., JARODZKA H., VAN DE WEIJER J.: Eye Tracking. A Comprehensive Guide to Methods and Measures., Oxford University Press, New York 2011.
3. SALVUCCI D.D., GOLDBERG J.H.: Identifying fixations and saccades in eye-tracking protocols. Proceedings of the symposium on Eye tracking research & applications – ETRA'00, ACM Press, New York 2000, 71–78.
4. MUCZYŃSKI B., GUCMA M., BILEWSKI M., ZALEWSKI M.: Using eye tracking data for evaluation and improvement of training process on ship's navigational bridge simulator. Scientific Journals Maritime University of Szczecin 33(105), 2013, 75–78.
5. MUCZYŃSKI B., GUCMA M.: (2013) Method of gaze data analysis for marine ship's simulator researches. Evaluation of offcer's of the watch eye metrics. Book of Abstracts of the 17th European Conference on Eye Movements, Journal of Eye Movement Research 6(3), Sweden, Lund 2013, 271.
6. www.smivision.com; access 10.09.2013.
7. SIEGENTHALER E., COSTELA F.M., OTERO-MILLAN J., MCCAMY M.B., DI STASI L., MACKNIK S.L., MARTINEZ-CONDE S.: New Eye Movement Measures in Human Factors Research. Book of Abstracts of the 17th European Conference on Eye Movements, Journal of Eye Movement Research 6(3), Sweden, Lund 2013, 90.
8. MARTINEZ-CONDE S., MACKNIK S.L., HUBEL D.H.: (2004) The role of fixational eye movements in visual perception. Nature reviews. Neuroscience, Vol. 5, No. 3, 229–40.
9. TSAI Y.F., VIIRRE E., STRYCHACZ C., CHASE B., JUNG T.-P. Task Performance and Eye Activity Relating to Cognitive Workload. Aviation, Space, and Environmental Medicine, Vol. 78, No. 5, 2007.
10. BROOKINGS J.B., WILSON G.F., SWAIN C.R.: Psychophysiological responses to changes in workload during simulated air traffic control. Biological Psychology, Vol. 42, No. 3, 1996.
11. SCHLEICHERA R., GALLEYB N., BRIESTC S., GALLEYD L.: Blinks and saccades as indicators of fatigue in sleepiness warnings: looking tired? Ergonomics, Vol. 51, No. 7, 2008, 982–1010.
12. MORRIS T.C., MILLER J.: (1996) Electrooculographic and performance indices of fatigue during simulated flight. Biological Psychology, Vol. 42, 1996, 343–360.
13. SMI – Experiment Suite Software Package.
14. POOLE A., BALL L.J.: Eye Tracking in Human-Computer Interaction and Usability Research: Current Status and Future Prospects. Encyclopedia of Human-Computer Interaction, Idea Group, Inc., Pennsylvania 2005.

Scientific Journals
Maritime University of Szczecin

Zeszyty Naukowe
Akademia Morska w Szczecinie

2013, 36(108) z. 1 pp. 121–124
ISSN 1733-8670

2013, 36(108) z. 1 s. 121–124

Navigational safety of LNG tankers in emergency situations

Vytautas Paulauskas, Donatas Paulauskas

Klaipeda University, Lithuania

Key words: navigational safety, LNG tankers, precaution measures, emergency situations, port areas

Abstract

LNG import terminals are under construction in the Baltic Sea ports Klaipeda and Świnoujście and should start operations in 2014. LNG tankers in Klaipeda port should cross port up to the end of the port. Probability of possible emergency situations with LNG tankers is very low, but in the same time it is necessary to take all possible precaution measures to avoid accidents with LNG tankers in any cases, especially in port areas.

"Black out" on the LNG ships is very dangerous in ports areas, because there is very limited channel's width and other port water areas, and it is necessary to steer vessel in such situations as well. Theoretical calculations of the precaution measures, simulations and practical training of the ship and tugs masters, port pilots and VTS operators should help in such emergency situations.

This article is oriented to explain theoretical calculation methods for the LNG tankers steering by tugs in case of "black out" situations, simulations' results and practical recommendations for the Port Authorities, port pilots, ships' and tugs' masters that will be possible to minimize LNG ships' incidents and accidents probability in port areas.

Introduction

LNG as energy for industry, for people requirements, for transport as a fuel and many other tasks is very important and LNG demand increase every year in many countries. In many countries and regions LNG import terminals are constructed or are under construction or planning. In the Baltic Sea are under construction LNG terminals are in Klaipeda and Świnoujście and should start to operate in 2014. LNG tankers in Klaipeda port must sail up to end of the port (about 6 miles by port waters). LNG Carriers are built up under very strict requirements by the authorities, but the in same time it is impossible to have 100% navigational safety guaranty [1, 2, 3]. Emergency situations with LNG tankers probability is very low, but in the same time it is necessary to take all possible precaution measures to avoid accidents with LNG tankers in any cases, especially in ports.

"Black out" on any ship is very dangerous in the ports areas, because there is very limited channels width and other port water areas, but it is necessary to steer vessel in such situations as well. Theoretical calculations of the precaution measures, simulations and practical training of the ship and tugs masters, port pilots and VTS operators should help in such emergency situations [4, 5, 6, 7].

Theoretical calculations methods for the LNG tankers steering by tugs in case of "black out" situations, simulations results and practical recommendations for the Port Authorities, port pilots, ships' and tugs' masters that will be possible to minimize LNG ships accidents probability in port areas [1, 6, 8, 9].

Navigational situations in planning LNG import ports and terminals

In the world there are more than 50 LNG import terminals. In the Baltic Sea there are under construction two LNG import terminals: in Klaipeda offshore LNG terminal and in Swinoustje onshore LNG terminal. In mentioned LNG terminals navigation has specific conditions, that means navigational channels (approach and inside ports) have limited width, there are bends in the channels, navigational channel in Klaipeda port is located close

to the oil and other terminals, which is visited by big ships, there are some public places close to the navigational channel [2, 3, 9, 10, 11].

In depending of the very high requirements to LNG tankers, in the same time nobody can guaranty that nothing happens with LNG tanker during passing navigational channel. In this case should be taken additional precaution measures to avoid big losses in case of incidents or accidents on LNG tanker. In any case, ships should be checked on "black out" situations. In this case in 30 s emergency generator must start to work, which is supplying the energy steering equipment (rudder machine). In the same time tugs' assistance should guaranty to keep LNG tanker in the channel up to hydro meteorological limitation conditions, that means LNG tanker at any time should be under control and should avoid touching moored to quay walls ships or waterfront constructions (quay walls, etc.) [1, 3, 5, 8, 9, 12].

On figures 1–3 there are shown Klaipeda port important places, which are located close to the navigational channel and cannot be touched by LNG tanker at any time [10, 13, 14].

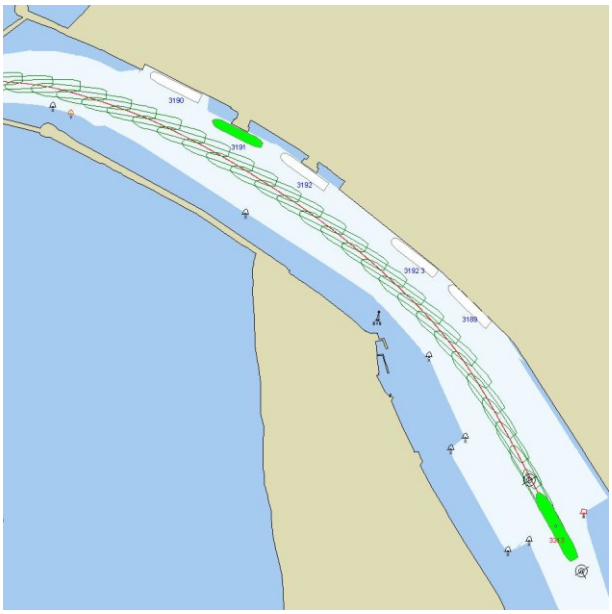

Fig. 1. LNG tanker sailing pass near Klaipeda oil terminal

In the same time other terminals, which are located close to the navigational channel are important for the port as well. Navigational passes are always important for the port navigational channels, terminals' design, that would be possible to guaranty safe navigation in ports [1, 3, 8, 9, 12]. As the example LNG terminal in Klaipeda port is located in south part of the port and LNG tanker must cross all the port until it reaches mooring place [10].

Fig. 2. LNG tanker sailing trajectory from entrance to the port until the mooring place

LNG terminal is located in the south part of Klaipeda port and ships turning basin is located close to the LNG terminal jetty.

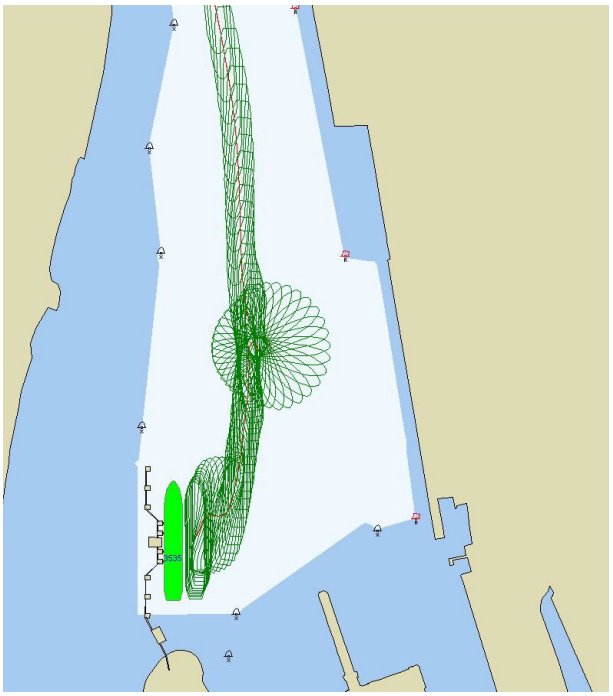

Fig. 3. Ships turning basin and LNG tanker mooring jetty

In typical navigation situation LNG tanker could sail to or from port entrance to the mooring place and from mooring place to the port gates. Klaipeda port entrance and inside navigational channels are wide and deep enough for typical LNG tankers (capacity up to 150,000–200,000 m²) in normal navigation conditions. In the same time there are always at least minimum probability of the failures, such as engine or steering system brake and etc.

In emergency situations LNG tanker must be safely steered by tugs until LNG tanker is reaching the safe place (anchoring or mooring place, etc.).

Very similar navigation situations are in other LNG ports and terminals.

Theoretical basis for the LNG tankers steering in emergency situations

LNG tanker steering in emergency conditions moments should be managed by tugs (in case of failure ship's propulsion equipment). In general moments, which are created by the ship and environment could be calculated as follows [2]:

$$M_{in} + M_k + M_\beta + M_p + M_N + M_a + M_{sr} + \\ + M_b + M_{sek} + M_T + M_{vil} + \ldots = 0 \quad (1)$$

where: M_{in} – inertia moment; M_k – moment on ship's hull; M_β – ship's hull as wing moment; M_p – ship's helm moment; M_N – moment which is created by ship's thrusters; M_a – aerodynamic moment; M_{sr} – moment which is created by current; M_b – moment which is created by waves; M_{sek} – shallow depths created moment; M_T – ship's propeller created moment; M_{vil} – moment created by tugs.

In the emergency conditions, in case of failure of ship's propulsion equipment for example in "black out" situation, ship cannot create moments by propulsion system, that means formula (1) could be expressed as follows:

$$M_{in} + M_k + M_\beta + M_a + M_{sr} + \\ + M_b + M_{sek} + M_{vil} + \ldots = 0 \quad (2)$$

For mentioned tasks, (in port conditions) formula (2) can be expressed as follows:

$$(I + \lambda_{66}) \frac{\mathrm{d}\omega}{\mathrm{d}t} \cdot \sin\beta \cdot \cos\beta + M_R + \\ + M_a + M_{sr} + M_{vil} = 0 \quad (3)$$

where: V – ship's mass; λ_ω – added water mass; $\mathrm{d}v/\mathrm{d}t$ – ship's acceleration; β – ship's drift angle; I – ship's hull inertia moment; λ_{66} – added moment; $\mathrm{d}\omega/\mathrm{d}t$ – angle velocity acceleration.

Finally, moment which is created by tugs should be equal or bigger as other moments. For the ship's steering possibilities it is necessary calculate moments. In case, if it is created moments by tugs are bigger as other moments, ship is able to steer, that means should be [2]:

$$M_{vil} \geq M_{in} + M_R + M_a + M_c + M_\beta + \cdots \quad (4)$$

where: M_{vil} – moment created by tug or tugs.

Mentioned moments could be calculated by the ship's theory or other methods, for example could be used numerical methods [2].

Practical calculations and testing of LNG tankers steering in emergency situations

For the practical calculations and testing was used LNG tanker, which length – 288 m, width – 49 m, draft 11.8 m, capacity – 150,000 m³ LNG.

Fig. 4. LNG tanker "Arctic Princess" (Norway): L = 288 m, B = 49 m, T = 11.8 m, DWT = 74,400 t

Calculation results receive by formula (4) showed, that four tugs with bollard pull 50 T are enough to steer LNG tanker with capacity of 150,000–170,000 m³ LNG in Klaipeda port in limited hydro meteorological conditions (wind up to 12–14 m/s, current up to 1.5–2.0 knots, waves on port entrance up to 1.5–2.0 m high).

Tests were made on SimFlex Navigator full mission Simulator [14] by Klaipeda port pilots in FORCE TECHNOLOGY (Denmark) during pilots' training session and by other ship masters and pilots. In case of training port pilots and good cooperation between ship's master, port pilots and tugs masters, it is possible to steer LNG tanker up to limited entrance to the port for such size ships hydro meteorological conditions. In the same time it is necessary to point out, that constant education and training of port pilots and tugs' masters is extremely important.

Some examples of the LNG tankers steering in emergency conditions in Klaipeda port tests are presented on figures 5–7.

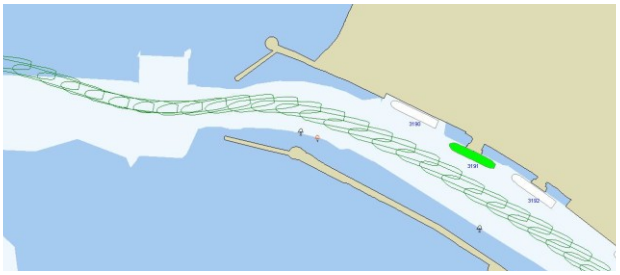

Fig. 5. LNG tanker sailing pass on departure in emergency situation (wind SW – 12 m/s, current out 1.2 kn, waves SW – 1.5 m) used four 50 T bollard pull tugs

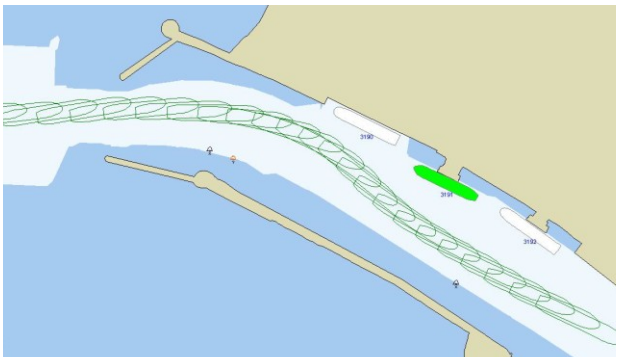

Fig. 6. LNG tanker sailing pass on entrance to the port in emergency situation ("black out" happens just before port gates, wind SW – 12 m/s, current out 1.2 kn, waves SW – 1.5 m), used four 50 T bollard pull tugs

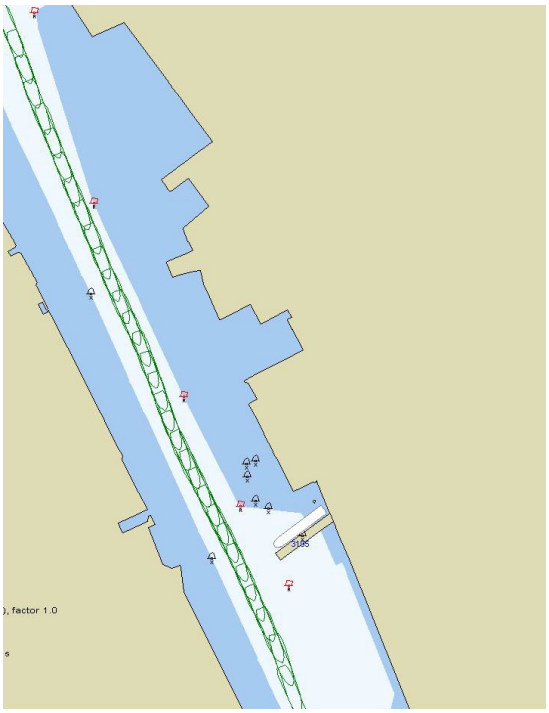

Fig. 7. LNG tanker sailing pass inside port navigational channel in emergency situation ("black out" happens during sailing in port inside navigational channel (wind SW – 12 m/s, current out 1.2 kn) used four 50 T bollard pull tugs

Conclusions

Emergency situations with LNG tankers probability is very low, but in the same time it is necessary to take all possible precaution measures to avoid incidents and accidents with LNG tankers in any cases, especially in ports.

In the emergency situations LNG tanker must be safely steered by tugs until LNG tanker reaches safe place (anchoring, mooring place, etc.).

Forces and moments, which are acting during ship's movement, could be calculated by the naval theory or other methods, for example numerical methods.

On the basis of LNG tanker's steering in emergency conditions calculation and testing results, as shown in the article, it is possible to consider that in case of good preparation of the port structures (VTS operators, port pilots, tug masters), education and training, there is possible to have successful steering of LNG tankers in emergency situations and avoiding incidents and accidents in port areas in any cases.

References

1. GUCMA L., MONTEWKA J.: Land borne laser rangefinder measurements for navigation safety assessment. European Journal of Navigation 3(4), 2005, 1–6.
2. PAULAUSKAS V., PAULAUSKAS D.: Laivo valdymas uoste. KU leidykla, Klaipėda 2009.
3. ZALEWSKI P., MONTEWKA J.: Navigation safety assessment in an entrance channel, based on real experiments. Guedes-Soares & Kolev Maritime Industry, Ocean Engineering and Coastal Resources, 2007, 1113–1117.
4. ALDERTON P.M.: Sea transport. Blackwell, Cambridge 1995.
5. BAUBLYS A.: Probability models for assessing transport terminal operation. Transport 22(1), 2007, 3–8.
6. EAU 2012: Recommendations of the Committee for Waterfront Structures – Harbours and Waterways (Ernst & Sohn, 2006).
7. PAULAUSKAS V., PAULAUSKAS D.: Evaluating the width of navigational channels. Transport 28(2), 2013, 166–174.
8. PAULAUSKAS V., LUKAUSKAS V., PLAČIENE B., BARZDŽIUKAS R.: Ships leaving a port under emergency conditions. Transport 27(3), 2012, 345–350.
9. PAULAUSKAS V.: Navigational risk assessment of ships. Transport 1, Vol. XXI, 2006, 12–18.
10. Klaipeda Seaport maps and charts, 2013.
11. PIANC Recommendations on maritime-port and terminal development (2010).
12. VENCEL E.S.: Teoriâ veroâtnostej. Nauka, 1969.
13. THEIRS G.F., JANSSES G.K.: A Port Simulation Model as a Performance Decision Instrument. Simulation 71(1), 1998, 117–125.
14. SimFlex Navigator – Ship simulator system.

Scientific Journals
Maritime University of Szczecin

Zeszyty Naukowe
Akademia Morska w Szczecinie

2013, 36(108) z. 1 pp. 125–130
ISSN 1733-8670

2013, 36(108) z. 1 s. 125–130

Influence of speed reduction on navigational safety of container ships

Marcin Przywarty[1], Lucjan Gucma[1], Marko Perkovic[2]

[1] Maritime University of Szczecin
70-500 Szczecin, ul. Wały Chrobrego 1–2, e-mail: {m.przywarty; l.gucma}@am.szczecin.pl
[2] University of Ljubljana

Key words: real-time simulation, speed reduction, navigational safety, movement parameters, manoeuvrability

Abstract
Paper presents results of a real-time simulation experiment which was carried out to study an influence of speed reduction on the navigational safety of container ships. In order to determine changes in the vessels manoeuvrability set of simulated sea trials was carried out. The tests included the measuring of the movement parameters of ships proceeding with different initial speed in different external conditions.

Introduction

Speed reduction or slow steaming is becoming increasingly popular among container ships operators on Baltic Sea particularly in light of the upcoming emission restrictions [1]. This paper presents results of a real-time simulation experiment which was carried out with use of the computer based Transas Navi-Trainer Professional 5000 (NTPRO 5000) Simulator (Fig. 1).

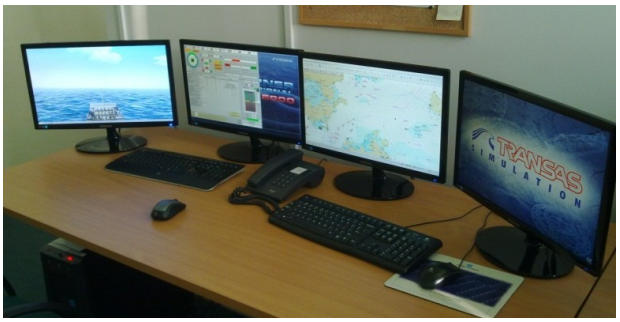

Fig. 1. Work station with NTPRO 5000 simulator

The main goal of the experiment was to study an influence of speed reduction on the manoeuvrability of container ships. In order to achieve the goal set of simulated sea trials was carried out. The tests included the measuring of the movement parameters of ships proceeding with different initial speed in different external conditions.

Assumption of the simulation experiment

Ships models

Simulations were carried out for two sizes of container vessels (Fig. 2), both in fully-loaded condition. The sizes of vessels were chosen with consideration of the characteristic size of the ships navigating in the Baltic Sea area. Particular parameters of the ships models are presented in table 1.

Fig. 2. Simulated container vessels

Both ships models are equipped with standard navigational equipment such as autopilot, GPS / dGPS receiver, echo-sounder, radar with ARPA, ECDIS, log, AIS, etc. NTPRO 5000 enables full

interaction between objects (ships models) and environment taking into account all 6 degrees of freedom. It also allows for recording values of dozens of parameters influencing the ship motion [2].

Table 1. Principal parameters of the simulated container vessels

Parameters	Vessel 1	Vessel 2
Capacity [TEU]	1610	4275
Displacement [t]	24080	73910
Length [m]	169	261.4
Breadth [m]	27.2	32.3
Bow draft	8.5	12.6
Stern draft	9.5	12.6

Research area and the external conditions

Research area was chosen as a location with high traffic density [3] and typical external conditions for southern part of Baltic Sea. The initial ship parameters were set as follows:

- position: latitude 51°N, longitude 14°E;
- heading: 000°;
- initial speed: different for different trials.

Depths in chosen area are about 50 m, so it can be assumed that their influence on ship motion is negligible. Simulations were carried out for three wind forces (0, 10 and 20 m/s) and for three relative directions (000°, 090°, and 180°). Heights and directions of waves were determined in accordance with wind force and direction [4].

Executed sea trials

For comprehensive assessment of speed reduction influence on manoeuvrability and navigational safety simulations of following sea trials were carried out:

- turning circle;
- zigzag manoeuvre;
- anti-collision manoeuvre;
- behaviour on straight section in different external conditions.

Turning circle

Turning circle tests were performed for both, port and starboard side according to the recommended procedures at speeds from FSAH to DSAH with a maximum rudder angle. It is necessary to do a turning circle of at least 540 degrees to determine the main parameters of this trial.

The essential information to be obtained from this manoeuvre consists of [5]:

- tactical diameter;
- turning radius;
- advance;
- transfer;
- loss of speed on steady turn;
- ROT (Rate Of Turn) on steady turn;
- time of one circulation on steady turn;
- roll angle.

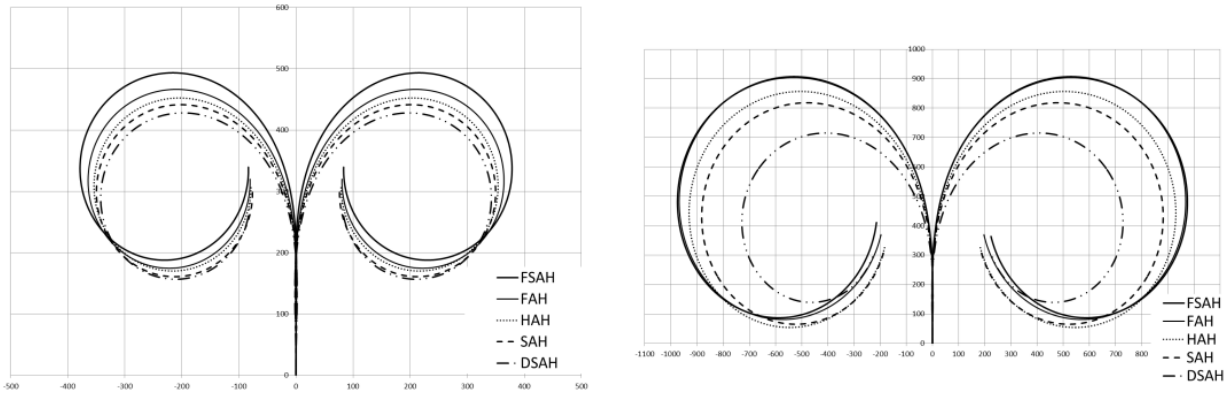

ship 1 ship 2

Fig. 3. Turning circles of 1610TEU (ship 1) and 4275TEU (ship 2) container vessel

Table 2. Parameters of turning circles in meters

	Tactical diameter [m]		Turning radius [m]		Advance [m]		Transfer [m]		ROT on steady turn [deg/min]		Time of circ. on steady turn [min]	
	ship 1	ship 2	ship 1	ship 2	ship 1	ship 2	ship 1	ship 2	ship 1	ship 2	ship 1	ship 2
FSAH	370	961	295	764	482	893	154	424	79	44	4.5	8.2
FAH	356	955	284	784	456	895	152	464	66	30	5.4	12
HAH	346	917	275	762	442	844	146	431	47	23	7.6	15.6
SAH	342	868	273	711	431	805	144	398	35	18	10.3	20
DSAH	335	712	262	518	418	701	142	307	18	13	20.0	27.7

Table 3. Parameters of turning circles in ships length

	Tactical diameter [L]		Turning radius [L]		Advance [L]		Transfer [L]	
	ship 1	ship 2	ship 1	ship 2	ship 1	ship 2	ship 1	ship 2
FSAH	2.2	3.7	1.7	2.9	2.9	3.4	0.9	1.6
FAH	2.1	3.7	1.7	3.0	2.7	3.4	0.9	1.8
HAH	2.0	3.5	1.6	2.9	2.6	3.2	0.9	1.6
SAH	2.0	3.3	1.6	2.7	2.6	3.1	0.9	1.5
DSAH	2.0	2.7	1.5	2.0	2.5	2.7	0.8	1.2

The weather conditions influence was omitted (wind force 0 m/s, no waves). Particular results are presented in tables 2 and 3. The smaller ship is marked as ship 1 and the bigger as ship 2. In table 2 distances are given in meters and in table 3 distances are given in ships length. Figure 3 shows dimensions of turning circles for both ships and for different initial speed. Variations of roll angles for both ships were similar, with maximum value less than 10°.

Zigzag manoeuvre

Zigzag manoeuvres were carried out for both container vessels according to the recommended procedures [5]. The weather conditions influence was omitted (wind force 0 m/s, no waves).

Following results of zigzag tests were gathered:

- Initial turning time (s) – the time from the instant, the rudder is put at the outset of the manoeuvre (first execute) until the heading is 10° off the initial course. At this instant the rudder is reversed to the opposite side (second execute).
- Overshoot angle (°) – the angle through which the ship continues to turn in the original direction after the application of counter rudder.
- Time to check yaw (s) – the time between the rudder execute and the time of the maximum heading change in the original direction.
- Reach (s) – the time between the first execute and the instant when the ship's heading is zero after the second execute.
- Time of a complete cycle (s) – the time between the first execute and the instant when the ship's heading is zero after the third execute.
- ROT (Rates Of Turn).
- Roll angle.

Particular results are presented in table 4. Results for 1610TEU container vessel are marked as ship 1 and the results for 4275TEU container vessel are marked as ship 2. Rates of turn and roll angles are presented in figures 4 and 5.

Anti-collision manoeuvre

Simulations of anti-collision manoeuvres were performed to assess the speed reduction influence

Table 4. Parameters of zigzag manoeuvres

	Initial turning time [s]		Overshoot angle [°]		Time to check yaw [s]		Reach [s]		Time of a complete cycle [s]	
	ship 1	ship 2	ship 1	ship 2	ship 1	ship 2	ship 1	ship 2	ship 1	ship 2
FSAH	32	48	18	8	39	162	115	135	223	266
FAH	39	66	17	8	43	226	140	189	278	372
HAH	53	84	17	7	73	284	194	236	390	464
SAH	73	106	16	7	93	363	261	299	521	591

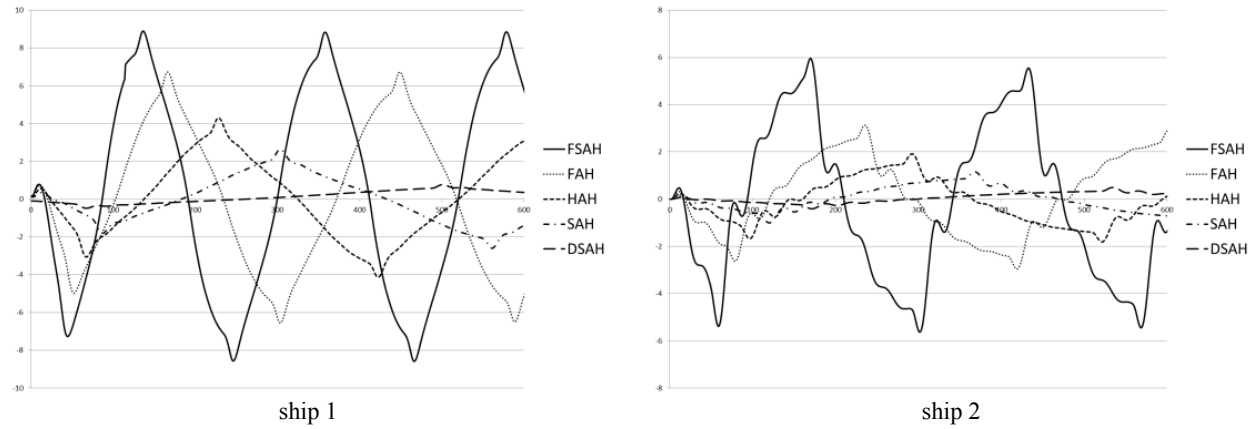

ship 1 ship 2

Fig. 4. Roll angles on zigzag manoeuvres of 1610TEU container vessel (ship 1) and 4275TEU container vessel (ship 2)

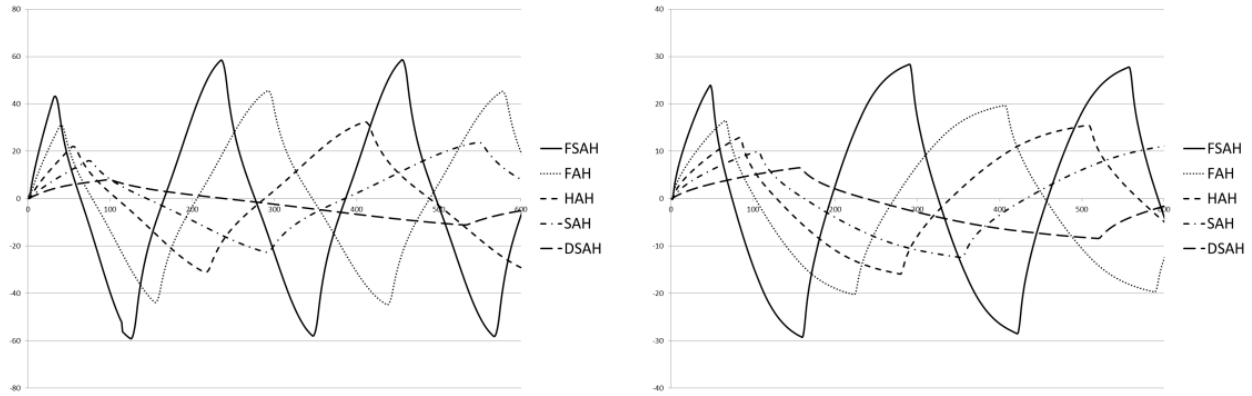

Fig. 5. Rates Of Turn on zigzag manoeuvres of 1610TEU container vessel (ship 1) and 4275TEU container vessel (ship 2)

Table 5. Parameters of anti-collision manoeuvres

	Time to change heading 30° [s]		Distance traveled to change heading 30° [m]		Distance traveled to change heading 30° [L]	
	ship 1	ship 2	ship 1	ship 2	ship 1	ship 2
FSAH	43	74	432	852	2.6	3.3
FAH	56	105	426	852	2.5	3.3
HAH	78	133	419	803	2.5	3.1
SAH	106	170	414	764	2.5	2.9
DSAH	208	253	405	654	2.4	2.5

on the navigational safety. Simulations were conducted for initial speeds form FSAH to DSAH and rudder angle 15° to starboard side. Following parameters were determined to establish when and in what distance the anti-collision manoeuvre should be started:

– time to 30° heading change;
– distance (advance) covered to 30° heading change.

The weather conditions influence was omitted (wind force 0 m/s, no waves). Particular results are presented in table 5. Results for 1610TEU container vessel are marked as "ship 1" and the results for 4275TEU container vessel are marked as "ship 2".

Behaviour on straight section

Simulation of ship behaviour on straight section was carried out to estimate speed reduction influence on the ship movement parameters in different external conditions. Following parameters were recorded:

– course-keeping ability;
– rolling;
– pitching;
– rudder angle.

Simulations of ship behaviour on straight section were carried out for both vessels and for different external conditions (wind force: 0, 10 and 20 m/s from relative directions 000°, 090° and 180°, waves height and directions were determined in accordance to wind force and direction). Minimum speeds necessary to keep the course are presented in table 6. Distributions of roll and rudder angles are presented in figures 6 and 7.

Table 6. Minimum speeds to keep the course in different external conditions

Wind speed [m/s]	Wind relative direction [deg]	Minimum speed to keep the course [kts]	
		ship 1	ship 2
0	–	< 5	5.3 (DSAH)
10	0	6	5.3 (DSAH)
	90	7	5.3 (DSAH)
	180	< 5	5.3 (DSAH)
20	0	12	9.5
	90	> 20	13
	180	7	5.3 (DSAH)

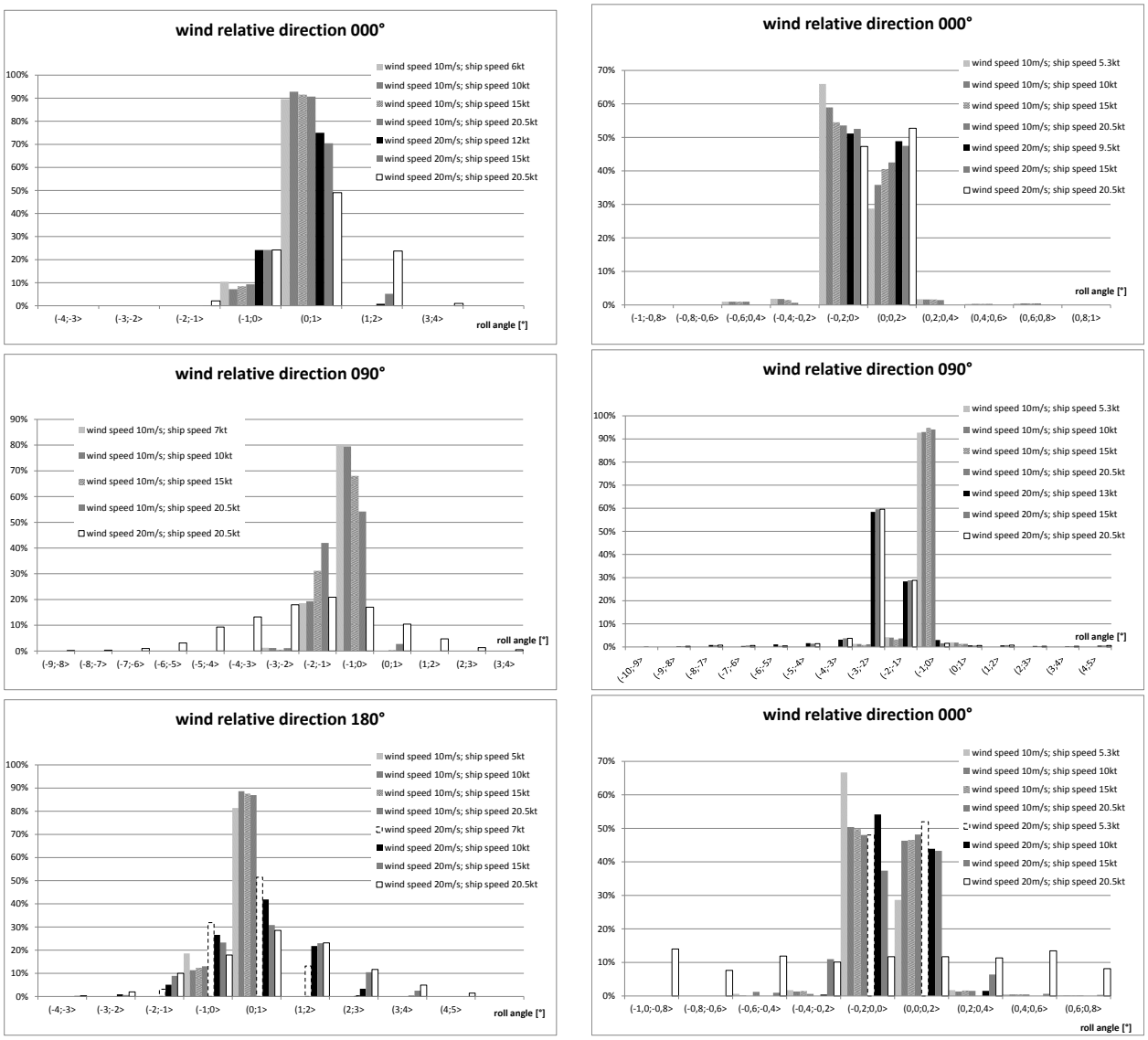

ship 1 ship 2

Fig. 6. Distribution of roll angles on straight sections in different external conditions for 1610TEU (ship 1) and 4275TEU (ship 2) container vessel

Conclusions

The main issue related to the speed reduction is the ability to maintain on the course in the bad external conditions. It was noticed that during adverse weather conditions vessels had not been able to keep the desired course while proceeding with reduced speed.

Reduction of speed does not have significant influence on spatial distribution of manoeuvres but it has strong effect on the ROT values, durations of manoeuvres and the roll angles. Due to this it should be taken into consideration that all manoeuvres should start earlier.

Particular conclusions:

– Speed reduction does not have significant influence on the dimensions of turning circles. Distinct change was noticed only for bigger ship for the minimal speed (DSAH).
– ROT, time of one circulation on steady turn and the roll angles strongly depend on the initial speed of vessel. The higher the initial speed is the higher is the ROT and the bigger are the roll angles. If the ROT is higher the duration of one circulation is shorter.
– All time-parameters measured during zigzag manoeuvre are dependent on initial speed. The higher the speed is the less values of parameters were determined.
– Slight changes in overshoot angles were noticed for different initial speeds. For smaller vessel from ca. 18° (FSAH) to ca. 16° (DSAH) and for bigger one from ca. 8° (FSAH) to ca. 6° (DSAH).
– Roll angle values on the zigzag manoeuvres are higher for the higher initial speed, values vary

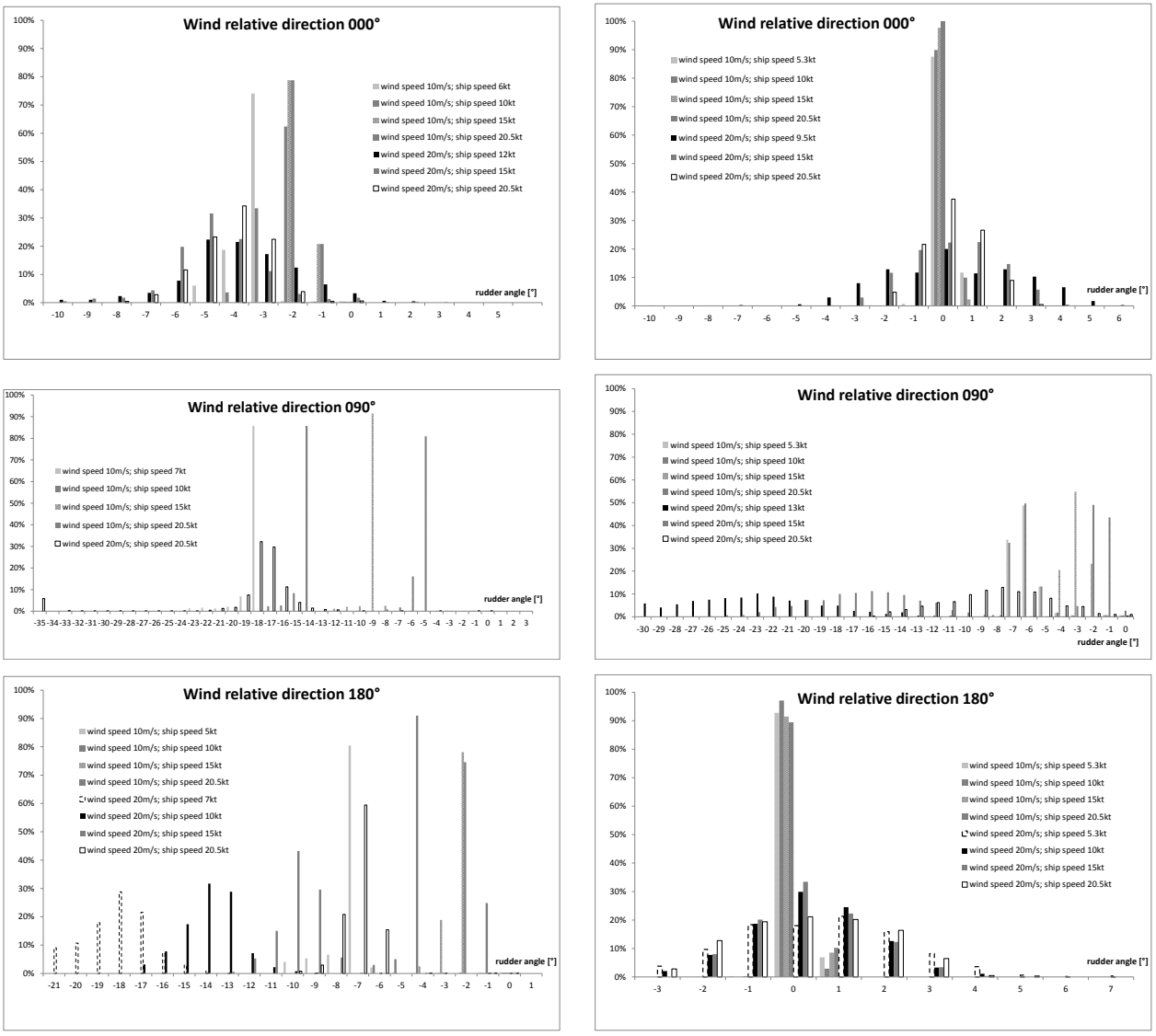

ship 1 ship 2

Fig. 7. Distribution of rudder angles on straight sections in different external conditions for 1610TEU (ship 1) and 4275TEU (ship 2) container vessel

between ca. 1° (DSAH) and ca. 9° (FSAH) for smaller vessel and between ca. 0.5° (DSAH) and ca. 6° (FSAH) for bigger vessel.

– Distances travelled during anti-collision manoeuvres are similar for all initial speeds, but the times of manoeuvres differ significantly. Maximum increase of time delay for anti-collision manoeuvre for DSAH in compare to FSAH is around 3 minutes which cause necessity to plan the manoeuvre earlier but does not influence significantly safety of navigation.
– Restrictions in speed reducing resulting from minimal speed necessary to maintain the desired course were observed. For smaller vessel and for wind speed 20 m/s from 090° relative direction minimum speed was higher than 20 knots.
– For simulations where the dependence between initial speed and the rudder angle was noticed it was observed that the higher the initial speed is the less values of rudder angles are necessary to maintain the course.
– Observed rudder angles higher than 15° will significantly influence effectiveness of steering system and increase rudder dragging forces.

References

1. FABER J., NELISSEN D., HON G., WANG H., TSIMPLIS M.: Regulated Slow Steaming in Maritime Transport. An Assessment of Options, Costs and Benefit. CE Delft, Delft 2012.
2. Transas Navigational Simulators
3. HELCOM (2012). Report on shipping accidents in the Baltic Sea area during 2011
4. PETTERSSON H., LINDOW H., SCHRADER D.: Wave climate in the Baltic Sea 2011. HELCOM Baltic Sea Environment Fact Sheet(s) 2012. Online.
5. WEŁNICKI W.: Mechanika ruchu okrętu. Wydawnictwo Politechniki Gdańskiej, Gdańsk 1989.

Scientific Journals
Maritime University of Szczecin

Zeszyty Naukowe
Akademia Morska w Szczecinie

2013, 36(108) z. 1 pp. 131–137
ISSN 1733-8670

2013, 36(108) z. 1 s. 131–137

Evacuation model managed through fuzzy logic during an accident in a LNG terminal

Goran Stanković, Stojan Petelin, Mitja R. Kožuh, Marko Perkovič
Peter Vidmar

University of Ljubljana, Faculty for maritime studies and transportation, Portorož, Slovenia

Key words: evacuation model, LNG terminal, risk analysis, fuzzy logic, safety evacuation

Abstract
Evacuation of people located inside the enclosed area of LNG terminal is a complex problem, especially considering that accidents involving LNG are potentially very hazardous. In order to create an evacuation model managed through fuzzy logic, extensive influence must be generated from safety analyses. A very important moment in the optimal functioning of an evacuation model is the creation of a database which incorporates all input indicators. The output result is the creation of a safety evacuation route which is active at the moment of the accident.

Introduction

Due to the ever increasing call for energy in the world, there is more and more need to use natural gas as an energy source and hence the need to open new LNG terminals as shipment by sea is inevitable. Basic information regarding LNG terminals is the capacity and number of LNG storage tanks, as well as the size and the capacity of the tankers which carry out the transport to the terminal. The potential hazard associated with LNG mainly comes from the possibility of an accident with consequences generated by LNG leakage. In such situations, a very possible occurrence is fire and thermal radiation. If the events lead to leakage of a greater quantity of LNG – into a pool – a cloud is created due to the evaporation which contains natural gas, water, steam and air. Due to its weight, the cloud, being heavier than the air, remains at the surface of the earth. The evaporated natural gas may be significantly influenced by the atmospheric conditions and the geographic-topographic features of the terrain. The cloud shifts according to the direction of the wind, while the speed of the wind additionally effects the mixing of the natural gas with the air. This mixture is flammable when the concentration of the natural gas in the air ranges between 5% and 15%. The dispersion of the cloud represents a danger to people, which is increased in the case of flammability. The rapid evacuation of people in such a situation is essential. The risk for employees at the LNG terminal is greatest. Therefore, there is a need for designing evacuation models which apply to those both inside and outside the enclosed part of the LNG terminal.

General description of the evacuation model

This paper describes an evacuation model intended for the people located inside the LNG terminal. The model uses data generated by conducting quantitative risk analysis (QRA) [1, 2] of events involved in LNG leakage accidents. The management or the control of the evacuation model is performed using fuzzy logic [3], where the final output result is the shortest safe evacuation route for each individual located in the LNG terminal.

Quantitative risk analysis

The objective of conducting the QRA is to identify the potential impact of the LNG leakage accident on the workers in the terminal. The analyses result in a time-based and spatial presentation of the

dispersion of the evaporated LNG, its concentration in the air, as well as thermal radiation. For more precise management of the evacuation, the area of the terminal is divided into cells (smaller blocks), as shown in figure1.

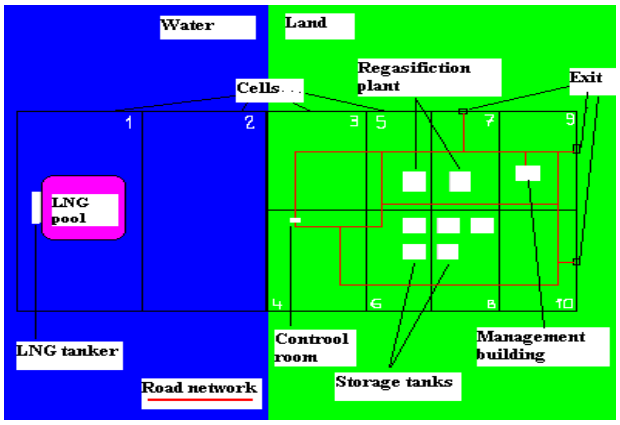

Fig. 1. Scheme of the modeled LNG Terminal

The areas which are a potential source of an LNG leakage accident are identified well in advance, including the maximum quantity of LNG that may leak. For each cell or area, the consequence from the accident is separately defined (possible size of a crack as a consequence of the accident, maximum quantity of the leaked LNG, the size of the leaked LNG, the area in which the LNG is leaking and so on) and in compliance with these data and other input parameters, the QRA is carried out. Potential accidents with LNG leakage involve cryogenic pipeline systems which are used to transport LNG, storage tanks, mooring LNG tankers during off-loading in storage tanks and so on. Intentional threats may range from insider threats to intentional external attacks. During such events, there is a small chance of complete leakage of LNG from each tank separately, but with the objective to obtain conservative calculations of the dimensions of an accident, we shall presuppose that the tanks have been completely emptied. In this case, we will review the example of an accident that occurs when mooring an LNG tanker during the course of off-loading. The accidents caused by terrorist attacks are scenarios considered to have the biggest negative impact. It has been estimated that in such cases, there is a possibility of a maximal crack in the tanker of 1500 mm [4], creating conditions for a pool with a diameter of up to 400 m [4, 5, 6, 7]. Our scenario thus includes a crack of 1500 mm and an LNG pool with a diameter of 400 m (Model 1). The behaviour of the evaporated natural gas from the LNG pool may be calculated by using a Fire Dynamics Simulator (FDS) on the basis of CFD modelling of the dispersion of the natural gas into the surrounding environment [8, 9, 10, 11, 12]. The speed and the direction of the wind plays an immense role when it comes to the length, speed, direction and the time frame of the dispersion of the evaporated natural gas, as well as the flammable concentration of the mixture of natural gas and air. Additionally, in case of fire, one can calculate the quantity of thermal radiation to the surrounding environment, consequently allowing the presentation of this in a spatial and time sense [13, 14]. The scenarios will be conducted using the created 3D model of an LNG Terminal for which the evacuation model will be made. The scenario for Model 1 simulates the evaporation of natural gas from the LNG pool on a water surface with a size of 160.000 m^2 (400×400 m). The dimensions of the presented model are 3000 m per x axis, 3000 m per y axis and 300 m per z axis. The atmospheric wind has a speed of 2 m/s and disperses the gas cloud in the direction of the wind. The temperature of the sea water is set to 20°C. The simulation of the dispersion is calculated with the use of the FDS program (Fire Dynamics Simulator) [15]. Additional obstacles are considered (vessel, buildings, storage tanks) which might have an influence on the spreading gas.

Figures 2 and 3 show examples of the length of the dispersion with concentration of methane in the air between 5% and 15% depending on the time of the leaked LNG from the moored tanker.

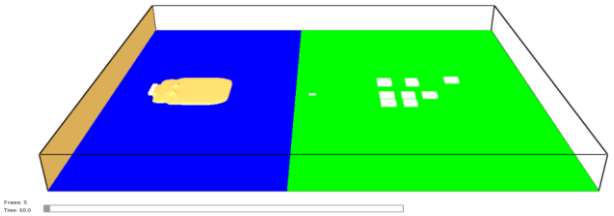

Fig. 2. Dispersion of the LNG vapour after 60 seconds

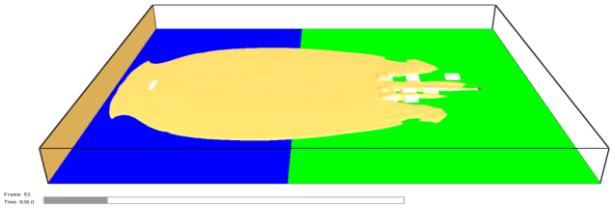

Fig. 3. Dispersion of LNG vapour after 636 seconds

Through the calculated data from the analyses, we identify the cell, time and magnitude of the danger for the people at the terminal. All of these data should be incorporated into the database. The objective of the database is to understand the influences of the accident, and for creating the rules and procedures under which the evacuation model will be managed with the use of fuzzy logic. For a better

evacuation model, it is necessary to perform as much as possible analyses with different input parameters for the speed and the direction of the wind, temperature data, location of the leakage, the type of the area / surface where the LNG is leaking and the like. Some scenarios can be excluded, since they do not pose a threat to the terminal. With this approach we achieve a simplification and reduce the time and efforts required for completing our database. Due to this, according to the scenario for Model 1, the directions of the wind N, NE and NW only will be included.

Evacuation model managed/controlled via fuzzy logic

Evacuations happen frequently. People are evacuated from their homes, businesses, ships, and more, in response to actual or predicted threats of hazards such as hurricanes, floods, tsunamis, volcanic eruption, and release of hazardous or nuclear materials, fires and explosions [16]. The term evacuation describes the withdrawal of persons from a specific area because of a real or anticipated threat or hazard. In the last decade the warning process and response, organizational response, behaviour in evacuations, evacuation planning and management has been more in focus than had been the case in the past. The stress has been on the quality of information, the timing of message delivery and compliance with warnings. The new warning technologies include cell phones, the internet, GPS devices, etc. Each individual in the LNG terminal, after being alerted to an accident through with alarm systems, is in a dilemma regarding the best evacuation route to choose. The slightest probability of risk given any chosen route implies potential fatality. The larger the scale of an accident, the greater the probability of an individual making an error in choosing a route. Having said this, there is a need for the development of an evacuation model which is to be managed using fuzzy logic and is meant to relocate individuals via safe routes, as well as via safe areas which are not endangered by the accident. The on-time evacuation of people is of essential significance for the decrease of risk; i.e. minimizing the human consequences of an accident event. Using fuzzy logic, the data from a database provides a clear picture of which cells of the terminal at which time after the recognition of the accident will be at a particular risk. It also provides images of the optimal evacuation routes at given times after the accident. The objective of the use of fuzzy logic is to process the data from the created database toward the selection of the shortest safe route for each individual located in the LNG terminal at a specifically determined time after the leakage of the LNG. Of great importance is the early detection of the accident. The devices for detecting gas or heat indicate the location where the LNG leakage accident happened [17]. This is the starting point for the creation of one dynamic evacuation model. The second important moment is detecting the direction of the wind. As we have mentioned, all locations have been pre-evaluated in terms of potential leakage, as well as the maximum quantities of leaked LNG. The location of the detected accident, the speed and direction of the wind, the atmospheric temperature and the temperature and the type of the surface where the accident takes place are the input parameters which indicate the selection of the scenario by which the dynamic evacuation routes for the individuals are created. For each cell of the terminal in compliance with the scenario, via the QRA, the program will provide insight into the time such a cell will be affected. Also, the safe-havens or shelters which are foreseen in case of an accident are also emphasized. In the end we determine which parts of the travel route at what time are safe for use during a dynamic evacuation. For a successful execution of the evacuation, a GPS device with an installed map, streets and routes and shelters of the LNG terminal which people can use is required. The device provides the accurate location of the individual at the time of the occurrence of the accident. With this, the individual represents the starting point A used to create his/her safety evacuation route. The evacuation route directs the individual to the end point B, which is at a location that will not be affected by the accident. The evacuation management device, at every 30 seconds, depending on the location of the individual identified via the GPS device, refreshes the analysis for creating a safe evacuation route, which in case of change in the initially shown route, and will alert the evacuee to any change, projecting the newly created evacuation route.

Evacuation model managed/controlled via fuzzy logic

The basic elements of any given fuzzy logic system [3, 18] are: rules, fuzzifier, inference engine, and defuzzifier. During the design of the fuzzy logic systems, one defines the input and output variables, identifies the membership functions and creates the database of fuzzy variables. There is a distinction between linguistic and numeric data – i.e. information. The linguistic data usually express a certain experience through words, while the numeric data in reference to a specific phenomenon are generated on the basis of measurements, experiments and statistical analyses. In our case, the

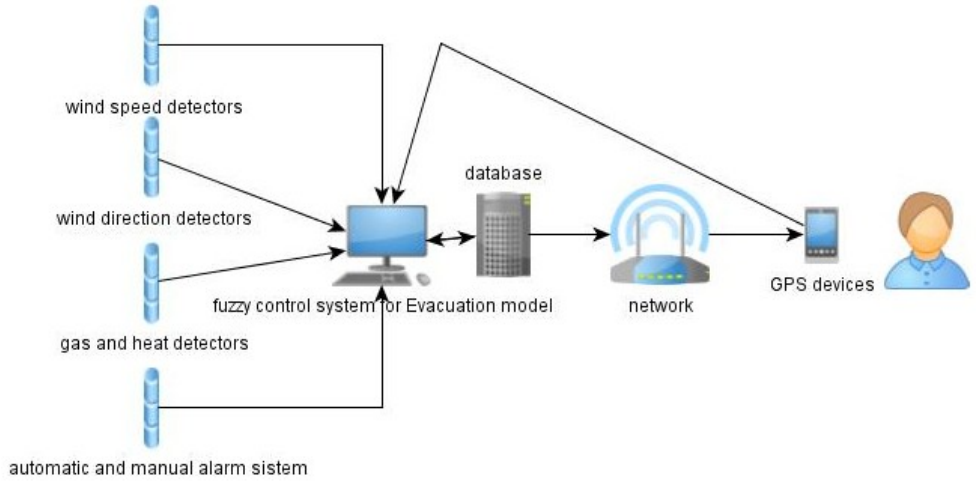

Fig. 4. General Structure of the fuzzy control system for an evacuation model

QRA provide us with both, linguistic and numeric data, on the basis of which the input and output variables are created, including the set of fuzzy rules. The basic task of fuzzy logic for management of the evacuation model is to make the proper selection of a route for evacuation for each individual in the terminal, which eliminates the possibility of an error during the selection of an evacuation route when such is created by an individual.

Evacuation model managed / controlled via fuzzy logic

The fuzzy logic controlled evacuation model (Fig. 4) uses wind speed and wind direction detectors, gas and heat detectors, automatic and manual alarm systems, and the positions of the terminal workers from different locations of the terminal area with the goal to collect all necessary information for input variables used by the fuzzy logic controller. The controlling is closely related to the previously accumulated experience from QRA, and is copied during the setting of the fuzzy logic controller.

Input and Output Membership Functions

There are four membership functions for the evacuation model for each of the input and output fuzzy variable. The table below (Table 1) shows the Input fuzzy variables – the speed of the wind within the area of the terminal (wind speed), as well as the time elapsed after the detection of the accident (time after disaster), as well as Output fuzzy variable – the remaining time to reach a point of unacceptable risk in cell X of the terminal (safe time). For purposes of facilitated use of the system fuzzy variables, the relevant abbreviated forms for the variables shall be used hereinafter.

The graphic display of the membership functions of the language variables is shown in figure 5.

Table 1. Fuzzy variables for wind speed, time after disaster, and safe time

Wind speed		Time after disaster		Safe time	
very slow	vs	very short	vs	very short	vs
slow	s	short	s	short	s
fast	f	medium	m	medium	m
very fast	vf	long	l	long	l

The *y*-axis shows the grade of membership for each fuzzy variable. The *x*-axis shows the input fuzzy variables (wind speed, time after disaster) and the output fuzzy variable (safe time). The set up and identification of these membership functions have been determined according to the QRA and a fulfilled database.

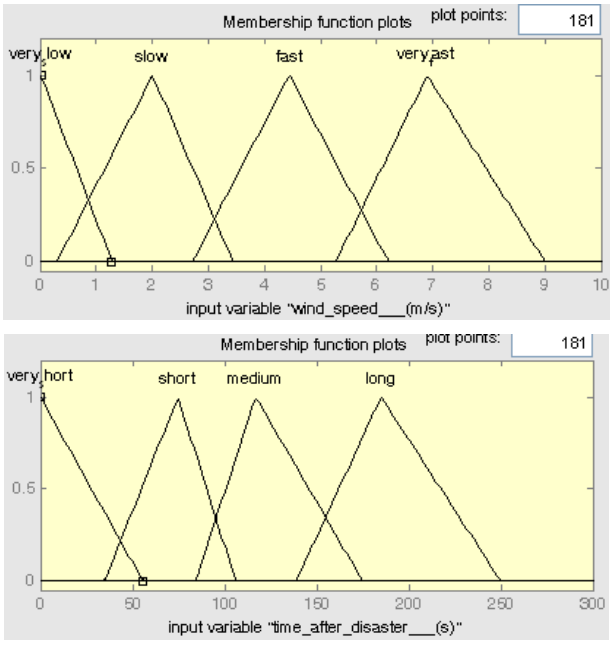

Fig. 5. Graphical presentation of the membership functions to the FUZZY LOGIC controller

1. If (wind_speed___(m/s) is very_slow) and (time_after_disaster___(s) is very_short) then (safe_time__(s) is long) (1)
2. If (wind_speed___(m/s) is very_slow) and (time_after_disaster___(s) is short) then (safe_time__(s) is medium) (1)
3. If (wind_speed___(m/s) is very_slow) and (time_after_disaster___(s) is medium) then (safe_time__(s) is medium) (1)
4. If (wind_speed___(m/s) is very_slow) and (time_after_disaster___(s) is long) then (safe_time__(s) is very_short) (1)
5. If (wind_speed___(m/s) is slow) and (time_after_disaster___(s) is very_short) then (safe_time__(s) is medium) (1)
6. If (wind_speed___(m/s) is slow) and (time_after_disaster___(s) is short) then (safe_time__(s) is medium) (1)
7. If (wind_speed___(m/s) is slow) and (time_after_disaster___(s) is medium) then (safe_time__(s) is short) (1)
8. If (wind_speed___(m/s) is slow) and (time_after_disaster___(s) is long) then (safe_time__(s) is very_short) (1)
9. If (wind_speed___(m/s) is fast) and (time_after_disaster___(s) is very_short) then (safe_time__(s) is short) (1)
10. If (wind_speed___(m/s) is fast) and (time_after_disaster___(s) is short) then (safe_time__(s) is short) (1)
11. If (wind_speed___(m/s) is fast) and (time_after_disaster___(s) is medium) then (safe_time__(s) is very_short) (1)
12. If (wind_speed___(m/s) is fast) and (time_after_disaster___(s) is long) then (safe_time__(s) is very_short) (1)
13. If (wind_speed___(m/s) is very_fast) and (time_after_disaster___(s) is very_short) then (safe_time__(s) is very_short) (1)
14. If (wind_speed___(m/s) is very_fast) and (time_after_disaster___(s) is short) then (safe_time__(s) is very_short) (1)
15. If (wind_speed___(m/s) is very_fast) and (time_after_disaster___(s) is medium) then (safe_time__(s) is very_short) (1)
16. If (wind_speed___(m/s) is very_fast) and (time_after_disaster___(s) is long) then (safe_time__(s) is very_short) (1)

Fig. 6. FUZZY Rule Base for evacuation model

Fuzzy Rule Base and Defuzzification

The rules of the FUZZY LOGIC controller are based on "IF-THEN" conditionality. The fuzzy rules for the fuzzy logic guided evacuation model are defined in figure 6.

In this case wind speed and time after disaster are the factors that affect the consequence expressed as safe time. We have two variables with Fuzzy Input with four membership functions. According to this the total number of rules applied to the output fuzzy variable safe time is sixteen. The number of rules can also be lesser in some cases, where it is believed that some rules are not necessary or will not change anything in certain situations. For each cell a separate matrix for fuzzy rules is being created in reference to each scenario which is part of the evacuation model. This is done with the objective that for each individual located in X cell, the fuzzy control system shall use the adequate matrix for the X cell which is intended for the scenario of the accident. As an example, table 2 shows the matrix for fuzzy rules for evacuation Mode l in an event when the individual is located in cell number 4.

Table 2. Matrix for FUZZY Rule Base for evacuation model

Safe time					
	time after disaster				
Wind speed		vs	s	m	l
	vs	l	m	m	vs
	s	m	m	s	vs
	f	s	s	vs	vs
	vf	vs	vs	vs	vs

FUZZY LOGIC controller is using the max-min composition (Mamandi). In the process of defuzzification, the centre of gravity of the received fuzzy set shows the output numerical value. As an example from the following chart (Fig. 7) we can see the max-min composition of the 16 rules in the case where the input variables are: wind speed 2 m/s, time after disaster 160 seconds. These values have a grade of membership of 1. The output numerical

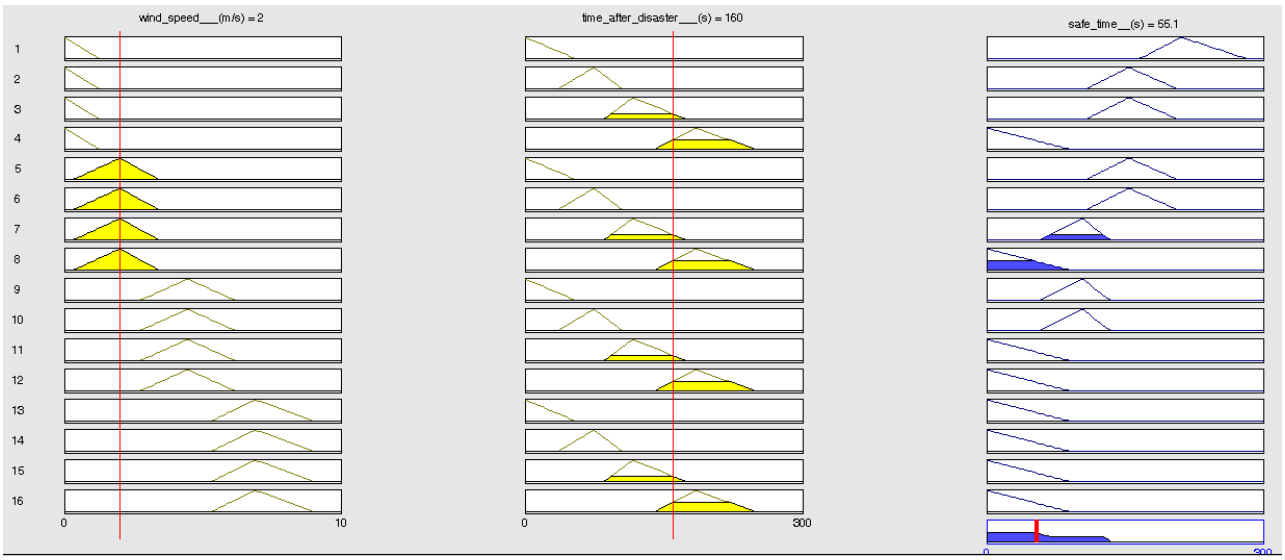

Fig. 7. Graphical presentation of the outcome of FUZZY LOGIC controller

value for safe time after the defuzzification for this case is 55 seconds.

Evacuation Route

In order for the evacuation model to successfully manage the obtained input and output data, it is necessary to produce a software solution which as a final product provides information to the GPS device of the individual in graphic and sound form via presentation of the evacuation route leading to an area which will not be affected by the influences of the accident. The designed program receives information from the fuzzy logic controller for each cell separately, when the cell will be affected by the accident, and in compliance with this, the program designs potential routes for each individual leading him or her to the final safe destination. The shortest route is the first option that appears on the GPS device of the individual for which the route was created. Under the selected Model 1 from the scenario, the individual is located in cell 4. QRA for the starting input data shows that cells 3 and 4 will be influenced by the accident approximately 200 seconds after the accident alert, cells 5 and 6 in approximately 320 seconds, cells 7 and 8 in approximately 380 seconds and cells 9 and 10 in approximately 480 seconds. The evacuation route, starting from cell 4, has an option to lead the individual to one of the three main exits of the terminal located in cells 7, 9 and 10 but also provides additional guidance. The created possible routes primarily indicate the shortest and safest route. Within the whole process of decision-making, an important factor is also the speed of movement of the individual which depends on whether the individual uses a vehicle or is on foot. In situations when time does not allow the individual to be evacuated outside the terminal, the program guides the individual to the nearest terminal safe-haven or shelter.

Conclusions

LNG leakage accidents are potentially very hazardous. Rapid reaction and evacuation of people is of primary significance. The new ideas for the creation of evacuation models may contribute to the creation of a good evacuation model with a high rate of success in the execution of any evacuation. Through the presented evacuation model, we have portrayed the management of an evacuation model using fuzzy logic for a specific scenario. The potential error during the selection of an evacuation route has been brought down to a minimum in comparison with the selection of an evacuation route by an individual who does not have all the information regarding the external influences on the accident. The advantage of the evacuation model managed via fuzzy logic on the basis of the created database through the carried out QRA is that it eliminates the possibility of an error during the selection of an evacuation route when such is created by an individual with less knowledge of influential temporal factors. Additionally, the program creates a separate safety evacuation route in real time for each individual located inside the terminal on the basis of his/her location after the accident alert. The estimated decrease in risk of course influences the location of new LNG terminals, which must be in compliance with certain safety rules. In any case, this is only a starting point in the development of an evacuation model managed through fuzzy logic. We should also review the possibility for expansion of the use of the model for the needs of the general population, located outside the LNG terminal.

References

1. Guidance on performing risk assessment in the design of onshore LNG installations including the ship/shore interface. Reference number of document: OGP Draft 116901, Date: 2013-02-06.
2. Guidelines for Chemical Process Quantitative Risk Analysis, Second edition, Center for chemical process safety of the American Institute of chemical engineers, 2000.
3. TEODOROVIĆ D., VUKADINOVIĆ K.: Traffic Control and Transport Planning: A Fuzzy Sets and Neural Networks Approach, Kluwer Academic Publishers, Boston–Dordrecht–London 1998.
4. PITBLADO R.M., BAIK J., HUGHES G.J., FERRO C., SHAW S.J.: Consequences of LNG Marine Incidents. CCPS Conference, Orlando 2004.
5. Hightower M., Gritzo L., Luketa-Hanlin A., Covan J., Tieszen S., Wellman G., Irwin M., Kaneshige M., Melof B., Morrow Ch., Ragland D.: Guidance on Risk Analysis and Safety Implications of a Large Liquefied Natural Gas (LNG) Spill Over Water. SANDIA REPORT, SAND2004-6258, Unlimited Release, Printed December 2004.
6. Hightower M.M., Luketa-Hanlin A., Gritzo L.A., Covan J.M.: Review of the Independent Risk Assessment of the Proposed Cabrillo Liquefied Natural Gas Deepwater Port Project. SANDIA REPORT, SAND2005-7339, Unlimited Release, Printed January 2006.
7. Luketa A., Hightower M.M., Attaway S.: Breach and Safety Analysis of Spills Over Water from Large Liquefied Natural Gas Carriers. SANDIA REPORT, SAND2008-3153, Unlimited Release, Printed May 2008.
8. MOUILLEAU Y., CHAMPASSITH A.: CFD simulations of the atmospheric gas dispersion using the Fire Dynamics Simulator (FDS). Journal of Loss of Loss Prevention in the Process Industries 22(2009), 316–323.
9. Gavelli F., Bullister E., Kytomaa H.: Application of CFD (Fluent) to LNG spills into geometrically, complex environments. Journal of Hazardous Materials 159, 2008, 158–168.
10. Oka H., Ota S.: Evaluation of consequence assessment methods for pool fires on water involving large spills from liquefied natural gas carriers. J Mar Sci Technol 13, 2008, 178–188.

11. JOHNSON D.W., CORNWELL J.B.: Modeling the release, spreading, and burning of LNG, LPG, and gasoline on water. Journal of Hazardous Materials 140, 2007, 535–540.
12. HISSONG D.W.: Keys to modeling LNG spills on water. Journal of Hazardous Materials 140, 2007, 465–477.
13. Raj P.K.: Large hydrocarbon fuel pool fires: Physical characteristics and thermal emission variations with height. Journal of Hazardous Materials 140, 2007, 280–292.
14. FAY J.A.: Model of spills and fires from LNG and oil tankers. Journal of Hazardous Materials B96, 2003, 171–188.
15. MCGRATTAN K.: NIST – FDS 5 (Fire Dynamics Simulator).
16. Liu M., Lo S., Yuen K.: A Study on Emergency Evacuation Planning In Case of Disasters. Proceedings of 2008 (tenth) Annual Meeting China Association for Science. Zhengzhou, China, 17–19 September 2008. CAST: China 2009.
17. A collection of booklets describing hazards and how to manage them. Energy Fire Protection and Emergency Response, Second Edition 2007, BP Fire Safety Series.
18. MENDEL J.M.: Fuzzy Sets for Words: A New Beginning. The IEEE International Conference on Fuzzy Systems, 2003.
19. NAMEE S.: Boonsap Witchayangkoon, Ampol Karoonsoontawong: (2012) Fuzzy Logic Modelling Approach for Risk Area Assessment for Hazardous Materials Transportation. American Transactions on Engineering & Applied Sciences, 28 January 2012.

Scientific Journals
Maritime University of Szczecin

Zeszyty Naukowe
Akademia Morska w Szczecinie

2013, 36(108) z. 1 pp. 138–143
ISSN 1733-8670

2013, 36(108) z. 1 s. 138–143

Reduction of ship steering gear load at high sea states by decreasing rudder angular velocity

Andrzej Stefanowski

Maritime University of Szczecin, Mechanical Faculty, Department of Control Systems and Robotics
70-205 Szczecin, ul. Podgórna 51/53, e-mail: a.stefanowski@am.szczecin.pl

Key words: steering gear, sea states, ship-autopilot system, simulations, rudder angular velocity

Abstract
The article discusses causes of steering gear overload at high sea states when a ship is kept on course in autopilot mode. The presented research results refer to simulations of a ship-autopilot system on a preset course in the presence of varying intensity disturbances (various sea states), with updated alterations of rudder angular velocity (the velocity changes are executed discretely) determined by the function block for conventional sea state determination.

Introduction

To achieve the required quality of course keeping (directional stability) of a ship sailing in various weather conditions, the power of control signals should be comparable with the power of disturbance signals. The intensity of disturbing signals acting on the ship proceeding in changing hydrometeorological conditions is highly variable – from very low (sea states up to 3) to very high (sea states 8 to 9). In most cases the installed power of an electro-hydraulic steering gear (executing a control signal) is fixed and when the ship is being kept on a preset course this power is utilized in its wide range, from minimum (good weather conditions) to the rated power and one pump unit in operation. In specific conditions, in navigationally difficult areas, for instance, national maritime administrations require that the ship's steering gear should work with two pump units in operation. In such cases, the steering gear power is increased by adding another pump unit working in parallel.

Steering gear power (for one pump unit) is chosen for a particular ship so as to satisfy the condition: rudder angular velocity at full ahead and ship's draft to the summer load line is not less than 2.33 degree per second. It should be noted that there is a requirement that time of changing the rudder from 35 degrees on one side to 30 degrees on the other side should not exceed 28 seconds [1]. The condition to obtain such rudder angular velocity is derived from another requirement: safe passing of ships proceeding on opposite courses, or from the practical condition, proposed by ship captains, to obtain a non-dimensional angular velocity (rate of turn) of the ship equal to 0.2 after it covers a distance equal to the ship's length [2]. The steering gear power selected to guarantee an appropriate rudder angular velocity (as a rule, the assumed velocity ranges from 3^o/s to 5^o/s) corresponds to the power of disturbances affecting the ship at sea state 3 to 4. Therefore, a lack of equilibrium is observed between control power and disturbances power at low and high sea states. As a consequence of this inequilibrium, the quality of course stability varies despite correct control algorithms. At low sea states, an average yaw angle amplitude is minimal, while at high sea states low power of the steering gear does not allow to effectively compensate the effects of disturbances (waves, wind, current). Along with an increase of sea state the amplitude of yaw angle also increases (up to five degrees), and so do rudder angles. Besides, reversals of the steering gear become more frequent. Although the mechanical, hydraulic and electrical requirements for the steering gear, according to classification society regulations, are very strict assuring high reliability,

failures of steering gear do occur, mainly due to exceeded design parameters − temperatures, number of reversals within one hour, or pressures – resulting from engine orders necessitating too intensive control signal sent by the heading controller. The algorithm of heading controller (mainly PID) should execute control assuring that the assumed quality criterion (figure of merit) is satisfied. One such criterion is economical – keeping the ship on the preset course, understood as a requirement to develop a maximum velocity in given conditions. Meeting this criterion will result in lower fuel consumption when covering one mile, for example (at constant propulsion power) thanks to shorter operation time of the main engine. A synthesis of the optimal algorithm of the controller for meeting the above criterion comes down to looking for a control that will minimize the functional:

$$\Delta\nu \cong \lim_{\tau\to\infty} \frac{1}{T}\int_0^T \left(m^2\Delta\psi^2 + \beta^2\right)\mathrm{d}t \qquad (1)$$

where:

- $\Delta\psi$ – heading angle deviation;
- β – rudder angle expressing mean speed loss from stopping forces due to the hull moving along the drift angle and with deflected rudder.

The functional includes a coefficient m^2, which is not the Lagrange multiplier determined from control constraints. For a given ship, it is a constant:

$$m^2 = \frac{B_1}{B_2} \qquad (2)$$

where:

- B_1 – hydrodynamic coefficient dependent on the shape of underwater part of the hull;
- B_2 – hydrodynamic coefficient dependent on the size and shape of the rudder.

The constant coefficient m^2 can be defined for each ship, and ranges from 4 to 16 [3].

However, the determined optimal controller algorithm for the above criterion, taking into account control constraints, causes steering gear overloading in high seas. One dangerous symptom of improper work of the steering gear in high waves is a large number of steering gear reversals performed in one hour. Steering gear is designed for 350–400 reversals per hour, while at sea states 8–9 the figure may reach even 2000. So frequent changes of rudder motion direction lead to fast wear of systems controlling the capacity of variable displacement hydraulic pumps (directional valves, telemotors), wear of electro-hydraulic directional valve springs, heating of pump drive motors, and may cause leaks in the hydraulic system due to pressure surges. The machine sends an alarm signal when allowable values of such parameters as temperatures or mean current of main electric motors are exceeded. This forces the crew to switch off the autopilot and start manual steering by a helmsman. Such situations could be avoided if the steering gear was more powerful. However, a more powerful steering gear, with a given moment at the rudder stock, translates into higher rudder movement speed, wider frequency band executed by the steering gear. Such states correspond to wider rudder angles being set at higher frequency (lower attenuation of controller signal). This, in turn, increases stopping forces from the rudder and ship speed reduction. The ultimate effects are higher fuel consumption and higher transport costs.

For the above reasons, the selection of a steering gear power is an optimization problem. On the one hand, safe manoeuvring criterion has to be met, on the other hand cost-effective operation of the ship in various sailing conditions has to be assured. As it is estimated that as much as 70% of ship's operating time falls to low and medium sea states, there is no reason to install power units of much higher capacity [3]. For the remaining 30% time of operation in difficult conditions created by high sea states action has to be taken to protect steering gear from overloading by giving up optimized control executing an assumed figure of merit.

Among many methods of reducing the intensity of steering gear operation with autopilot at high sea states common actions include [3, 4, 5, 6]:

- increasing the dead zone width of the P-type heading angle controller, or the power amplifier of the controller;
- reducing the gain of derivating part of heading angle controller;
- filtering out higher frequencies in the heading angle signal;
- reducing rudder angular velocity;
- increasing the idle time of steering gear;
- changing the criterion (functional) for algorithm optimization (adaptive controllers).

The above actions are performed automatically in modern autopilots, depending on the results of analysis of signals from the course keeping stability system. It should be noted, however, that each of the above actions limiting the steering gear power causes the mean yaw amplitude to increase. Further in this article proposals will be made in reference to the control of steering gear angular velocity depending on the intensity of its work, defined by the function block analyzing the control signal.

Assessment of steering gear work intensity operating at high sea states

As it was stated previously, during the steering gear-autopilot co-operation at high sea states the power unit gets heated (electric motors of pump drives, pumps, hydraulic oil, hydraulic cylinders). Besides, the steering gear performs a large number of reversals per time unit, harmful for its durability. The alarm system monitors the condition of the machine by observing temperatures or mean currents of electric motors and, in case a parameter is exceeded, engine personnel are alerted on a dangerous situation that may lead to a failure. The personnel are obliged to immediately reduce the load by disconnecting the autopilot and continuing the voyage with the ship being steered by a helmsman. Return to automatic mode (autopilot) should take place only after the power unit cools down (alarm signal disappears) and upon selecting new autopilot settings in the heading controller. The alarm system does not monitor the intensity of steering gear loads by counting the number of reversals within a time unit. Although such count is possible by counting the number of changes in the sign of rudder angle derivative, it is difficult due to a lack of proper devices onboard with such functionality. Besides, counting the number of reversals by recording the actions of electrohydraulic directional valves controlling the flow of hydraulic fluid from fixed displacement pumps to hydraulic cylinders is also troublesome due to numerous additional switchings, resulting from the action of feedback around the three-point controller of the steering gear (follow-up control with dynamic correction).

The author proposes an assessment of steering gear work intensity based on the results of an algorithm analyzing the signal of rudder angle variance and rudder angular velocity variance taken in appropriate proportions. The algorithm is executed by a function block, whose diagram is shown in figure 1.

The block input gets a rudder angle signal $\beta(t)$ from a rudder stock sensor. The constant component is eliminated from the signal by its differentiation, then integration. The obtained signal $\beta 1(t)$ is amplified $k1$ times, then squared. The signal $[\beta 2(t)]^2$ is subtracted from the square of properly amplified signal of rudder angular velocity (amplified $k2$ times). The obtained difference is averaged by a first order inertial element with a relatively large time constant. The resultant signal $X(t)$ is considered as a measure of the steering gear work intensity. A characteristic feature of the above system operation is the fact that the signal $X(t)$ assumes 0 value for $k1/k2 = \omega_0$ ($k1$, $k2$ – gains of rudder angle term and rudder angle derivating term), whilst ω_0 is a signal frequency $\beta(t)$ for navigation in calm water, and the signal increases as sea state rises. The results of the presented function block operation are described in detail in [7].

It is proposed to use the block output signal $X(t)$ for changes of rudder angular velocity in order to reduce the intensity of steering gear work intensity.

Application of the function block for rudder angular velocity control

Reduction of steering gear load when it is controlled by an autopilot at high sea states can be achieved by decreasing the angular velocity of rudder ($P = M\omega$). The choice of a new rudder angular velocity should satisfy the regulations (minimum 2.33°/s), and cause such reduction of load that in given conditions the autopilot could be used and that the new control would not lead to a substantial decrease of the relevant figure of merit (e.g. significant drop in ship's speed).

Technical solutions allowing to control the rudder angular velocity may vary. A simple method consists in decreasing the displacement of hydraulic pumps by reducing their rotary speeds. Electric motors of these pumps should be multiple-speed motors or fed by voltage inverters with controlled U/f ratio, with discrete control obtained by changing the number of pole pairs or discretely forcing a new U/f ratio.

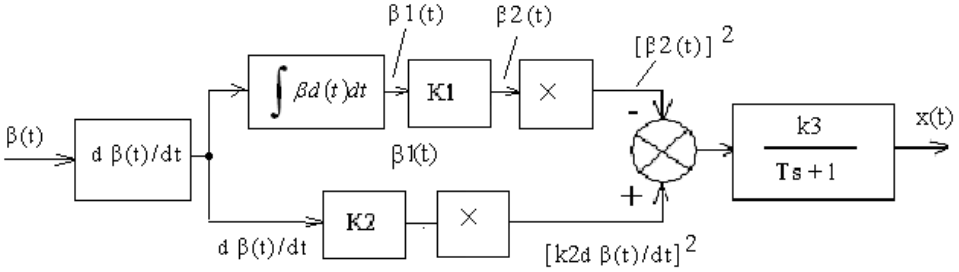

Fig. 1. Diagram of the function block, $\beta(t)$ – rudder angle signal

It is proposed that two rotary speeds are chosen, dependent on the level of function block signal $x(t)$ and preset levels of switching two-point controller governing motor speeds. The idea of this solution is illustrated in figure 2.

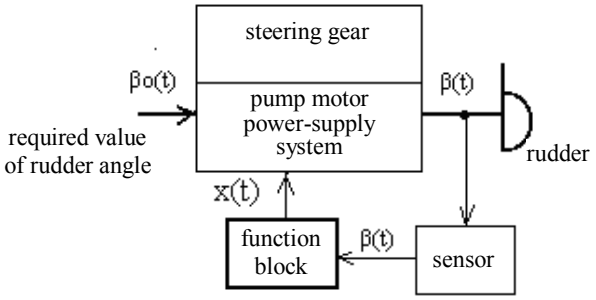

Fig. 2. Method of using the function block for changes of rudder movement speed

To explain the operating effectiveness of the rudder angular velocity control system at high sea states by means of a function block, we have modelled a heading angle stability system with a PID controller (without parameter adaptation) (Fig. 3).

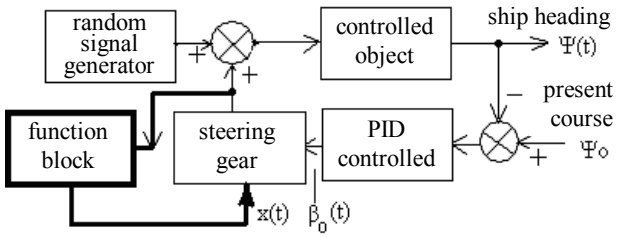

Fig. 3. Model of heading angle stability system with rudder angular velocity control

The assumed model is a simplified, linear model of ship dynamics with the transmittance expressed by the formula [8]:

$$G(s) = \frac{0.05}{s(20s+1)}$$

A steering gear with fixed displacement pump and fixed delivery direction is modelled as a non-linear follow-up system with a three-point controller without dynamic correction, with a constant coefficient of integrating real part gain and with a restriction of an output signal at a level of ±30 degrees. A change of rudder angular velocity in this model is obtained by changing the gain coefficient of the integral real term (with inertia).

A schematic diagram of a steering gear model is shown in figure 4.

The integral gain coefficient for a steering gear working at normal (designed) movement speed is assumed at $k = 4°/s$ while for a gear being shifted at a reduced velocity – at a level 2.5°/s. A time constant of the integral real term is assumed to be $T = 0.8$ s.

Responses to a step change of a setpoint $\beta_0(t)$ of the modelled steering gear working at various speeds are shown in figure 5.

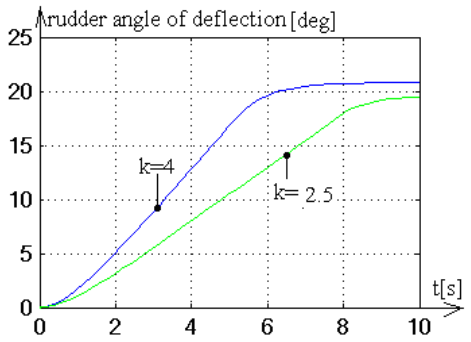

Fig. 5. Responses to step changes executed by the steering gear model at full ($k = 4$) and reduced ($k = 2.5$) velocity

Controller settings were chosen so as to give 10% overshoot when a ship changes its heading (at no disturbances condition).

A random setpoint was sent at the model input, reflecting the action of forces and moments on the hull due to waves. The output signal was a random signal with the following power spectrum density:

$$S(\omega) = \frac{2Dr\alpha\left(\alpha^2+\beta^2+\omega^2\right)}{\omega^4+2\left(\alpha^2-\beta^2\right)\omega^2+\left(\alpha^2+\beta^2\right)^2}$$

where: β – resonance frequency of the spectrum, $\alpha = 0.21\,\beta$, Dr – process dispersion.

The function block was tuned to a frequency $\omega = 0.1$ ($X = 0$). The values of parameters β and Dr were taken from available publications, for waves corresponding to sea state 8 ($Dr = 3.398$ m^2, $\beta = 0.55$ rad/s, $\alpha = 0.115$ rad/s) [3].

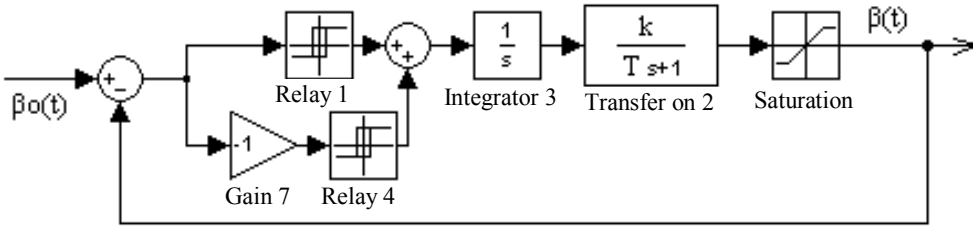

Fig. 4. A steering gear model

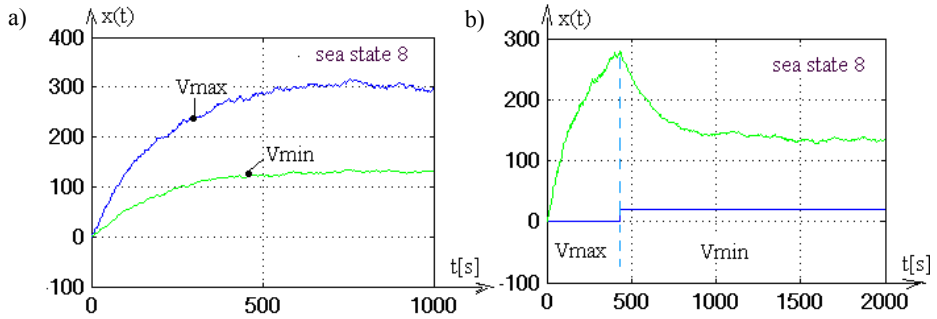

Fig. 6. Changes of the output signal $x(t)$ of the function block; a) for full and reduced velocity of steering gear movement, b) when switching the gear from full to reduced movement speed

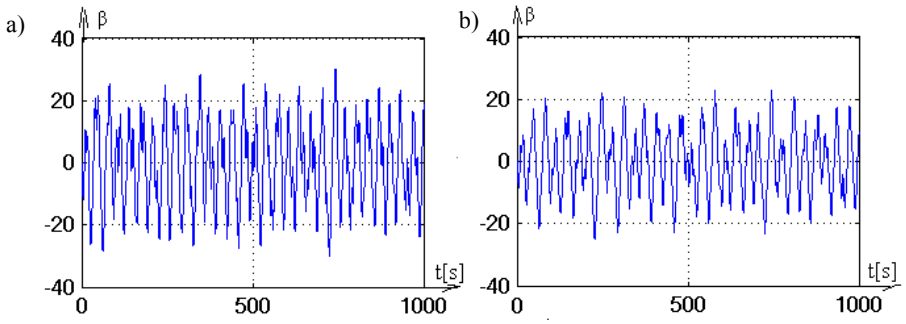

Fig. 7. Rudder angle signal; a) full rudder angular velocity, b) lower rudder angular velocity

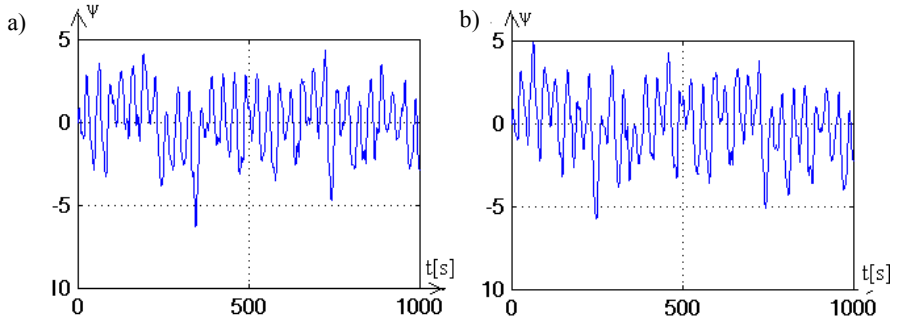

Fig. 8. Ship's yawing angle signal; a) full rudder angular velocity, b) lower rudder angular velocity

The simulation was performed using the MATLAB Simulink.

Figures 6, 7 and 8 demonstrate the results of simulated action of the function block (signal $X(t)$), rudder angle signal (signal $\beta(t)$) and ship's yaw angle signal (signal $\psi(t)$) for sea state 8, at full and reduced angular velocity of the rudder.

The change of output signal was used to reflect automatic alterations of rudder angular velocity from full to reduced and the other way by adding a switching block to the system.

A substantial hysteresis was applied in this block to assure stable operation of the system in case the function block signal drops after a reduced velocity signal input. Levels of switching a two-point controller were set at 280 and 100, so that the system could switch the gear to a lower velocity before reaching the saturation of signal $X(t)$ (about 300) and to prevent the gear from returning to full velocity after a drop of signal $X(t)$ value after velocity reduction. The action of the system with the switching function is shown in figures 6b and 9.

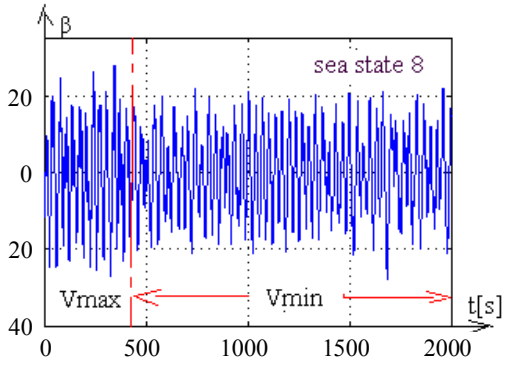

Fig. 9. Change of the rudder angle signal after steering gear angular velocity alteration

Conclusions

It follows from the presented simulation results that a reduction of rudder angular velocity critically decreases the output signal of the function block, and the mean amplitude of rudder angle and slightly increases the yaw angle. A decrease in mean rudder angle amplitude is significant, which reduces the intensity of gear operation. Besides, the number of rudder movement directions in a period of time slightly drops. The use of the function block and its output signal $X(t)$ enables the automation of the process of switching the rudder angular velocity when sailing at high sea states from full to reduced velocity (and *vice versa*), which should enhance the safety of ship operation by decreasing the probability of steering gear failure.

References

1. Przepisy Polskiego Rejestru Statków. Wydawnictwo PRS, 2007.
2. STEFANOWSKI A.: Normowanie prędkości przestawiania steru statku. Materiały V MKNT EXPLO-SHIP 2008. Akademia Morska w Szczecinie, Szczecin 2008.
3. LERNER D.M., ŁUKOMSKIJ J.A. i inni: Uprawlienije morskimi podwianymi obiektami. Sudostrojenie, Leningrad 1979.
4. STEFANOWSKI A.: Układ adaptacji autopilota typu TS. Nadieżnost i Effektiwnost Techniczeskich Sistiem – mieżdunarodnyj sbornik naucznych trudow, KGTU, Kaliningrad 2009.
5. WYSZKOWSKI S.: Autopiloty okrętowe. Wydawnictwo Morskie, Gdańsk 1982.
6. WAGUSZCZIENKO L.L., CYMBAŁ N.N. Sistiemy awtomaticzeskogo uprawlienia dwiżeniem sudna. Łatstar, Odessa 2002.
7. STEFANOWSKI A.: Ocena warunków pracy maszyny sterowej statku na podstawie sygnału bloku funkcyjnego. Proceedings of the XIV International scientific and technical conference on marine traffic engineering. Maritime University of Szczecin, 2011, 459–467.
8. LISOWSKI J.: Statek jako obiekt sterowania automatycznego. Wydawnictwo Morskie, Gdańsk 1981.

Others

9. KOCHENBURGER R.J.: Modelowanie układów dynamicznych przy użyciu maszyn matematycznych. Wydawnictwo Naukowo-Techniczne, Warszawa 1975.
10. STEFANOWSKI A.: Monitorowanie obciążenia elektrohydraulicznych maszyn sterowych statków. Nadieżnost i Effektiwnost Techniczeskich Sistiem – mieżdunarodnyj sbornik naucznych trudow, KGTU, Kaliningrad 2010.
11. STEFANOWSKI A.: Zastosowania elektronicznego modelu prędkości kątowej statku. Budownictwo Okrętowe 4, 1983.
12. STEFANOWSKI A., ZWIERZEWICZ Z.: Assessment of ship steering gear load on an analysis of rudder angle signal. Scientific Journals Maritime University of Szczecin 30(102), 2012, 126–131.

Scientific Journals
Maritime University of Szczecin

Zeszyty Naukowe
Akademia Morska w Szczecinie

2013, 36(108) z. 1 pp. 144–148
ISSN 1733-8670

2013, 36(108) z. 1 s. 144–148

IR technology in marine applications

Waldemar Świderski

Military Institute of Armament Technology
05-220 Zielonka, ul. Prymasa Wyszyńskiego 7

Key words: infra-red radiation, marine applications, infra-red technique, measuring devices, observations

Abstract
The infra-red radiation was discovered in 1800 by English astronomer Sir Wiliam Hirchel but practical applications could be dated to the beginning of XX century. First advanced scientific investigations, as well as works relating to the military applications of IR technique were carried out during the First World War. Many applications of IR radiation exist until now. It is generally accepted that taking into account the destination the devices of IR techniques can be divided on three main groups: measuring devices, observation and automatic recognition systems. Devices of this type can be found both in Navy and civil marine.

Introduction

The infra-red radiation was discovered in 1800 by English astronomer Sir Wiliam Hirchel but practical applications can be dated to the beginning of XX century [1]. First advanced scientific investigations, as well as works relating to the military applications of IR technique were carried out during the First World War. Many applications of IR radiation exist until now.

There are different segmentations of infrared radiation on sub-ranges in literature [2]. The conventional segmentation of spectral band of infrared radiation mostly applies four ranges. First range (near infrared NIR) is limited from 0.7 μm to 1.1 μm length of waves and it is dominated by returned radiation of sun. The systems of low-light-level television (L3TV) and image amplifiers and night vision systems work in this range. The second range is limited from 1.1 μm to 2.5 μm length of waves and called as short-wave infrared (SWIR). Third range of middle-wave infrared (MWIR) is limited from 2.5 μm to 7.0 μm length of waves. This range is usually limited to the band of 3.0 μm to 5.0 μm, because atmosphere suppression strongly limits working range of this area. The infrared range of MWIR is mainly used to detecting and observation of objects at increased temperatures. The long-wave infrared (LWIR) is limited from 7.0 μm to 14.0 μm length of waves, but practically used is the narrower range from 8.0 μm to 12.0 μm, mainly to detecting and observation of low-temperature objects.

It is generally accepted that taking into account the destination the devices of IR techniques can be divided on three main groups: measuring devices, observation and automatic recognition systems. Devices of this type can be found both, in Navy and civil marine.

In civil marine they are mainly used in:

- navigation;
- maritime life rescue;
- maritime pollution combating.

In the Navy they are mainly used in:

- observation and recognition systems;
- rocket and missile homing systems.

Civil Marine Applications

Navigation

Maritime navigation provides safe move of a ship or yacht from one place to the other. Navigation also answers the question where floating object is at any moment (position), as well as how to avoid dangerous situations on the way and to reach target point successfully. All this comes to solution of two tasks: definition of position and lay-out of proper

course [3]. There are many methods to specify the position of floating object like: satellite navigation, geo-navigation, radar navigation, pilotage, celestial navigation, radio navigation and inertial navigation. In spite of the fact that in these methods are applied more and more technically and technologically advanced devices like GPS, radar or electronic maps, a necessity still exists for direct observation of potential threats which could be found on course of a vessel (ship or yacht). The optical observation, even reinforced by the use of optical devices working in the range of visible spectrum, cannot be effective in difficult and unfavourable atmospheric conditions. Therefore, the use of observation devices working in the range of infrared spectrum (thermal cameras) is very useful at limited visible conditions.

Several examples of use of thermal cameras in navigation are presented below:

- captains can use thermal imaging cameras to help them navigate more safely at night (Fig. 1);
- an approaching "blip" on radar screen can also mean danger. Thermal imaging allows the seeing vessels on the horizon and provides decision making capabilities before it is too late;
- icebergs and floating ice can damage a vessel severely or even sink it. It will however become clearly visible thanks to thermal imaging so that the captain can take appropriate action to avoid collisions.

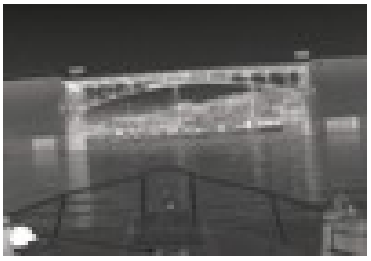

Fig. 1. Seeing at night

Maritime life rescue

Maritime life rescue of people is carried out in Poland mainly by two state institutions:

- SAR (Search and Rescue) Service;
- Navy.

SAR Service has life boats class SAR-3000, SAR-1500, R17, as well as R27 to use in operation of rescue actions. Moreover, Maritime Rescue Stations are equipped with specialist cross-country cars pulling life boats class RIB. Two multipurpose rescue vessels M/S "Kapitan Poinc" and M/S "Czesław 2" are prepared to lead rescue actions [4].

Navy possesses own rescue ships, as well as two types of multipurpose helicopters adapted to work on the sea: PZL W-3RM Anakonda and Mi-14 PS. Additionally, the Maritime Regional Units of the Border Guard are equipped with life boat class SAR-1500, which can be directed in a region of rescue actions including the sea.

The sea rescue belongs to a field of activities where the modern solutions and technical applications should be applied without delays [5]. This is connected with the need of safety assurance, as well as rescue of lives and properties. The rescue actions are very often carried in difficult atmospheric conditions and at different seasons of the year including day and night. From the other side there is very limited range and resolution of devices working in range of visible spectrum. In case of search mission of men a decisive factor of a successful operation is the time. The use of devices working in range of infrared (thermal cameras) makes possible detection of search objects in difficult and variables hydrometeorology conditions existing during rescue actions. Unfortunately, in this type of equipment are only equipped life boats class SAR 3000 (Fig. 2) and helicopters. Thermal imaging can help to quickly find a person that is floating in the water before hypothermia sets in (Fig. 3).

Fig. 2. Life boat class SAR-3000 (www.sar.gov.pl)

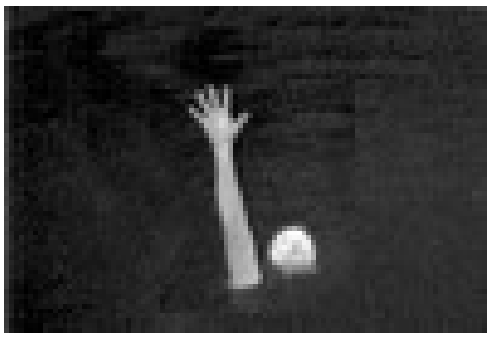

Fig. 3. Man overboard (www.flir.com [6])

Fighting the fires on vessels during rescue actions is a goal for life boats and rescue vessels also. Thermal camera is helpful in estimating the fire situation. It helps in localizing sources of fire,

fighting fires hidden in unapproachable spaces and inspecting sites of the fire. It also enables to measure temperature of difficult to access elements, chimney ducts, ventilation ducts, electrical switchboards, systems, machines and devices. Knowing the temperature of an object helps to minimize the losses. The use of camera helps to perform the actions fast and efficiently at minimum extinguishing media and losses.

Maritime pollution combating

The multi-purpose rescue vessels are also designated for recovering oil pollutions and recognizing their types (mainly gases: explosive, H_2S, NH_3, CO and O_2).

A thermal imaging camera is extremely useful for detecting oil spills that are floating on the water not only in the case of an accident but also when loading or unloading fuel tankers. Oil floating on the water becomes clearly visible on a thermal image.

The stationary gas detection system is designed to detection of presence of gases in air and it is equipped with sensor of gases. Generally, it uses following sensors: electrochemical, catalytic, semiconductor and infrared.

Gases to be detected are often corrosive and reactive. With most sensor types, the sensor itself is directly exposed to the gas, often causing the sensor to drift or die prematurely. The main advantage of IR instruments is that the detector does not directly interact with the gas (or gases) to be detected. The major functional components of the analyzer are protected with optical parts. In other words, gas molecules interact only with a light beam. Only the sample cell and related components are directly exposed to the gas sample stream. These components can be treated, making them resistant to corrosion, and can be designed such that they are easily removable for maintenance or replacement. Today, many IR instruments are available for a wide variety of applications. Many of them offer simple, rugged, and reliable designs. In general, for toxic and combustible gas monitoring applications, IR instruments are among the most user's friendly and require the least amount of maintenance. There are virtually unlimited numbers of applications for which IR technology can be used. Gases whose molecules consist of two or more dissimilar atoms absorb infrared radiation in a unique manner and are detectable using infrared techniques. Infrared sensors are highly selective and offer a wide range of sensitivities, from parts per million levels to 100 percent concentrations [7].

Thermal cameras make possible detection and observation of gases in surrounding too. Thanks of infrared image it can be perceived where effluence of gas comes into being and also in which direction a cloud of gas moves. Imaging by thermal camera is the best solution for taking into consideration other methods of detecting emission of gases. Present methods and technologies depend on a punctual contact sensor that "feels" the gas in air flowing nearby of detection device. However, thermal camera displays a real image of flowing gas and it makes possible to undertake the immediate reaction and analyse the size of emitted gas.

Navy applications

Observation and recognition systems

Every floating object can be detected and identified on basis of radiation features, obtained in different ranges of electromagnetic radiation, from which the most useful are: visible, microwave and infrared.

The development of infrared technology was mainly stimulated by its military applications. First thermal camera used for military application was developed in 1952. First thermal cameras were large and heavy. The study of infrared detectors with large sensitivity and speed of reaction (InSb, Ge:Hg) made possible to obtain images with larger temperature resolutions than for first thermal detectors. The company Perkin-Elmer worked out a thermal camera for the USA Ground Forces in 1960 and Hughnes Aircraft Company and Texas Instruments made a thermal camera for the Air Force in 1965 [3]. Thermal cameras for the Navy appeared later.

The detection process in infrared band can be separated into four independent primary areas which can be characterized as follows: target to background radiation contrast, attenuation process, detection system and signal processor. Detection can take place only if target feature can be discriminated against the background. This requires (as a minimum) two criteria to be fulfilled. In the first place, the radiation contrast between target and background must generate a detector's output voltage exceeding the system noise level. Secondly, the radiation contrast must be discernible from the total observed scene.

For naval targets this approach is partly applicable. Naval targets must be found in a clutter background trough Fourier analysis or by the use of polarization type approaches. Hot exhaust gases, such as those produced by ships, show broad emis-

sion spectra with selective peaks than can be used for detection purposes [8].

The infrared signature of an object is essentially the appearance of that object to an IR sensor (Fig. 4). From the point of view of an IR camera, it is a quantitative measurement of the object's apparent infrared brightness as a function of wavelength. This is affected by many factors, including the shape and size of the object, standoff distance, atmospheric conditions, temperature and emissivity of the object, the background against which it is viewed, and the IR wavelength sensitivity of the camera.

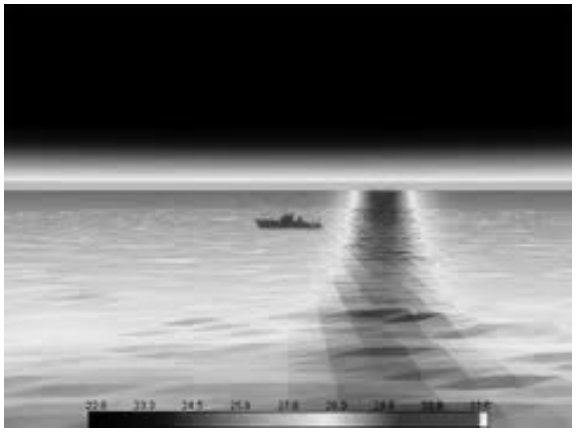

Fig. 4. Infrared image (www.thermoanalytics.com)

On basis of a data base including infrared signatures of floating objects (ships, vessels, boats and the like) it can detect and identify these objects because their infrared signatures are characteristic for every of them (Fig. 5).

A military objective in characterizing the infrared signatures of target objects is to understand the likely infrared signature of threats and develop the means to detect them, as well as to reduce the infrared signatures of owned offensive weaponry.

Fig. 5. Infrared signature of vessel (www.sail_world.com)

The first Polish ship that had to receive optoelectronic observation system was the corvette "Gawron" (Fig. 6) but this project was given up in February 2012.

Fig. 6. Corvette of "Gawron" type (www.wyborcza.pl)

Rocket and Missile Homing Systems

Different classes of rockets and missiles have launching platforms on air, ground, sea and underwater. Marine missiles are launched from ship launchers and could be type of water-air, water-ground, water-water, water-depth and water-outer space missiles. Depth missiles are launched from submarine launcher and could be type of depth-ground, depth-depth, depth-water and depth-air missiles.

Homing in infrared (passive guidance) is one of method used in rockets and missiles. This method may be used in automatic and semi-automatic systems. Infrared camera (IR detector) located in the head of a missile (rocket) is homing this missile on a target being a source of infrared radiation.

An example of missile equipped with infrared homing system is Naval Strike Missile (NSM - Fig.7). The target selection technology provides NSM with a capacity for independent detection, recognition, and discrimination of targets at sea or on the coast. This is possible by the combination of an imaging infrared (IIR) seeker and an onboard target database. NSM is able to navigate by GPS, inertial and terrain reference systems.

Fig. 7. Naval Strike Missile (www.kongsberg.com)

In December 2008 the NSM was selected by the Polish Navy that ordered in total 50 land-based

missiles (including 2 for testing) under the contracts concluded in 2008 and 2011 and delivery planned for 2013–2016 [9].

In June 2013 Poland completed the Coastal Missile Division equipped for the beginning with 12 NSM and 23 vehicles on Jelcz chassis (inc. six launchers, two TRS-15C radars, six fire control and three command vehicles) [10]. Ultimately, the Coastal Missile Division will be equipped with 48 missiles and six launchers. As it is believed Poland is going to establish second missile division in the near future.

Conclusions

Some possibilities of use of infrared technique in marine applications were presented in the paper. Their use increases the safety of navigation, possibility of people life rescue, chances of defeating threats and environmental contamination, as well as military capacities of the Polish Navy. Unfortunately, the scale of utilization of these systems in Poland is small as there is a little sale at present both, in Navy and civil marine applications.

The quicker development of infrared technology in the last years may be observed and it also creates new possibilities for using modern infrared systems in marine applications.

Infrared camuflage of different military objects and ships is a problem in which MIAT is going to be involved. The development of infrared camuflage materials and the evaluation of their effectiveness is the problem area where signatures of object and background come together. For camulage materials two conditions must be fulfilled to be effective in the thermal infrared: temperature similarity and spatial similarity. Models and measurements to test prototype camuflage materials and to optimize their performance are planned to be used in MIAT in future works.

References

1. MINKINA W.: Pomiary termowizyjne – przyrządy i metody. Wydawnictwa Politechniki Częstochowskiej, Częstochowa 2004.
2. ŚWIDERSKI W.: Metody termograficzne w nieniszczących badaniach materiałów kompozytowych do zastosowań specjalnych. Monografia habilitacyjna, Wojskowy Instytut Techniczny Uzbrojenia, Zielonka 2010.
3. www.navipedia.pl
4. www.sar.gov.pl
5. Praca zbiorowa. Pomiary termowizyjne w praktyce. Pomiary Automatyka Kontrola, Warszawa 2004.
6. www.flir.com
7. TRENCZEK S., WOJTAS P.: Rozwój pomiaroznawstwa stosowanego od pomiarów wskaźnikowych do monitorowania i nadzorowania bezpieczeństwa. Prace Naukowe Instytutu Górnictwa Politechniki Wrocławskiej, Nr 117, 2006, 327–339.
8. JACOBS P.A.: Thermal Infrared Characterization of Ground Targets and Backgrounds. Toutorial Texts in Optical Engineering, Vol. TT26, SPIE, Washington 1996.
9. GÓRKA M.: Superrakiety w starej marynarce. Gazeta Wyborcza, Warszawa 2008.
10. www.altair.com.pl

Scientific Journals
Maritime University of Szczecin

Zeszyty Naukowe
Akademia Morska w Szczecinie

2013, 36(108) z. 1 pp. 149–155
ISSN 1733-8670

2013, 36(108) z. 1 s. 149–155

Determination of ship's positions applying the selected M-estimation methods basing on radar observations

Sławomir Świerczyński, Krzysztof Czaplewski

Polish Naval Academy
81-103 Gdynia, ul. Śmidowicza 69, e-mail: krzysztof@czaplewski.pl

Key words: ship's positions, M-estimation methods, radar observations, navigational data, water areas

Abstract
The paper presents an analysis of the selected robust adjustment methods applied in geodesy, proving thereby justifiability in choosing the applied attenuation function. With a use of the radar navigation methods, the said methods were applied in the process of determination of the observed vessel's positions.

Introduction

The geometrical measurement structures can be defined in two-dimensional system, for example (X, Y), wherein a parameter to measure are the directions from which the angle is computed. The measurement structure in navigation may reflect the real navigation equipment. It can be a network of coastal radar stations, assigned for collecting navigational data (bearings or distances), necessary for fixing positions of ships in water areas. They are situated along the coast line and they can be formed into different geometrical configurations of radar survey stations. Figure 1 presents an exemplary measurement grid, wherein the coastal radar stations are used for surveying purpose.

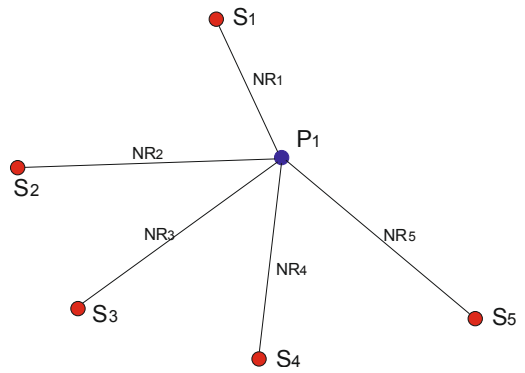

Fig. 1. Measurement structure [own study]

With a use of such a measurement structure, comprising the coastal radar stations, it is feasible to carry out surveys at some time intervals. A bearing is here one of the parameters to measure. On taking measurements we can see that there may come up incidents when there are found gross errors biased survey results. Such errors may result from improper installation or calibration of the measurement equipment, wrong readings from measurement equipment caused by momentary changes of measurement environment parameters etc. The errors of such character are called often gross errors and may considerably affect the measurement results' values. To eliminate a case of determination of false radar echoes, there can be applied the robust estimation methods of properly selected attenuation functions.

In the adjustment calculus there are known several M-estimation methods, which differ in a form of the attenuation function or the weight function. The most popular are the Huber's, Hampel's and the Danish methods. For the purpose of the here presented study, there was carried out analysis of these three functions of attenuation in respect of their influence on the position fixing accuracy in consideration of the gross errors biased measurements.

The Danish attenuation function is characterized with such properties, that beyond the admissible interval $\Delta\bar{v} \in \langle -k{:}k \rangle$, it ex-potentially decreases and takes the following form:

$$t(\bar{v}_n)=\begin{cases}1 & \text{for } \bar{v}_n \in \langle -k:k \rangle \\ \exp\left\{-l\left(|\bar{v}_n|-k\right)^g\right\} & \text{for } |\bar{v}_n|>k\end{cases} \tag{1}$$

In that case the equivalent values of weights are settled according to the formula:

$$\hat{p}_n = t(\bar{v}_n)p_n = \begin{cases}p_n & \text{for } \bar{v}_n \in \langle -k:k \rangle \\ \exp\left\{-l\left(|\bar{v}_n|-k\right)^g\right\}p_n & \text{for } |\bar{v}_n|>k\end{cases}$$

The Hampel's attenuation function, the next one applied in the calculations, has two additional intermediate intervals (leftward and rightward from the admissible interval $\Delta\bar{v} \in \langle -k:k \rangle$), where the attenuation function $t(\bar{v})$ linearly reduces its values. The above mentioned function and the weight function resulting therefrom have the forms as follows:

$$t(\bar{v}_n)=\begin{cases}1 & \text{for } \bar{v}_n \in \langle -k:k \rangle \\ \dfrac{|\bar{v}_n|-k_b}{k-k_b} & \text{for } |\bar{v}_n| \in (k:k_b\rangle \\ 0 & \text{for } |\bar{v}_n|>k_b\end{cases} \tag{3}$$

$$\hat{p}_n = t(\bar{v}_n)p_n = \begin{cases}p_n & \text{for } \bar{v}_n \in \langle -k:k \rangle \\ \left(\dfrac{|\bar{v}_n|-k_b}{k-k_b}\right)p_n & \text{for } |\bar{v}_n| \in (k:k_b\rangle \\ 0 & \text{for } |\bar{v}_n|>k_b\end{cases} \tag{4}$$

where k_b is a number which settles the limits of the additional intervals. Generally, it was assumed that $k_b = 4,...,6$.

The last attenuation function taken for analysis, the Huber's function, is the most „radical" one, as it assigns the zero values of weights to all the observations, corrections of which are not within the interval admissible for them and takes the form as follows:

$$t(\bar{v}_n)=\begin{cases}1 & \text{for } \bar{v}_n \in \langle -k:k \rangle \\ 0 & \text{for } \bar{v}_n \notin (-k:k)\end{cases} \tag{5}$$

Therefore, the following weight function results:

$$\hat{p}_n = t(\bar{v}_n)p_n = \begin{cases}p_n & \text{for } \bar{v}_n \in \langle -k:k \rangle \\ 0 & \text{for } \bar{v}_n \notin (-k:k)\end{cases} \tag{6}$$

The equalization problem with application of the gross errors robust method may take the following form:

$$\left.\begin{aligned}
&\mathrm{V} = \mathrm{A}\hat{\mathrm{d}}_\mathrm{X} + \mathrm{L} && \text{functional model}\\
&\mathrm{C_X} = \sigma_0^2\mathrm{Q_X} = \sigma_0^2\mathrm{P}^{-1} && \text{original statistic model}\\
&\widehat{\mathrm{C}}_\mathrm{X} = \sigma_0^2\widehat{\mathrm{Q}}_\mathrm{X} = \sigma_0^2\widehat{\mathrm{P}}^{-1} && \text{equivalent statistic model}\\
&\widehat{\mathrm{P}} = \mathrm{T}(\overline{\mathrm{V}})\mathrm{P} && \text{equivalent weights}\\
&\Psi(\hat{\mathrm{d}}_\mathrm{X}) = \mathrm{V}^\mathrm{T}\widehat{\mathrm{P}}\mathrm{V} = \mathrm{V}^\mathrm{T}\mathrm{T}(\overline{\mathrm{V}})\mathrm{P}\,\mathrm{V} = \min && \text{equalization criterion}\\
&\mathrm{V}^\mathrm{T}\mathrm{T}(\overline{\mathrm{V}})\mathrm{P}\,\mathrm{V} = \hat{\mathrm{V}}^\mathrm{T}\mathrm{T}\left(\hat{\overline{\mathrm{V}}}\right)\mathrm{P}\hat{\mathrm{V}} && \text{equalization criterion}
\end{aligned}\right\} \tag{2,7}$$

where:

$\widehat{\mathrm{P}} = \mathrm{T}(\overline{\mathrm{V}})\mathrm{P}$ – equivalent weight matrix;

$\mathrm{C_X}$ – equivalent covariance matrix;

$\widehat{\mathrm{Q}}_\mathrm{X}$ – equivalent co-factors matrix;

$\mathrm{T}(\overline{\mathrm{V}})$ – diagonal attenuation matrix.

For this way adopted assumptions the equalization problem solution is of iterative character. To solve the problem there may be adopted an algorithm suggested in [9, 10], where the first stage of the calculation process is equalization applying the classical least squares method. In the equalization process we assume that the observed position forwarded by the watch officer to the traffic supervision system operator is an expected position of the coordinates as follows:

$$\mathrm{P}_\mathrm{j}^0 = \begin{bmatrix}\mathrm{X}_\mathrm{j}^0 \\ \mathrm{Y}_\mathrm{j}^0\end{bmatrix} \tag{8}$$

for the measuring structure adopted to these considerations the equalization problem's functional model takes the following form:

$$v_{ij} = \frac{\partial NR_{ij}}{\partial X_{P_j}}\hat{d}_{X_{P_j}} + \frac{\partial NR_{ij}}{\partial Y_{P_j}}\hat{d}_{Y_{P_j}} + NR_{ij}^0 - NR_{ij}^{obs}\Big|_{\substack{i=1,\ldots,n\\ j=1,\ldots,m}} \tag{9}$$

where:

v_{ij} – corrections to the measured bearing taken from the i-th radar station (i = 1,…,5);

NR_{ij}^0 – radar bearing value for $P_j^0\left(X_j^0, Y_j^0\right)$;

P_j – j-th position of the ship (j = 1,…,4);

Assuming that:

V – corrections vector;

A – matrix of coefficients with unknowns;

$\hat{\mathrm{d}}_\mathrm{X}$ – searched vector of increments in the expected coordinates;

L – free terms matrix.

Thus the matrix system of corrections' equations takes the form as follows:

$$\mathrm{V} = \mathrm{A} \cdot \hat{\mathrm{d}}_{\mathrm{X}} + \mathrm{L} \tag{10}$$

With taking advantage of the indeterminate method, a solution of this equations system is:

$$\hat{\mathrm{d}}_{\mathrm{X}} = -\left(\mathrm{A}^{\mathrm{T}}\mathrm{P}\mathrm{A}\right)^{-1}\mathrm{A}^{\mathrm{T}}\mathrm{P}\mathrm{L} \tag{11}$$

where: P – is the performed observations weights matrix ($i = 1,\ldots,5$), ($j = 1,..,4$)

Therefore, estimators of the equalized coordinates of the ship at sea are as follows:

$$\hat{\mathrm{P}}_{\mathrm{j}} = \mathrm{P}_{\mathrm{j}}^{0} + \hat{\mathrm{d}}_{\mathrm{XY}} = \begin{bmatrix} X_j^0 \\ Y_j^0 \end{bmatrix} + \begin{bmatrix} \hat{d}_{X_{P_j}} \\ \hat{d}_{Y_{P_j}} \end{bmatrix} = \begin{bmatrix} \hat{X}_j \\ \hat{Y}_j \end{bmatrix} \tag{12}$$

where: $\hat{\mathrm{P}}_{\mathrm{j}}\left(\hat{\mathrm{X}}_{\mathrm{j}}, \hat{\mathrm{Y}}_{\mathrm{j}}\right)$ – the estimated position of a vessel at sea.

To find out which of the standardized corrections may represent gross errors (not within $\Delta\bar{v}$), there was determined the corrections vector covariance matrix for $m_0 = 1$.

$$\hat{\mathrm{C}}_{\hat{\mathrm{V}}(\mathrm{m_o}=1)} = \mathrm{P}^{-1} - \mathrm{A}\left(\mathrm{A}^{\mathrm{T}}\mathrm{P}\mathrm{A}\right)^{-1}\mathrm{A}^{\mathbf{T}} \tag{13}$$

and next there was carried out classification, whether for every $i - \bar{v}_i \in \Delta\bar{v}$

In case all $\bar{v}_i \in \Delta\bar{v}$, then we abandon further calculations; otherwise, if any correction $\bar{v}_i \notin \Delta\bar{v}$ there were followed up the next iteration steps:

It is assumed that $j = 0$ then:

$$\mathrm{V}^{(\mathrm{j})} = \mathrm{V}, \quad \mathrm{P}^{(\mathrm{j})} = \mathrm{P}, \quad \mathrm{C}_{\mathrm{V}(m_o=1)}^{(\mathrm{j})} = \hat{\mathrm{C}}_{\hat{\mathrm{V}}(m_o=1)}^{(\mathrm{j})}$$

and the control parameters for all the functions of attenuation $l = 0.02$, $g = 2$, and for the Huber's function $k_b = 6$ and the function of attenuation and the matrix of attenuation are calculated; afterwards it has to be checked which of the standardized corrections is laid within the admissible interval:

Then iteration is carried out; we increase j by 1, it means: $j := j + 1$, and calculate the matrix of weights, of increments, so the matrix of corrections:

$$\left.\begin{aligned} \mathrm{P}^{\mathrm{j}} &= \mathrm{T}\left(\bar{\mathrm{V}}^{(\mathrm{j}-1)}\right)\mathrm{P}^{(\mathrm{j}-1)} \\ \mathrm{d}_{\mathrm{X}}^{(\mathrm{j})} &= -\left(\mathrm{A}^{\mathrm{T}}\mathrm{P}^{(\mathrm{j})}\mathrm{A}\right)^{-1}\mathrm{A}^{\mathrm{T}}\mathrm{P}^{(\mathrm{j})}\mathrm{L} \\ \mathrm{V}^{[\mathrm{j}]} &= \mathrm{A} \cdot \mathrm{d}_{\mathrm{X}}^{(\mathrm{j})} + \mathrm{L} \end{aligned}\right\} \tag{14}$$

Having in mind the assumed precision of calculations we check differences between the corrections vectors elements: $\mathrm{v}^{(\mathrm{j})}$ and $\mathrm{v}^{(\mathrm{j}-1)}$.

In case the differences are more essential than the assumed ones, we have to calculate the corrections vector covariance matrix for $m_0 = 1$.

$$\begin{aligned} \mathbf{C}_{\mathbf{V}(m_o=1)}^{(\mathbf{j})} &= \left(\mathrm{P}^{(\mathrm{j})}\right)^{-1} - \mathrm{A}\left(\mathrm{A}^{\mathrm{T}}\mathrm{P}^{(\mathrm{j})}\mathrm{A}\right)^{-1}\mathrm{A}^{\mathrm{T}} \\ m_{v_i}^{(j)} &= \sqrt{\left[\mathbf{C}_{\mathbf{V}(m_o=1)}^{(\mathbf{j})}\right]_{ii}} \qquad \bar{v}_i^{(j)} = \frac{v_i^j}{m_{v_i}^{(j)}} \end{aligned} \tag{15}$$

Now a value of the attenuation function and the matrix of attenuation are calculated. We increase j by 1, and begin the next step of iteration. The iteration process is finished with such equalization, for which the obtained standardized corrections values are laid within the interval admissible therefor and resulting therefrom the new attenuation matrix would not cause any decrease of the weights matrix value and, in turn, the corrections values (within the assumed limits of calculations precision).

Equalization problem and its solution

The calculations were analyzed taking advantage of the measured navigational observations such as the bearings. There were carried out observations of the ship along the Gulf of Gdańsk; the surveys were performed at five coastal stations, at asymmetrical time intervals. Due to the long measuring sequence, this paper presents the surveys of four ship's positions. Values of the bearings are shown in table 1. For a purpose of this research,

Table 1. The bearings and coordinates of the ship sailing in the Gulf of Gdańsk

Survey point	Coastal radar stations					$\mathrm{P}_{\mathrm{j}}^{0}$
	Hel	Gdynia	Gdańsk North Port	Górki Zachodnie	Krynica Morska	
P_1	140.2°	93.3°	27.6°	29.5°	293.9°	φ = 54° 31.279'N λ = 18° 55.539'E
P_2	156.1°	100.5°	29.3°	27.3°	288.8°	φ = 54° 29.829'N λ = 18° 53.472'E
P_3	172.8°	112.5°	33.3°	21.8°	282.7°	φ = 54° 27.769'N λ = 18° 50.539'E
P_4	180.2°	121°	38.1°	15.1°	278.4°	φ = 54° 26.485'N λ = 18° 48.712'E

one survey was biased with a gross error. In practice, it may happen in case a bearing is taken falsely by the radar operator, improper identification of a surveyed object or an error in indications of the navigational equipment connected with radar. The gross error comes out for the positions P_1, P_2, P_3 and P_4 in all bearings taken at the coastal station in Gdańsk.

To simplify the calculation process there was decided that the further calculations are to be performed applying the rectangular coordinates system, not the terrestrial coordinates one. The calculations were carried out for each location of the ship at the moment of taking a bearing. Due to limits of size of this paper the authors present results of the calculations performed for one position P_2.

While carrying out equalization of the performed observations in the first step applying the least squares method, for the selected functions of attenuation the following results were obtained:

1) In case of the Danish function of attenuation:

The vector of increments in the expected coordinates is:

$$\hat{d}_X = -\left(A^T P A\right)^{-1} A^T P L = \begin{bmatrix} \hat{d}_{X_{P_1}} \\ \hat{d}_{Y_{P_1}} \end{bmatrix} = \begin{bmatrix} 3059.04 \\ -1193.10 \end{bmatrix}_{[m]}$$

Thus, the correction vector takes the value:

$$V = \begin{bmatrix} v_1 \\ v_2 \\ v_3 \\ v_4 \\ v_5 \end{bmatrix} = \begin{bmatrix} 1.42 \\ -4.80 \\ 11.05 \\ -7.33 \\ 5.21 \end{bmatrix}$$

Consequently, the estimator of the observed ship's position at sea, with a use of the observations carried out at the coastal station is as follows:

$$\hat{P}_1 = \begin{bmatrix} \hat{X}_1 \\ \hat{Y}_1 \end{bmatrix} = \begin{bmatrix} X_1^0 \\ Y_1^0 \end{bmatrix} + \begin{bmatrix} \hat{d}_{X_{P_1}} \\ \hat{d}_{Y_{P_1}} \end{bmatrix} =$$

$$= \begin{bmatrix} 6040883.49 \\ 363431.40 \end{bmatrix} + \begin{bmatrix} 3059.04 \\ -1193.10 \end{bmatrix} = \begin{bmatrix} 6043942.53 \\ 363590.33 \end{bmatrix}$$

Basing on the obtained results we set out which of the standardized corrections can represent gross errors. Assuming for the calculations $\gamma = 0.95$, wherefrom $k = 2$. The admissible interval $\Delta\bar{v}$ form is as follows: $\Delta\bar{v} \in \langle -k;k \rangle = \langle -2;2 \rangle$. Then the corrections vector's covariance matrix $\hat{C}$ for $m_o = 1$.

$$\hat{C}_{\hat{V}(m_o=1)} = P^{-1} - A\left(A^T P A\right)^{-1} A^T =$$

$$= \begin{bmatrix} 0.06837 & -0.07554 & 0.00954 & 0.06422 & 0.04995 \\ -0.07554 & 0.17395 & -0.06657 & -0.03361 & 0.04429 \\ 0.00954 & -0.06657 & 0.13804 & -0.09869 & 0.03454 \\ 0.06422 & -0.03361 & -0.09869 & 0.14578 & 0.01412 \\ 0.04995 & 0.04429 & 0.03454 & 0.01412 & 0.22387 \end{bmatrix}$$

then we have to carry out the classification:

$$\bar{\hat{v}}_1 = \frac{\left(\hat{v}_1\right)_{(m)}}{\left(\sqrt{0.06837}\right)_{(m)}} = 5.42 \quad \notin \Delta\bar{v}$$

$$\bar{\hat{v}}_2 = \frac{\left(\hat{v}_2\right)_{(m)}}{\left(\sqrt{0.17395}\right)_{(m)}} = -11.52 \quad \notin \Delta\bar{v}$$

$$\bar{\hat{v}}_3 = \frac{\left(\hat{v}_3\right)_{(m)}}{\left(\sqrt{0.13804}\right)_{(m)}} = 29.73 \quad \notin \Delta\bar{v}$$

$$\bar{\hat{v}}_4 = \frac{\left(\hat{v}_4\right)_{(m)}}{\left(\sqrt{0.14578}\right)_{(m)}} = -19.20 \quad \notin \Delta\bar{v}$$

$$\bar{\hat{v}}_5 = \frac{\left(\hat{v}_5\right)_{(m)}}{\left(\sqrt{0.22387}\right)_{(m)}} = 11.01 \quad \notin \Delta\bar{v}$$

The obtained results prove that none of the standardized corrections' estimators is laid within the admissible interval. If the geodesy methods were applied, it would be necessary to reject any measurements biased with such errors and to repeat the surveys. However, it is difficult for a port approaching ship to turn back to let us perform surveys at the previously measured positions. So, remaining not influenced by such errors we perform equalization of the measurement results, making the observation results robust to gross errors with application of the function of attenuation.

Finally the following solution is found:

$$\hat{d}_X = -\left(A^T \bar{\hat{P}} A\right)^{-1} A^T \bar{\hat{P}} L = \begin{bmatrix} -284.73 \\ -267.45 \end{bmatrix}_{(m)}$$

$$\hat{V} = A \cdot \hat{d}_X + L = \begin{bmatrix} 0.04 \\ 1.28 \\ 21.64 \\ 2.15 \\ 2.08 \end{bmatrix}_{(m)}$$

$$\hat{P}_1 = \begin{bmatrix} \hat{X}_1 \\ \hat{Y}_1 \end{bmatrix} = \begin{bmatrix} X_1^0 \\ Y_1^0 \end{bmatrix} + \begin{bmatrix} \hat{d}_{X_{P_1}} \\ \hat{d}_{Y_{P_1}} \end{bmatrix} =$$

$$= \begin{bmatrix} 6040883.49 \\ 363431.40 \end{bmatrix} + \begin{bmatrix} 3059.04 \\ -1193.10 \end{bmatrix} = \begin{bmatrix} 6043942.53 \\ 362238.30 \end{bmatrix}$$

2) For the Hampel's function:

The vector of increments in the expected coordinates is:

$$\hat{d}_X = -\left(A^T P A\right)^{-1} A^T P L = \begin{bmatrix} \hat{d}_{X_{P_1}} \\ \hat{d}_{Y_{P_1}} \end{bmatrix} = \begin{bmatrix} 3059.04 \\ -1193.10 \end{bmatrix}_{[m]}$$

So, the corrections vector takes the following value:

$$V = \begin{bmatrix} v_1 \\ v_2 \\ v_3 \\ v_4 \\ v_5 \end{bmatrix} = \begin{bmatrix} 1.42 \\ -4.80 \\ 11.05 \\ -7.33 \\ 5.21 \end{bmatrix}$$

Thus, the following is the estimator of the observed position of the ship at sea, with a use of the observations taken at the coastal stations:

$$\hat{P}_1 = \begin{bmatrix} \hat{X}_1 \\ \hat{Y}_1 \end{bmatrix} = \begin{bmatrix} X_1^0 \\ Y_1^0 \end{bmatrix} + \begin{bmatrix} \hat{d}_{X_{P_1}} \\ \hat{d}_{Y_{P_1}} \end{bmatrix} =$$

$$= \begin{bmatrix} 6040883.49 \\ 363431.40 \end{bmatrix} + \begin{bmatrix} 3059.04 \\ -1193.10 \end{bmatrix} = \begin{bmatrix} 6043942.53 \\ 362238.30 \end{bmatrix}$$

Basing on the obtained results we were capable to define which of the standardized corrections may represent gross errors. Assuming $\gamma = 0.95$ for calculation purpose it is obtained thereby that $k = 2$. The admissible interval $\Delta\bar{v} \in \langle -k;k \rangle = \langle -2;2 \rangle$. Within this function range we also assume a value $k_b = 6$. Then there is calculated the corrections vector's matrix for $m_o = 1$, and next carry out classification, which of the standardized corrections is laid within the admissible interval:

$$\bar{\hat{v}}_1 = 5.42 \quad \notin \Delta\bar{v}, \qquad \bar{\hat{v}}_2 = -11.52 \quad \notin \Delta\bar{v}$$
$$\bar{\hat{v}}_3 = 29.73 \quad \notin \Delta\bar{v}, \qquad \bar{\hat{v}}_4 = -19.20 \quad \notin \Delta\bar{v}$$
$$\bar{\hat{v}}_5 == 11.01 \quad \notin \Delta\bar{v}$$

Finally, we obtain the following solution:

$$\hat{d}_X = -\left(A^T \hat{P} A\right)^{-1} A^T \hat{P} L = \begin{bmatrix} 3241.08 \\ -932.85 \end{bmatrix}_{(m)}$$

$$\hat{V} = A \cdot \hat{d}_X + L = \begin{bmatrix} -0.01 \\ -5.39 \\ 11.12 \\ -6.83 \\ 5.6 \end{bmatrix}_{(m)}$$

$$\hat{P}_1 = \begin{bmatrix} \hat{X}_1 \\ \hat{Y}_1 \end{bmatrix} = \begin{bmatrix} X_1^0 \\ Y_1^0 \end{bmatrix} + \begin{bmatrix} \hat{d}_{X_{P_1}} \\ \hat{d}_{Y_{P_1}} \end{bmatrix} =$$

$$= \begin{bmatrix} 6040883.49 \\ 363431.40 \end{bmatrix} + \begin{bmatrix} 3241.08 \\ -932.85 \end{bmatrix} = \begin{bmatrix} 6044124.57 \\ 362498.54 \end{bmatrix}$$

3) For the Huber's function:

The following is the vector of increments in the expected coordinates:

$$\hat{d}_X = -\left(A^T P A\right)^{-1} A^T P L = \begin{bmatrix} \hat{d}_{X_{P_1}} \\ \hat{d}_{Y_{P_1}} \end{bmatrix} = \begin{bmatrix} 3059.04 \\ -1193.10 \end{bmatrix}_{[m]}$$

Thus, the corrections vector takes the value:

$$V = \begin{bmatrix} v_1 \\ v_2 \\ v_3 \\ v_4 \\ v_5 \end{bmatrix} = \begin{bmatrix} 1.42 \\ -4.80 \\ 11.05 \\ -7.33 \\ 5.21 \end{bmatrix}$$

Consequently, the following is the estimator of the observed position of a ship at sea, with a use of the observations taken at the coastal stations:

$$\hat{P}_1 = \begin{bmatrix} \hat{X}_1 \\ \hat{Y}_1 \end{bmatrix} = \begin{bmatrix} X_1^0 \\ Y_1^0 \end{bmatrix} + \begin{bmatrix} \hat{d}_{X_{P_1}} \\ \hat{d}_{Y_{P_1}} \end{bmatrix} =$$

$$= \begin{bmatrix} 6040883.49 \\ 363431.40 \end{bmatrix} + \begin{bmatrix} 3059.04 \\ -1193.10 \end{bmatrix} = \begin{bmatrix} 6043942.53 \\ 363590.33 \end{bmatrix}$$

On the basis of the obtained results it was defined which of the standardized corrections may represent gross errors. Adopting to the calculations $\gamma = 0{,}95$, we find that $k = 2$. The admissible interval $\Delta\bar{v}$ is as follows: $\Delta\bar{v} \in \langle -k;k \rangle = \langle -2;2 \rangle$. A this point there is calculated the corrections vector's covariance matrix for $m_o = 1$, and then carried out classification, which of the standardized corrections is laid within the limits if the admissible interval:

$$\bar{\hat{v}}_1 = 5.42 \quad \notin \Delta\bar{v}, \qquad \bar{\hat{v}}_2 = -11.52 \quad \notin \Delta\bar{v}$$
$$\bar{\hat{v}}_3 = 29.73 \quad \notin \Delta\bar{v}, \qquad \bar{\hat{v}}_4 = -19.20 \quad \notin \Delta\bar{v}$$
$$\bar{\hat{v}}_5 == 11.01 \quad \notin \Delta\bar{v}$$

Ultimately, the following solution is obtained:

$$\hat{d}_X = -\left(A^T \hat{P} A\right)^{-1} A^T \hat{P} L = \begin{bmatrix} 3059.04 \\ -1193.10 \end{bmatrix}_{(m)}$$

Table 2. Ship's position, sizes of increments and estimated coordinates

Survey point	Reckoned ship coordinates	Estimated coordinates	Coordinates after applying the Danish function	Coordinates after applying the Hampel's function	Coordinates after applying the Huber's function
P_1	X = 6043505.62 Y = 365741.39	X = 6044148.28 Y = 365520.70	X = 6043729.09 Y = 365941.95	X = 6046533.702 Y = 363772.566	X = 6046396.96 Y = 363590.33
P_2	X = 6040883.49 Y = 363431.40	X = 6041537.69 Y = 363401.64	X = 6041168.22 Y = 363698.85	X = 6044124.571 Y = 362498.544	X = 6043942.53 Y = 362238.30
P_3	X = 6037160.10 Y = 360149.01	X = 6037735.18 Y = 360230.87	X = 6037090.70 Y = 360606.77	X = 6038780.569 Y = 360472.854	X = 6040363.66 Y = 359950.24
P_4	X = 6034840.44 Y = 358101.69	X = 6035222.02 Y = 358103.18	X = 6036314.75 Y = 358474.98	X = 6037828.994 Y = 358733.697	X = 6037916.67 Y = 358267.96

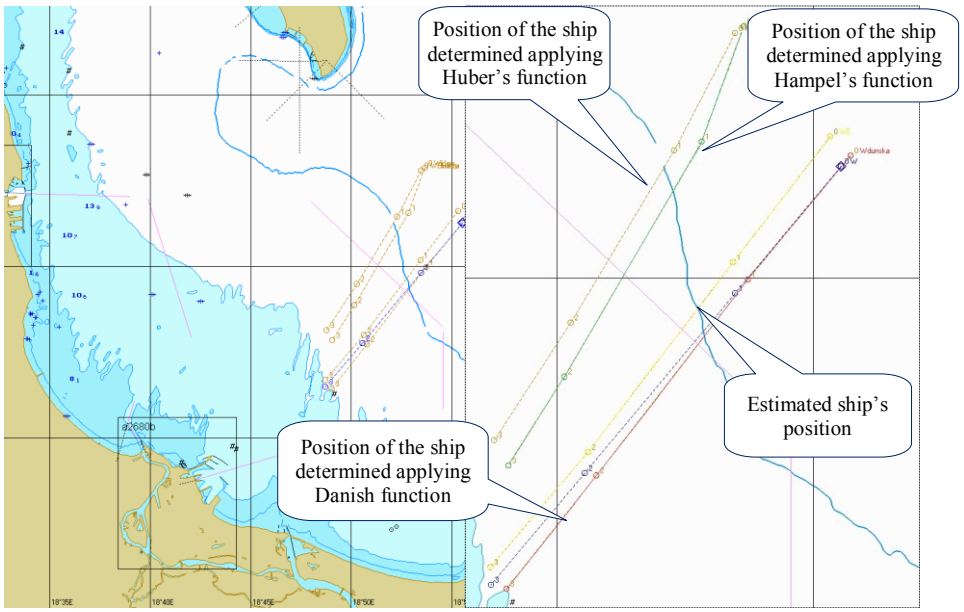

Fig. 2. Graphical presentation of the calculation results [own study]

$$V = \begin{bmatrix} v_1 \\ v_2 \\ v_3 \\ v_4 \\ v_5 \end{bmatrix} = \begin{bmatrix} 1.42 \\ -4.80 \\ 11.05 \\ -7.33 \\ 5.21 \end{bmatrix}$$

$$\hat{P}_1 = \begin{bmatrix} \hat{X}_1 \\ \hat{Y}_1 \end{bmatrix} = \begin{bmatrix} X_1^0 \\ Y_1^0 \end{bmatrix} + \begin{bmatrix} \hat{d}_{X_{P_1}} \\ \hat{d}_{Y_{P_1}} \end{bmatrix} =$$

$$= \begin{bmatrix} 6040883.49 \\ 363431.40 \end{bmatrix} + \begin{bmatrix} 3059.04 \\ -1193.10 \end{bmatrix} = \begin{bmatrix} 6043942.53 \\ 362238.30 \end{bmatrix}$$

Having finished the final calculations the increments sizes and the estimated ship coordinates were displayed in table 2, and the graphical interpretation of the calculation results in figure 2.

Conclusions

On taking measurement of parameters necessary for determination of vessels positions it has to be taken into consideration that in effect of any disturbances in the survey process the measurement results may be biased with serious errors; at the extreme situation the errors can considerably deviate from the expected results. In case a gross error occurs it is advised to repeat the survey and correct the results. For a ship sailing in water area re-survey is impossible. Within each time interval the ship travels along a certain route distance and turning back to the last measuring point is unfeasible. In consequence, incorrect determination of the ship's position may cause mistaken chart navigation and finally appear a threat to navigation safety. Applying the M-estimation methods can considerably correct such errors and reduce their influence on marking out the plot of route on the chart.

A key problem in robust estimation is selection of the proper attenuation function, affecting the position fixing accuracy. In the paper three methods of robust equalization are presented. The performed analysis proved that for the presented case it appears the best to apply the Danish attenuation function. When the other functions – of Hampel or

of Hubert are applied, in case of the serious errors, the results show displacing the vessel's position to an unexpected point.

References

1. WIŚNIEWSKI Z.: Metody opracowania wyników pomiarów w nawigacji i hydrografii, Monografia, AMW, Gdynia 2004.
2. WIŚNIEWSKI Z.: Rachunek wyrównawczy w geodezji (z przykładami), UWM, Olsztyn 2009.

Others

3. CZAPLEWSKI K.: Positioning With Interactive Navigational Structures Implementation. Annual of Navigation No. 7, Monograph, Gdynia 2004.
4. CZAPLEWSKI K., ŚWIERCZYŃSKI S.: Zautomatyzowane stanowisko nawigacji radarowej. Zeszyty Naukowe AMW w Gdyni 2(185), 2011.
5. ŚWIERCZYŃSKI S., CZAPLEWSKI K.: Determination of the precise observed ship's position using the traffic control systems and applying the geodesic estimation methods. Scientific Journals Maritime University of Szczecin 32(104) z. 2, 2012, 167–172.
6. GUCMA M., CHRZANOWSKI J., JANKOWSKI S., JUSZKIEWICZ W., MONTEWKA J., PRZYWARTY M.: Urządzenia radarowe w praktyce nawigacyjnej. Akademia Morska, Szczecin 2010.
7. KOPACZ Z., MORGAŚ W., URBAŃSKI J.: Ocena dokładności pozycji okrętu. AMW, Gdynia 2007.
8. STUPAK T.: Data transmission in VTS Zatoka Gdańska. Zeszyty Naukowe, Transport, Politechnika Śląska, z. 59, nr 1691, Gliwice 2005.
9. WĄŻ M., CZAPLEWSKI K:. Automatyzacja nawigacji radarowej. Zaszyty Naukowe AM w Szczecinie 13(85), 2008..
10. WĄŻ M.: Synchroniczna sieć radarowa. Zeszyty Naukowe AMW w Gdyni 186A, 2008.
11. URBAŃSKI J., KOPACZ Z., POSIŁA J.: Nawigacja Morska. AMW, Gdynia 2000.

Scientific Journals
Maritime University of Szczecin

Zeszyty Naukowe
Akademia Morska w Szczecinie

2013, 36(108) z. 1 pp. 156–161
ISSN 1733-8670

2013, 36(108) z. 1 s. 156–161

The Automatic Identification System operating jointly with radar as the aid to navigation

Sławomir Świerczyński, Krzysztof Czaplewski

Polish Naval Academy
81-103 Gdynia, ul. Śmidowicza 69, e-mail: krzysztof@czaplewski.pl

Key words: Automatic Identification System, radar, information, navigation, safety of traffic

Abstract
The paper presents joint operation of AIS-AtoN and radar. There was brought forward a fact of divergence of the information visualized in radar in cases when AIS receivers are produced by different manufacturers. It happens that the AtoN AIS information is not displayed by radar screen. It is also essential that not every ship is provided with AIS equipment; therefore the users cannot always fully take advantage of AtoN AIS in respect of functionality.

Introduction

The Automatic Identification System (AIS), an autonomous broadcast system designed and popularized at the turn of the 21st century, was implemented to enhance navigational safety. It was designed as a tool to facilitate identification of vessels via exchange of identification data and to aid the planning of anti-collision manoeuvres. It also supports the functioning of maritime traffic systems by complementing data of particular influence on the safety of navigation vessel to vessel, vessel to coastal station, coastal station to vessel. AIS – type devices include:

- class A designed for SOLAS – convention vessels;
- class B designed for non-convention vessels;
- base stations;
- simplex and duplex AIS relay devices;
- derived from class A devices installed on a navigation mark, the so-called AtoN AIS (AtoN – *Aids to Navigation*) [1].

Aid to navigation (AtoN) is any external device for a vessel, whose task is to assist in indicating its position, warning about danger or obstruction. Typical structures helpful in maritime navigation are, among others, lighthouses, beacons, buoys, etc. AIS as an aid to navigation (AtoN) provides information which facilitates the identification of navigation signs in any weather conditions. Additionally, it complements the already existing signals transmitted by navigation marks and missing marking on a body of water, using a synthetic and virtual AtoN AIS where installation of a physical AtoN is technically difficult or impossible [2]. This article refers only to the AIS system installed on navigation marks. Further in the article, the term AISAtoN will be used to define it.

One of the main elements of the AIS system are AIS coastal stations. They receive signals from transponder-equipped vessels (both class A and B) to enable their identification and the reading of static and dynamic parameters. They are connected to form extensive nets in order to facilitate exchange of information and to deliver it to central databases. Incorporating AIS AtoN into this system allows additional delivery of information in the interests of navigational safety, not only for vessel identification. Such comprehensive information makes it possible to conduct an analysis of fixed and floating structures, and to plan the functioning and expansion of the AtoN system. There are three kinds of AIS AtoN devices:

– real AIS AtoN;
– synthetic AIS AtoN;
– virtual AIS AtoN.

A real sign is physically located on the water and the AIS device is installed on it. In the case of

the synthetic AtoN, information is transmitted to the coastal station which sends it to other system users. The virtual AIS AtoN does not physically exist and information about it is transmitted by coastal stations. It is used for marking hazards to navigation, where a more permanent AtoN has not been established yet or establishing it is, for various reasons, uneconomical [1].

AIS devices fitted on AtoN, apart from identification, provide information and data which enhance the level of services offered by the existing AtoN, such as real heights of tides and the local weather conditions in the vicinity of the AtoN. For monitoring floating AtoN their position is obtained from an electronic positioning system indicated by a GPS receiver (e.g. RTK GNSS) or a position from "the guar zone" if the AtoN goes beyond that zone. Additionally, in real time the device conducts diagnostics and sends the information to the system to monitor the system's efficiency and performance. It is transmitted as a Message Type 21 (Message 21 – AtoN report). In case of damage, change of position (e.g. due to floating) or lack of lighting at night, AtoN could pose a hazard for safe navigation and therefore, an additional navigation warning should be generated as message 12 (Message 12 – Addressed safety related message) containing information on the status of the AtoN in a given body of water.

Using AIS to aid navigation is very significant, so ITU depicted the AIS message 21 for the exclusive use with AtoN, which does not mean that other messages can be used for AtoN. The primary purpose of using AIS AtoN is to enhance safety of navigation via the following activities [2]:

- identification of AtoN irrespective of weather conditions and its display on AIS receivers and electronic maps;
- complementing existing navigational information;
- transmitting accurate position of floating AtoN and indicating whether a floating AtoN is off position;
- marking or delineating tracks, routes, areas, limits or offshore structures (e.g. wind turbines and oil platforms);
- providing hydrometeorological information from connected sensors.

AIS AtoN messages can be generated based on information acquired from AIS installed on AtoN. The device then sends a message about AtoN identification, weather conditions and sea state. It delivers messages from other AIS AtoN devices for monitoring purposes and transmits information on synthetic and virtual AIS AtoN which, for reasons practical or economical, are not always physically used on AtoN. A synthetic AtoN is composed of a GNSS receiver, a central processing unit and a packet radio or GSM placed on the AtoN. The data is sent to coastal stations where it is converted into AIS format and transmitted to other devices which view this data as if it came from an AIS device on AtoN. On an ECDIS graphic display presentation there should be an AtoN and the coastal station transmitting messages from this AtoN.

On AIS AtoN nautical charts it is indicated by a magenta circle surrounding the existing AtoN symbol and an adjacent legend stating AIS. The font will be upright for a fixed AtoN and italic for a floating AtoN. To indicate a virtual AIS AtoN, there will be a V-AIS next to the symbol, which is shown in figure 1 [3].

Fig. 1. AIS AtoN symbols shown on paper maps [own study]

Symbols displayed on all shipborne navigational systems and equipment are defined in IMO resolution [4] (Fig. 2).

Fig. 2. AIS AtoN symbols displayed on all shipborne navigational systems and equipment [own study]: a) AIS Based AtoN, Real Position of Charted Object, b) AIS Based AtoN, Virtual position

AIS as an aid in navigation cooperating with radar

One has to bear in mind that not all vessels are equipped with AIS devices, as stipulated by the SOLAS Convention, which specifies which vessels should be outfitted with AIS devices (SOLAS, Chapter V, Rule 19) [5]. Depending on the devices the vessel is equipped with, AIS information can be not displayed at all (class B AIS devices) or can be shown on a display (class A AIS devices) and on an electronic map or radar. Users who do not possess ECDIS or radar will not be able to fully avail themselves of AIS AtoN's functionality. There are also differences in information display on ECDIS and radar, depending on producers. Radar is the primary navigation device used by a watch officer while manoeuvring a vessel and with low visibility it is his only "eyes". With norm PKN-IEC / PAS

Fig. 3. Radar echo of the DRAUGEN oil platform [own study]

60936-5, which is a translation of the English version of the international technical specification IEC/PAS 60936-5:2003, Poland presents a minimal, advised part of AIS information – a section of message 1, 2 (AIS class A) and optionally 18 and 19 (AIS class B) – which can be introduced in radar of own vessel to be presented in graphic or alphanumeric form.

Depending on producers of the devices, not all information from AIS is displayed on radar. Figure 3 shows a radar image where one can see an echo of the DRAUGEN oil platform in the Norwegian Sea – target No. 13. An AIS receiver indicates the structure as AtoN (Fig. 4).

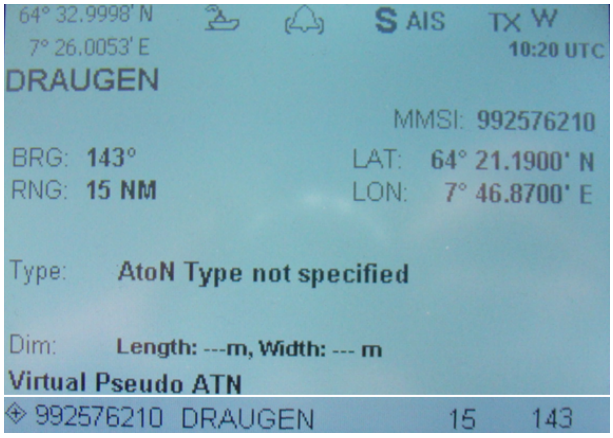

Fig. 4. Information about the DRAUGEN platform on display of AIS receiver [own study]

As can be observed on the radar's screen, the information about the structure is displayed as radar echo, despite the fact that the AIS display function is switched on. The AIS graphic mark is not shown. A similar situation can be seen in the next two figures (Figs 5 and 6) with echoes from the oil platform and the vessel NORMAND MERMAID moored by the platform. The figures show AIS information from this vessel and the one under way in the direction of the oil platform of vessel ESVAGT DON.

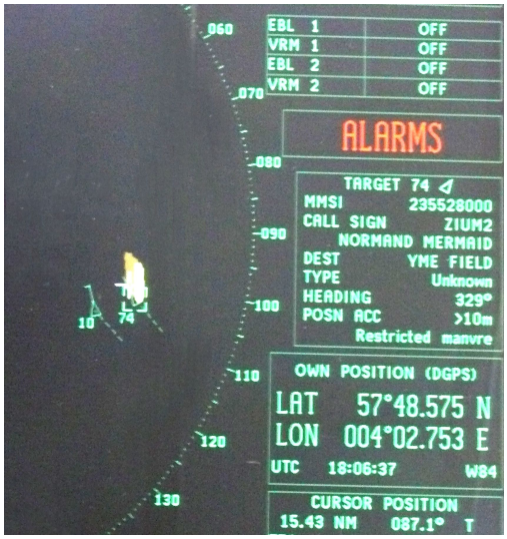

Fig. 5. Display of information from NORMAND MERMAID [own study]

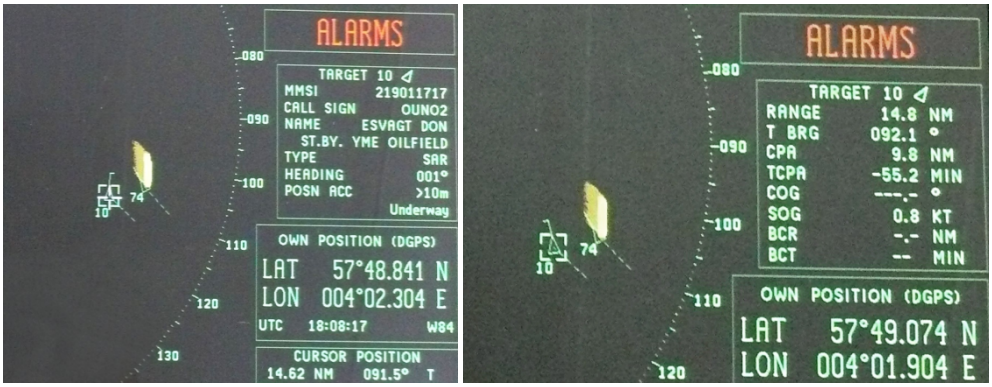

Fig. 6. Display of information from ESVAGT DON [own study]

On the display of AIS receiver and on the electronic map we receive information about additional AtoN which show oil platforms in the North Sea (Figs 7 and 8], whereas the radar does not display this information. Fixed marine structures such as wind turbines and oil and gas platforms are considered to be hazardous for navigation, so according to the authors it is vitally important to include information about them in the AIS AtoN system.

The figures that follow (Figs 9, 10, 11) show yet another example where the AIS system presents information about platform A6A as AtoN, whereas the indicator's screen shows echo from this structure – target No. 80, however, there is no graphic mark from the AIS system.

With the advancement of integrated navigation systems presenting, more often than not, information on multifunction indicators, emerging is a problem with excess of displayed information. Radar echo from a fixed structure, with AIS additionally placed on this structure, together with a graphic mark representing it on the map, provides

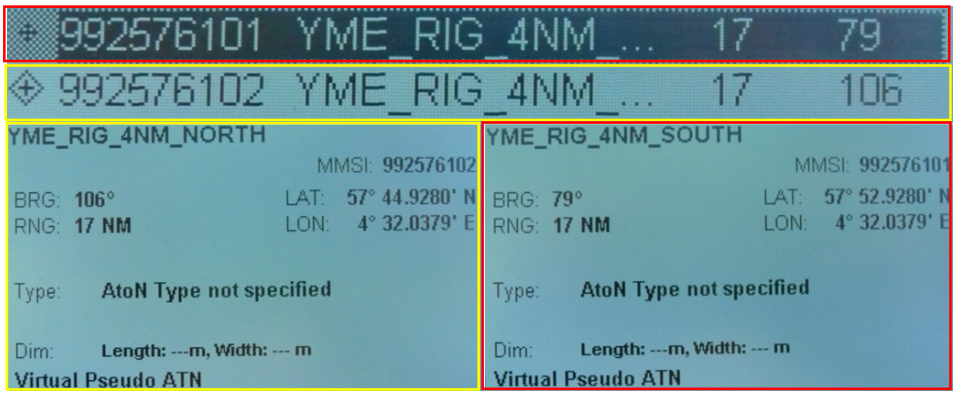

Fig. 7. Presentation of information about AtoN on the AIS receiver's display [own study]

Fig. 8. Presentation of information about AtoN on an electronic map [own study]

Fig. 9. Radar echo from oil platform A6A [own study]

Fig. 10. Presentation of information about platform A6A on the AIS receiver's display [own study]

three pieces of information representing the same structures. Simultaneous display of these pieces of information "clutters" the display. Hence the question – is there a need for filtering this information? Information about a given AtoN comes from three independent sources, so even if one of them malfunctions, the information will still be displayed.

In the case of virtual AIS AtoN, information is presented on an AIS and ECDIS display. Not all vessels are equipped with AIS class A receivers and electronic maps, which means that information about hazards such as submerged wrecks or floating rocks will not be delivered to the users of such vessels. Needless to say, radar indicators will not display the above-mentioned structures. In many cases where radar is the primary source of navigational information, the display of a graphic mark of such a virtual AIS AtoN on the screen of radar's indicator could warn the watch officer about any hazard.

Conclusions

Applying AIS as an aid to navigation poses a valuable source of information not only about vessels, but also about any and all signs and marks which provide help in navigation, weather conditions and sea state in a given body of water. Incorporating AIS AtoN into one system makes it possible to monitor in real time and to deliver

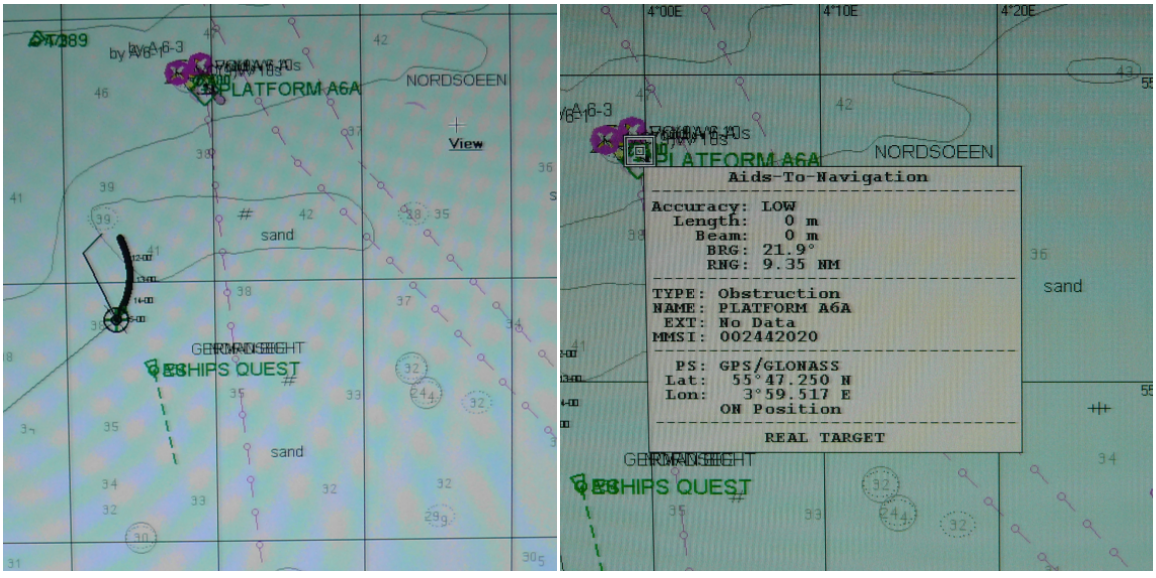

Fig. 11. Presentation of information about platform A6A on an electronic map [own study]

information indispensable for the safety of navigation and constitutes within AIS a new source of data, not only about vessels. Thanks to GNSS positioning, using AIS AtoN provides navigators with accurate information about signs and marks.

Currently the SOLAS convention specifies which vessels have to be fitted with AIS. Many vessels do not possess devices in which a user might make full use of the received information, about the situation around the vessel, and thus AIS is considered to be an additional source of information with regard to information acquired from radars or observation. Moreover, indicators of different producers present varied information or present it in various ways, which may lead to lacks of vitally important information in the sense of navigational safety.

Increasing the number of vessels equipped with AIS and widespread use of AIS AtoN should lead to the modernisation of devices and inter-device information transfer.

References

1. Wawruch R., Stupak T.: Analiza zastosowań AIS do unikania zderzeń. Prace Wydziału Nawigacyjnego Akademii Morskiej w Gdyni, Gdynia 2007.
2. IALA Aids to Navigation Manual. IALA NAVGUIDE. Edition 5, 2006.
3. Regulations of the IHO for international (INT) charts a chart specifications of the IHO – Edition 4.4.0 – September 2013.
4. IMO SN/Circ.243 Guidelines for the presentation of Navigation-related symbols, terms and abbreviations.
5. Międzynarodowa konwencja o bezpieczeństwie życia na morzu SOLAS 1974 z późniejszymi zmianami.

Others

6. GUCMA M., CHRZANOWSKI J., JANKOWSKI S., JUSZKIEWICZ W., MONTEWKA J., PRZYWARTY M.: Urządzenia radarowe w praktyce nawigacyjnej. Akademia Morska, Szczecin 2010.
7. IEC 62288 Ed. 2: Maritime Navigation and Radiocommunication Equipment and Systems – Presentation of navigation-related information on shipborne navigational displays – General requirements, methods of testing and required test results.
8. IEC 62320-2 AIS AtoN stations – Minimum operational and performance requirements – methods of test and required test results.

Scientific Journals
Maritime University of Szczecin

Zeszyty Naukowe
Akademia Morska w Szczecinie

2013, 36(108) z. 1 pp. 162–167
ISSN 1733-8670

2013, 36(108) z. 1 s. 162–167

Radar target detection based on methods of image pattern matching

Ling Tong, Frank Heymann, Thoralf Noack

German Aerospace Center (DLR)
17235, Neustrelitz, Kalkhorstweg 53, Germany

Key words: detection, tracking, radar images, image pattern matching, algorithms

Abstract
This paper studies the performance of pattern matching algorithms with the goal of the detection and tracking of vessel targets in maritime radar images. We compare different methods using a database which consists of radar images from two different manufactures. The data covers a timespan of roughly 4 hours with a one second time resolution. The performance of 3 template matching and 5 feature detector algorithms is tested and the most suitable algorithm is chosen for further optimizations. These optimizations are based on the properties of the radar images and the properties of the radar target.

1. Introduction

Radar, an acronym for "radio detection and ranging", which uses radio waves to discover objects and to determine their spatial locations, is an essential tool for maritime surveillance. ARPA (Automatic Radar Plotting Aid) is an added tracking feature on the basis of the traditional radar. It can provide attitude data and collision avoidance information automatically and continuously by calculating the course and speed of the objects to be tracked. However, due to their functional limitations [1], the existing ARPA products are still not able to be used for a reliable tracking. Therefore, accurate and fast detection of radar targets is still one of the principal unresolved technical issues.

In this paper we focus on the target detection in radar images using the technique of 2D image processing and methods of computer vision. The paper is structured as follows; Section 2 describes the utilized database and the strategy of our study. Section 3 gives an introduction to a sample collection of image matching algorithms used in this study. In section 4 we present and discuss our results. Some improvements for an effective and efficient application of the approaches in radar target tracking are presented in section 5. In section 6 we finally conclude our findings.

2. Database and strategy

The data used in this paper consists of radar images from the radar training location of the "Schifffahrts Institut Warnemünde" in Rostock. The radar screen was stored every second as an image file using a VGA2USB [2] converter. During our 4 hour measurement campaign we were able to collect the data from two different manufactures, namely Sperry Marine [3] and SAM [4]. The final database consists of 18.6 gigabyte (Sperry 11.9 GB, SAM 6.7GB) stored in 16339 PNG image files (Sperry 9494, SAM 6845).

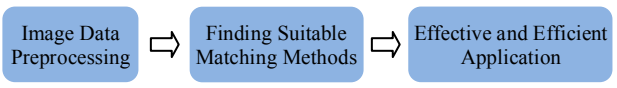

Fig. 1. Strategy of our study

The strategy of our study is illustrated in figure 1 and consists of three steps.

After storing and sorting the data files, we optimize the images according to the properties of the maritime radar. For example, as shown in figure 2, we are only interested in the circle in which the radar reflections are visualized and not in the additional graphical user interface. In addition, we extract a sample collection of targets (subpatterns) which are selected by eye. As shown in figure 3 the

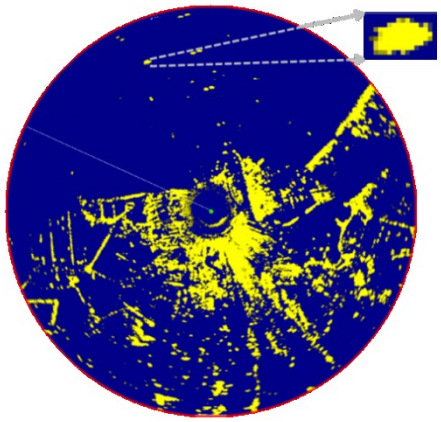

Fig. 2. This figure shows the subpattern extraction. The large blue circle is the radar screen and the smaller rectangle describes a zoomed version of the extracted pattern patch

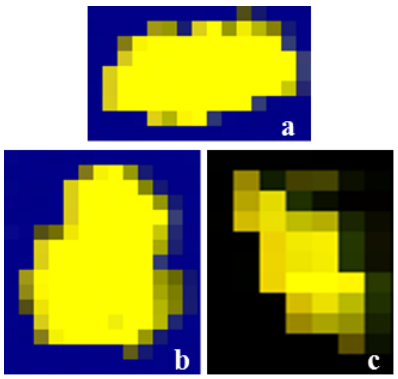

Fig. 3. This figure shows three zoomed versions of our subpattern collection. The subpattern a and b are from the SAM radar while the c subpattern is from Sperry Marine. These patches show similaritys with an elliptical shape

subpattern consists of the target itself and an one pixel border, which is defined by a threshold operation using the median value between 0 (black) and 255 (white), namely 127, as threshold value.

In the next step we attempt to identify the most suitable pattern matching algorithm, which is provided by the open source image processing library OpenCV [5]. We start the search with the test in which each method has to find the subpattern (Fig. 2) in the original image it was extracted from. We consider only methods for further investigation which pass this initial test. The additional test is described in more detail in section 4.

In the final step we chose the most suitable extraction algorithm to test it on real life data. The method and all optimizations are described in section 5.

3. Image matching approaches

Image Pattern matching algorithms can be broadly classified into two major categories of approaches: Feature Based Matching (FBM) and Area Based Matching (ABM) [6], as shown in table 1.

Table 1. Feature Based Matching and Area Based Matching

Image Matching Algorithms	Matching Entities	Matching Strategy
Feature Based Matching	Features: Curves, Edges, Regions	Feature Extraction, Feature Description and Descriptor Matching
Area Based Matching	Gray levels	Similarity Measure or Distance Measure

Feature-based matching approaches extract image features, such as special points, curves, edges, regions, etc., and attempt to establish the correspondence between the features of the pattern patch and the input image. Its matching strategy is based on the image processing of feature extraction, feature description and descriptor matching.

Area-based matching which is also known as *Template Based Matching* (TBM) matches a sample template patch against an input image by "sliding" the patch over the image. Its matching algorithm is based on a distance or a similarity measure of the intensity values of template patch and input image.

3.1. Feature Based Matching (FBM) approaches

Feature based matching has found widespread application in many areas of computer vision, such as face recognition, 3D stereo Reconstruction, and images registration.

In the FBM, only the selected points with certain features, such as end points, curves, corners, edges, regions, etc., are to be matched. As illustrated in figure 4, in the first stage of matching process, the image pair is preprocessed by using a so-called feature detector that attempts to extract specific feature key points. In the second stage, the feature vectors, namely the descriptors are calculated to describe the visual information of a feature point's

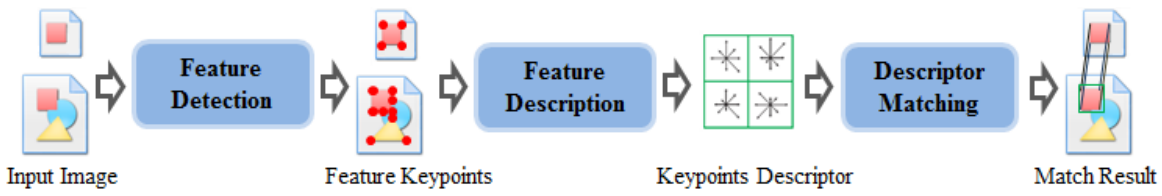

Fig. 4. Schematic process flow of the feature based image matching approaches

neighborhood [5] which can be used to characterize the feature point and make it distinguishable from the others. To learn more about feature description please read the reference book [7]. The corresponding feature pairs between the pattern patch and the input image would be found in the last stage.

In view of the issue that the targets to be matched in the radar image only have few pixels (about 100 pixels), as shown in figure 3, and information carried by pattern patches are consequently few, the most important stage in our case is the detection of the key points with significant feature, and thus we chose a standard feature descriptor and a standard feature matcher, and test the feature detectors listed below:

- SIFT: SIFT [8], stands for Scale Invariant Feature Transform. The detector is resistant to the most common image transformation, such as scale, rotation and lighting.
- SURF: The Speed-Up Robust Feature detector (SURF) published by Bay [9] in 2006 overcomes the computational cost of SIFT without affecting the quality of the detected points.
- Harris: Harris Feature Detector was presented by Harris [10] in 1988 for the detection of corner feature-points.
- FAST: The FAST Feature Detector [11] modified the Harris corner detector in order to speed up the algorithm without compromising the results.
- Dense: Using Dense Feature Detector, the features points are distributed densely and regularly over the image.

3.2. Template Based Matching (TBM) approaches

Template based matching is a technique of computer vision widely used in finding areas of an input image that are similar to a template image patch by pixel-wise "sliding" the patch over the input image, using one of the matching methods described in this section.

The way to achieve template based matching is by using a similarity or distance measure between a template image and an exactly matching region in the image. It is necessary to find the maximum similarity or minimum distance [12]. The result similarity $S(x, y)$ can be computed from the image data I and the template patch T as:

$$S(x,y) = \sum_{x_T=0}^{w-1} \sum_{y_T=0}^{h-1} \left| T(x_T, y_T) - I(x + x_T, y + y_T) \right| \quad (1)$$

x, y are the coordinates of the image, and x_T, y_T define the location in the template patch with a width w and a height h. The summation will be done over the template patch.

- Cross Correlation (CC): The CC multiplicatively matches the template patch against the input image, and in each position the cross correlation between the template patch and the corresponding part of the input image is computed.
- Correlation Coefficient (CCOEFF): The CCOEFF matches a template patch relative to its mean against the corresponding part of the input image relative to its mean.
- Sum of Squared Differences (SSD): The SSD minimizes the squared difference between a template patch and the corresponding region of the input image.

4. Results – Comparative study

To identify the suitable matching approaches listed in the last section, two kinds of tests are executed, i.e. the initial test and the real time (RT) performance test. To pass an initial test, each method has to find the subpattern, as shown in figure 2, in the original image it was extracted from. We consider only methods which pass this initial test for further investigation. In the RT performance test, we test the approaches which already pass the initial test if they meet our real time requirement, namely each image should be processed less than one second. This section aims to list our test results, and that begins with an explanation of the outcome of the testing of the different matching approaches.

- SIFT/SURF: These two methods are also called texture based detectors [13]. They cannot detect enough feature points for matching if the target has only few pixels just like the targets in our pattern patches in figure 3. SIFT and SURF feature detectors didn't pass our initial test.
- Harris/FAST: The issue that the Harris and FAST detectors detect corners prioritized over edges [13] while the features in our patch, as shown in figure 3, are dominated by edge, makes the two detectors not reliable in the initial test.
- Dense: The dense method passes the initial test but the computing time of matching is so long, namely about 5 or 6 seconds (tested on a PC with 2 processors clocked with 3 GHz and 4 GB memory) that cannot meet our requirements of real-time tracking (one image per second). Therefore, the dense feature detector cannot be taken into account.
- CC: The method CC fails our initial test. Due to the issue that the best match will be the coordination point with the maximum result of the cross-correlation, this method fails when there is an object in the image brighter, namely with

Table 2. An instance of when the cross correlation is unable to provide the correct match

$\begin{bmatrix} a & b \\ c & d \end{bmatrix} * \begin{bmatrix} m & m \\ m & m \end{bmatrix}$ Template patch — Image patch with constant grey value $(a, b, c, d > 0$ and $m > 0)$	$\begin{bmatrix} a & b \\ c & d \end{bmatrix} * \begin{bmatrix} n & n \\ n & n \end{bmatrix}$ Template patch — Image patch with constant grey value $(a, b, c, d > 0$ and $n > m > 0)$
Result: $m \cdot (a + b + c + d)$	Result: $n \cdot (a + b + c + d) > m \cdot (a + b + c + d)$

larger grey value, than the target. Table 2 shows schematically an instance of when the cross correlation is unable to provide the correct match, i.e., the cross correlation of the template patch and an Image patch with constant grey value m (the first cross correlation) is less than the cross correlation of the template patch with a brighter patch with constant grey value n (the second cross correlation), under the premise that both template patch and image patch are not a black patch (a, b, c, d, n and $m > 0$). In this case, the second cross correlation always has larger score, regardless of what the template is! To avoid this flaw of the method CC, we can subtract the mean value of the template and calculate the coefficient of the cross correlation, namely, correlation coefficient.

– CCOEFF: This method passes the initial test. Using this method, we get a higher score of similarity only when the darker parts of the template patch overlap darker parts of the input image, and brighter parts of the template patch overlap brighter parts of the input image. This method meets also the RT requirement.
– SSD: The SSD passes our two tests, and it is faster than CCOEFF.

To compare the matching approaches, we list the advantages and drawbacks of the tested approaches for the application in the field of radar target detection in table 3, according to their working principles and their application conditions.

The feature based matching approaches use only some distinctive features instead of the entirety of the image, therefore, the data processing can be more computationally efficient. On the other hand, FBM normally requires sophisticated image processing for feature extraction and a reliable matching depends consequently on the robustness of feature detection. In view of these facts, featured based approaches are typically applied when the pattern patch has "strong" features, i.e. the local structural information is more significant than the information carried by the intensity levels of the image, such as the applications in face recognition and panorama generation. Obviously, our pattern patches are not that case. Accordingly, the FBM approaches may only be applied as a supplement in special cases of radar target detection.

The template based matching approaches are best suited for detecting objects which do not have sufficient strong features, or for the matches that are estimated directly based on the bulk of intensity values. Moreover, although the TBM requires a vast data processing, the computing time is short enough for a real time tracking.

According to the comparative study of the above algorithms, we decide to utilize the template based matching approach *SSD* for the target detection.

Table 3. Comparison of image matching approaches

Approach		Advantages	Drawbacks	Suggestion
FBM	SIFT/ SURF	scale, rotation and lighting invariant	cannot find enough key points in case of lack of pixels	fails the initial test
	Harris/ FAST	scale, rotation lighting and noise invariant	detecting corners prioritized over edges	not reliable in the initial test
	Dense	dense feature points	too slow (about 5 or 6 seconds)	fails RT requirements
TBM	CC	the simplest measure	not invariant to lighting, scale and rotation	not reliable in the initial test
	CCOEFF	invariant to lighting	not invariant to scale and rotation	suitable
	SSD	invariant to lighting, fast	not invariant to scale and rotation	suitable

5. Efficient and effective application of TBM in radar target tracking

The analysis in the last section shows that the TBM also has its drawbacks, such as that the intensity distribution of the template and input image must be similar, in particular, the TBM is not invariant to rotation, and it often requires a vast data processing. In order to overcome these drawbacks and achieve a radar target tracking, the following measures have been taken for the effective and efficient application of the template based matching approaches.

5.1. Adaptive Template Update

In this paper we attempt to follow a target of interest through a series of radar images by finding the location in each image which best matches the pre-selected template patch containing the target.

The major drawback of applying the template based matching in the field of radar target detection is that the TBM is not invariant to rotation. In addition, the intensity distributions of targets sometimes vary greatly between images of long time intervals. That means the template patch that we used at the beginning of the match may not be suitable for the matches after a certain time. Therefore, we continually update the template, to reduce this drawback.

To minimize the erroneous matches caused by the target rotation, we extract the match result of the previous moment and save it as the template patch for the matching process at the next moment, this is the so-called winner update scheme, i.e., after each matching, the "winner" of the match will be saved as new template for the next match. It is necessaray to ensure the correctness of the winner, otherwise a wrong object will be tracked in the next moments.

In consideration of the size difference of the target between two adjacent images, the size of the new template should be adaptability changed. To implement this idea, at each moment, the new template patch which is obtained from the previous moment should be checked if there is still one pixel background border on all sides, as shown in figure 3 in section 2. In fact, this one pixel border plays the role as a buffer in order to compensate a size change of the target in the next image.

5.2. Setting a Region of Interest (ROI)

Another drawback of template based matching is that it required a "wasteful" pixel-wise scanning of the input image and computing a similarity or distance measure for each position of the whole image. The radar scan area is usually larger than the area that a ship can reach within the interval of adjacent radar images in a dataset.

Take for example, the SAM radar [4] images in our datasets. The scan area of this radar images is a circle with a radius of 3 nm (nautical miles). The interval of adjacent radar images is one second. The current world's water speed record as of 1978 is 511 km/h (i.e., about 0.077 nm/s) which was achieved by the boat Spirit of Australia [14]. In comparison with the 3 nm circle this 0.077 nm is only a tiny part of the entire image. Thus, it is really not necessary to scan the entire image. In response to this issue, setting a region of interest can reduce the computational cost on one hand, and it can also avoid unnecessary erroneous match on the other hand.

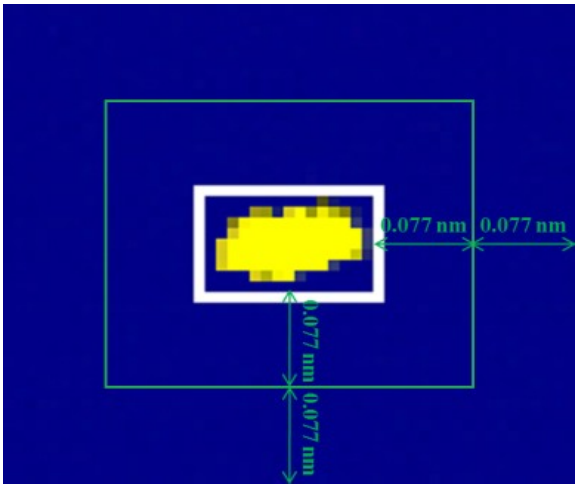

Fig. 5. This Figure illustrates what we define as Region of Interest (ROI)

As depicted in figure 5 that we extend a length of 0.077 nm on each side of the target forms thereby a rectangular area. The area inside of the green rectangle is the region with possibilities that the target may appear in the next second. The further extension of 0.077 nm on each side of green rectangle which can also be called as buffer zone is used to ensure that the target cannot come outside of the region by any possibility, such as, in the case that one image is missing, or the reflection area of the target in next radar image increases suddenly.

The conservative allocation of such a large buffer zone aims to cover all the unknown exceptions. Coupled with the buffer zone, we obtain the region of interest. The size of ROI in pixels in radar images can be calculated from the radial ratio of range setting, i.e. nm/pixel.

Now, the scanning and matching process only takes place within the region of interest. The relative position of the ROI in the input image responds to the position changes of the target. Consequently,

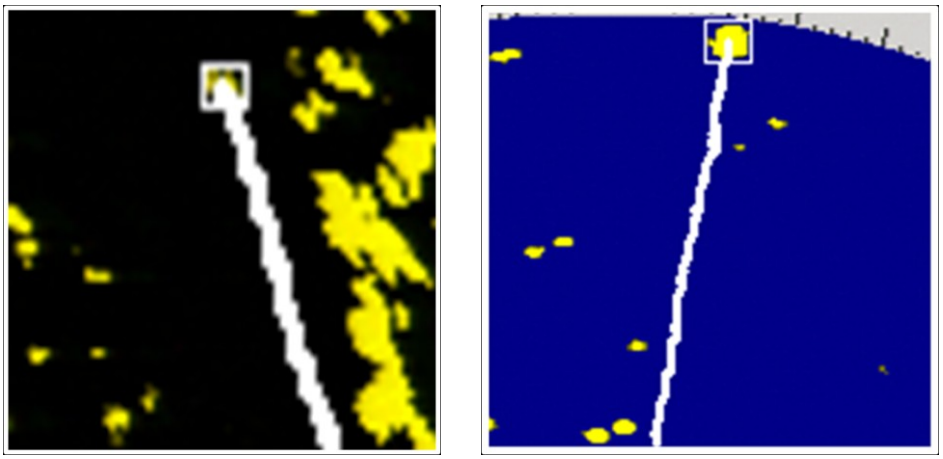

Fig. 6. Sample Tracking Results: a) Sperry Marine Radar [3], b) SAM Radar [4]

the location of ROI should be recalculated every time after the matching and saved for the extraction of the ROI in the next input image.

5.3. Tests with radar image datasets

Through the above two improvements, erroneous matches are reduced, computational resources are saved, and the performance is increased.

In order to test the prototype of our radar target detector, the detector is instantiated with radar image datasets from two radars: *Sperry Marine* and *SAM*. Both radar devices were installed at Rostock coast. As shown in figure 6, the white curve shows the track of the target.

In figure 6a the detector has successfully tracked the target for 3.5 minutes (210 images), and in figure 6b the track was 7.5 minutes (500 images), without losses (100% tracking proofed by eye). The test results showed that a target can be detected and tracked when its intensity distribution does not vary greatly in adjacent radar images, i.e. the case of non-interference.

Conclusions

In this paper we tested 8 pattern matching approaches and we also discussed the possibilities of the applications of these approaches in the field of radar target detection. Finally, we identified the template based matching approach *SSD* is more suitable for detecting targets in radar images. In order to more effectively and efficiently apply this approach, and achieve radar target tracking, several improvements are implemented in a software prototype of radar target detector. To test our solution, the detector is instantiated with image datasets from two radars that were installed at Rostock coast. The test results showed that a target can be detected and tracked, when its intensity distribution does not vary greatly in adjacent radar images, i.e. the case of non-interference. A comprehensive validation will be done in future work.

References

1. JIAO Z., LUO Z.: The Analysis of the Limitation of the ARPA. Navigation College, Wuhan University of Technology. Reports 2007-6 (Notice: published in Chinese language), 2007.
2. Compact external frame grabber – VGA2USB LR. Epiphan Systems Inc., Ottawa, Ontario 2009.
3. VisionMaster FT Series of Naval Radars. Northrop Grumman Corporation – Sperry Marine.
4. Radarpilot 1100 specification. SAM Electronics GmbH. Hamburg, Germany.
5. LAGANIERE R.: OpenCV 2 Computer Vision Application Programming Cookbook. Published by Packt Publishing Ltd, Olton Birmingham 2011, UK.
6. BABBAR G., BAJAJ P., CHAWLA A., GOGNA M.: A comparative study of image matching algorithms. International Journal of Information, Technology and Knowledge Management, July-December, 2(2), 2010, 337–339.
7. SZELISKI R.: Computer Vision: Algorithms and Applications. Springer, London Dordrecht Heidelberg New York 2010.
8. LOWE D.G.: Distintive image feature from scale-invariant keypoints. International Journal of Computer Vision 60(2), 2004, 91–110.
9. BAY H., ESS A., TUYTELAARS T., VAN GOOL L.: Speeded-up robust features (SURF); Computer Vision ECCV 2006, Vol. 3951, Lecture Notes in Computer Science, 2006, 404–417.
10. HARRIS C.: A combined corner and edge detector; Fourth Alvey Vision Conference, Manchester, UK. p. 147–151.
11. TRAJKOVIC M., HEDLEY M.: FAST corner detector. Image and Vision Computing 16, 1998, 75–87.
12. BRUNELLI R.: Template Matching Techniques in Computer Vision: Theory and Practice. John Published by Wiley and Sons Ltd, United Kingdom 2009.
13. GUERRERO M.: A Comparative Study of Three Image Matcing Algorithms: Sift, Surf, and Fast. All Graduate Theses and Dissertations, Paper 1040, Utah State University, 2011.
14. Museum C. o. C.B. Ken Warby – the fastest man on water. Official Newsletter of the Concord Heritage Society March 2011, No. 176.

Scientific Journals
Maritime University of Szczecin

Zeszyty Naukowe
Akademia Morska w Szczecinie

2013, 36(108) z. 1 pp. 168–176
ISSN 1733-8670

2013, 36(108) z. 1 s. 168–176

Safety assessment for a cruise ship terminal

Peter Vidmar, Marko Perkovic, Tanja Brcko

University of Ljubljana, Faculty of Maritime Studies and Transport
6320 Portorož, Pot Pomorščakov 4, Slovenia

Key words: cruise ships, safety assessment, degree of risk, hazards, ship terminal

Abstract

Cruise ships arriving in the port of Koper carry approximately 1000 to 3000 passengers and crew members. Such a concentration of people presents a high degree of risk in the event of a major disaster, because it is difficult to control, due to limited space, the dynamics of people in the event of a general panic, the presence of large amounts of fuel, proximity of the city center and other vessels and cargo at the port.

To avoid the possibility of hazard events, a good safety assessment must be done prior to a ship's arrival. One of the methodologies for systematically assessing the risk is a Formal Safety Assessment, a tool for determing and evaluating the risk of potential hazards at a cruise ship terminal. This paper discusses the diverse aspects of safety analysis.

Introduction

Cruising is an important element of maritime commerce, as it is on the cruise ship where tourism and transport come together [1]. Cruises also appear to be gaining in popularity; in 1999 cruise ships carried almost 9 million passengers, while in 2006 at least 17 million passengers took vacations on cruise ships. In Slovenia's port of Koper authorities are struggling with the need to adapt to the growing cruise ship trade, which includes the need to accept larger ships. Safety analysis is also necessary, for while in general cruising offers a safe vacation and has a good overall safety record, hazards do exist: from fire, collision, and grounding.

While the international shipping community has long been concerned with maritime safety, in the last decade or so the safety of cruise ship has become more of a concern. Cruise ships are not only subject to various local, national and international rules and requirements relevant for safe operation and construction, they must also comply with the safety standards set by the International Maritime Organization (IMO) enforced through the International Convention for Safety of Life at Sea (SOLAS).

The Formal Safety Assessment (FSA) is a tool for risk evaluation developed by IMO to enhance the safety of ships, passengers and crews, and the environment. The FSA uses five steps: hazard identification (HAZID), risk assessment, risk control options, cost benefit assessment and decision-making recommendations. Its goal is a systematic approach to safety in all aspects regarding particular vessels. This paper examines the FSA in relation to a cruise terminal and the existing safety plan of a cargo seaport.

We should add that the US Coast Guard and Passenger Vessel Association published a manual for safety risk assessment of passenger ships at sea and in ports (PVA Risk Guide – A Guide to Improving the Safety of Passenger Vessel Operations by Addressing Risk). This manual helps improve the process of risk (hazard) identification, to plan how to reduce risk levels and protect ship or ports from possible hazards. It is a tool which could be adapted for different operations or environments where risk assessment is needed. They divided risk handling activities (risk assessment, risk management and risk communication) into ten steps: problem definition, expert gathering, hazard identification, probability assignment, consequence assignment, calculation of relative risk, development of counter measures, estimation of benefit, estimation of cost and cost-benefit analysis [2].

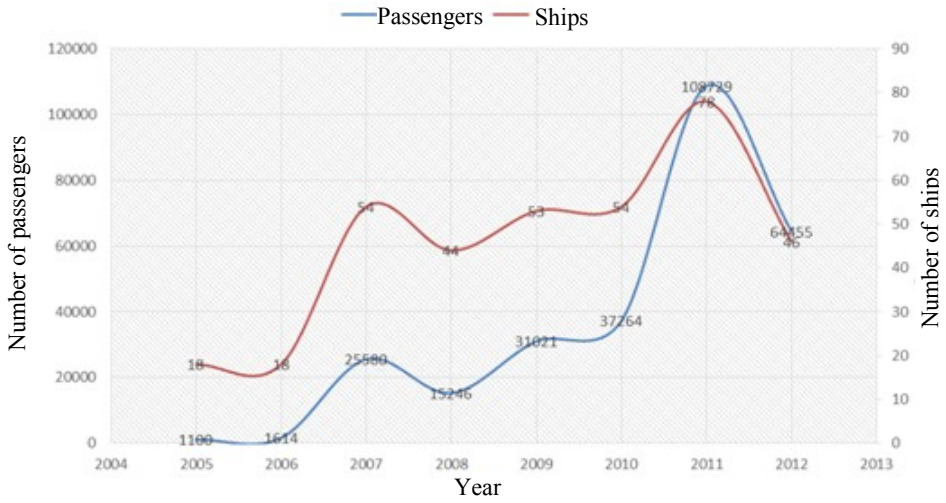

Fig. 1. Passenger vessels and passengers calling Port of Koper

Risk evaluation criteria

Risk evaluation begins with the conception of appropriate risk acceptance criteria. Port and terminal operators identify potential hazards strictly related with ship hazards, when the ship is approaching or leaving the port or is moored at a terminal. The following quote is taken from MSC 72/16: "The term risk acceptance is established in many industries and regulations; however, it is worth noting that the term itself can be misleading. The risk is not acceptable, but the activity might imply the risk to be acceptable because of the benefits." It is therefore important to make the distinction between risk tolerability and risk acceptability [3].

The term "risk evaluation criteria" rather than "risk acceptance criteria" is perhaps more appropriate to risk assessment. "Risk evaluation" is the official term at IMO (FSA Guidelines) and reflects organization's position that risks are not acceptable; yet decisions involving risks are accepted because their benefits are deemed to outweigh the risks. Risk evaluation criteria use the following categories: unacceptable, tolerable and broadly acceptable. These are further described below:

Intolerable: – Risk level is intolerable. Risks must be reduced irrespective of costs.

Tolerable (ALARP): – Risk level is tolerable provided that risks are managed to ALARP (As Low as Reasonably Practicable).
– Risks shall be reduced as long as the risk reduction is not disproportionate to the costs.
– Need only to implement cost beneficial Risk Control Options (RCOs).

Partially acceptable: – Risk level is negligible. Not necessary to consider RCOs.

In the following the modelled risk level for cruise ships and ship terminal will be evaluated using risk evaluation criteria concerning individual risk and societal risk.

Individual risk

Individual risk is the frequency for an individual fatality per year, the likelihood that the most exposed crew member or passenger will die as a result of an accident or event on board a cruise ship. This report only considers events related to ship operation. Accidents due to leisure activities and occupational risks are not within our scope.

The criterion accepts that higher risk is tolerable for crew members than for passengers, as they have "volunteered" to take on whatever risks may be involved in sailing and also benefit financially from operating the cruise ship. We should stress, too, crew members are more aware of their risks and have been trained to carry out their job responsibilities safely and effectively. It should also be noted that the basis on safety regulation in the UK is encapsulated in the Health and Safety at Work Act [4] which requires the duty holder to ensure and demonstrate that risk to employees, part time employed persons and the general public is As Low As Reasonably Practicable (ALARP). The Health and Safety Executive (HSE) publishes from time to time the risk levels it considers as intolerable or tolerable under certain circumstances and while these risk levels cover all industrial activities in the UK, the primary instrument for risk control is ALARP dynamics. Trbojevic [5] has emphasized

the individual risk criteria based on existing European standards and guidelines.

Table 1. Individual risk evaluation criteria

Risk criteria	Value
Maximum tolerable risk for crew members	10^{-3} per year
Maximum tolerable risk passengers	10^{-4} per year
Negligible risk	10^{-6} per year

Societal risk

A societal risk criterion takes the possibilities of catastrophic accidents of major societal concern into account to ensure that the risks imposed on the society from the activity are controlled. Depending on the system under consideration, both individual and societal risk evaluation criteria might apply. Societal risk posed by a cruise ship terminal facility is measured by the exposure probability of a group of people to risks, and where a large number of people are affected by possible accidents and would be exposed to a hazardous level of harm (fatality) due to all types of potential accidents at the facility or through its activity. The societal risk is dependent on both, the density of people in the vicinity of a hazardous terminal (e.g., LNG, Chemical or oil terminal) and the location of the population in relation to the facility. The societal risk is generally presented in the form of an FN curve, expressing the relation between the annual probability (F) of exceeding a given number of fatalities and the number (N) [5]. In most countries the risk assessment is performed on the basis of potential fatalities to the exposed population. Different countries use slightly different criteria for risk acceptability. In the UK, the Health and Safety Executive (HSE) guidelines are to use the individual risk as the principal measure, but also to use the societal risk criteria for land use planning. The acceptability criteria levels for risks for facilities in the UK are specified by HSE (1989). Facilities are permitted only when these (published) criteria are met. In the Netherlands, however, both the individual risk criteria and the societal risk criteria must be met when considering those events whose hazardous effects extend to such distances at which the conditional probability for lethality is higher than 1% [6, 7].

Societal risk criteria is more complex a concept than individual risk and there is continual debate as to whether the methodologies adopted are suitable. FN curves are, however, a common way of presenting societal risk and are considered by some parties the best way of illustrating this data. The method of deriving societal risk evaluation criteria in this report is based on IMO MSC 72/16 – Decision parameters including risk acceptance criteria [8]. The risk level is plotted as a cumulative function of consequence and frequency on a log-log graph:

$$F1 = \frac{r \cdot EV}{\sum_{N=1}^{N_u} \frac{1}{N}} \quad (1)$$

where:

- $F1$ – is the frequency of accidents involving one or more fatalities;
- N_u – is the upper limit of the number of fatalities that may occur in one accident;
- r – the number of fatalities due to transportation divided by contribution to GNP by transportation. It can be calculated as r = fatalities/$ GNP;
- EV – is the economic value of the industry. In this case, the EV here is represented by a reference vessel and is derived from the income from cruise voyages.

As presented by MSC 85/INF.2 [3] the ALARP area can now be defined by use of the above formula. The criteria applied in this study are presented in table 2.

Table 2. Limits for societal risk

Parameters for societal risk criteria	Value	Denomination
F upper (dotted line between ALARP and Intolerable)	$6.9 \cdot 10^{-1}$	fatalities
F lower (dotted line between ALARP and Negligible)	$6.9 \cdot 10^{-3}$	fatalities

Cruise ship accident statistics

In order to perform safety analysis, whether qualitative or quantitative, it is essential to obtain reliable failure data. Qualitative risk analysis requires less detailed statistical failure data compared to Quantitative Risk Assessment (QRA). A ship year is defined as one ship sailing for one year. Given the increase in the number of large ships in recent years it is necessary to distinguish between "smaller" cruise ships and "large" cruise ships; the following tables have been split into two groups (20–60,000 GRT and > 60,000 GRT).

The graph shows an increasing accident trend. The data takes into account the significant increase in the number of cruise ships that have entered the market during the previous decade – particularly for vessels > 60000 GRT.

Most claims involved with accidents were personal injury-related, 50% being for passengers or third-party property and 27% for injury to crew [9]. However, passenger ships were eight times less likely to collide than the average and much less likely to cause third-party damage or pollution.

Related to the study conducted there is no particular event when the accident inside a port, at a cargo terminal led to passenger fatalities at a cruise ship terminal. Accidents usually occur due to the cruise ship itself and its nautical operations. Events that usually lead to accidents are listed in table 3.

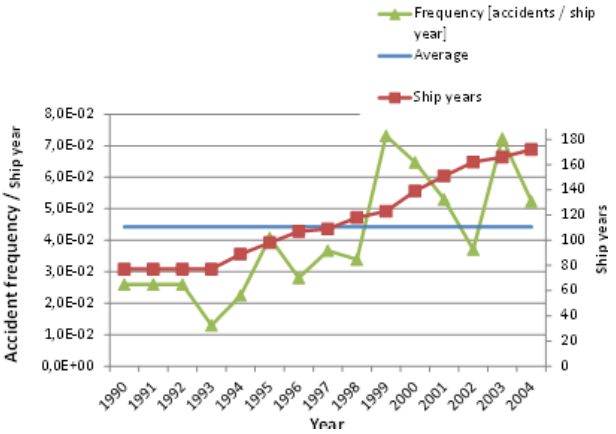

Fig. 2. Accident frequency, year-by-year (per ship-year)

Table 3. Hazardous events during operation phases

Operation phases	Possible hazardous events
Passenger embarkation	Passenger and crew injuries while alongside Passenger violence Fire/explosion in terminal Noise Overloaded gangway/collapse Injuries to unattended children
Getting underway (arrival and departure)	Lifting injuries while loading wheelchairs Fall in water/man overboard Collision with another vessel Loss of control (ice, wind, restricted visibility) Slips, falls at gangway Fire during fuelling
Cruise	Injuries due to machinery failure High speed collision, grounding Situational management (loss of awareness, distraction, multiple events) Electric shock Exposure to elements Medical emergency/evacuation Vessel fire Engine failure Noise due to conflicting groups
Docking	Squish injury Dock fire Contact with unknown/hidden objects Complacency (hard docking)
Disembarkation	Sewage spills Injuries due to overloaded gangway Slips and falls while disembarkation Careless attendance to handicapped passengers
Outside events (accident on ship neighbour)	Spills at neighbouring cargo terminal Gas or chemical release at neighbouring cargo terminal Fire or explosion at neighbouring cargo terminal

The threat to humans depends on the type of accident. The accidents registered for cruise ships from 1990 to 2004 are presented in figure 3.

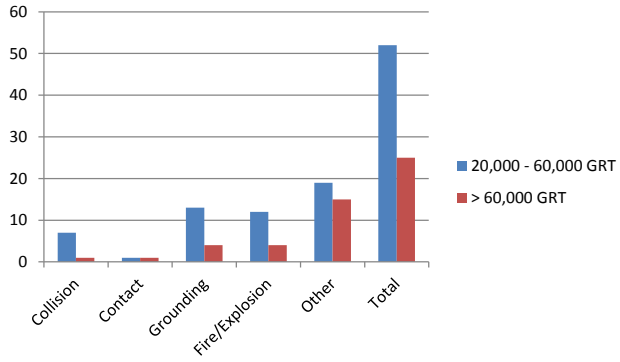

Fig. 3. Cruise ship accidents by type from 1990–2004

"Other" refers mostly to hull and machinery related incidents which have generally been low in fatalities over the years. "Grounding" and "Fire / Explosion" have been the most serious of relevant historical events. The influence or potential consequences of an external accident to a cruise ship and its passengers is not mentioned reports and references. The risk analysis presented below [4] shows how the risk may be quantified on the basis of the simulation of different accident scenarios.

Accident frequency calculation

The exposure during the 1990–2004 period has been 1742 ships years (1222 + 520). 1742 ship years will be used for the accident frequency calculations. The frequency calculations can be summarized as the fraction of accident per accident type and the total number of accidents. However, the number of accidents with fatalities is too few to represent any significant accident trend (Table 4).

Consequences

The consequence of an accident is defined as the expected number of fatalities if such accident occurs. In order to perform consistent and comparable consequence assessments, fixed bands of expected numbers of fatalities were defined. Bands are defined to suit the reference vessel of 110,000 GRT with a total capacity of 4000 persons. Ten fatality bends cover the full range of accident severities, from a minor scenario to a catastrophic accident resulting in a large number of fatalities. For purposes of accuracy in regard to the current world fleet, the estimated number of fatalities was also estimated for a ship of 75,200 GRT and 40,876 GRT.

Additional risk could occur and influence the safety level for passengers due to other activities conducted in a port area. The literature does not emphasize accidents in ports that have influenced

Table 4. Accident frequency calculations, vessels > 20,000 GRT

Cruise ship **Ships > 20,000 GRT**	Collision	Contact	Grounding	Fire/Exp.	Other	SUM
LMIS accidents recorded 1990–2004	8	2	17	16	34	77
Ship years 1990–2004 [ship years]	1742	1742	1742	1742	1742	1742
Cruise ship accident frequency [per ship year]	**4.59E–03**	**1.15E–03**	**9.76E–03**	**9.18E–03**	**1.95E–02**	**4.42E–02**
Return period [No. of ship years per accident]	218	871	102	109	51	23
Number of fatalities, 1990–2004	0	0	0	21	1	22

the safety level of a moored cruise ship or terminal. Therefore, the initial probability could not be defined as possible for collision, contact, grounding and fire accidents. Potential consequences and risks should therefore be calculated applying a deterministic approach.

The occurrence of accidents at cargo terminals with spills of flammable or toxic fluids are risks and require special consideration. Potentially large spills with fire could have a negative influence on a moored cruise ship in a range of 500 m, depending on spill dynamics, weather conditions and several other factors analyzed below. This events have a very small probability, however, because of the potentially severe consequences should be considered and analyzed.

Fig. 4. ERPG 2 zone for a methanol spill in a 11.5 t puddle (Port of Koper)

Figure 4 illustrates the ERPG 2 zone (1000 ppm) for a spill of 11.5 t of methanol in water. Threat zones are calculated applying a heavy gas model. Results indicate that this is a consideration to be implemented in a cruise ship terminal PSA. Second (described in Fig. 5a) is a supposition of a spill and fire of a flammable liquid in a close neighbour to the cruise ship. The initial probability of the spill event is assumed to be $5e^{-5}$/ship year.

A final recognized industrial risk present in the port of Koper is the possibility of a leakage of styrene that may start at the chemical terminal and with north or north east winds a highly poisonous cloud can affect a cruise vessel. The case of expected concentration inside cabins is presented with figure 5b.

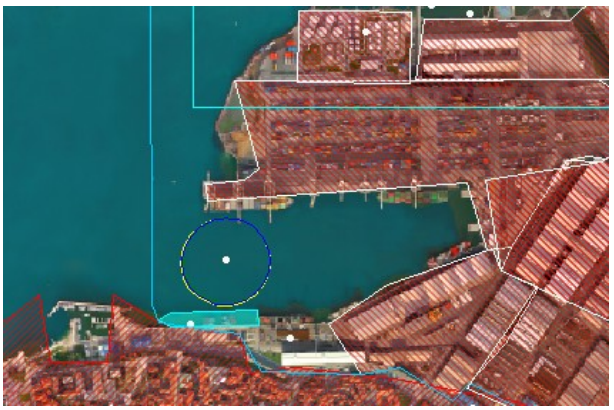

Fig. 5. a) Thermal zones of 12 kW/m^2 for ignition of 12 t of gasoline in a pool (Port of Koper)

It is important to note that the identified fatality bands only apply to the reference vessels defined for this study. Each final event is connected to an estimated number of fatalities. The expected number of fatalities is selected from one of the ten possible bands, as defined before. The event tree and probabilities for each event have been carried out together with other participants involved in the Hazard Identification process. The assumption of fatalities is based on the review of the calculated consequences for each event. A further event tree for an oil spill occurring near a cruise ship is presented in figure 6.

The percent value represents the share of the total number of passengers on the analyses ship brand. Most important are levels 2 and 3, which consider intervention by the containment group. Without containment the slick could spread uncontrollably and reach zones with a higher probability of ignition. In the proposed event tree the percent of fatalities on each event is predicted on a qualitative basis, proposed by the HAZID group of expert, in our case the authors. Those values could therefore be enhanced.

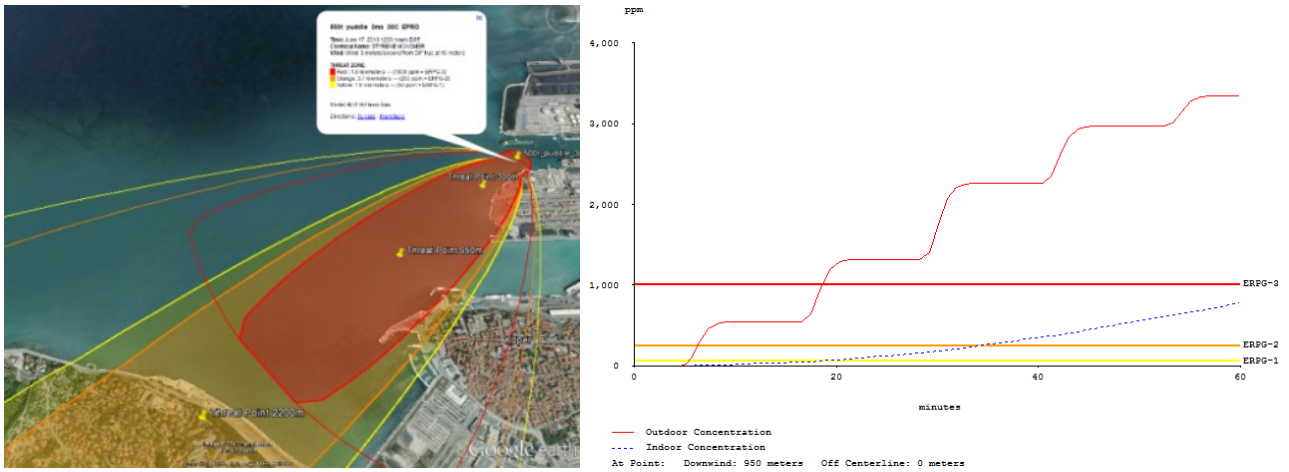

Fig. 5. b: ERPG zones (left) indoor and outdoor concentration passenger terminal for the evaporation of 500 t of Styrene

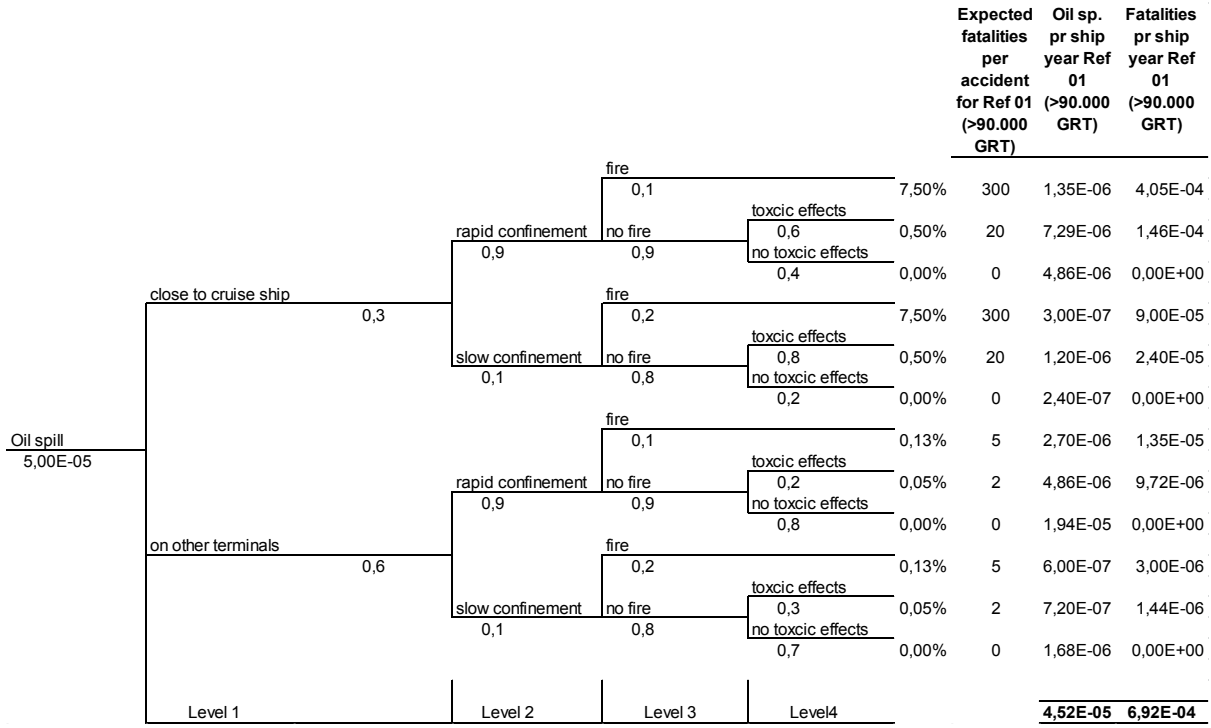

Fig. 6. Cruise ship neighbour oil spill event tree

Table 5. Results for cruise ship neighbour oil spill event tree

Cruse ship neighbour oil spill			
Ships in Band	Number of ships in band	Theoretical Fatalities per ship year	Theoretical Number of Fatalities per year
Ref 01 (>90,000 GRT)	30	0.00069	0.02
Ref 02 (60,000–90,000 GRT)	53	0.00047	0.03
Ref 03 (20,000–60,000 GRT)	89	0.00036	0.03
Total	**172**		**0.08**
Theoretical predicted fatalities per year in current world fleet	Theoretical predicted average number of fatalities per ship year	Theoretical predicted average number of ship years per fatality (current fleet)	
0.08	**4.53E–04**	**2209.4**	

– Large scale incidents (sinking, flooding and rapid capsizing) with an estimated 80% casualty rate shape the results for the oil spill event tree. This is because the estimated numbers of fatalities is large and the estimated frequencies are not low enough to compensate. Any change in

the estimated likelihood or consequence of these large scale incidents will have a direct effect on the results of the risk modelling.
- A return period of 2209.4 ship years per fatality (due to oil spill).
- 0.08 fatalities (due to oil spill) per year for the cruise fleet (172 Ships).

The estimated numbers of fatalities for the two other sizes of vessels are also representative of today's fleet and have also been derived and are used later in the results section to provide an overall average number of fatalities that could be expected. The method required establishing the particulars of a reference vessel and determining the likely outcome in terms of fatalities for all scenarios. The total number of persons on board is assumed to make an impact on the total numbers of fatalities only when whole ship events are modelled. Evacuation is indirectly factored into the event tree analysis by assuming a normal distribution of evacuation. It was assumed that, on average, evacuation will work according to procedures.

Risk level

Individual risk levels can be derived from the ship risk level when the number of crew and passengers is known. The table 6 details the number of passengers and crew on board the three different reference vessels. From the table, an estimated number of persons on board the world cruise fleet (1990–2004) can be calculated and an estimated number of persons on an average size cruise ship can be derived.

The fatality frequencies, calculated from the event-tree(s), are used as input to calculate the individual fatality frequencies for crew and passengers. Risk for crew and passengers have been modelled in a similar way except for the fact that crew is on board for a longer period (higher exposure).

From table 7 it can be seen that the individual risk exposure to a crew member is 7.5E-5 fatalities per crew year. This corresponds to one crew fatality approximately every 13,290 crew years. Similarly, the individual risk exposure to a cruise ship passenger is 5.77E-6 fatalities per year. This implies that a

Table 6. Risk exposure for crew and passengers

Selection of Representative Ships within 3 size bands	Selected Band for Group of Ships (GRT)	Number of Ships in Band
Reference Ship 01	> 90.000 GRT	30
Reference Ship 02	60.000–90.000 GRT	53
Reference Ship 03	20.000–60.000 GRT	89

	No. of ships in each band	Ships complement (representative ship)	Total carrying capacity of each ship band
Number of persons onboard ships in current cruise fleet	30	4000	120,000
	53	2728	144,584
	89	2080	185,120
		Total	449,704

	Total No. of Ships	Total Capacity of Ships	Average No. of persons on each ship
Average number of person on a ship representative of today's fleet	172	449,704	2615

	Working period / stay onboard	Total exposure per ship year
Crew Exposure	Average 6 months onboard	0.5
Passenger Exposure	Maximum 2 weeks per year	0.0384

Table 7. Individual risk summary

Hazard	Fatalities [per ship year]	Individual Risk of Pax & Crew [Fatalities Per Year]	Individual Risk for Pax [Fatalities Per Year]	Individual Risk for Crew [Fatalities Per Year]	Return period for passengers in years	Return period for Crew in years
Collision	2.35E–01	8.97E–05	3.44E–06	4.49E–05	290,506	22,285
Contact	7.91E–03	3.03E–06	1.16E–07	1.51E–06	8,617,509	661,069
Grounding	1.41E–01	5.38E–05	2.07E–06	2.69E–05	484,206	37,145
Fire / explosion	9.67E–03	3.70E–06	1.42E–07	1.85E–06	7,050,441	540,856
Oil spill	4.53E–04	1.73E–07	6.64E–09	8.66E–08	150,601,788	11,553,014
Sum of all incident causes	**3.93E–01**	**1.50E–04**	**5.77E–06**	**7.52E–05**	173,249	13,290
Return period in years	2.54	6645	173,249	13,290		

single fatality occurs approximately every 173,249 passenger years.

The individual risk level for crew and passengers is in the ALARP area, which means that according to the IMO guidelines the risk for crew and passengers should be reduced as long as the risk reduction is not disproportionate to the costs; i.e. only cost beneficial RCOs need to be implemented.

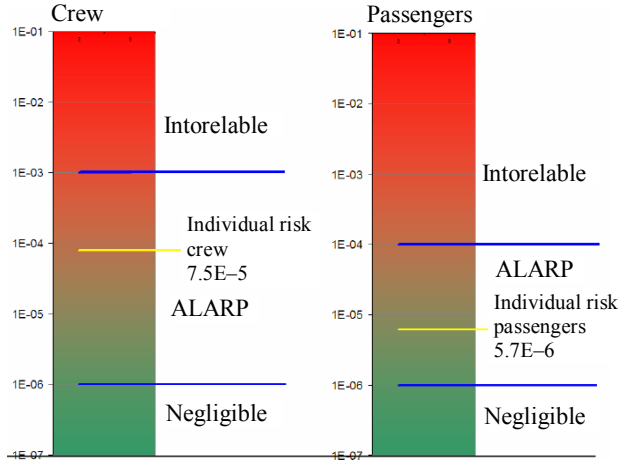

Fig. 7. Individual risk level

The individual risk could also be presented as an area derived from the consequence models and the topography of the populated area together with the assumption of the cruise ship passengers and crew.

Fig. 8. Individual risk zones for cruise ship neighbour oil spill

The highest dependence of results derives from the initial probability of the event. In this case the oil spill probability is assumed to be 5E–5. The probability could be calculated from the historical data as has been the case for other accidents. In this case the data were not available for such an event because there are very few events available for the analyzed port. Related to the reason of an oil spill there is a probability it happens as a consequence of collision or grounding from the sea side, but also as a consequence of an industrial accident on the land side. The value 5e–5 is taken as a calculated risk of a land side spill. The calculated probability for collision in the analyzed port is 2E–5 /year and for grounding 5.8E–5. Assuming that 10% of those accidents could lead to a spill the frequencies are ten times lower. In this case the higher probability has been assumed for further calculation.

Societal risk

Based on the calculated individual risk frequencies the societal risk in computed. Integrate the probability of death for each event over the population specified N_u represents the number of people killed by a given event. Figure 9 illustrates the modelled risk level for cruise ships in an FN diagram. The risk level is calculated as the sum of the frequency per ship year for these accidents. The limits for societal risks are provided in table 2. The risk level is within the ALARP region.

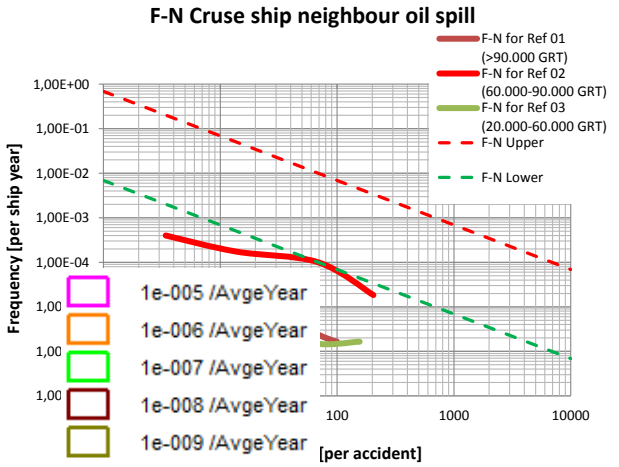

Fig. 9. Societal risk level for Cruise ship neighbour oil spill

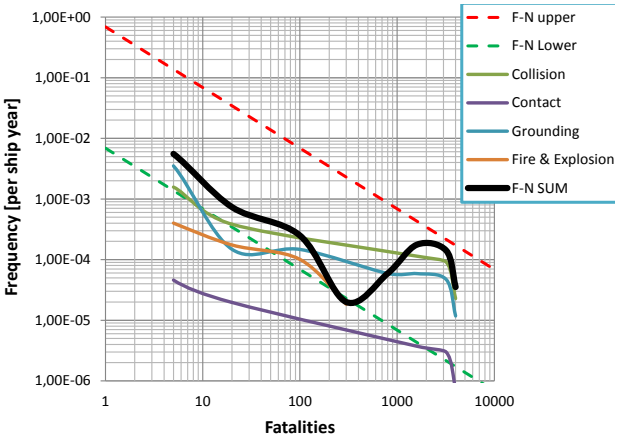

Fig. 10. Societal risk level based on accident type

Figure 10 shows the risk level for other four accident types evaluated for cruise ships over 90,000 GRT. From the figure it is evident that collision and

grounding accidents are the main risk contributors, while contact and fire / explosion accidents do not contribute significantly to the overall risk picture.

Table 8. Risk overview per hazard

Hazard	Accudent frequency [per ship year]	% of all accidents	Fatalities [per ship year]	% of all
Collision	4.59E–03	10	2.35E–01	58.8
Contact	1.15E–03	3	7.91E–03	2.0
Grounding	9.76E–03	22	1.41E–01	35.3
Fire / explosion	9.18E–03	21	9.67E–03	2.4
Others	1.95E–02	44	5.81E–03	1.5

Conclusions

44% of cruise ship accidents fall into the "other" category. However, the four modelled hazards account for 98% of fatalities. Collision and grounding amount to 94% of fatalities (59% + 35%). Smaller accidents with 2 to 5 fatalities can be expected every year in a fleet of 172 ships. The great majority of risks are within the large scale accident category due to the large numbers of estimated fatalities. Catastrophic accidents with large numbers of fatalities account for 80% of the risk even though the frequency of such events is quite low.

The results are highly dependent on historic incident data and modelling of collisions and to a lesser extent groundings. The data used are not up to date and should be updated for the analysis of the current world fleet of cruise ships. Further research should be initiated to investigate whether our results apply to modern cruise ships.

References

1. WILD P., DEARING J.: Development of and prospects for cruising in Europe. Maritime Policy and Management, 27(4), 2000, 315–337.
2. United States Coast Guard, Passenger Vessel Association. PVA Risk Guide: A Guide to Improving the Safety of Passenger Vessel Operations by Addressing Risk, 2007.
3. Maritime Safety Committee. MSC 85/INF.2, Formal Safety Assessment – Cruise Ship, IMO, 2008.
4. Institution of Chemical Engineers. Nomenclature for Hazard and Risk Assessment in the Process Industry Rugby. 1992.
5. TRBOJEVIC V.M.: Risk criteria in EU. ESREL'05, Poland, 2005, 27–30.
6. BOTTELBERGHS P.H.: Risk analysis and safety policy developments in the Netherlands. Journal of Hazardous, 2000.
7. RAJ P.K., LEMOFF T.: Risk analysis based LNG facility sitting standard in NFPA 59A, Journal of Loss Prevention in the Process Industries 22, 2009, 820–829.
8. International Maritime Organization. MSC 72/16, Formal Safety Assessment – Decision parameters including risk acceptance criteria –Submitted by Norway, 2000.
9. UK P&I Club. Press release, UK club's analysis: Two per cent of claims incur 72% of the costs. London 1999.

Others

10. HIGHTOWER M.M., LUKETA-HANLIN A., GRITZO L.A., COVAN J.M.: Review of the independent risk assessment of the proposed Cabrillo liquefied natural gas deepwater port project, Sandia National Laboratories, 2006.
11. BOTTELBERGHS P.H.: Risk analysis and safety policy developments in the Netherlands. Journal of Hazardous Materials 71, 2000.
12. GUCMA L.: Evaluation of oil spills in the Baltic Sea by means of simulation model and statistical data. International Maritime Association of Mediterranean, Balkema 2007.
13. DNV Energy. Nautical Risk assessment LNG transport Rostock, December 2007.
14. MACDONALD D.: Practical Hazops, Trips and Alarms, IDC Technologies, imprint of Elsevier, 2004.
15. DOUGAL D.: An introduction to Fire dynamics, John Wiley & Sons Ltd., 1998.

Scientific Journals
Maritime University of Szczecin

Zeszyty Naukowe
Akademia Morska w Szczecinie

2013, 36(108) z. 1 pp. 177–181
ISSN 1733-8670

2013, 36(108) z. 1 s. 177–181

Experimental evaluation of the Constant False Alarm Rate (CFAR) algorithms used in maritime FM-CW radars

Ryszard Wawruch

Gdynia Maritime University, Department of Navigation, Faculty of Navigation
81-345 Gdynia, al. Jana Pawła II/3, e-mail: wawruch@am.gdynia.pl

Key words: algorithms, practical efficiency, maritime radar, video signals, experimental research

Abstract

Paper presents basic information on the Constant False Alarm Rate (CFAR) algorithms and assessment of their practical efficiency in maritime FM-CW radar. Experimental research comprised qualitative assessment of the different CFAR algorithms done by the comparison of radar video signals presented by installed in the Gdynia Maritime University FM-CW radar type CRM-203 utilised these algorithms and pulse radars with digital (Raytheon Pathfinder MK2 and NSC 34) and analogue (Racal Decca AC 1690) display units.

Introduction

In order to detect objects by radar it is necessary to separate in radar signal coming back to the scanner, target returns received from the objects against so called background created by unwanted echoes: atmospheric and inner (receiver) noises, clutters and interferences. In maritime navigation objects means coastline and sea surface objects like ships, aids to navigation and different fix and drifting objects creating obstruction to navigation (ice, etc.). Clutters are created by returns generated by sea (surface clutters) and clouds and precipitation (volume clutters). Separation is done by power threshold above which any return is considered to probably originate from object. If the threshold is low, more targets will be detected but radar video signal will contain returns from coastline and sea surface objects together with unwanted noises, clutters and interferences. It means that radar sensitivity will be high but the probability of proper object detection against unwanted echoes relatively low. If the threshold is high, effect will be contrary to the above mentioned – radar sensitivity will be low but the probability of proper detection relatively high.

Described threshold may be introduced manually by radar operator or in semi or fully automatic manner by the equipment using adaptive algorithm realizing Constant False Alarm Rate (CFAR) detection. In all cases it is done by control of the gain and anti-clutter sea functions. The role of the CFAR algorithm is to determine the power threshold above which any return will be considered to originate from a objected with required probability level. If the background against which objects are to be detected does not change in space and time, a fixed threshold level may be chosen to provide required probability of false detection (false alarm). Probability of false alarm is a function of the signal-to-unwanted echoes (noise, clutter and interference) ratio of the target returns and depends on the probability density function of the unwanted echoes assumed for this condition to be Gaussian (Additive White Gaussian Noise – AWGN). However, in the event of maritime radar, unwanted echoes, mainly sea clutter, are time correlated and change both spatially and temporary. It means, they may not be assumed as AWGN and changing threshold has to be used. The threshold level shall adequately raise and lower to maintain a constant probability of false alarm.

More detailed information on principles of automatic radar detection may be found in [1, 2].

Principle of CFAR detection

In the CFAR algorithm so called cell under test (CUT) has to be selected. It may be the distant cell

containing strongest return or return with amplitude higher than the defined level. In the simplest CFAR algorithm, the threshold level is defined by radar operator. In algorithm working in automatic manner the threshold level is calculated by estimating the level of unwanted returns (noise, clutter, interference) around the CUT. This is done by selecting a block of cells around the CUT and calculating their average power level. To avoid impact of the CUT itself on this estimation, cells directly adjacent to the CUT are treated as guard cells and ignored. A target is declared present in the CUT if its amplitude is both higher than amplitude of returns in all directly adjacent cells and higher than average power level. This algorithm is known as cell-averaging CFAR (CA-CFAR). In other CFAR schemes calculation of the average power value is performed separately for cells to the left and right of the CUT and criterion of the greatest-of or least-of these two power levels is used to define the local power threshold. These are greatest-of CFAR (GO-CFAR) and least-of CFAR (LO-CFAR) algorithms. More sophisticated CFAR algorithms select adaptively the threshold level taking into account clutter statistical distribution, e.g. K-distribution for sea clutter. To this family of CFAR schemes belong the ordered statistic (OS-CFAR) and clutter map (CMAP-CFAR) algorithms.

The efficiency of the CFAR algorithm defines radar detection capability and sensitivity. The knowledge of its efficiency and limitations, particularly in bad weather condition is important for radar user mainly in case of new radar technologies like Frequency Modulated Continuous Wave (FM-CW) radar introduced nowadays on seagoing vessels and in Vessel Traffic Services (VTS). At present manufacturers and ship and VTS personnel do not have sufficient experience in utilizing this new technology at sea. There are not available any information which CFAR algorithm is most suitable for radars installed in VTS and on ships sailing in different sea areas and in different weather condition in the accessible bibliography and radar manufacturer instructions. Usually manufacturers inform users simply e.g.: that their radars have: automatic detection (Norcontrol), so called “clean sweep” function (Atlas Elektronik), four types of algorithms define as near, near buoy, rough sea, harbour (Furuno), two types of algorithms define as harbour and open sea (Sperry Marine) only and do not present how these functions are realised and how shall be used.

The scarcity of information about automatic detection function realized in maritime radars especially practical usefulness of the particular types of applied CFAR algorithms and recommendation on the principle of their utilisation was the reason of conducting experimental research in the Gdynia Maritime University using FM-CW radar type CRM-203 constructed by BUMAR Elektronika S.A. This radar, as a prototype has different CFAR algorithms available to the user and due to that is convenient for research purposes.

Description of the research

Experimental research has been conducted since winter 2011. It comprises qualitative assessment of the different CFAR algorithms done by the comparison of the radar video signals presented by FM-CW radar type CRM-203 and pulse radars with display units: digital (Raytheon Pathfinder MK2 and NSC 34) and analogue (Racal Decca AC 1690). All these radars are installed in the university building on shore nearby the south entrance to the port in Gdynia The distances between radar scanners positions on the roof of university building are not bigger than a few meters and the field of view of particular radars may be considered as the same (Fig. 1). Basic parameters of the FM-CW radar are presented in table 1.

Table 1. Basic parameters of the FM-CW radar type CRM-203

Parameter	Value
Output power	1 mW, 10 mW, 100 mW, 2 W
Carrier frequency	9.3–9.5 GHz
Frequency deviation switched according to the required scale range	54 MHz at 6 NM, 27 MHz at 12 NM, 13.5 MHz at 24 NM
Range scales	0.25–48 NM
Modulation	Direct Digital Synthesizer (DDS) based linear FM-CW
Sweep repetition period	1 ms
IF bandwidth	4 MHz
Frequency curve slope of IF amplifier	6 dB/oct; 12 dB/oct; 18 dB/oct
Beam width (horizontal/vertical)	0.70°/22°
Polarisation	Horizontal
Analog-to-digital converter	14 bits
FFT signal processing	8192-points FFT
Sampling frequency	8 MHz
Display resolution	1280 × 1024 pixels
Range and bearing accuracies	1% of selected range or 50 m (whichever is greater), 0.7°

More detailed information about FM-CW and pulse radars utilised in the research may be found in [3, 4, 5, 6].

Fig. 1. The field of view of radar antennas

Following parameters of the CFAR algorithm may be chosen in the FM-CW radar type CRM-203:

1. Type of algorithm:
   - FIX (detection without CFAR, voltage threshold given manually by operator);
   - CAGO (normalized ambient average left, greatest of);
   - CASO (normalized ambient average right, smallest (lower) of);
   - CA (duplex normalized ambient average);
   - OS (ordered statistic);
   - CMAP (clutter map).
2. Length of the cell used in CFAR algorithm: 4, 8, 16, 32, 64 and 128.
3. Level of the voltage threshold between 0 and 255 with increment of 1.
4. Attenuation level between 0 and 255 with increment of 1.

These CFAR parameters may be defined for the following different parameters of the scanner, transceiver and processing algorithms:

1. Scanner rotation speed between 12 and 30 rpm/min with increment of 1 rpm/min.
2. Anti clutter sea – three levels: 6 dB/oct; 12 dB/oct; 18 dB/oct.
3. Receiver gain level before signal digitalisation (automatic/manual) between 0 dB and 63 dB with increment of 1 dB.
4. Carrier frequency – 10 different values in the band 9300–9500 MHz defined by manufacturer.
5. Type of window algorithm: Bartlett, Blackman, Gaussian, Hamming, Hanning, Harris, Kaiser, rectangular, triangle and Von Hann.
6. Differentiation – switched on/off.
7. Pulse clutters correlation – switched on/off.
8. Fix clutters correlation – switched on/off.
9. Clutter chart – switched on/off.
10. Binary integrator with the "M-of-N" rule – switched on/off and utilising any value of integers between 0 and 30 as *m* and *n* parameters.

Tests has been conducted in different weather conditions in all seasons of the year, including dif-

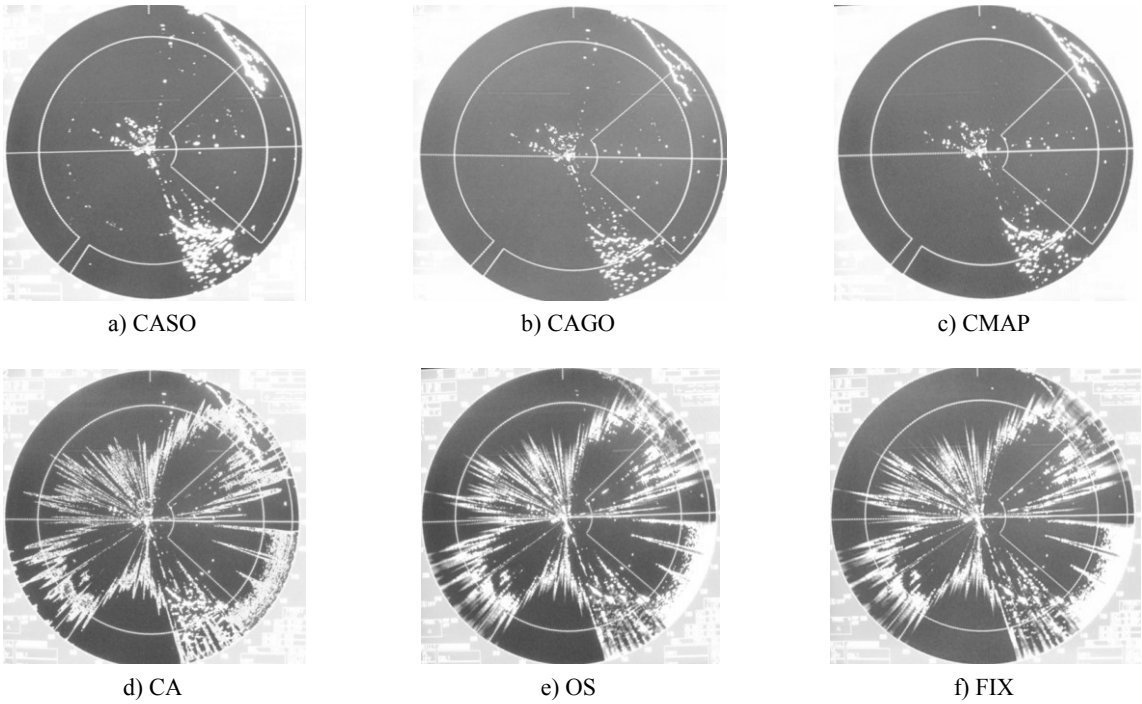

a) CASO b) CAGO c) CMAP

d) CA e) OS f) FIX

Fig. 2. Radar video signal received on the range of 12 nautical miles for the same weather condition and the same all radar parameters, including detection parameters except type of the CFAR algorithm (length of cell 128, level of voltage threshold 2, attenuation 40)

ferent sea state, ice, snow and rain conditions. There have been checked effects of the utilisation of different types and parameters of CFAR algorithm. The assessment was conducted by the comparison of the radar video signal presented on display monitors of the FM-CW and pulse radars on the following ranges of observation:

1. 22,224 meters (12 nautical miles) enabling presentation of the whole Polish part of the Gulf of Gdańsk.

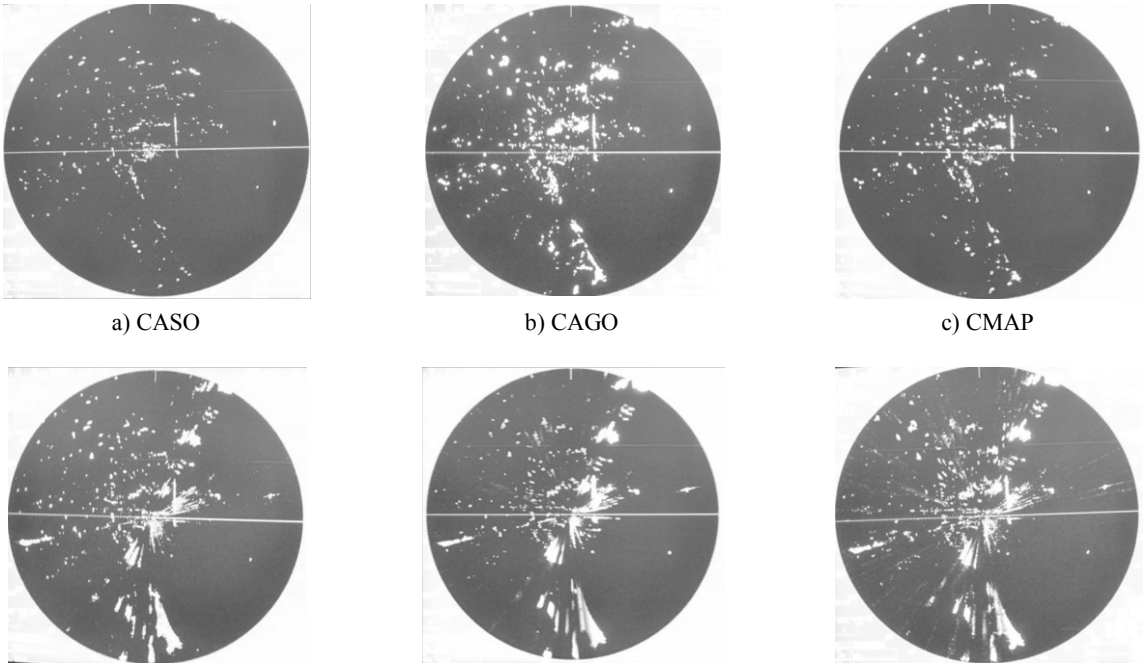

a) CASO b) CAGO c) CMAP

d) CA e) OS f) FIX

Fig. 3. Radar video signal received on the range of 1.5 nautical miles for the same weather condition and the same all radar parameters, including detection parameters except type of the CFAR algorithm (length of cell 128, level of voltage threshold 2, attenuation 40)

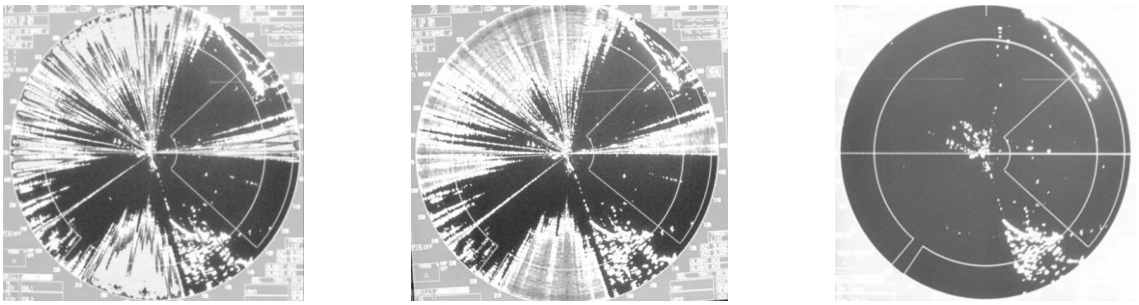

a) length of cell: 4 b) length of cell: 64 c) length of cell: 128

Fig. 4. Radar image on the range of observation 12 nautical miles received for CASO CFAR algorithm and different values of the length of cell

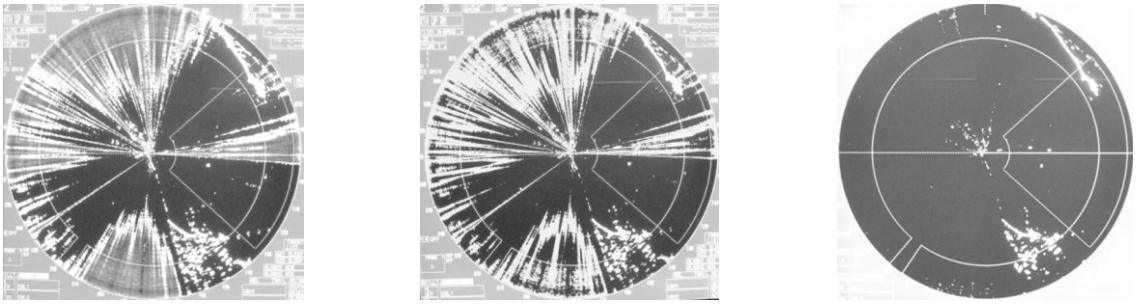

a) threshold 0 b) threshold 50 c) threshold 100

Fig. 5. Radar image on the range of observation 12 nautical miles received for CASO CFAR algorithm and different values of the voltage threshold

2. 2778 meters (1.5 nautical miles) to check the utility of the particular types and parameters of the CFAR algorithm on the smaller distances for returns received from object in the Gdynia harbour and town.

Results of the research

Samples of the research results are presented on figures 2–5. Figure 2 shows radar video signal received on the range of 12 nautical miles for the same weather condition and the same all radar parameters, including detection parameters except type of the CFAR algorithm (length of cell 128, level of voltage threshold 2, attenuation 40).

As may be observed on figure 2 two groups of CFAR algorithms give very often completely different effects. Pictures a, b and c (schemas CASO, CAGO and CMAP) present radar image with different sensitivity but without distortion characteristic for images received using schemas CA, OS and FIX (pictures d, e and f). Similar effect of the application of particular CFAR algorithms was received for range of observation equal to 1.5 nautical miles (Fig. 3).

On the ranges of observation 6 nautical miles and bigger the best radar image was received for CFAR CASO algorithm. CAGO schema was more efficient on the smaller ranges. But even for these two CFAR algorithms, application of improper values of other CFAR parameters (length of the cell and voltage threshold and attenuation levels) may result in considerable distortion of presented radar video signal (Figs 4 and 5).

Conclusions

On the basis of the carried out measurements, it was stated that:

1. The best FM-CW radar image and detection possibility were obtained for CASO CFAR algorithm on the ranges equal to 6 nautical miles and bigger and for CAGO algorithm on the smaller ranges of observation.
2. The efficiency of particular CFAR algorithms depends strongly on values of the length of cell and levels of voltage threshold and attenuation selected by the operator.
3. The usage of differentiation, correlation (pulse and fix clutters) and integration functions accessible in the tested radar influences the efficiency of the CRAR algorithm.
4. The efficiency of the CRAR algorithm depends on the transmitter carrier frequency used by radar inside X band.
5. It was not observed influence of the scanner rotation speed (in the range between 12 and 30 rpm) on the efficiency of the CRAR algorithm.
6. During the research was possible to obtain the same detection distances of coastline, floating aids to navigation and ships by tested FM-CW radar type CRM-203 and the modern pulse radars Raytheon NSC34 and Pathfinder MK2.
7. The large number of available reciprocally correlated controls effecting radar detection possibility and quality of radar image impedes work out of the recommendation regarding setting picture on the tested radar.

Experimental researches described in this paper are time-consuming due to the necessity of waiting for particular weather conditions mainly ice and snow conditions in the winter time period. They are continued in order to define some recommendations on the principle of use of particular CFAR algorithms and their results will be presented during the next MTE conference.

References

1. HAMISH M.: Modern Radar Systems, Artech House Inc., Boston, London 2008.
2. KOMAROV I., SMOLSKIY S.: Fundamental of Short-Range FM Radar. Artech House Inc., Boston, London 2003.
3. PLATA S., WAWRUCH R.: CRM-203 Type Frequency Modulated Continuous Wave (FMCW) Radar. In Adam Weintrit (ed.) Marine Navigation and Safety of Sea Transportation, CRC Press Taylor & Francis Group, Boca Raton, London, New York, Leiden 2009, 207–210.
4. STUPAK T., WAWRUCH R., PLATA S.: Hydro-Meteorological Disturbaces Influence on Radar Picture Investigation. International Radar Symposium "IRS 2010", Conference Proceedings, German Institute of Navigation (DGON), Vilnius 2010, Vol. 1, 336–338.
5. WAWRUCH R.: Detection Possibility of the Frequency Modulated Continuous Wave (FM CW) Radar. In Adam Weintrit (ed.) Marine Navigation and Safety of Sea Transportation. Advances in Marine Navigation. CRC Press Taylor & Francis Group, Boca Raton, London, New York, Leiden 2013, 247–251.
6. WAWRUCH R., STUPAK T.: Detection Possibilities of Pulse and FMCW Radars-Comparative Analysis. International radar Symposium „IRS 2009", Proceedings, German Institute of Navigation (DGON), Technical University of Hamburg, Hamburg, 2009, 131–134.

Scientific Journals
Maritime University of Szczecin

Zeszyty Naukowe
Akademia Morska w Szczecinie

2013, 36(108) z. 1 pp. 182–187
ISSN 1733-8670

2013, 36(108) z. 1 s. 182–187

Control system design for dynamic positioning using vectorial backstepping

Anna Witkowska

Gdańsk University of Technology, Electrical and Control Engineering Department
80-233 Gdańsk, ul. Narutowicza 11/12, e-mail: awitkowska@ely.pg.gda.pl

Key words: dynamic positioning, backstepping, nonlinear passive observer

Abstract
The problem of synthesis a dynamic positioning system for low frequency model of surface vessel was considered in this paper. The recursive vectorial backstepping control design was used to keep a fixed position and heading in presence of wave disturbances. The passive observer was introduced to smooth the measurements and to estimate the velocities needed for the control algorithm. The computer simulation results were given to demonstrate the effectiveness of that combination of controller-observer system to compensate environmental disturbances.

Introduction

In view of the manoeuvre difficulties caused by the weight of ships, it is not an easy task to improve the quality of navigation, especially for ships moving at slow speed (called dynamic positioning). Dynamic positioning (DP) system for marine vehicles is a challenging practical problem. It includes station keeping, position mooring and slow speed references tracking. Of that three, the main purpose of DP is to maintain a certain accurate position and course, regardless of the interference such as wave and wind. This task should only be achieved under its own propulsion and using navigation systems. An application of the appropriate control method for DP is directly related to the adopted model, its purpose, structure and number of the installed actuators.

The station keeping for DP system can be achieved using only three control inputs when it is considered a fully actuated ship operating in the horizontal plane. Hence, the dynamic positioning system can be designed by using feedback from position and heading angle. These state variables are in some cases available through satellite navigation systems as GPS / DGPS, supported by the gyros and accelerometers. But in general more signals like for example velocities accelerations and stationary varying disturbances due to wind, ocean current and nonlinear wave effects, are necessary in the control law. In the process of ship steering, direct measurement of longitudinal and transverse velocity is not available when they attain low speed values. However, it is possible to calculate the estimated value of velocity on the basis of the position and direction measurements by the state observer. In most cases, an accurate state measurements are disturbed by the wind, waves and sea currents, as well as by the interference of the measuring sensors. Therefore, the estimates should be filtered by using so-called wave filtering (WF) techniques. Oscillatory disruptions of a WF motion components are filtered before feedback is applied. However, the remaining LF motion components which are associated with the deviation from the given position and direction are compensated by the control system.

The examples of several solutions mentioned above have been recently obtained. Most of them base on signal filtering, state estimation and appropriate selection of the control method. The first DP systems were designed using conventional PID controllers in cascade with low-pass and notch filters. Here, the wave disturbances were filtered

before feedback was applied in order to avoid unnecessary control action. Model-based controls for dynamic positioning includes also LQG, sliding mode control [1], robust H∞ control [2, 3], nonlinear backstepping method [4] and another state – space techniques [5]. The artificial intelligence [6], fuzzy logic [7] and neural nets [8] were also used for DP. A number of researches were carried out within the scope of application.

In the DP systems, wave filtering and state estimation were resolved using Kalman filters [9, 10] or Luenberger observer. There is the most important drawback of that two observers-if the extended Kalman filter and Luenberger observer are combined with a state feedback controller, using state estimates, then a global expotential stability cannot be quaranteed. Alternative solution for the state feedback controllers is the backstepping observer [4] or passive observer and wave filtering [11]. These methods were designed by using Lyapunov stability theorem and Kalman Yakubovich – Popov theorem to ensure GES property. Passive observer in comparison to the backstepping observer has less tuning parameters, so it is easier to apply. In this study the vectorial backstepping controller in configuration with passive observer was considered to keep fixed position and heading at low forward speed. Both of these methods were designed based on Lyapunov stability theorem and assuming an a priori knowledge of mathematical vessel model.

Ship model

The mathematical vessel model of the ship used for DP in a horizontal plane is described in [5].

Kinematic model

Since we only consider the surge, sway and yaw the kinematic equations are given by:

$$\boldsymbol{\eta}' = \mathbf{R}(\psi)\,\boldsymbol{\nu} \tag{1}$$

where the state vector $\boldsymbol{\eta} = [x, y\ \psi]^{\mathrm{T}}$ denotes the position (x, y) and heading $0 < \psi < 2\pi$ of the ship in the earth-fixed frame. The vector $\boldsymbol{\nu} = [u, v, r]^{\mathrm{T}}$ denotes linear velocities in surge, sway and angular velocity in yaw coordinated in the body fixed frame. The rotation matrix $\mathbf{R}(\psi)$ with the property $\mathbf{R}^{\mathrm{T}} = \mathbf{R}^{-1}$ is given by:

$$\mathbf{R}(\psi) = \begin{bmatrix} \cos\psi & -\sin\psi & 0 \\ \sin\psi & \cos\psi & 0 \\ 0 & 0 & 1 \end{bmatrix} \tag{2}$$

Low Frequency model

During dynamically positioning it is a common assumption to consider the low speed, low frequency model omitting the centrifugal / coriolis forces, moments and nonlinear damping effects:

$$\mathbf{M}\nu' + \mathbf{D}\nu = \boldsymbol{\tau} + \boldsymbol{\tau}_w \tag{3}$$

where the matrix of inertia $\mathbf{M} \in \mathbf{R}^{3\times3}$ and the damping matrix $\mathbf{D} \in \mathbf{R}^{3\times3}$ will defined in detail later. The control input vector $\boldsymbol{\tau} \in \mathbf{R}^3$, $\boldsymbol{\tau} = [\tau_x,\ \tau_y,\ \tau_n]^{\mathrm{T}}$ of forces and moments provided by the actuator system and the vector $\boldsymbol{\tau}_w$ of slowly varying forces and moments that act on the hull due to environmental disturbances such as wind, currents and waves or unmodelled dynamics can be written as:

$$\boldsymbol{\tau} = \mathbf{B}\mathbf{K}(U)\,\mathbf{u} \tag{4}$$

$$\boldsymbol{\tau}_w = \mathbf{R}(\psi)^{\mathrm{T}}\,\mathbf{b} \tag{5}$$

where $\mathbf{B} \in \mathbf{R}^{3\times n}$ is a thruster configuration matrix, $\mathbf{K}(U) \in \mathbf{R}^{n\times n}$ is a diagonal matrix of speed – dependent force coefficients, $n \geq 3$ is the number of independent actuators and $\mathbf{u} \in \mathbf{R}^n$ is the control inputs vector.

Wave Frequency model

The following wave frequency model can be used for each degrees of freedom ($i = 1,2,3$), producing forces added to the position and heading measurements:

$$h_i(s) = \frac{2\zeta_i \varpi_{0i} \sigma_i}{s^2 + 2\zeta_i \varpi_{0i} s + \varpi_{0i}^2} \tag{6}$$

where: ζ_i – relative damping ratio, ϖ_{0i} – dominating wave frequency, σ_i – wave intensity parameter.

A state space realization of WF model can be expressed as:

$$\boldsymbol{\chi}' = \boldsymbol{\Omega}\boldsymbol{\chi} \tag{7}$$

$$\boldsymbol{\eta}_w = \boldsymbol{\Gamma}\boldsymbol{\chi} \tag{8}$$

Here, $\boldsymbol{\eta}_w = [x_w, y_w, \psi_w]^{\mathrm{T}}$ denotes position and heading measurement vector, $\boldsymbol{\chi} \in \mathbf{R}^6$ is a state vector, $\boldsymbol{\Omega} \in \mathbf{R}^{6\times6}$ is a constant matrix resulted directly from transformation of the transmittance (6) to the state space model:

$$\boldsymbol{\Omega} = \begin{bmatrix} 0_{3\times3} & I_{3\times3} \\ \Omega_{21} & \Omega_{22} \end{bmatrix} \tag{9}$$

$$\Omega_{21} = -\mathrm{diag}\left(\varpi_{01}^2, \varpi_{02}^2, \varpi_{03}^2\right) \tag{10}$$

$$\Omega_{22} = -\mathrm{diag}\left(2\xi_1\varpi_{01}^2, 2\xi_2\varpi_{02}^2, 2\xi_3\varpi_{03}^2\right) \tag{11}$$

The constant matrix $\mathbf{\Gamma} \in \mathbf{R}^{3\times 6}$ converts the vector $\boldsymbol{\chi}$ to space $\mathbf{R}^3$:

$$\mathbf{\Gamma} = \begin{bmatrix} 0_{3\times 3} & I_{3\times 3} \end{bmatrix} \tag{12}$$

The bias state may be modelled by a first-order Markov process:

$$\mathbf{b}' = -\mathbf{T}^{-1}\mathbf{b} \tag{13}$$

where $\mathbf{T} \in \mathbf{R}^{3\times 3}$ is a diagonal matrix representing positive bias time constants.

DP controller

In this section the control input vector $\mathbf{u}$ was designed to guarantee that $\boldsymbol{\eta}(t)$ and $\boldsymbol{\nu}(t)$ are bounded and to ensure asymptotic convergence of position and heading to their desired constant values, $\boldsymbol{\eta}(t) \to \boldsymbol{\eta}_d$, at $\boldsymbol{\nu}(t) \approx 0$ for all $t \geq 0$.

The classical vectorial backstepping method was used, discussed in detail [4]. The reference signals needed for control are the desired state vector $\boldsymbol{\eta}_d = [x_d, y_d, \psi_d]^{\mathrm{T}}$ and its first and second order derivatives. All reference signals, the heading angle ψ_d and position (x_d, y_d) are assumed to be bounded. The control design based on mathematical ship model (1)–(5) and consists of two steps.

At the first step of backstepping the virtual control variable $\boldsymbol{\nu}$ is designed for subsystem (1). The system is considered in a new error variables $\mathbf{z}_1 \in \mathbf{R}^3$ and $\mathbf{z}_2 \in \mathbf{R}^3$ given by:

$$\mathbf{z}_1 = \left[z_{11}, z_{12}, z_{13}\right]^{\mathrm{T}} = \boldsymbol{\eta} - \boldsymbol{\eta}_d \tag{14}$$

$$\mathbf{z}_2 = \boldsymbol{\nu} - \boldsymbol{\alpha} \tag{15}$$

where $\boldsymbol{\alpha} = [\alpha_1, \alpha_2, \alpha_3]^{\mathrm{T}}$ is a desired virtual control for $\boldsymbol{\nu}$, calculated with respect to the control Lyapunov function candidate. At the second step the actual control law $\mathbf{u}$ is designed for the subsystem (3) based on second Lyapunov theory. The following feedback control law is proposed:

$$\mathbf{u} = \mathbf{K}^{-1}\mathbf{W}^{-1}\mathbf{B}^{\mathrm{T}}\left(\mathbf{B}\mathbf{W}^{-1}\mathbf{B}^{\mathrm{T}}\right)^{-1} \cdot \cdot \left[\mathbf{D}\boldsymbol{\nu} - \mathbf{M}\mathbf{R}^{\mathrm{T}}\left(\mathbf{C}_2\mathbf{z}_2 + \mathbf{z}_1 + \mathbf{R}'\boldsymbol{\nu} + \mathbf{C}_1\mathbf{z}_1' - \boldsymbol{\eta}_d''\right) - \mathbf{R}^{\mathrm{T}}\mathbf{b}\right] \tag{16}$$

where the first and second control Lyapunov function candidates and the desired virtual control are given by $V_1 = 0.5\mathbf{z}_1{}^{\mathrm{T}}\mathbf{z}_1$, $V_2 = \mathrm{V}_1 + 0.5\mathbf{z}_2{}^{\mathrm{T}}\mathbf{z}_2$ and $\alpha = -\mathbf{C}_1\mathbf{z}_1 + \boldsymbol{\eta}'_d$. Now, the error dynamics can be written as:

$$\mathbf{z}_1' = -\mathbf{C}_1\mathbf{z}_1 + \mathbf{z}_2 \tag{17}$$

$$\mathbf{z}_2' = \mathbf{C}_2\mathbf{z}_2 - \mathbf{z}_1 \tag{18}$$

While all reference signals $\boldsymbol{\eta}_d$ are constant and the state variables $\boldsymbol{\eta}(t)$, $\boldsymbol{\nu}(t)$ are available measurably, then the equilibrium point $(\mathbf{z}_1, \mathbf{z}_2) = (0, 0)$ is GAS. It ensures convergence $\boldsymbol{\eta}(t) \to \boldsymbol{\eta}_d$ and $\boldsymbol{\nu}(t) \to \boldsymbol{\alpha}$. Stability is established by using LaSalle's theorem, since $V_2 > 0$ and $V_2' \leq 0$. Among the other things it is satisfied where designed parameter matrices $\mathbf{C}_1 = \mathbf{C}_1{}^{\mathrm{T}} > 0$ and $\mathbf{C}_2 = \mathbf{C}_2{}^{\mathrm{T}} > 0$ are chosen in a diagonal form.

DP model – based observer

The model-based observer described in detailed in [11] was used to reconstruct the system's non-measured states. The chosen observer was designed on the basis of the Lyapunov stability theory. The measured position and heading, $\mathbf{y}_m$ can be seen as a superposition of the LF motions and WF motions:

$$\mathbf{y}_m = \boldsymbol{\eta} + \boldsymbol{\eta}_w \tag{20}$$

The idea of passive observer is to reconstruct $\boldsymbol{\eta}$, $\boldsymbol{\eta}_w$ based on output $\mathbf{y}_m$ and vector forces $\boldsymbol{\tau}$. On the basis of a complete model which consists of a ship model (1)–(5), bias model (13) and WF model (7)–(12), the resulting observer is composed of the following equations including: state estimators (21–22), measurements estimator (23), bias estimator (24), wave estimator (25):

$$\dot{\hat{\boldsymbol{\eta}}} = \mathbf{R}\left(\mathbf{y}_m\right)\hat{\boldsymbol{\nu}} + \mathbf{K}_2\tilde{\mathbf{y}} \tag{21}$$

$$\dot{\hat{\boldsymbol{\nu}}} = -\mathbf{M}^{-1}\mathbf{D}\hat{\boldsymbol{\nu}} + \mathbf{M}^{-1}\mathbf{R}\left(\mathbf{y}_m\right)^{\mathrm{T}}\hat{\mathbf{b}} + \mathbf{M}^{-1}\boldsymbol{\tau} + \mathbf{R}\left(\mathbf{y}_m\right)^{\mathrm{T}}\mathbf{K}_4\tilde{\mathbf{y}} \tag{22}$$

$$\hat{\mathbf{y}} = \hat{\boldsymbol{\eta}} + \mathbf{\Gamma}\hat{\boldsymbol{\chi}} \tag{23}$$

$$\dot{\hat{\mathbf{b}}} = -\mathbf{T}^{-1}\hat{\mathbf{b}} + \mathbf{K}_3\hat{\mathbf{y}} \tag{24}$$

$$\dot{\hat{\boldsymbol{\chi}}} = \boldsymbol{\Omega}\hat{\boldsymbol{\chi}} + \mathbf{K}_1\tilde{\mathbf{y}} \tag{25}$$

Here, $\tilde{\mathbf{y}} = \mathbf{y}_m - \hat{\mathbf{y}}$ is the estimation error and $\mathbf{K}_1 \in \mathbf{R}^{6\times 3}$, $\mathbf{K}_2$, $\mathbf{K}_3$ and $\mathbf{K}_4 \in \mathbf{R}^{3\times 3}$ are diagonal observer gain matrices. The observer – gains $\mathbf{K}_1$, and $\mathbf{K}_2$ can calculated for the same order as shown in [11], based on the wave frequency model parameters (6). As can be seen the $\mathbf{K}_3$ and $\mathbf{K}_4$ are unknown diagonal matrices in the observer model besides sea state, which was assumed to be known.

Simulation Research

In this section the performance of the control system was verified. The scaled mathematical model of supply vessel was used as a case study [5, 12]. The vessel system matrices were given below:

$$\mathbf{M} = \begin{bmatrix} 1.1274 & 0 & 0 \\ 0 & 1.8902 & -0.0744 \\ 0 & -0.0744 & 0.1278 \end{bmatrix} \quad (26)$$

$$\mathbf{D} = \begin{bmatrix} 0.0358 & 0 & 0 \\ 0 & 0.1183 & -0.000124 \\ 0 & -0.000041 & 0.0308 \end{bmatrix} \quad (27)$$

Assuming that ship is equipped with two main aft propellers, one bow tunnel thruster and two rudders in the aft of the ship, matrixes **B**, **K** and the control allocation weights **W** are given by:

$$\mathbf{B} = \begin{bmatrix} 1 & 1 & 0 & 0 & 0 \\ 0 & 0 & 1 & -1 & -1 \\ 0.0656 & -0.0656 & 0.7874 & 0.4987 & 0.4987 \end{bmatrix} \quad (28)$$

$$\mathbf{W} = \mathrm{diag}([1\ 1\ 0.25\cdot(1+\exp(200\cdot U^2)) \exp(1/(0.02+0.6\cdot U))\cdot 2.5\cdot 10^{-8} \exp(1/(0.02+0.6\cdot U))\cdot 2.5\cdot 10^{-8}]) \quad (29)$$

$$\mathbf{K} = 0.0025\cdot\mathrm{diag}([6.55\ 6.55\ 1.37\cdot\exp(-47\cdot U^2)\ 3.9+ + 6.4\cdot 10^3\cdot U^2\ 3.9+6.4\cdot 10^3\cdot U^2]) \quad (30)$$

The tested controller-observer system were modeled in the computing environment called Matlab / Simulink. Simulations were carried out in time domain. Numerical integration was done using Runge-Kutta method in fourth-order integration with a period equal to 0.1 s. During a simulation tests all the simulation deploy the same parameters settings as follows. The initial conditions were chosen as: $\boldsymbol{\eta}(t_0) = (0, 0, 0)$, $\boldsymbol{\nu}(t_0) = (0.01, 0.01, 0.01)$ and the initial values of all estimates were set as zero. The desired position and orientation were changed after 30 s to the value $\boldsymbol{\eta}_d(t) = (10, 10, 45°)$.The simulation studies were carried out in the presence of wave disturbances (6). The parameters of the wave frequency model were set at $\zeta_i = 0.1$, $\omega_{0i} = 0.65$ rad/s, $\sigma_i = 0.5$ m. The amplitudes of the wave were set at 2.0 m, 2.0 m, 3° respectively for surge, sway and yaw directions. The observer – gains $\mathbf{K}_1$ and $\mathbf{K}_2$ were calculated on the basis of the appropriate wave frequency model parameters as shown in [11] and a bias time constants was assumed $\mathbf{T} = \mathrm{diag}(100, 100, 100)$. The tuned controller and observer parameters were $\mathbf{K}_3 = 0.01\cdot\mathrm{diag}(0.1, 0.1, 0.1)$, $\mathbf{K}_4 = 0.0208\cdot\mathrm{diag}(0.1, 0.1, 0.1)$, $\mathbf{C}_1 = \mathrm{diag}(0.05, 0.05, 5)$, $\mathbf{C}_2 = \mathrm{diag}(4, 4, 0.5)$.

The simulation tests aim at checking the operation correctness of the vectorial backstepping controller with passive observer. The following data (Figs 1–5) show the ability of the system to the convergence of the position and heading to their desired values, wave filtration and state estimation. The first 150 seconds of tests present the results with an observer and a wave filtering. During the next time state variables were not observed and filtered.

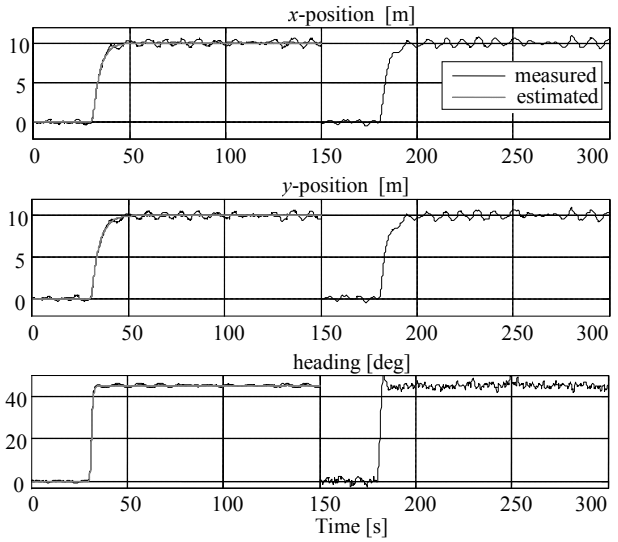

Fig. 1. Measured and filtered position and heading

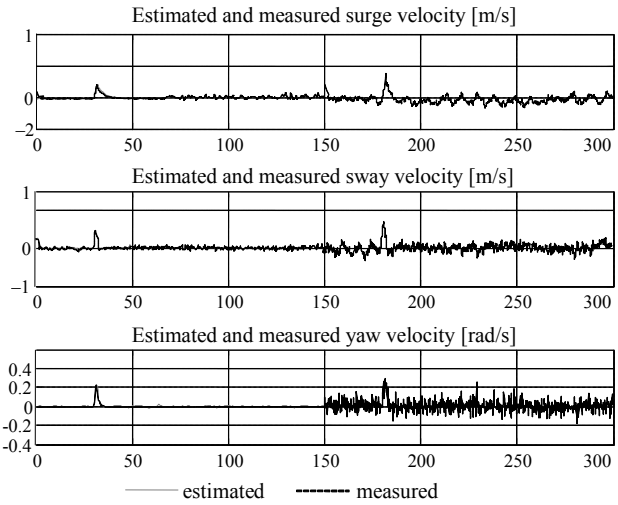

Fig. 2. Observer error of surge, sway velocities and yaw angle

The time-histories shown in figure 1 confirm a good ability of the backstepping controller to keep fixed position and heading in the presence of wave disturbances. The system confirms also good ability to state estimation and wave filtering. The gray line present measured position, black line estimated. The surge, sway velocity and yaw angle were also estimated from observer (Fig. 2). It is seen that all the observer errors tend to zero for velocities, position and heading. Velocity estimation error does not exceed 2% of the steady-state. The next figures present forces and moments in surge, sway and yaw direction during a simulation

test without and in the presence of obsever and wave filtering. In a figure 4 we can see a actual ship position in the system with observer and without observer and wave filtering. The DP system with backsepping controller and passive observer gives an excellent positioning performance.

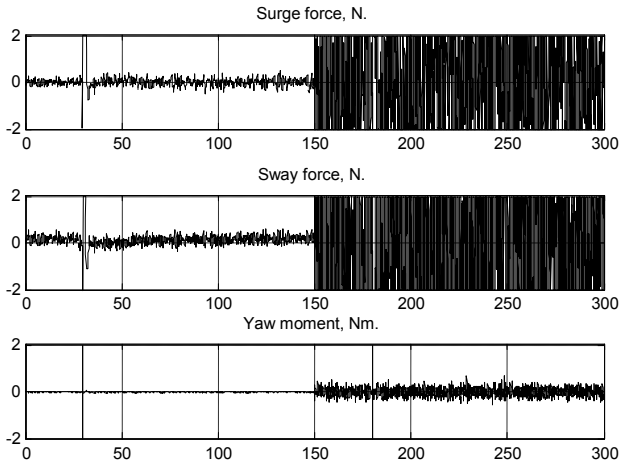

Fig. 3. Forces and moments in surge, sway and yaw direction

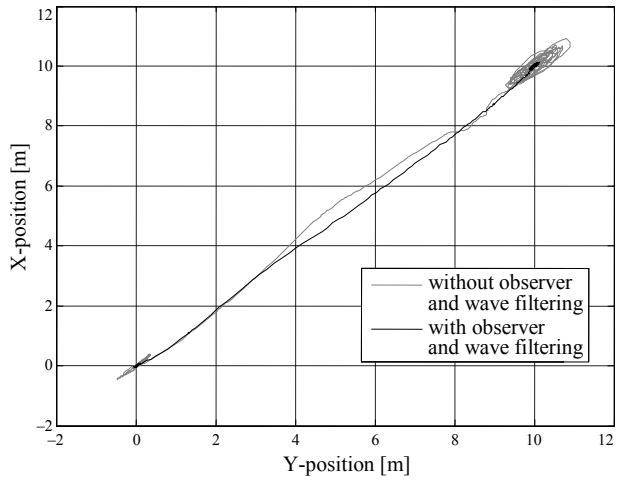

Fig. 4. Actual ship position

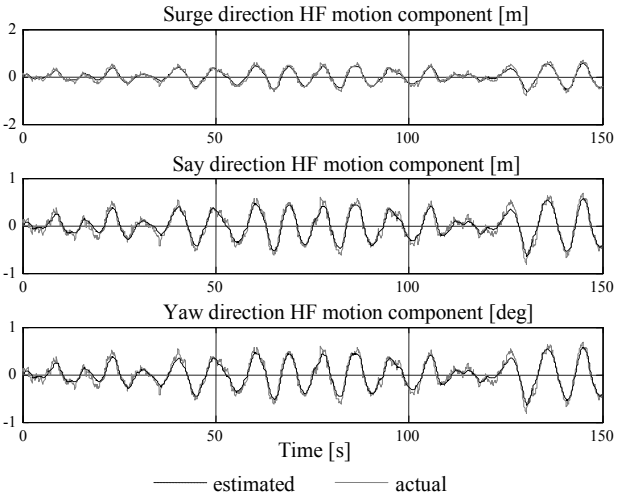

Fig. 5. Actual and estimated HF motion components

The system realizes also estimation of the first order wave motions components that cause oscylatory motion of the vessel. The HF motion components in surge, sway and yaw direction, vessel were presented in a figure 5. We can see that actual HF motion components are fully estimated in each direction.

Conclusions

Ships with DP system are used to perform operations on the sea, especially in the output of crude oil. Functions, that these vessels implement, are able to eliminate the tugs work and are able to quickly respond to changes in weather or operating parameters. This gives the versatility of using this type of vessels.

In this paper the backstepping controller was used to keep fixed position and heading in the presence of wave disturbances. The passive observer was introduced to smooth the measurements and to estimate the velocities needed for the control algorithms. These combinations of controller-observer confirm the good ability of the control system to keep fixed position and heading in the presence of different wave disturbances. The simulation results have shown that these combinations of controller-observer effectively compensate environmental disturbances.

References

1. TOMERA M.: Nonlinear controller design of a ship autopilot. International Journal of Applied Mathematics and Computer Science, Vol. 20, No. 2, 2010, 271–280.
2. GRIMBLE M., ZHANG Y., KATEBI M.R.: H∞-based ship autopilot design. Ship Control Symposium, Ottawa 1993, 678–683.
3. MESSER A., GRIMBLE M.: Introduction to robust shiptrack-keeping control design. Transactions of the Institute of Measurement and Control. Vol. 15, No. 3, 1993, 104–110.
4. KRSTIC M., KANELLAKOPULOS I., KOKOTOVIC P.V.: Nonlinear and Adaptive Control Design. John Wiley and Sons Ltd., New York 1995.
5. FOSSEN T.I.: Marine Control Systems: Guidance, Navigation, and Control of Ships, Rigs and Underwater Vehicles. Marine Cybernetics, Trondheim 2002.
6. Xu R., Wang Q., Song Y., Zheng R., Chen M.: Study on Ship Dynamic Positioning System's Thruster Allocation Based on Genetic Algorithm. International Conference on Information Science and Technology. Nanjing, Jiangsu 2011.
7. CAO Y., LEE T., GARRETT D., CHAPPELL: Dynamic Positioning of Drilling Vessels with a Fuzzy Logic Controller. Dynamic Positionig Conference. Houston 2001.
8. CAO Y., ZHOU Z., VORUS W.: Application of a Neural Network Predictor / Controller to Dynamic Positioning of Offshore Structures. Dynamic Positionig Conference. Houston 2000.
9. BANKA S., DWORAK P., BRAASEL M.: On control of nonlinear dynamic mimo plants using a switchable structure of

linear modal controllers. Measurement Automation and Monitoring, Vol. 56, No. 5, 2010, 385–391.
10. GRIMBLE M., FUNG P.: Dynamic Ship Positioning Using a Self-tuning Kalman Filter. Transaction on Automatic Control. IEEE, Vol. AC-28, No. 3, 1983.
11. FOSSEN T.I., STRAND J.P.: Passive nonlinear observer design for ships Using Lyapunov Methods: Experimental Results with a Supply vessel. Automatica, Vol. 35, No. 1 (Jan), 1999, 3–16.
12. GODHAVN J.M., FOSSEN T.I., BERGE S.P.: Non-linear and adaptive backstepping designs for tracking control of ships, International Journal of Adaptive Control and Signal Processing 12(8), 649–670.

Others

13. SKJETNE R.: The Maneuvering Problem. Ph.D. thesis, Norwegian University of Science and Technology, Trondheim 2005.
14. WITKOWSKA A., TOMERA M., ŚMIERZCHALSKI R.: A Backstepping approach to ship course control. Int. J. Appl. Math. Comput. Sci., Vol. 17, No. 1, 2007, 73–85.
15. WITKOWSKA A., ŚMIERZCHALSKI R.: Designing a ship course controller by applying the adaptive backstepping method. Int. J. Appl. Math. Comput. Sci., Vol. 22, No. 4, 2012, 985–997.

Scientific Journals
Maritime University of Szczecin

Zeszyty Naukowe
Akademia Morska w Szczecinie

2013, 36(108) z. 1 pp. 188–194
ISSN 1733-8670

2013, 36(108) z. 1 s. 188–194

Implementation and verification of course controllers in the inland navigation simulator (InSim)

Paweł Zalewski

Maritime University of Szczecin
70-500 Szczecin, ul. Wały Chrobrego 1–2, e-mail: p.zalewski@am.szczecin.pl

Key words: InSim, shiphandling simulation, PID controller, fuzzy controller, ship's course control algorithm

Abstract
The formal verification of performance properties of a ship's course control algorithm used in the InSim simulator of Maritime University of Szczecin is presented in the paper. Implementation of fuzzification, fuzzy rules and defuzzification techniques allowed the construction of a controller tuned in accordance to expert knowledge as an alternative to the industry PID standard. Both controllers' structures are analysed. Their verification leads to the assessment and comparison of dynamic properties of a modelled ship's course control. Further development of course controllers into track controllers has been discussed as well.

Introduction

The desired ship's motion both, in reality and simulation, can be achieved by control of the vessel's momentary vector state parameters. In restricted water areas two basic cases of ship's steering are distinguished:

1) while proceeding via straight or curved route segments between consecutive waypoints with fixed allocation of engine / thrusters;
2) while manoeuvring with variable allocation of engine / thrusters.

Two types of autopilot have been implemented into the Inland Navigation Simulator (InSim) developed in Maritime University of Szczecin for navigator's support in case No. 1: PID and fuzzy. These autopilots monitor 4 variables of the state vector: course tracking error $\Delta\psi(t)$, derivative of course $\omega_z = \mathrm{d}\psi(t)/\mathrm{d}t$, transverse shift of ship's body origin (usually centre of gravity) from the set trajectory $\Delta y(t)$ and linear speed of this displacement v_y. Additionally, for realistic steering gear model implementation, the rudder angle offset $\Delta\delta_R(t)$ is monitored. In the article the structure of autopilots' course control module (monitoring the first two variables) is analysed and its performance validated (Fig. 1).

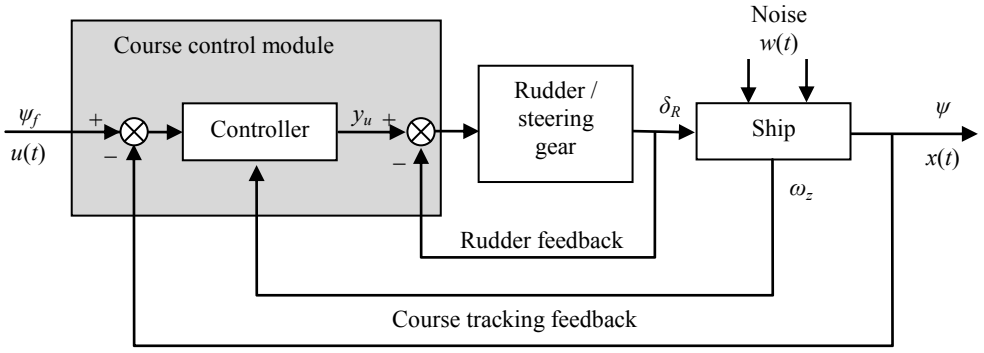

Fig. 1. Diagram of a ship's course control

Symbols in the figure 1 mean:
$u(t)=\psi_f$ – preset course value (set point);
$x(t)=\psi$ – instantaneous course value;
ω_z – instantaneous course derivative value (angular velocity);
y_u – steering gear allocation value (allocated rudder angle);
δ_R – measured rudder angle;
w – noise vector;
and: $\Delta\psi = \psi_f - \psi$, $\Delta\delta_R = \delta_R - y_u$.

The track keeping function which requires monitoring of the displacement variables $\Delta y(t)$ and v_y, is implemented via cascade control arrangement in which another controller's output drives the set point of a course controller. The structure of this second "displacement" controller is equivalent to the first "course" controller and its performance can be verified accordingly.

PID controller of ship's course

PID (Proportional–Integral–Derivative) controller is the most popular device used contemporary either in continuous or discrete control systems [1, 2, 3, 4]. Application of a PID controller guarantees better dynamic properties (control time, control curve-trajectory) and static properties (error) in relation to the P, PI, PD type controllers. There are following parameters of a PID controller:

– gain (proportional) coefficient k_p;
– integration time T_i;
– differentiation time T_d.

Generally, the impact of these parameters on the controlled process (achievement and maintaining of set course) can be interpreted as follows:

– the proportional component compensates current deviation between the set and the instantaneous (current) value of the controlled parameter;
– the integral component compensates for the accumulation of these deviations in the past;
– the derivative component compensates for the expected deviations in the future.

Dynamic time characteristics (output $y_u(t)$ as a result of application of the input signal $\Delta\psi(t)$ in the time t) of the PID controller in the basic, continuous form are described by the equation [5]:

$$y_u(t) = k_p\left(\Delta\psi(t) + \frac{1}{T_i}\int_0^t \Delta\psi(t)\,\mathrm{d}t + T_d\,\frac{\mathrm{d}\Delta\psi(t)}{\mathrm{d}t}\right) \tag{1}$$

For modelling purposes it is convenient to introduce the equation (1) in the operator form – by means of a continuous time transfer function to a domain of complex variable s:

$$G_{PID}(s) = \frac{Y_u(s)}{\Delta\Psi(s)} = k_p\left(1 + \frac{1}{sT_i} + sT_d\right) \tag{2}$$

Switching from the continuous to discrete time transfer function (as used in the simulator) requires substitution of the variable s in equation (2), after numerical forward Euler integration, by:

$$s = \frac{z-1}{T_s} \tag{3}$$

where:
T_s – sampling time.

Derivative action of a PID controller can cause amplification of the noise (interference) in the measured process value $\Delta\psi(t)$ and, consequently, cause unnecessary changes or oscillations of the output signal $y_u(t)$. To avoid this undesirable effect, a filter element is introduced to the architecture of the controller in its derivative component. Therefore, an ideal PID controller, after substituting (3)

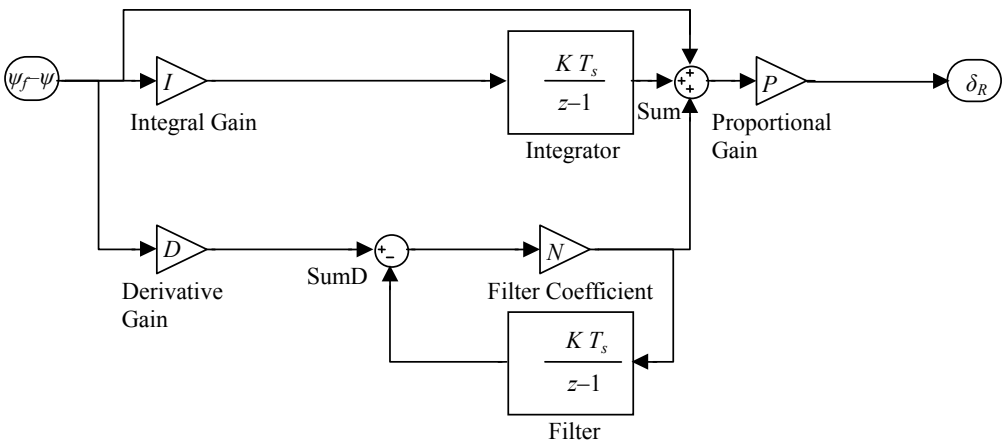

Fig. 2. Diagram of the InSim discrete PIDF controller

in (2), takes the form of a PIDF (Proportional – Integral – Derivative – Filter) as in formula (4):

$$G_{PIDF}(z) = k_p\left(1+\frac{1}{z-1}\frac{T_s}{T_i}+\frac{T_d}{\frac{1}{N}+\frac{T_s}{z-1}}\right) \quad (4)$$

where: N – is the filter coefficient.

Block diagram of the InSim PIDF controller architecture in discrete time domain (4), designed in MATLAB / Simulink is shown in the figure 2.

Symbols in the figure 2 mean:

K – gain value, $P = k_p$, $I = \frac{1}{T_i}$, $D = T_d$.

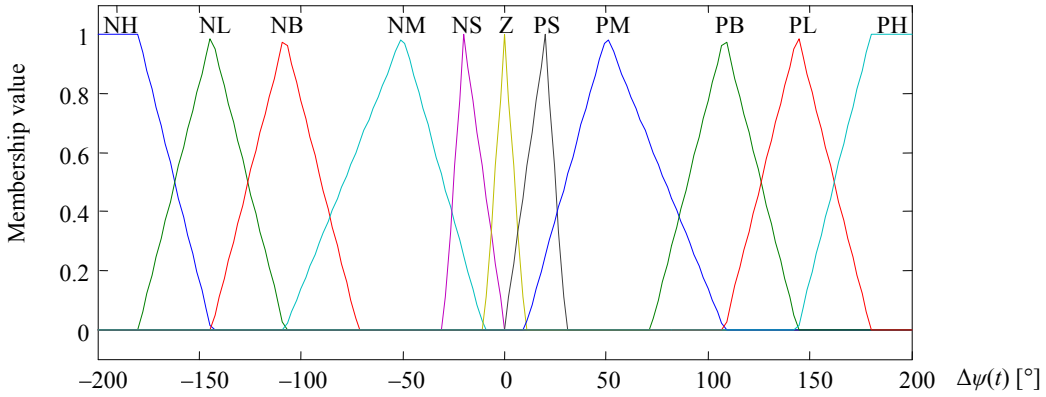

Fig. 3. Membership functions to the fuzzy sets of course error

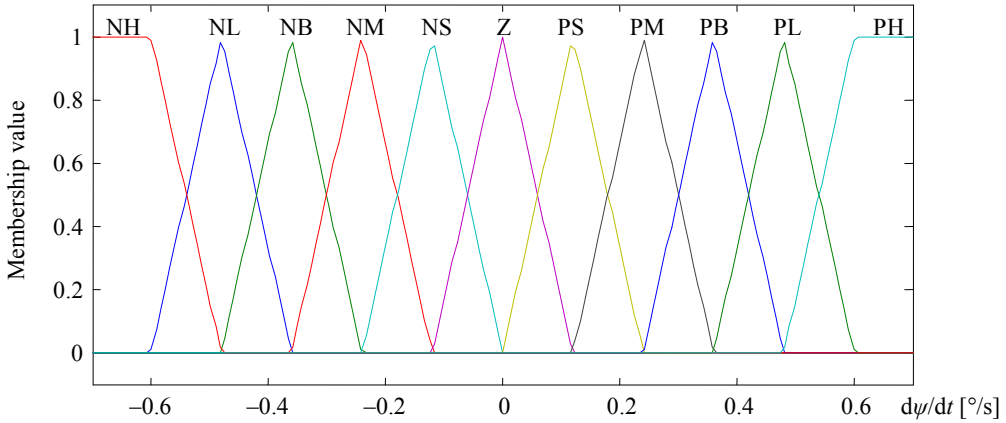

Fig. 4. Membership functions to the fuzzy sets of rate of change of course error

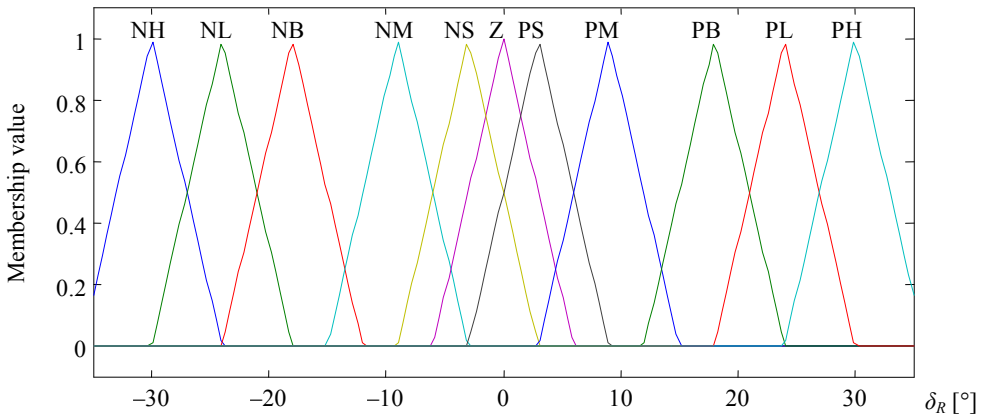

Fig. 5. Membership functions to the fuzzy sets of rudder angle allocation

Fuzzy controller of ship's course

According to assumptions given in the introduction, input variables in a fuzzy controller of ship's course, correspondingly to the PID controller are: difference between the set course value and the current course value – course's deviation (error) $\Delta\psi(t)$, rate of change of the course's deviation – course's derivative $\omega_z = \mathrm{d}\psi(t)/\mathrm{d}t$, and the output variable is: allocated rudder angle $y_u = \delta_R(t)$.

Membership functions of each variable of the controller to the fuzzy sets marked linguistically *NH* (negative high), *NL* (negative large), *NB* (negative big), *NM* (negative medium), *NS* (negative small), *Z* (close to zero), *PS* (positive small), *PM* (positive medium), *PB* (positive big), *PL* (positive large), *PH* (positive high) are presented in the figures 3, 4 and 5.

Introducing fuzzy rules, all the major components of the navigator's knowledge of ship's steering are directly evident from the fig. 6 in the following manner:

1. If the heading error $\Delta\psi$ and change in heading error ω_z are both, big and have identical signs, then use very big maximum rudder input correspondingly.
2. For zero $\Delta\psi$ and ω_z, the rudder angle should be zero, but if $\Delta\psi$ and ω_z move positive (to starboard), then the rudder should move negative (to port).
3. If ω_z moves significantly positive, then the rudder should move even more negative. Similar reaction follows for $\Delta\psi$ and ω_z negative, where the rudder angle should be made positive. For the case where $\Delta\psi$ and ω_z have opposite signs and depending on the magnitude of the signals, the rudder input should be either positive or negative.

For small $\Delta\psi$ and ω_z, the changes to the rudder position should be smaller and applied slower to keep system's stability and lower heading oscillations (yawing). For instance by lowering the "gain" of the controller near zero the noise will not be amplified. Also, if the ship's angular position is moving sufficiently fast to remove the heading error, then be conservative in using the rudder to further help ship's rotation since this is unnecessary.

These rules can be presented in the form of *If…Then…*, for example:

If $\Delta\psi(t)$ *is NH And* $d\psi(t)/dt$ *is NH Then* $\delta_R(t)$ *is PH*
If $\Delta\psi(t)$ *is NH And* $d\psi(t)/dt$ *is NL Then* $\delta_R(t)$ *is PH*
If $\Delta\psi(t)$ *is NL And* $d\psi(t)/dt$ *is NH Then* $\delta_R(t)$ *is PH*
…

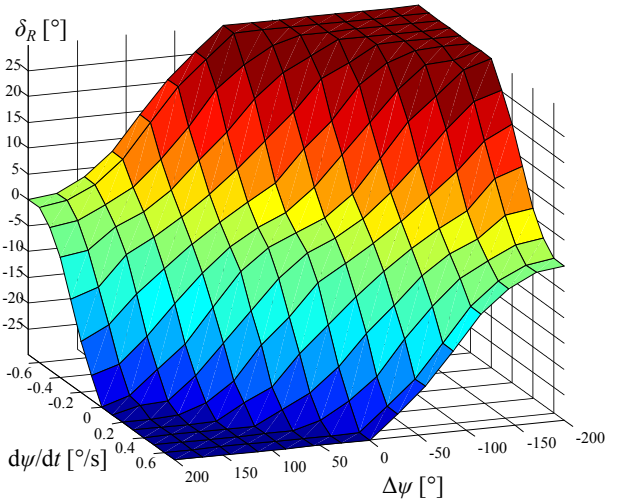

Fig. 6. Relation among rudder angle, course error and course error rate (angular velocity) as 3D response surface

They comprise navigator's expertise of ship's course control. Based on the assumed inputs and outputs there are $11^2 = 121$ such rules, a combination of 11 linguistic variables of fuzzy sets, two inputs and one output presented in the form of the response surface plot in the figure 6.

The principle of determining the "crisp" value of rudder angle δ_{Rc}, using the centre of gravity of the membership function [6], for the fuzzy output with two rules activated (5) is presented in the figure 7.

In the presented case, the small deflection of the rudder to port follows the detection of a small angular velocity to the starboard side at near zero deviation from the set course.

$$\delta_{Rc} = \frac{\int \delta_R m_C(\delta_R)\,\mathrm{d}\,\delta_R}{\int m_C(\delta_R)\,\mathrm{d}\,\delta_R} \tag{5}$$

where: $m_C(\delta_R)$ – membership function of a conclusion set resultant from combination of two activated sets; in the figure 7 these are *Z* and *NS* marked by gray colours.

Verification of implemented course controllers performance

Validation of course controllers implemented in InSim has been designed to verify the performance (evaluation of the dynamic properties) of the provided state vector control. Considering the control of one of the state vector parameters such as vessel course, changing the absolute value of the course in range of 0° to 180°, leads to the ship's response similar to oscillatory process shown in the figure 8.

The analyzed indicators of control quality are [6] (Fig. 8):

1) static accuracy:

$$e_f = \psi_s - \psi_f \tag{6}$$

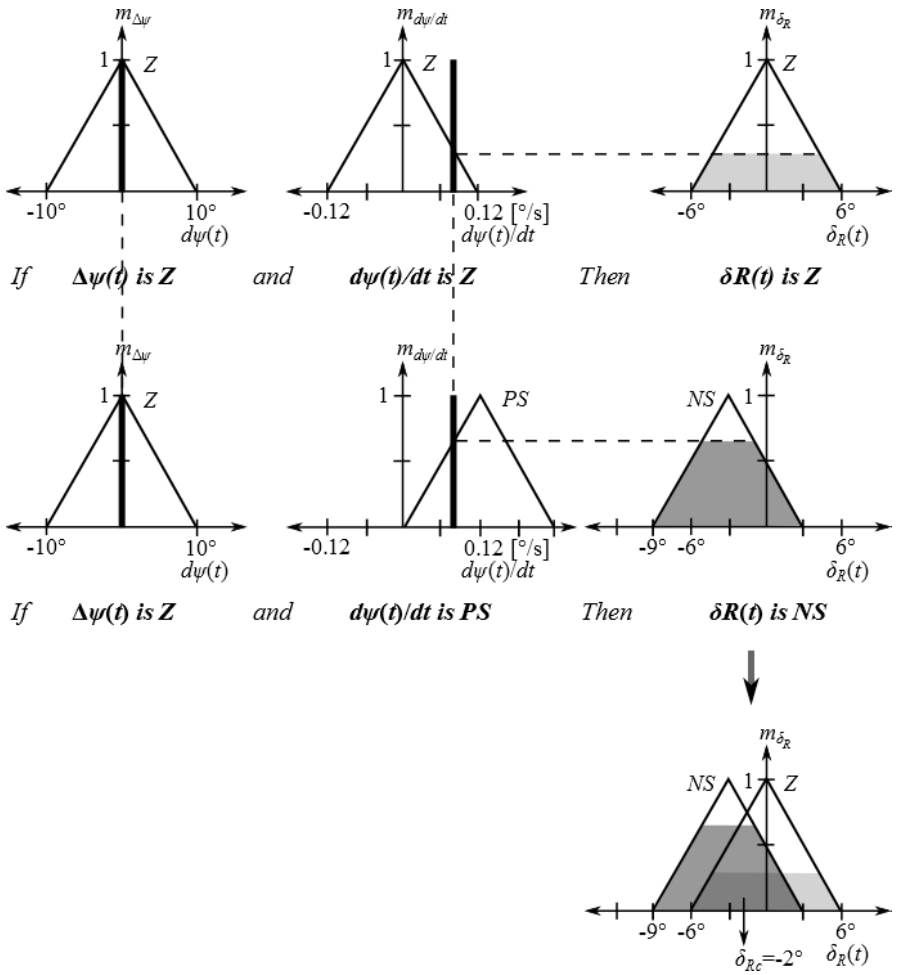

Fig. 7. Determination of the "crisp" value of rudder angle in the fuzzy controller of ship's course

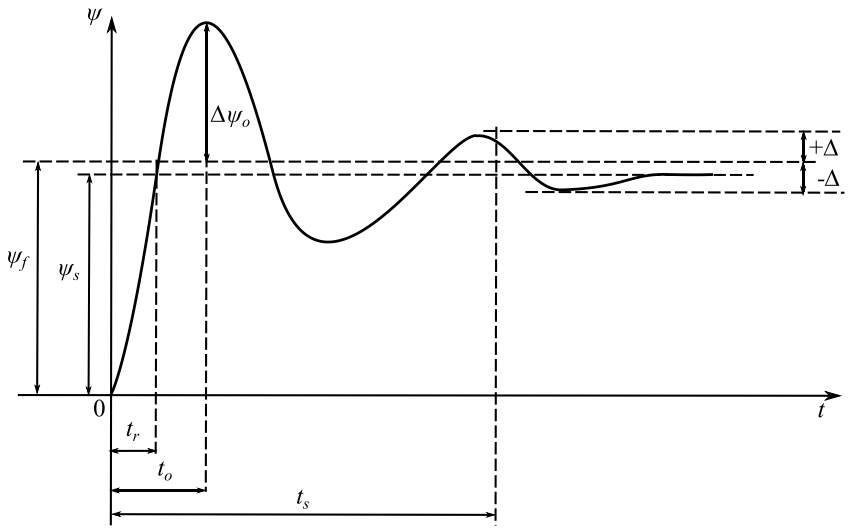

Fig. 8. Oscillatory behaviour of the function of ship's course as a result of controller's actions

2) indicators related to the step response of the control system – the responsiveness to the excitations:
   a) lag or "pseudo dead time" – the time between the output (rudder) change and the point at which the tangent line drawn through the steepest part of the process curve (the point of inflection) crosses the original process line (t_l);
   b) control time (t_s);
   c) rise time (t_r);
   d) the time to reach the maximum response (t_o);

e) the maximum overshoot ($\Delta\psi_o$):

$$\Delta\psi_o = \psi_{\max} - \psi_s \tag{7}$$

$$\Delta\psi_o[\%] = \frac{\Delta\psi_o}{\psi_s}\cdot 100 \tag{8}$$

3) quality indicators related to the frequency characteristics – stability reserve:
   a) reserve of gain ΔK or module ΔL,

$$\Delta K = \frac{1}{\left|G(j\omega_\pi)\right|} \tag{9}$$

where: $j \in \mathrm{N}$; $\varphi(\omega_\pi) = -180°$;
   b) reserve of phase $\Delta\varphi$;
4) indices based on integrating the error following a disturbance or set point change:
   a) IAE – Integral of absolute value of error:

$$I_1 = \int_0^\infty \left|e(t) - e(\infty)\right| \mathrm{d}t \tag{10}$$

   b) ISE – Integral of square error:

$$I_2 = \int_0^\infty \left(e(t) - e(\infty)\right)^2 \mathrm{d}t \tag{11}$$

   c) ITAE – Integral of time times absolute value of error:

$$I_3 = \int_0^\infty t\left|e(t) - e(\infty)\right| \mathrm{d}t \tag{12}$$

   d) ITSE – Integral of time times error squared:

$$I_3 = \int_0^\infty t\left|e(t) - e(\infty)\right| \mathrm{d}t \tag{13}$$

Tuning the controller parameters according to the criterion of minimizing the quality indicators (Figs 9 and 10) has been performed on the basis of theoretical and empirical knowledge of the process in MATLAB using model of the river barge [7] according to the following steps:

1) determination of the design level of operation (DLO), which corresponds to finding of the expected values of the rudder settings, major disruptions;
2) determination of the controller's parameters by methods based on process approximation (for instance Ziegler Nichols methods for PID, inputs and output membership function changes according to expert knowledge);
3) recording of the controller's output while running simulated process of ship's motion;
4) evaluation of the tuning quality and eventual return to the second stage with the changed parameters of the controller.

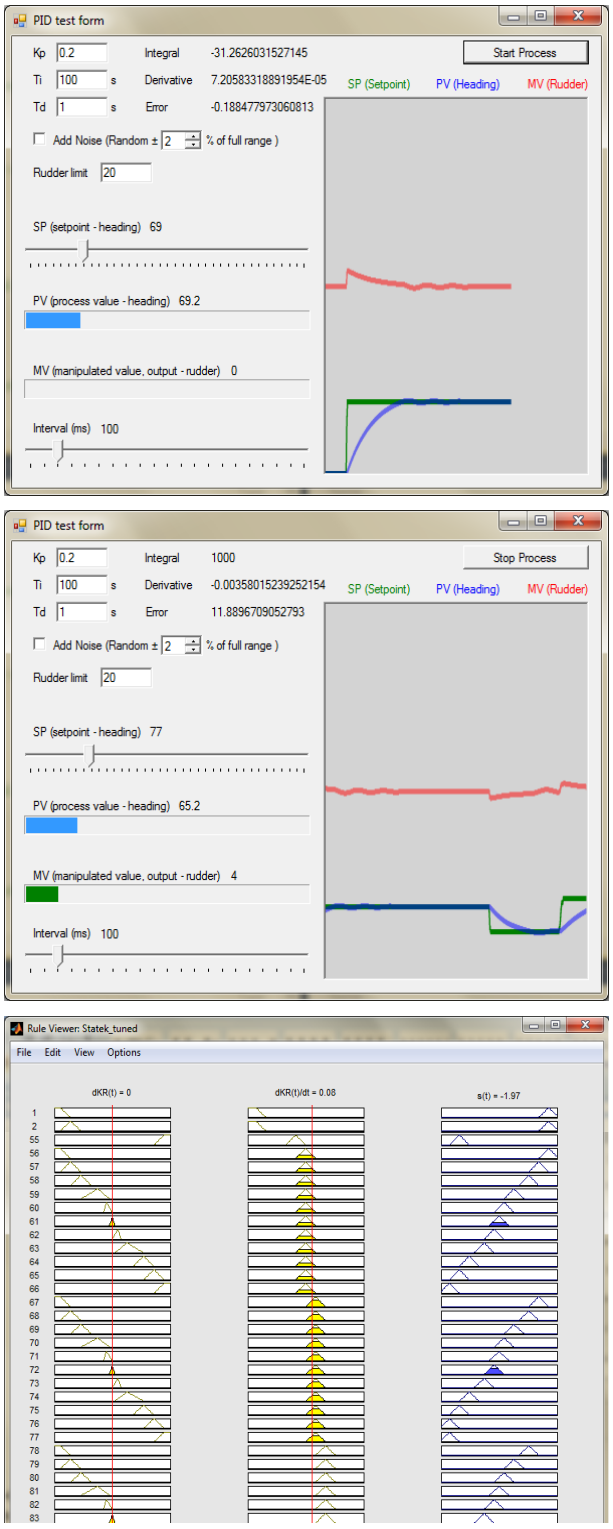

Fig. 9. Interface of controllers' tuning application in InSim

Conclusions

Two types of controllers have been implemented for the InSim shiphandling simulator. Their assessment and comparison of dynamic properties of resultant modelled ship's course control lead to preliminary conclusion that these controllers can be used alternatively in InSim ships' models.

References

1. LISOWSKI J.: Statek jako obiekt sterowania automatycznego. Elektrotechnika i elektronika okrętowa 9, Wydawnictwo Morskie. Gdańsk 1981.
2. KACZOREK T., DZIELIŃSKI A., DĄBROWSKI W., ŁOPATKA R.: Podstawy teorii sterowania. WNT, Warszawa 2005.
3. ÅSTRÖM K.J., HÄGGLUND T.: Advanced PID Control, Research Triangle Park. NC: Instrumentation, Systems, and Automation Society, 2006.
4. ZALEWSKI P.: Systemy autonomiczne w procesie oceny bezpieczeństwa jednostek pływających na akwenie ograniczonym. Wydawnictwo Naukowe Akademii Morskiej w Szczecinie, Szczecin 2013.
5. BRZÓZKA J.: Regulatory i układy automatyki. Wydawnictwo MIKOM, Warszawa 2004.
6. PIEGAT A.: Modelowanie i sterowanie rozmyte. Akademicka Oficyna Wydawnicza EXIT, Warszawa 2003.
7. ARTYSZUK J.: Modelowanie i symulacja ruchu jednostek pływających w zagadnieniach bezpieczeństwa i efektywności manewrowania. Wydawnictwo Naukowe Akademii Morskiej w Szczecinie, Szczecin 2013.

This paper presents results from a research project "Budowa zintegrowanego nieautonomicznego symulatora nawigacyjno-manewrowego jednostek śródlądowych" financed by MNiSW Nr 0973/R/T 02/2010/10.

Scientific Journals
Maritime University of Szczecin

Zeszyty Naukowe
Akademia Morska w Szczecinie

2013, 36(108) z. 1 pp. 195–199
ISSN 1733-8670

2013, 36(108) z. 1 s. 195–199

Numerical study on the influences of canal geometry on ship squat

Minggui Zhou, Zaojian Zou

Shanghai Jiao Tong University

Key words: accurate prediction, safety passage, restricted waters, numerical calculations, squat

Abstract

Accurate prediction of the ship squat is of significance to ensure safety passage of ships in restricted waters. In this paper, a first-order Rankine source panel method is adopted to predict the squat of a ship sailing in restricted canal. Taking KVLCC2 tanker as example, numerical calculations are carried out for the ship travelling in a canal with different conditions. The results of squat are compared with measurement data and the results from empirical formulas. The influence of canal geometry on ship squat is investigated.

Introduction

The hydrodynamic behavior of a ship in restricted waters such as harbours, channels or canals is very different from that in open deep waters. The restricted space underneath and alongside a ship has an important influence on both, sinkage and trim of the ship, also known as squat, which is more pronounced than in deep and open water. Squat is caused by the drop in pressure under the bottom of the ship, where the relative speed of the water is higher. Due to the squat effect, the hydrodynamic forces on the ship may increase largely; ship manoeuvrability and controllability will become poor and risks of grounding may increase due to insufficient underkeel clearances, especially for large vessels. Accurate prediction of the squat is of significance to evaluate ship hydrodynamic performance correctly and to ensure safety passage of the ship in restricted waters.

Ship squat both, in unrestricted waters and restricted waters can be predicted experimentally and numerically. Zhou et al. (2013) [1] summarized the commonly used empirical methods of squat prediction for a ship sailing in restricted waters. Normally a blockage factor Ac/As, the ratio of the cross section area of the canal to the wetted cross section area of the ship, is applied in the empirical formulas to consider the influence of canal geometry. However, the influence of other parameters, such as bank geometry or the lateral position of the ship, is not taken into consideration. In 2006 a comprehensive model test program was carried out at the fully automated towing tank of Flanders Hydraulics Research (Flemish Government, Antwerp, Belgium) with ship models sailing parallel to different bank geometries. The mathematical model that has been developed based on these tests takes account of complex bank geometries [2], but the parameters for the mathematical model are not published. Lataire et al. (2013) [3] investigated the influences of the blockage on the squat of the KVLCC2 Moeri tanker moving in a rectangular fairways, an improved model for the squat was proposed and took into account the forward speed, propeller action, lateral position in the fairway, total width of the fairway and water depth. Briggs et al. (2013) [4] compared the measured ship squat from the Panamax canal for four ships with numerical and empirical methods and the comparisons demonstrated that the Beck, Newman and Tuck (BNT), Ankudinov, and PIANC predictions fell within the range of squat measurements and can be used with confidence in deep draft canal design.

In this paper, a first-order Rankine source panel method is introduced and applied to predict the squat of a ship sailing in restricted canals. Taking KVLCC2 Moeri tanker as example, the numerical

method is firstly applied to calculate the ship squat for different lateral positions and different underkeel clearances in a canal and the numerical results are compared with the measurement data given in [3]. Then calculations are conducted for the ship sailing in different canal geometries with the same blockage factor. The influence of canal geometry on ship squat is analyzed.

Mathematical formulation

A ship sailing with a constant speed in restricted canals is considered, as shown in figure 1. A body-fixed coordinate system *o-xyz* is defined, where the origin *o* is located at the intersection of the mid-ship section and the undisturbed free surface, the *x*-axis pointing towards the bow of the ship, the *y*-axis towards the starboard, and the *z*-axis vertically downwards. Here, we assume that the cross-section shape of the canal is uniform in the *x*-direction. *h* is the water depth, *T* is the draft of the ship, y_p and y_s are the distances from the centerline of the ship to the toe of portside bank and to the toe of starboard side bank, respectively.

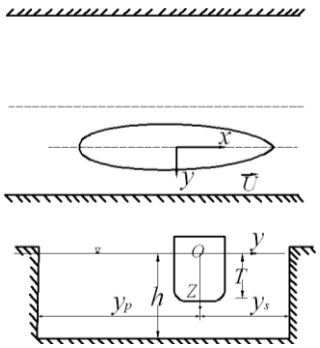

Fig. 1. Sketch map of a ship sailing in a restricted canal

It is assumed that the fluid is incompressible and inviscid, and the flow is irrotational. There exists a velocity potential ϕ which should satisfy Laplace's equation in the fluid domain:

$$\nabla^2\phi = 0 \tag{1}$$

The following boundary conditions should also be satisfied:

– on the ship hull surface S_B:

$$\nabla\phi \cdot \vec{n}_B = 0 \tag{2}$$

where $\vec{n}_B = (n_{B1}, n_{B2}, n_{B3})$ is the unit normal vector towards inside the hull;

– on the wall surfaces of the canal S_W:

$$\nabla\phi \cdot \vec{n}_W = 0 \tag{3}$$

where $\vec{n}_W = (n_{W1}, n_{W2}, n_{W3})$ is the unit normal vector towards outside the fluid;

– on the water bottom $z = h$:

$$\phi_z = 0 \tag{4}$$

– on the free surface S_F ($z = \zeta(x,y)$), the combined free surface condition is:

$$\nabla\phi \cdot \nabla\left(\frac{1}{2}\nabla\phi \cdot \nabla\phi\right) - 2U\nabla\phi \cdot \nabla\phi_x + U^2\nabla\phi_{xx} - g\phi_z = 0 \tag{5}$$

– on the boundary surface at infinite S_∞, the disturbance due to ship motion decays to zero:

$$\nabla\phi|_{R\to\infty} = (0,0,0) \tag{6}$$

where $R = \sqrt{x^2 + y^2 + z^2}$.

Moreover, it should satisfy the radiation condition at infinity. We solve the boundary value problem by a first-order Rankine source panel method. By using the Rankine source, the Laplace's equation and the disturbance decay condition at infinity are satisfied automatically.

For the first-order Rankine source panel method, a Rankine source is distributed on the ship hull surface, the free surface and canal bank surfaces. These surfaces are discretized into panels, on each of which a Rankine source with constant strength is distributed. The strengths are determined by satisfying the corresponding boundary conditions. To satisfy the radiation condition, the numerical technique of raised panels with staggered grid above the free surface is utilized; while the boundary condition on water bottom is satisfied by the method of images. Since the boundary conditions on the free surface are nonlinear, an iterative scheme is used to satisfy these conditions. Refer to literature [5] for more details of the numerical method.

Once the boundary-value problem is solved, the velocity potential ϕ is obtained and the pressure *p* in the flow domain can be obtained by Bernoulli equation. Then the hydrodynamic forces and moments on ship hull can be calculated by integrating the hydrodynamic pressure over the hull surface. From the vertical force and pitching moment, the sinkage and trim can be calculated according to dynamic equilibrium during the iteration procedure for the nonlinear free surface boundary conditions.

Case for study

The KVLCC2 Moeri tanker in full scale (SIMMAN, 2008) [6] is adopted to carry out the numerical calculations. The main dimensions of KVLCC2 are listed in table 1.

Table 1. Main dimensions of KVLCC2

Length between perpendiculars	L [m]	320.0
Breadth	B [m]	58.0
Moulded depth	D [m]	30.0
Draft	T [m]	20.8
Displacement	∇ [m^3]	312622
Wetted area w/o rudder	S_W [m^2]	27194
Block coefficient	C_B	0.8098

The calculation conditions are shown in table 2. In order to verify the Rankine source panel method, the case that KVLCC2 is sailing in a rectangular canal with varying lateral position and water depth (Group1, 2 and 3 in table 2) is firstly calculated and the numerical results are compared with the measurement data published in [3]. Bank effect on the ship squat can be investigated as well. Then the numerical calculations for the KVLCC2 travelling in different canal geometries with the same cross section area and in different water depth are carried out (Group 4 to 7 in table 2).

Since KVLCC2 has a transom stern, the flow around the stern is very complicated. To deal with the transom stern, it is supposed that the wave surface leaves the hull at the transom edge; and the method of adding "virtual length" is adopted, that is, a virtual extension is generated and added to the length of the vessel. The virtual length ΔL is related with the characteristics of transom stern and ship speed. In this paper the ship speed is lower than the designed speed and $\Delta L = L / 25$ is applied.

The discretized domain of the free surface and the wall surface extends from $2.0L$ to $1.0L$ in the longitudinal direction, while the width of the discretized domain in transverse direction is determined according to the distance between the ship and banks.

The panel arrangements on the hull surface and the free surface are shown in figure 2.

Results and analysis

Bank effect on ship squat

The squat results of Group 1, 2 and 3 are selected to study the bank effect on the ship squat and compared with the measurement data to verify the numerical method. Here the width of the canal is 5B and the ship speed is 8 knots. For all the cases, the bow squat (S_b) is larger than the stern squat (S_s). In practical use, the maximum ship squat is the most concerned. Thus, figure 3 shows the bow squat of KVLCC2.

From the comparison it can be seen that when the ship is not very close to the canal bank (y_s = 145 m and 87 m), the calculation results are a little smaller than the measurements. However, when the ship-bank distance is smaller (y_s = 58 m and 43.5 m), the discrepancy between the calculation results and measurement data becomes larger.

Table 2. Overview of the calculation conditions

Group No.	Slope of the canal bank	Breath of the canal on the free surface Ws [m]	Breath of the canal on the bottom W_b [m]	y_s [m]	h/T	U [m/s]
1	vertical wall	290.00	290.00	145, 87, 58, 43.5	1.50	4.115
2	vertical wall	290.00	290.00	145, 87, 58, 43.6	1.35	
3	vertical wall	290.00	290.00	145, 87, 58, 43.7	1.10	
4	vertical wall	290.00	290.00	145	1.20	3.087, 4.115, 5.144
5	1/3	364.88	215.12	107.56		
6	1/5	414.80	165.2	82.6		
7	1/8	489.68	90.32	45.16		

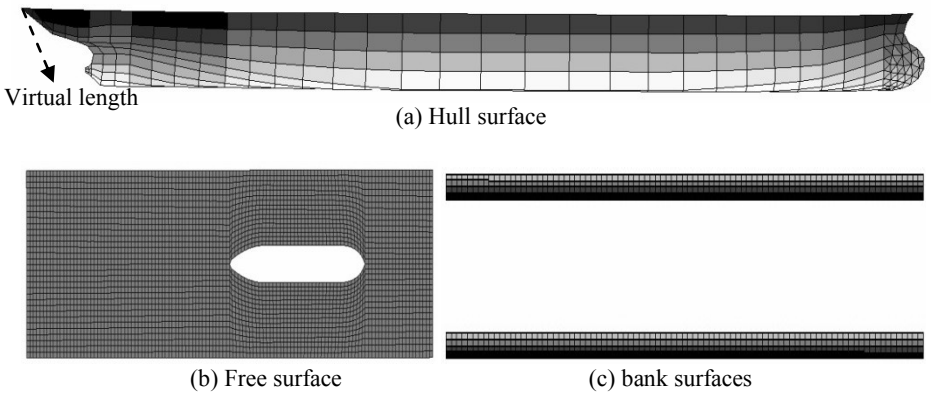

(a) Hull surface

(b) Free surface (c) bank surfaces

Fig. 2. Panel arrangements

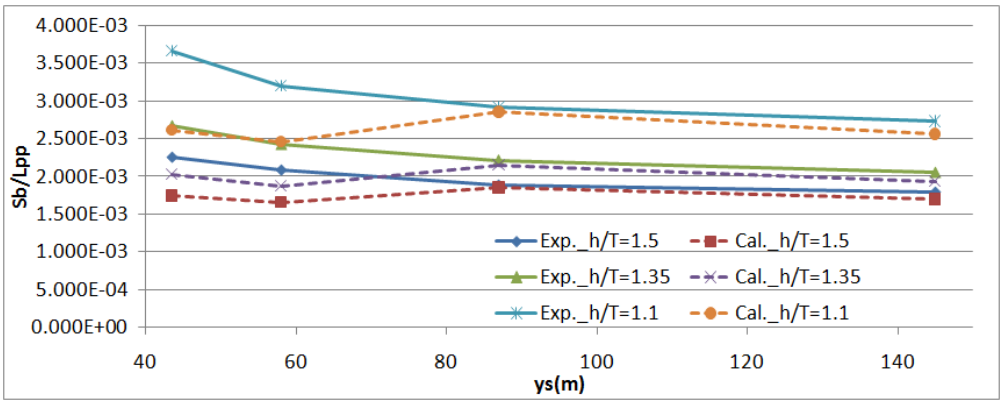

Fig. 3. Comparison of numerical results and measurement for different lateral positions

The reason for the above discrepancy may be that, when the ship is closer to the bank, the vertex is generated between the ship and the bank. Thus, the viscous effect becomes more obvious and has to be taken into account. The Rankine source panel method based on potential theory doesn't perform well under such condition by neglecting the viscous effect. In addition, the effects of rudder and propeller is neglected, the flow field around the ship, especially near the ship stern is not accurate, which may also cause the error. It can also be seen that with the decrease of water depth, the ship squat becomes larger.

The calculation error of all these cases is given in table 3. When y_s is larger, the calculation error is below 10%; while when y_s is smaller, the error is around 20%~30%.

Table 3. Calculation error of the Rankine source panel method

y_s	$h/T = 1.5$	$h/T = 1.35$	$h/T = 1.1$
43.5	23.02%	24.30%	28.55%
58	20.90%	22.95%	23.21%
87	2.15%	2.51%	2.23%
145	5.65%	5.82%	6.12%

From the above analysis, it is found that the Rankine source panel method can be used to predict ship squat when the ship is not close to the canal bank.

Influence of canal geometry on ship squat

In this subsection Group 4, 5, 6 and 7 in table 2 are selected. The KVLCC2 is moving along the centerline of the canal and the ship speed varies from 6 knots to 10 knots. Since the different canal geometries have the same cross section area, the same blockage factor ($Ac/As = 6$) for all the cases are applied to investigate the influence of canal geometry on the ship squat. All the results of the bow squat (S_b) are given in table 4.

Table 4. Non-dimensional ship squat with different canal geometries and ship speed

Group No.	Canal bank slope	Squat S_b [m]		
		$U = 3.087$	$U = 4.115$	$U = 5.144$
4	vertical wall	1.191E–03	2.185E–03	3.536E–03
5	1/3	1.021E–03	1.891E–03	3.079E–03
6	1/5	1.027E–03	1.904E–03	3.097E–03
7	1/8	1.111E–03	2.013E–03	3.244E–03

The squat values in table 4 indicate that, with the same blockage factor and $h/T = 1.2$, the KVLCC2 has the largest squat when sailing along the vertical bank. The second largest squat happens

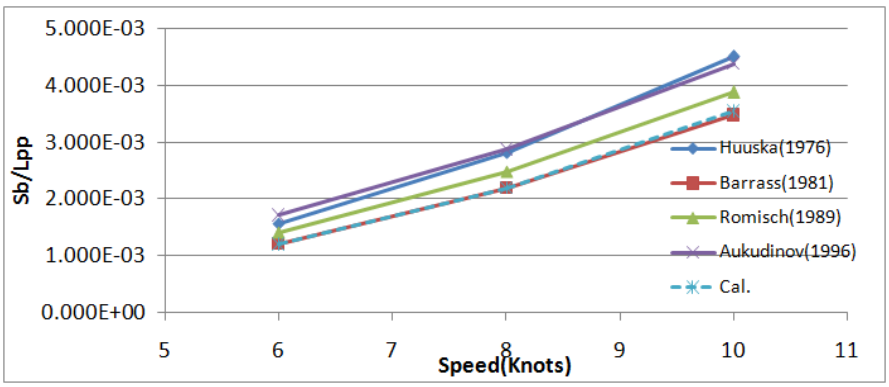

Fig. 4. Squat comparison with empirical formulas, $h/T = 1.2$ and $Ac/As = 6$

when the bank slope is 1/8, and then followed by sloping bank 1/5 and 1/3. The vertical bank has the dominant influence on ship behaviour and always causes a larger ship squat than other bank geometries no matter in shallow or deep water. For the cases with a sloping bank, if the water is deep enough, the steeper the bank is, the larger the ship squat becomes. When the water is very shallow, the ship behaviour is affected by both the canal bank and the bottom. That is why the squat for sloping bank 1/8 is larger than those of the banks with other slopes.

Figure 4 shows the comparison of the numerical results and those calculated by the commonly used empirical squat formulas. Since all the four geometries have the same blockage factor, the ship squat is the same according to the empirical formulas. Here, the squat for vertical bank is adopted. The comparison shows that the numerical results agree well with the popular formulas, especially with Barrass (1981) formula.

Conclusions

In this paper, a first-order Rankine source panel method is adopted to predict the squat of a ship sailing in laterally and vertically restricted canals. Numerical calculations are carried out for the KVLCC2 tanker travelling in a canal at different lateral positions, water depth, ship speed and bank geometries. The calculated squat is compared with measurement data and the results from empirical formulas. Through the analysis, it is found that the Rankine source panel method can be applied to the ship squat prediction when the ship is not close to the bank. The method can also predict the ship squat differences among different canal geometries with the same blockage factor. The ship squat is most obvious when the ship sails along a vertical bank. For the cases with a sloping bank, when the water depth is very shallow, the ship travels along a 1/8 sloping bank may have a larger squat than the other two geometries.

The study in this paper investigated the influence of canal geometry on ship squat that cannot be calculated by the empirical formulas, which is useful for the practical use. Future study will be focused on taking account the viscous effect and the propeller and rudder geometry into the numerical model.

Acknowledgements

This work is supported by the National Natural Science Foundation of China (Grant No. 51061130548) and the China Scholarship Council.

References

1. ZHOU M., ZOU Z., YAO J.: Prediction of ship squat in restricted waters. Journal of Ship Mechanics, Wuxi 2013.
2. LATAIRE E., VANTORRE M.: Ship-bank interaction induced by irregular bank geometries. Proceedings 27th Symposium on Naval Hydrodynamics, Seoul 2008.
3. LATAIRE E., VANTORRE M., DELEFORTRIE P.: A prediction method for squat in restricted and unrestricted rectangular fairways. Ocean Engineering, 2012.
4. BRIGGS M.J., KOPP P.J., ANKUDINOV V.K., SILVER A.L.: Comparison of measured ship squat with numerical and empirical methods. Journal of Ship Research, New York 2013.
5. Yao J., Zou Z.: Calculation of ship squat in restricted waterways by using a 3-D panel method. The 9th International Conference on Hydrodynamics, Shanghai 2010.
6. SIMMAN2008. Workshop on Verification and Validation of Ship Maneuvering Simulation Methods. Copenhagen 2008. www.simman2008.dk.

Editorial Staff / Redakcja

Editor / Redaktor – Paulina Mańkowska

Statistically editors / Redaktorzy statystyczni – Lech Kasyk, Grzegorz Nicewicz

Editorial study and proofreading / Opracowanie językowe i korekta – Adriana Nowakowska

Layout design / Opracowanie graficzne – Monika Jagielska

Editorial translator / Tłumacz redakcji – Adriana Nowakowska

Computer typesetting / Skład komputerowy – Irena Hajdasz

Wydawnictwo Naukowe Akademii Morskiej w Szczecinie

70-506 Szczecin, ul. T. Starzyńskiego 8
tel. 91 480 96 45, 91 480 96 16, e-mail: bw@am.szczecin.pl
www.wydawnictwo.am.szczecin.pl

Wydanie I. Nakład 150 egz. Objętość: 25 a.wyd.
Drukarnia: Agencja Reklamowa „TOP" Agnieszka Łuczak, 87-800 Włocławek, ul. Toruńska 148